Development, Analysis and Testing of a Hybrid Passive Control Device for Seismic Protection of Framed Structures

By

Justin D. Marshall

Dissertation submitted to the faculty of
Virginia Polytechnic Institute and State University
in partial fulfillment of the requirements
for the degree of

Doctor of Philosophy

in

Civil Engineering

Approved:

Dr. Finley A. Charney, Chairman

Dr. W. Samuel Easterling

Dr. Thomas M. Murray

Dr. Raymond H. Plaut

Dr. Mahendra P. Singh

Dr. Elisa D. Sotelino

15 December 2008

Blacksburg, Virginia

Development, Analysis and Testing of a Hybrid Passive Control Device for Seismic Protection of Framed Structures

Justin D. Marshall

Abstract

A new seismic protection strategy called the hybrid passive control device (HPCD) has been developed which combines typical passive energy dissipation devices. It consists of a high damping rubber (HDR) sandwich damper in series with a buckling restrained brace (BRB). The HPCD provides energy dissipation at small deformations without significantly decreasing the structural period. The significant energy dissipation capacity of a BRB is provided for significant seismic events in the second phase. The transition between these two phases consists of an increasing stiffness as the device transitions from rubber damper to BRB. The HPCD reduces deformations, forces and accelerations from seismic events. The hyperelastic or stiffening effect also prevents resonant build-up and aids in collapse prevention due to p-delta effects.

The first phase of this work included characterization of high damping rubber compounds and analytical modeling of the HPCD concept. Experimental testing was completed to measure both the static and dynamic material properties of six different rubber compounds. The two most promising rubber compounds were selected for possible inclusion in the device. Analytical models of these selected materials were developed for nonlinear solid finite element analysis. The most promising configuration of the device was selected from several options. The selected configuration was analyzed using the commercial finite element program ABAQUS. These models were used to confirm the validity of the theoretical behavior of the device. Additionally these tests were used to determine which of the rubber compounds performed best.

Experimental testing of a half-scale HPCD specimen was carried out in the Structures and Materials Research Laboratory at Virginia Tech. The prototype was tested under cyclic and static loads. The experimental tests confirmed the potential of the hybrid device while highlighting minor issues with the design of the prototype. The final component in the research was an analytical study using hybrid devices in a 9-story steel moment frame structure. The devices were found to provide improved response over a special steel moment frame and a moment frame combined with a buckling restrained brace frame.

Acknowledgements

This dissertation represents the culmination of a significant amount of work on the part of many people. The first person I want to mention is my wife Ginger. Her support throughout all my educational pursuits and especially these last years has been critical to my success. I also want to thank my children, Andrew, Hawley and Audrey, who have not seen as much of their dad as they would have liked. I have to thank my parents for the ideals and character they instilled in me and the work ethic they taught me from my early years. I also want to thank my Heavenly Father for all the blessings, comfort and support he has given me throughout my life.

I would especially like to acknowledge Dr. Charney for the opportunity to work on this project. His advice, knowledge and experience have been freely given. He has also given me the latitude to work independently which proved in some cases to be maybe a little too much. I greatly enjoyed the discussions we had that started on technical matters and often became personal. I also want to thank each of my committee members: Dr. M.P. Singh, Dr. Elisa Sotelino, Dr. Ray Plaut, Dr. Sam Easterling and Dr. Tom Murray. Each has had a significant effect on my educational progress through classroom and personal interaction. I have learned a great deal and am honored to have had the opportunity.

The experimental testing in the lab would not have been possible without Brett Farmer and Dennis Huffman. They were always available and willing to help me when something didn't go according to plan. The best part was that when I needed help with how to do something they were ready with an idea that made my life easier than implementing my own convoluted plan.

I would also like to acknowledge my fellow graduate students. I don't think I would have made it through without them. I hesitate to name names as someone will surely be left out, but Andrei, Devin, Brad, Sean, Rakesh, Adam, Chris, Matt, and Ashley have all been great friends. Someone is always in need of help, and having so many good people around makes life and work easier.

Finally I would like to acknowledge those who have financially contributed to my education. The Charles E. Via Fellowship has been a wonderful blessing to me. I would also like to acknowledge the National Science Foundation under project #0612798 and the Virginia Tech ASPIRES program for funding this research. Lastly, I would like to thank Corry Rubber Corporation for sharing their expertise and donating materials to this research.

Table of Contents

List of Figures

Chapter 2

Chapter 3

Chapter 4

Chapter 5

Chapter 6

Chapter 7

Appendix A

List of Tables

Chapter 4

Chapter 6

Chapter 7

Chapter 8

Chapter 1. Introduction

1.1. Defining the Problem

Engineers are renowned for their ability to creatively solve real world problems through the application of science and mathematics. In the field of structural engineering typical problems include designing structures to be safe and effective throughout their lifetime. The success of the solution resides in the economy, visual appeal and effectiveness of the structure. Unfortunately in many cases when the structure fails, not only does the engineer lose credibility, but the loss of money and lives can be significant. There are many examples, some recent, where the drastic failure of a structure has significant costs both financially and emotionally. In some cases the failure is a result of a prolonged problem finally reaching the breaking point. In other cases, extreme loading causes an immediate and drastic failure. This research focuses on preventing failure due to extreme loading during earthquakes.

Gravity load design of structures is the first thing that budding structural engineers encounter in their education. This includes designing structural elements for loads the building or bridge must support, including appropriate safety factors and serviceability conditions. Along the way they are introduced to lateral loads. These loads originate primarily though not exclusively from two sources, wind and earthquakes. Not only do these loads require different systems to prevent collapse, they can greatly increase the effect of gravity loads as the building is pushed away from center. The dynamic nature of these loads requires greater understanding of basic structural behavior, including terms like mode of vibration, resonant frequency and damping.

In wind events, the pressure on the building must be resisted by the structural system while remaining elastic. In earthquakes, the forces are generated by the building's inertia resisting motion while the foundation shakes with the surrounding earth. The magnitude of the forces generated is very high. It is not practical to design structures to remain elastic during major seismic events. The practice of increasing the strength, which typically increases stiffness, of the structure serves in many cases to increase the inertial forces due to changing dynamic properties. Here is the problem: how can we effectively design buildings to perform well under these conditions? Further questions can also be asked about what state the building should be in following the event. Do you want a building to preserve life by avoiding collapse or do you want to be able to immediately re-enter the building with only minor repairs? This work proposes a

solution in the form of a device that controls structural response under minor to major earthquakes and reduces vibrations under wind forces.

1.2. The Proposed Solution

A significant number of innovative devices and materials have been proposed and successfully used for seismic protection. Each of these devices and methods has strengths and weaknesses. Base isolation has been shown to be effective at reducing accelerations on structures by allowing a near rigid body motion of the structure and deflecting a large portion of the seismic energy away. Multiple control devices exist that initially stiffen the structure and then dissipate significant energy upon yielding. One problem with these devices is that stiffening a structure can move the first vibration period down to a region where the earthquake response is increased, sometimes significantly. Viscous and viscoelastic dampers are used to add energy dissipation to the lateral force resisting system. These devices are effective for all levels of vibration.

The solution proposed in this work is called the hybrid passive control device (HPCD). The HPCD is a combination of two typical passive control devices combined in a way to create a unique and innovative device which enhances the strengths and offsets the weaknesses of the individual devices. The HPCD is a two-stage device. The first stage is a viscoelastic solid device consisting of a high damping rubber (HDR) material. The benefit of the first stage is energy dissipation for all deformation levels. It dissipates energy during wind events and minor earthquakes without requiring structural repair. The second stage of the HPCD is a hysteretic yield device. The benefits of this phase are the ability to dissipate significant energy and an increase in the stiffness of the device. The increased stiffness reduces displacements and prevents instability which could lead to collapse. The second phase of the HPCD only engages during major earthquakes and focuses the permanent damage into elements that can be replaced without affecting the core structure. In addition to the HPCD, other hybrid configurations are developed here and analyzed as part of this research.

1.3. Scope of Work

The scope of work includes the initial development, analysis and testing of the HPCD as well as development and analysis of other hybrid passive control configurations which take advantage of the combination of typical passive elements. The initial step was to determine the configuration of the device. Several designs were developed and considered. With the basic design in hand, the

selection and analysis of high damping rubber was another early step. Several highly damped rubber compounds were physically characterized statically and dynamically. The data was used to create a material model in the commercial finite element analysis (FEA) program ABAQUS. The analytical model was calibrated using the test data. Once the basic device configuration was chosen, it was further developed and a scale model was fabricated. The scaled prototype was tested to determine if the concept of the device had merit. The performance of the device in a structural frame was investigated through an analytical study using standard nonlinear structural analysis software. Building structures were designed for two geographic areas and subjected to scaled earthquake records corresponding to the local seismicity. The maximum base shear, roof drift and roof acceleration were used as the primary performance standards along with residual drift. Buildings with the HPCD and other hybrid configurations were compared to a special steel moment frame and other typical passive control measures. The purpose of the analysis is to demonstrate the benefits of the hybrid concept in the control of structures under various levels of lateral loads and make a preliminary investigation of the effect of some of the variables associated with the hybrid devices.

1.4. Organization of Dissertation

Chapter 2 of this work provides a background review and current status on the development of passive structural control technology. Applications to structures in the United States and other areas of the world are also discussed. The innovative materials and configurations of damping devices and base isolation systems are reviewed to demonstrate the great flexibility that exists in passive control systems. It also demonstrates that the HPCD adds to the state of the art.

Chapter 3 provides a primer on the behavior and analysis of high damping rubber materials. HDR is a complex material having many beneficial engineering properties. The trade-off is the difficulty in modeling the dual nature and highly nonlinear force-deformation behavior of filled vulcanized rubber. A portion of the body of research in constitutive models is presented along with the background necessary to understand rubber behavior and how it is analytically modeled.

Chapter 4 presents the test methods used to characterize the rubber compounds considered for use in the device. The test results are presented with a discussion of what they mean to the analytical model and theoretical performance of the device. The latter portion of the chapter consists of using the test results to generate analytical models of the HDR compounds. Chapter

4 also consists of a discussion about which rubber compound provides the best performance and merits inclusion in the HPCD.

Chapter 5 includes a nonlinear FEA of the device to verify that the theoretical basis of the device can be supported analytically.

Chapter 6 includes a detailed description of the HPCD. It also includes the testing procedure and results for experimental tests of a scaled prototype of the HPCD. The device is subjected to both cyclic and static loads to test the various components of the hybrid device.

Chapter 7 describes and presents the results of an analytical study. The goal is to compare several hybrid passive control configurations to typical passive control methods. Nonlinear dynamic response history analysis of a 9-story steel moment frame is used to determine the effect of hybrid configurations on the performance of a steel moment frame structure under seismic events.

Chapter 8 includes the summary, conclusions and recommendation for future research and development associated with this research.

Appendix A gives the reduced static test data for the six high damping rubber compounds.

Appendix B presents the design calculations for the scaled HPCD prototype.

Chapter 2. Literature Review

2.1. Introduction

Structural engineers have the challenge of designing buildings to withstand the forces of nature. These forces include gravity loads, both live and dead loads, such as self-weight, non-structural components, human occupancy, snow, and rain ponding. In some situations flood loads, hydrostatic pressure and soil pressure must also be included. In addition to static loads, dynamic loads or resulting deformations are often critical to structural performance and safety. Small-scale vibrations such as footfalls or machine induced motions are one class of dynamic loads. Another set of dynamic effects includes wind, seismic and blast loads. Wind loads generally require stiffening of a structural system to reduce horizontal displacement and to limit vibration to levels below the threshold of human perception. Wind loads can be classified as either large or small scale vibrations depending on the geographic location. Seismic loads are another case entirely. Designing for seismic loads can be accomplished through simple strengthening. This method works in low seismic areas but is not effective in areas of high seismicity. The reason simple strengthening is not feasible is that adding strength typically adds stiffness. Additional stiffness reduces the period of the structure which increases the inertial loads and requires greater strength. The additional stiffness also increases accelerations which can cause severe damage to the contents of the building. Effective seismic design provides the appropriate combination of stiffness, strength and ductility. The stiffness and strength reduce deformations during ground shaking. The ductility allows the structure to dissipate energy through yielding of structural components without collapsing. The problem with this design methodology is that the cost of ductility can be structural damage beyond repair or to an extent that significant costs are incurred prior to re-occupying the building.

In response to this problem, engineers have developed ways to introduce elements in a structure to control response. The study and analysis of these devices forms a part of the field of structural control. The over-arching goal as it pertains to civil structures is to control response under lateral loads while maintaining life safety as a minimum standard. These control systems can be designed to reduce wind induced vibrations or to dissipate energy during an earthquake without damaging essential structural elements.

2.2. Structural Control

The field of structural control is highly multi-disciplinary and complex. It has its roots in the aerospace industry but has quickly moved into the arena of civil structures (Housner et al. 1997). Within civil structures the primary goal of structural control is to provide the necessary strength, ductility or energy dissipation capacity to save lives by preventing collapse. A secondary goal is for structures to be able to withstand whatever hazard is present and still function with minimal repair. Although the inclusion of these types of devices add up-front building costs, the protection of occupants and reduction of lost production time can more than offset the initial investment.

The major fields of structural control are passive, active, hybrid and semi-active control (Housner et al. 1997). The focus of this survey is on passive energy dissipation systems. Active, semi-active and hybrid control systems are briefly discussed for information only.

2.2.1. Active Control

Active structural control is accomplished through devices which monitor the structure and apply appropriate controls in the form of an applied force or displacement. The goal is to dissipate energy or counteract excessive deformations by modifying the properties of the structure. Active control systems provide significant benefits to structures in many types of events. These systems are very complex and include sensors embedded in the structure, actuators with an external power source and a computerized structural monitoring and analysis system (Spencer and Soong 2002). One concern with these systems is the large power requirement which can be an issue in a significant natural hazard. Stability may also be a concern due to large forces being applied to the structural system (Housner et al. 1997). The way these systems work is through a network of sensors, actuators and controllers. The controller monitors the applied forces or displacements and the response of the system to external excitation. The controller can then determine what the actuator can do to counteract the motion and return the structure to its undeformed condition. The sensors could be accelerometers, strain gages, fiber optics or another type of measurement device. Examples of actuators include piezoelectric devices, hydraulic actuators or any other system relying on external power to generate force or cause motion.

Active control systems are most commonly found in aerospace applications where active control is required to maintain stability. Applications to civil structures have not been as prevalent. An

example of active control in civil structures is found in Japan where 20 full scale structures were outfitted with active control systems with a primary function of controlling wind vibrations to enhance occupant comfort (Housner et al. 1997).

2.2.2. Semi-Active Control

Semi-active control measures typically require a small power supply but rely on structural deformations to develop forces in the energy dissipation element. The power source is used to adjust the mechanical properties of the device based on feedback from sensors monitoring the structure. Examples of these devices include electrorheological (ER) fluid, magnetorheological (MR) fluid, and variable-orifice fluid dampers (Spencer Jr. and Nagarajaiah 2003; Symans and Constantinou 1999). The advantage of these devices is that they are controllable. The power requirements for these devices tend to be less than active systems even to the degree of running on batteries. Properly implemented semi-active control devices have the potential of outperforming passive devices (Spencer and Soong 2002). Semi-active devices input no energy into the structure and avoid the stability problem with active systems.

The first full-scale implementation of a semi-active control was on the I-35 Walnut Creek Bridge. An adjustable hydraulic actuation system powered by a 12-volt automotive battery was installed on an in-service bridge. A two-year study found that the control system reduced dynamic stresses by 50% and prolonged the service life of the structure (Patten et al. 1999).

2.2.3. Hybrid Control

Hybrid devices employ a combination of active and passive devices. The role of the active device is to offset the weakness of the passive device and vice versa (Spencer and Soong 2002; Spencer Jr. and Nagarajaiah 2003). The hybrid actuator-damper-bracing control system is composed of a viscoelastic damper and a hydraulic actuator. The control strategy is designed to minimize use of the active controller and maximize the benefits of the passive damper. The passive system is designed to be active during small and moderate seismic events with the active controller being effective for significant ground motion. Analysis of one-story and six-story structures concluded that the intelligent strategy was effective for reducing seismic response (Zhang et al. 2006). A value of the hybrid system illustrated by the previous reference is that power requirements for an active system can be reduced by using passive devices as part of the control system (Housner et al. 1997).

2.3. Passive Control Methods

Passive control devices require no external power. They use the relative deformation between the attachment points of the device to the structure to dissipate energy. Many types and multiple configurations of passive energy dissipation devices exist. Two categories of passive devices are rate-independent and rate-dependent. Rate-independent devices dissipate energy through mechanisms that depend only on the displacement in the device. Examples of these include metallic yielding, friction, and shape-memory alloy (SMA) devices (Whittaker and Aiken 1993). The energy dissipation capacity of rate-dependent devices depends on the velocity across the device. These devices include viscous fluid dampers (VFD), viscoelastic (VE) solid dampers and viscous damping walls. Depending on which VE materials are utilized, the magnitude of the displacement can have an effect on the energy dissipation capacity, making the energy dissipation capacity of VE dampers dependent upon both the velocity and the displacement.

The goal of structural control systems within the realm of civil structures is to resist, reduce or dissipate detrimental dynamic loads. For the application investigated in this research, the specific goal is to reduce vibrations due to wind and limit displacement, acceleration and structural damage during earthquakes. This is accomplished by adding an energy-dissipating element to the structure that spares the other elements from damage. Mathematically, this can be seen from an energy balance equation applicable to passive energy dissipation systems shown in Equation 2-1 (Uang and Bertero 1990).

$$E_i = E_k + E_s + E_h + E_\xi \qquad \textbf{Equation 2 - 1}$$

E_i is the energy input into the structure with E_k being the kinetic energy of the structure and E_s the elastic strain energy in the structural members. The two energy dissipation terms in the equation, E_h and E_ξ, account for hysteretic energy dissipated by the structural members and equivalent viscous damping inherent in the structure, respectively.

Energy dissipation is required to survive significant seismic events without collapse. A superior solution would be to design energy dissipation into the system, which reduces damage to the primary structural system which supports gravity loads. This reduction in primary system structural damage can be accomplished through the use of energy dissipation devices or supplemental dampers. In the case of base isolation, the aim is to reduce the input energy by decoupling the structure from the ground. This method allows the structure to deflect a portion of

the earthquake energy away so structural elements can remain elastic (Naeim and Kelly 1999). Another name for these systems is earthquake protection systems. Another class of control systems is called dynamic vibration absorbers. Included in this class are tuned mass dampers, tuned liquid dampers, tuned liquid column dampers and combinations of the various devices. These devices are tuned to a specific frequency, usually the first mode, to reduce vibrations at the specified frequency. Their application to seismic response is limited due to the tuning of the device which requires remaining in the elastic range for optimal performance (Constantinou et al. 1998).

Although most applications of structural control have been for steel or reinforced concrete (RC) structures, light-framed timber structures have also been investigated. Wood structures generally have a higher level of inherent structural damping (up to 15%). The cost of this damping is inelastic damage to the structural system. To solve this problem, base isolation and passive energy dissipation have been applied to and analyzed for wood-frame buildings as well (Symans et al. 2002).

Passive damping systems have been studied and implemented in buildings and bridges all over the world. Japan, Europe, the former Soviet Union, New Zealand and many countries in North America have buildings with passive structural control systems. Several state-of-the-art or current state of the practice articles catalog the uses of passive control devices throughout the world (Guerreiro et al. 2006; Kasai and Ooki 2006; Lu and Zhao 2004; Martinez-Rueda 2002; Mazzolani 2001; Symans et al. 2008). For resources which are overall reviews of passive energy systems for seismic control, including a discussion of mathematical modeling, linear and nonlinear analysis, design procedures and code requirements, see Hanson and Soong (2001) and Constantinou et al. (1998).

To better illustrate the effects of changes in the structure on earthquake response, Figure 2-1 shows acceleration-displacement response spectra with three levels of damping. The horizontal axis represents displacement. The vertical axis represents lateral acceleration which corresponds directly with base shear forces. The diagonal lines from the origin represent different periods of vibration. Assuming that the original structure has a fundamental period on the middle diagonal line and 5% damping, places the response at point A. If the structural stiffness is increased, the period increases shifting us to the upper diagonal line at point B. At this point displacements are

reduced at the expense of increased base shear. If the first mode period on the original structure is reduced through base isolation the response would move to the bottom diagonal line at point C. Here the structure experiences large displacements and reduced forces.

Adding damping or energy dissipation is another option. Increasing damping from 5% to 20% on the base structure moves the response from point A to point F. This results in reduced displacement and base shear. The same effect is seen if damping is added to the base isolated structure. This causes the response to move from C to E. The same effect is seen on the upper line with a shift from B to D. The higher stiffness structure with added damping has reduced response for both quantities. A reduction in base shear due to added damping is only true if the structure remains elastic. If the structure becomes nonlinear, the behavior can be highly unpredictable. It should also be noted that these response spectra only represent linear responses one ground motion.

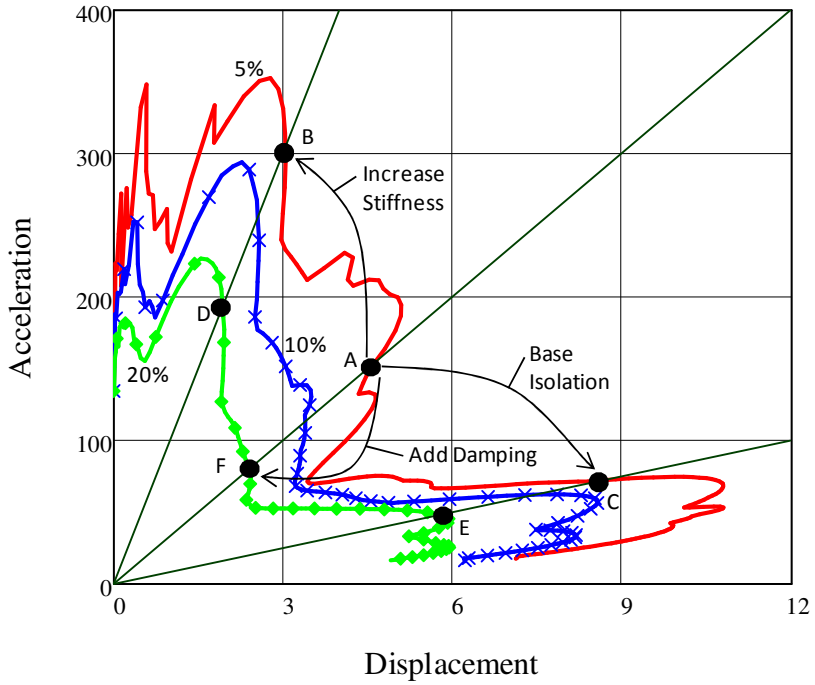

Figure 2 - 1 Acceleration-Displacement Response Spectrum

2.3.1. Base Isolation/Seismic Isolation

Base isolation differs from other passive control measures in that the goal is to isolate the structure from seismic input. Base isolation systems move the first vibration frequency outside the range where earthquake energy is focused. Decoupling the horizontal motion of the building

from the ground allows this to occur. The result is a significant reduction in the energy the structural system must either absorb or dissipate. Base isolation also has the benefit of reducing both story drift and acceleration. Reduction of story acceleration significantly aids in protection of non-structural components and building contents. In many cases, sensitive equipment in buildings costs more than the building itself, so protecting it provides a significant financial benefit. Isolation of structures has been implemented for buildings and bridges around the world.

One of the early attempts at isolating a structure from ground motions was undertaken by John Milne using cast iron plates and solid metal balls. His original design was modified several times, specifically the diameter of the metal spheres, because of the performance of the building under wind loads (Naeim and Kelly 1999). This example also illustrates another problem with base isolation. During normal wind events, some stiffness must be present to resist excessive displacements. An example of this is the Pestalozzi School in Macedonia, the first isolation system with elastomeric bearing pads in 1969. Glass blocks were used to lock the building in place under wind loads. During a seismic event these blocks are designed to crush and the elastomeric bearings would then act to isolate the structure (Naeim and Kelly 1999). The drawback to this system is that these fuses must be replaced after each event. Other configurations of base isolation systems, including a hotel designed by Frank Lloyd Wright, attest to the success of the concept over the last 100 plus years (Buckle and Mayes 1990).

One issue with isolation systems is that large displacements must be accounted for at the isolation plane. This requires special detailing of piping, electrical and mechanical systems to compensate for significant movement. Because of these details, construction of isolation systems can be very expensive. There is also a limitation on the geometry of buildings that can be effectively isolated due to an already long period and overturning issues. An additional drawback to base isolation is that near-field earthquake motions with a strong velocity pulse cause problems with isolated structures (Housner et al. 1997). Base isolation can be highly effective for the right structure in the right location, but is not ideal for every situation.

Current research and practice in seismic isolation employs elastomeric laminated bearing pads, friction-pendulum devices or sliding devices that allow the structure to displace at or near the foundation level. It is often used in combination with a damping device to reduce the energy imparted to the structure and the displacement across the isolation level. Fluid viscous dampers,

friction surfaces and lead-core bearing pads are commonly used for energy dissipation, although other systems have and are being used.

High-damping natural rubber (HDNR) has been used as the elastomeric material in laminated bearing pads to function both as the horizontally flexible material and the energy dissipating element. Because this material is used in the supplemental damping device developed and analyzed in this research, this portion of the review will focus on HDNR's implementation and development as a base isolation material. Other elastomers for isolation pads include low-damping natural and synthetic rubber. These rubbers, however, require an added energy dissipating element such a lead plug insert, viscous damper, frictional device or metallic damper to reduce displacements at the isolation level.

To achieve the desired horizontal flexibility and vertical stiffness, bearing pads are laminated by alternating steel plates and thin horizontal layers of elastomeric materials. This is done to reduce the bulging and settling that would occur in a taller rubber bearing. In some cases, bent plates are used so the bearing is horizontally stiff in one direction and flexible in the orthogonal direction. Figure 2-2 illustrates some different types of laminated bearing pads.

HDNR bearings were used in the first seismically isolated building in the United States. The Foothill County Law and Justice Center in Rancho Cucamonga, California, which is located only 13 miles from the San Andreas Fault and completed in 1985, was the first building isolated on this type of bearing (Tarics et al. 1984). The same HDNR system was used in the Fire Command and Control Facility in Los Angeles County (Anderson 1989).

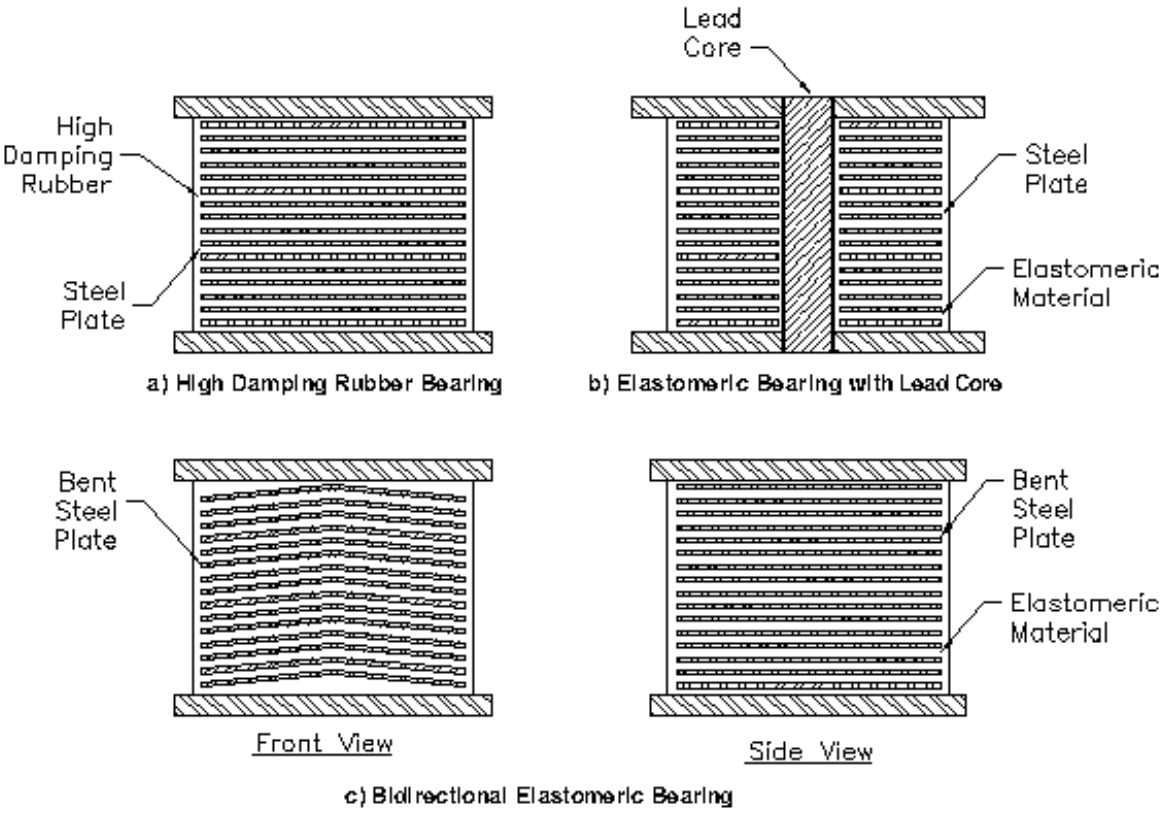

Figure 2 - 2 Laminated Elastomeric Bearing Pads

HDNR is an ideal material for use in laminated bearings because of its nonlinear stress-strain behavior (see Figure 2-3). At low strains (< 20%) the material has a high initial stiffness, which provides the stiffness required for wind loads. In the mid-range of strains, up to 150 or 200%, the stiffness is reduced, which allows the horizontal flexibility necessary to achieve isolation. In the higher strain levels, the rubber has a hyperelastic or stiffening effect which provides a stopgap to bearing failure or excessive displacement (Fuller et al. 1996b). The levels at which these changes in stiffness occur is based on the specific compound of HDNR. An additional benefit is that the inherent damping of the material eliminates the requirement for a supplemental damping element to limit displacement, providing for a simpler isolation system (Derham et al. 1985). The work by Derham, Kelly and Thomas was the first implementation of filled natural rubber and was part of a ten-year study by the University of California at Berkeley and The Malaysian Rubber Producers' Research Association in England. Later work on the properties of HDNR compounds showed that various compounds of carbon-black filled natural rubber are available in a shear modulus range of 70 to 175 psi and material loss factors over 11% (Fuller et al. 1996b). Fuller, Ahmadi and Pond completed a study on the longevity of the rubber dampers. Based on unfilled

natural rubber bearings, test results show a stiffening of 5 – 15% over a period of 37 years. Because of the different chemistry of HDNR, laboratory ageing tests showed that the material stiffens by approximately 20%. The dynamic modulus and damping exhibited a smaller change than the stiffness properties. They also concluded that there is a desire to increase the inherent damping above the current values (Fuller et al. 1996a).

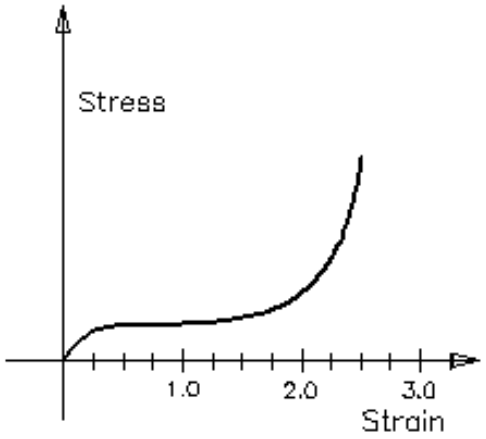

Figure 2 - 3 Representative Stress-Strain Diagram for HDNR

In the United States, the number of HDNR base isolated buildings has continued to increase. The Traffic Management Center for Caltrans in Kearny Mesa, California used 40 HDNR isolators provided by Bridgestone Engineered Products Rubber Company (Walters et al. 1995). Hospitals and government buildings are also popular structures for HDNR isolation systems. The M.L. King/C.R. Drew Diagnostic Trauma Center used 70 HDNR bearings in combination with sliding bearings (Naeim and Kelly 1999). Another medical facility isolated with HDNR is the Arrowhead Regional Medical Center. The center consists of six separate structures, five of which are isolated. The hybrid isolation system consists of a combination of high damping and linear rubber bearings with velocity dependent dampers (Asher et al. 2001). The Los Angeles City Hall was retrofitted after damage in three major seismic events. The isolation system consists of 416 HDNR bearings, flat sliding bearings and 52 viscous dampers in the isolation plane (Youssef and Hata 2005).

Outside of the United States, high damping rubber bearings are used extensively for isolation systems. In Japan, the number of seismically isolated buildings has increased annually by at least 100 buildings per year from 1996 to 2003 (Kani et al. 2006). Kani, Takayama and Wada (2006) report on multiple base isolated structures and their performance during seismic events

based on building occupants' interviews. The buildings cited in the paper using HDNR bearings include the Hokuriku Vocational School in Nagaoka City, a dormitory structure in Hakata, a condominium building in Minami and an office building in Chuo. All of these reinforced concrete structures performed well during seismic events. Another interesting application of HDNR isolation was for a wood frame building study in Japan. HDNR bearings were studied on a two-story timber structure and found to be effective at reducing displacement and acceleration (Sakamoto et al. 1990). Shaking table studies of a seismically isolated 2/5 scaled structural steel frame completed in Taiwan demonstrated a 40% reduction in displacement and a 40-60% reduction in floor accelerations (Pu et al. 2004). In Malaysia, two three-story reinforced concrete buildings were constructed; one with a conventional fixed base, the other isolated with HDNR bearings with 10% damping (Malek and Basir 2001).

Active base isolation implementation and research can also be found in Europe, specifically in Italy. The list of buildings in Italy using HDNR bearings includes the five building complex of Telecom Italia in Ancona, an apartment building in Squillace Marina, a Navy building in Ancona, a Navy Medical Centre and apartment building in Augusta and the Department of Mathematics and Faculty of Agriculture buildings at the University of Basilicata (Mazzolani 2001). Another study illustrates the use of HDNR bearings with low friction sliding bearings to retrofit two four story reinforced concrete buildings (Oliveto et al. 2004).

Base isolation as a passive control method is effective for historically significant buildings because it can reduce the earthquake forces to elastic levels. Because of the reduced accelerations, no additional structure is required, and the historical architecture can be preserved. One example of this is museums including the Bronzes of Riace at the Museum of Reggio Calabria, the National Museum of Perugia and the Satyr of Mazara del Vallo. These applications are three-stage high damping rubber systems (Martelli 2006). Another historic structure in Italy protected by base isolation is the cloister façade of the Sao Vicente de Fora monastery. The isolation system, partially illustrated in Figure 2-4, includes high-damping bearings at the base of the façade columns (De Luca et al. 2001). A minaret in Egypt damaged during the Egypt/Dashur 1992 earthquake was retrofitted using HDNR bearings and vertical anchoring steel bars. The now base isolated Manjaq Al-Yusufi, a Mamluk-style minaret, was completed in 1349 A.D. (El-Attar et al. 2005). The Capelinhos Lighthouse, a landmark on the Fayal Island, Azores was constructed in 1903 and damaged by volcanic induced seismic events in the 1950s. An HDNR

base isolation solution was used to bring this building up to current seismic performance standards (Guerreiro et al. 2006).

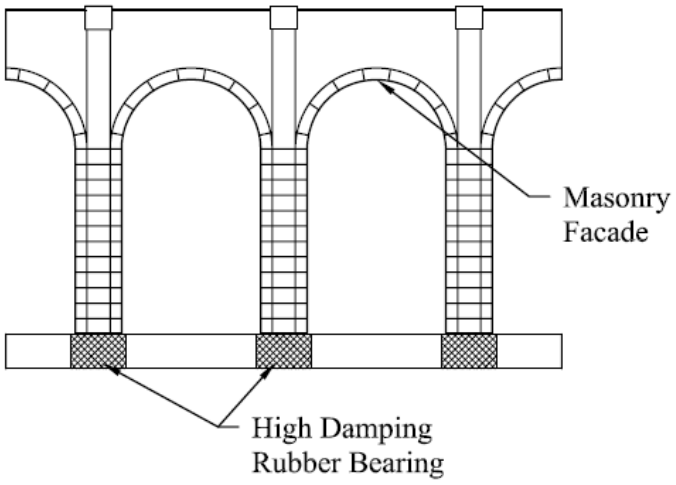

Figure 2 - 4 Schematic of Cloister Façade [after (De Luca et al. 2001)]

Although this is by no means a complete list of applications, it displays the past success and future potential of HDNR as an isolator and damper. Another aspect of HDNR research is the complex material properties. The damping is neither hysteretic nor viscous but a combination of the two. The stress-strain behavior is nonlinear with a continuously changing stiffness. Because of this complexity, a large body of work exists on modeling the physical behavior of carbon-filled rubbers. A review of this literature will be provided in a later chapter.

2.3.2. Rate-Independent Dampers

Rate-independent devices are classified as such due to the relative independence of the energy dissipation to the velocity across the damper. “Hysteretic devices” is another commonly used name for these devices. Metallic yielding devices and friction devices are the two primary classes of hysteretic devices. These devices significantly affect the dynamics of the structure by adding stiffness initially and energy dissipation as the devices yield and deform plastically. In this manner, these devices help with wind loads by stiffening the structure but can also act as an earthquake attractor by shortening the period and increasing the input seismic energy. Figure 2-5 shows idealized hysteresis loops for rate-independent devices.

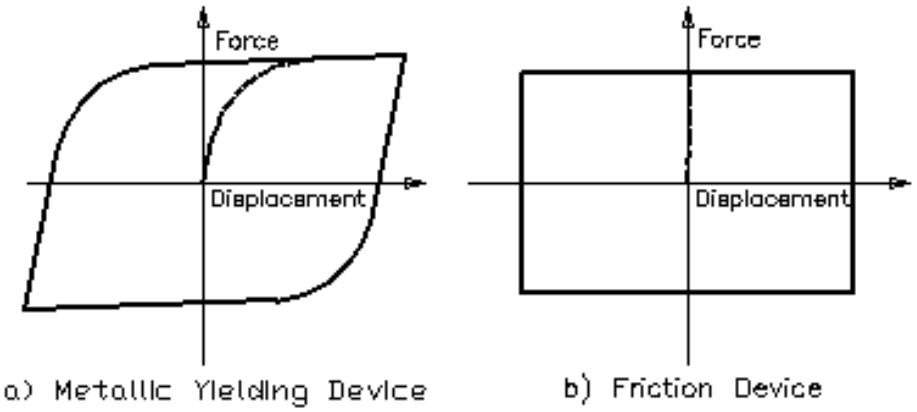

Figure 2 - 5 Rate-Independent Idealized Hysteresis Loops

2.3.2.1. Metallic Yielding Dampers

Metallic yielding devices use the ductility of metals to dissipate energy. Mild steel is the standard in these devices; however, the use of lead and shape memory alloys (SMA) has also been investigated (Towashiraporn et al. 2002). Stainless steel and aluminum alloys are also contenders for seismic protection devices because of their properties (Di Sarno and Elnashai 2003).

In the 1970s, research using metallic yielding devices to dissipate seismic energy was initiated (Kelly et al. 1972; Skinner et al. 1975). Some devices presented in this early research include torsional beams, flexural strips and U-shaped plates. Later work included added damping and stiffness (ADAS) devices which dissipate energy by yielding of specially shaped plates.

2.3.2.1.1. Added Damping and Stiffness (ADAS) Device

ADAS devices use a series of parallel plates typically connected to a chevron brace at the bottom and the structural frame at the top, as shown in Figure 2-6. The plates are tapered to match the shape of the moment diagram such that the yielding occurs throughout the plate to achieve the most energy dissipation per volume of steel. The plates are subject to bending about the weak axis. The initially used shape was hourglass or X-shaped plate (Bergman and Goel 1987; Whittaker et al. 1991). Using the same functionality as the ADAS device with triangular shaped plates, the tapered plate energy absorber (TPEA) device was also developed and found to be effective at dissipating energy (Tsai and Tsai 1995; Tsai et al. 1993).

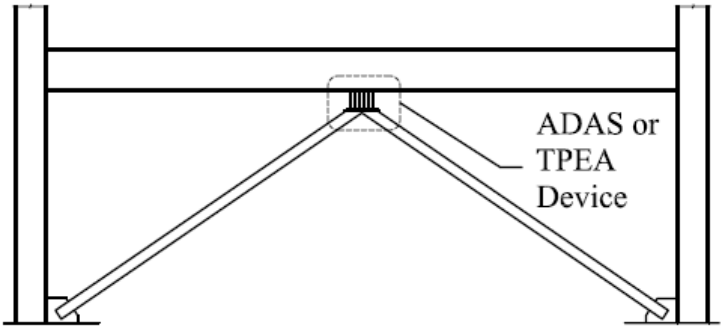

Figure 2 - 6 Chevron Brace Configuration for ADAS/TPEA Device

For the ADAS device, both ends of the plates were clamped, resulting in double curvature bending. Because of the hourglass shape of the plate, it yields uniformly over its height. The TPEA device had clamped-pinned end conditions. The triangular shape of the plate served the same function as the X-shaped plate, with yielding spread over the entire plate. Figures 2-7 and 2-8 illustrate the ADAS and TPEA devices' plate geometry.

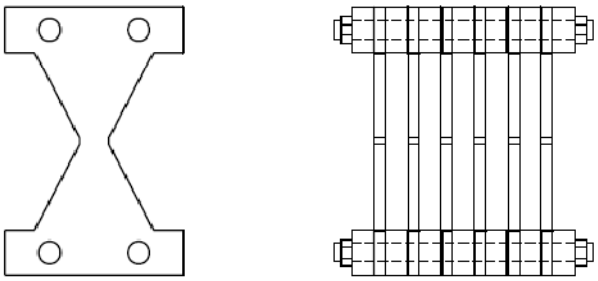

Figure 2 - 7 Additional Damping and Stiffness (ADAS) Device

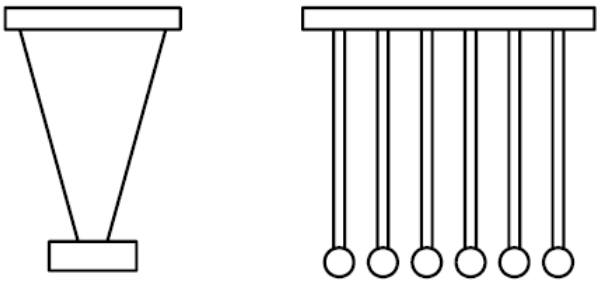

Figure 2 - 8 Triangular Plate Energy Absorbing (TPEA) Device

A retrofit of reinforced concrete (RC) buildings in Mexico City employed ADAS devices both within the structural envelope and in buttresses outside the building (Martinez-Romero 1993). Seismic retrofit in the United States of the Wells Fargo Bank in San Francisco due to damage from the Loma Prieta earthquake included ADAS devices attached to chevron braces (Perry et al. 1993). The initial work on plate dampers found that they are effective at reducing displacements,

in part because of added stiffness. They are also effective at dissipating energy through a stable and repeatable hysteresis. A later study on a building damaged by the Mexico City earthquake concluded that a retrofit with ADAS elements was superior to a retrofit with steel braces. The yielding was concentrated in the ADAS devices (Tena-Colunga and Vergara 1997). A later study conducted on a four-story steel structure in Iran also concluded that a retrofit with an ADAS device provided exceptional dynamic performance (Tehranizadeh 2001). As a variation on the ADAS device, it was implemented in a tension-only cable system. This system uses crossed cables which slip or rotate at the ends, causing the ADAS device to dissipate energy (Phocas and Pocanschi 2003).

Research using low yield strength steel (LYS) and a rhombic shape plate for an ADAS-type device was introduced to overcome weaknesses in the original device, (see Figure 2-9). Due to issues with maintaining fixity of the plate, this device uses symmetry to achieve the prescribed condition at the center of the plate. Additionally, LYS exhibits a greater degree of strain hardening and improved ductility over A36 steel, which reduces the instances of fracture and fatigue failure under cyclic loading (Shih et al. 2004).

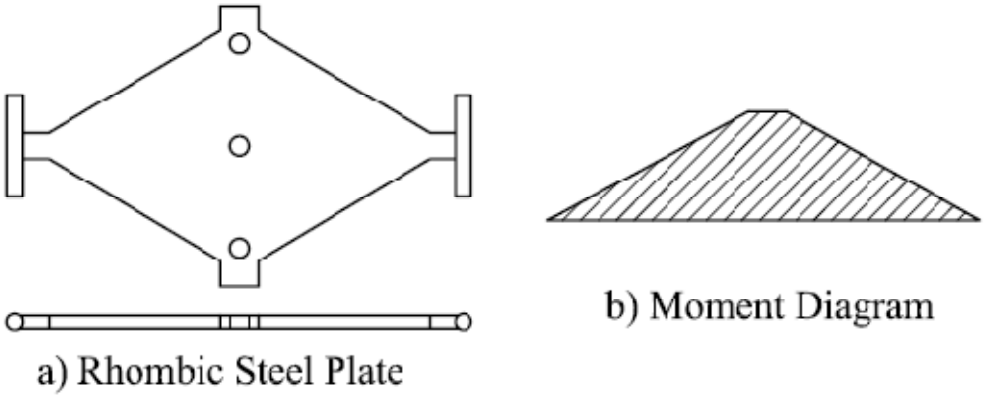

Figure 2 - 9 Rhombic Low Yield Strength Steel (LYS) Plate

The longitudinal ADAS (LADAS) device, shown in Figure 2-10, is another variation on the original ADAS device. The shape of the yielding element in the LADAS device is similar to that of the LYS rhombic device. The LADAS would be implemented in a diagonal or horizontal brace rather than being directly attached to a beam. Testing has proved its effectiveness in reducing seismic response of structures (Tsai et al. 2005b).

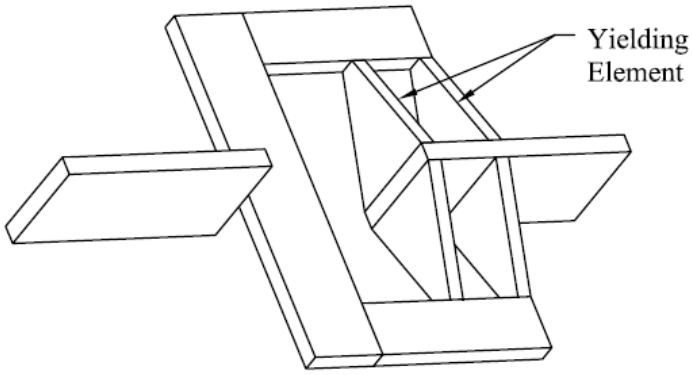

Figure 2 - 10 Longitudinal Added Damping and Stiffness Device [after (Tsai et al. 2005b)]

2.3.2.1.2. Yielding Inner Frame

According to Tyler (1985), the initial concept of the yielding inner frame was suggested by David Smith and Robert Henry of Auckland, New Zealand in the late 1970s. The initial frame was a solid round bar formed into a rectangle. Each corner of the frame was attached to the end of an X-brace. Under loading, the frame would form into a parallelogram and through yielding dissipate energy. An example of this is shown in Figure 2-11. In the tests performed by Tyler, the device performed well through 200 cycles. One weakness of the initial device was a constant cross-section of the yielding element.

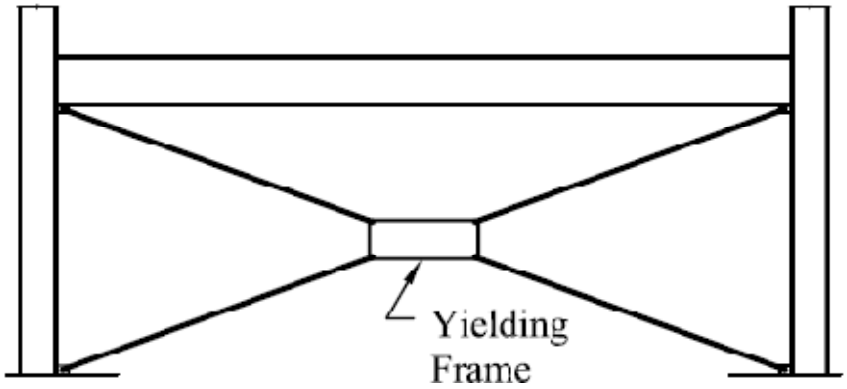

Figure 2 - 11 Yielding Inner Frame in a Structural Bay

Using the same reasoning as for the ADAS and TPEA devices, configurations with a varying cross-section were developed to provide a greater volume of material to yield. This was accomplished by matching the moment diagram with the cross-sectional area through tapering or adding additional plates (Ciampi and Samuelli-Ferretti 1990). Figure 2-12 provides sketches of these frame elements.

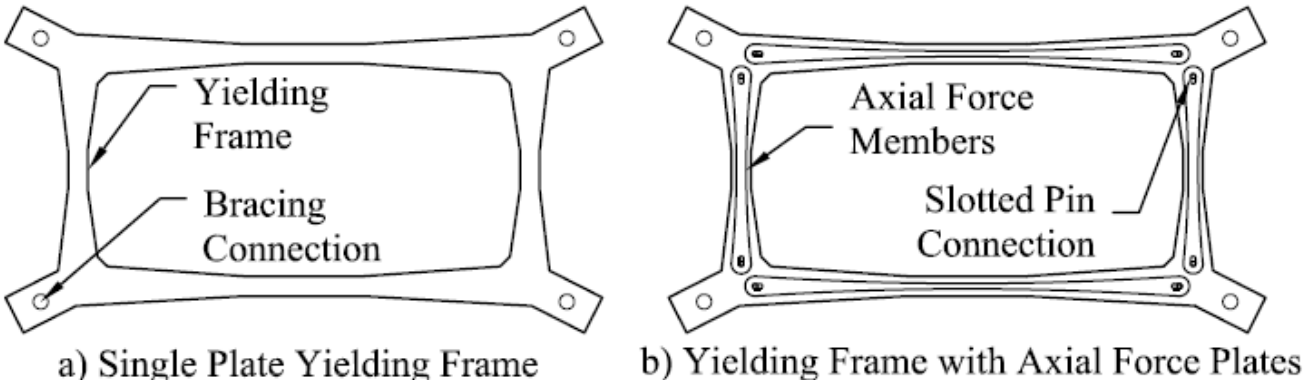

Figure 2 - 12 Single Plate Yielding Frames [after (Ciampi and Samuelli-Ferretti 1990)]

Single plate yielding dampers are sketched in Figure 2-12. Further work by Ciampi and his research group culminated in the E-shaped and C-shaped metallic devices. These devices would be connected to chevron bracing in the middle with the edge holes attached to the beam above, (see Figure 2-13). The geometry is efficient in that uniform plastic deformation occurs for small displacements. These devices are attached to chevron bracing and provide the same plane-stress load condition for yielding as the original yielding frame (Ciampi 1995; Ciampi et al. 1993a; Ciampi et al. 1993b).

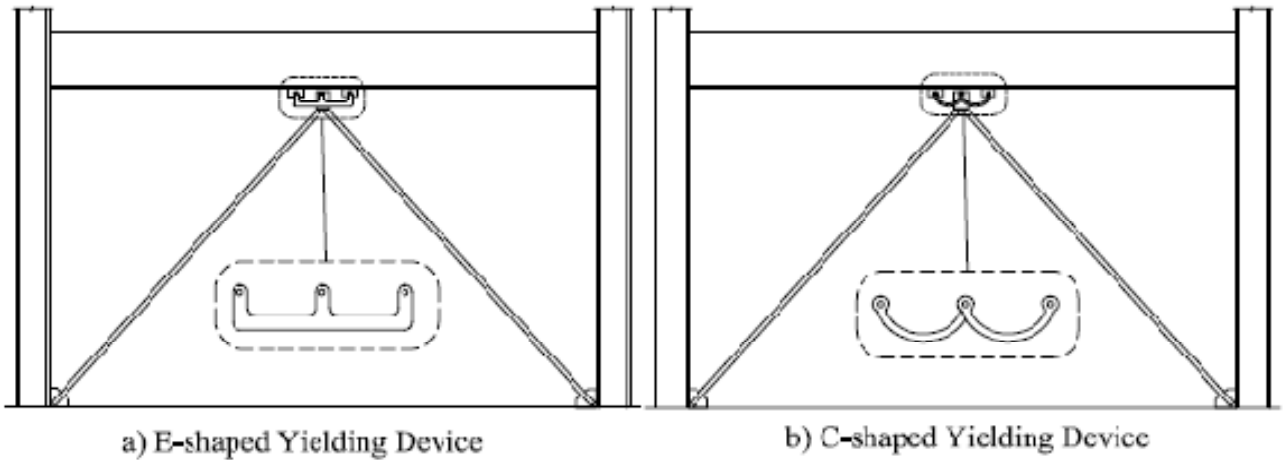

Figure 2 - 13 E-shaped and C-shaped Metallic Yielding Devices

Work at the University of Rome 'La Sapienza' developed a lightweight dissipative bracing system using C-shaped damping elements attached to a hinged rectangular frame connected at the corners to tension-only cross-bracing. Under load, the rectangular frame would deform into a trapezoid with the C-shaped elements yielding due to the elongation or shortening of the diagonal along which it was attached. The frame at the center of the bay is referred to as the

articulated quadrilateral. The device is diagrammed in Figure 2-14. Shaking table tests of a two-story steel frame verify the device effectiveness at reducing inter-story drift and base shear (Ciampi 1995; Ciampi et al. 1993a; Ciampi et al. 1993b). A study on yielding damped braced frames (YDBF) examined the behavior of frames with varying sizes of inner frames. The research found that the YDBF elements yielded and the frames remained elastic (Sabouri-Ghomi and Roufegarinejad 2005). The use of the yielding inner frame has been proven to be an effective solution for dissipating seismic energy in both new and retrofit applications. The key element is efficient yielding of the material. This is best accomplished by matching the shape of the dissipation element to the moment diagram.

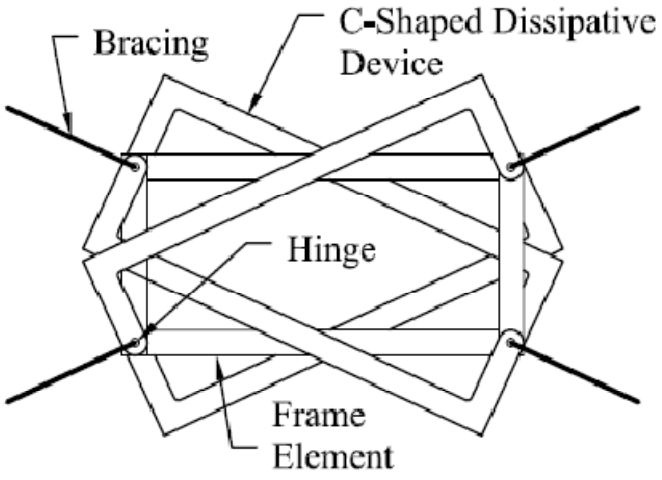

Figure 2 - 14 Articulated Quadrilateral Dissipative Device [after (Ciampi 1995)]

2.3.2.1.3. Buckling-Restrained Brace (BRB)

Buckling-restrained braces (BRB) or unbonded braces (UBB) act as both a structural brace and a hysteretic damper. They are made up of a steel core, a confinement material and steel restraining tube. A typical BRB is sketched in Figure 2-15. The steel core is designed to yield in both tension and compression. Because of the provided confinement, the behavior will be nearly symmetric during load reversals. In most cases the core is dog-boned or has a tapered cross-section so the yielding can be focused in the desired region. The bond-breaker material or a small gap is provided between the core and confinement material so the effects of friction are minimized. The confining material is most commonly a mortar or cement material with very small or no aggregate. Based on the cited research, the early beginnings of a brace restrained against buckling were in the 1970s in Japan (Black et al. 2004; Fahnestock et al. 2006; Xie 2005). The earliest referenced work in this group is from Xie in which he states that the earliest

work is a steel plate encased in a precast concrete wall (2005). Since that time period, significant work has been carried out to improve the original configuration.

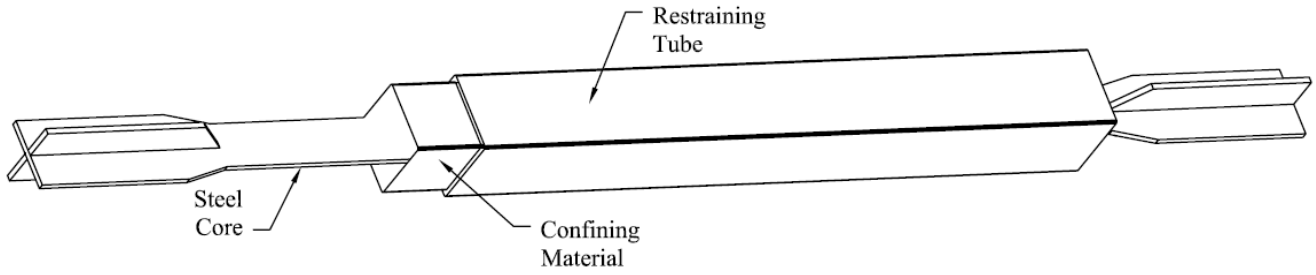

Figure 2 - 15 Buckling Restrained Brace (BRB)

Researchers in Asia and the United States have been active in developing and using BRBs since the 1994 Northridge, 1995 Kobe and 1999 Chi-chi earthquakes. Recent experimental testing of BRBs demonstrated their ability to provide a stable, repeatable and ductile response. The device performance exceeded the specified requirements in terms of ultimate deformation and cumulative plastic strain in testing (Black et al. 2004; Tsai et al. 2004). A variation of the typical BRB configuration called the confined yielding brace (CYB) replaces the mortar used to confine the steel core with a confined non-cohesive material. Because of this change, a debonding material is not required around the steel core. Additional modifications to the typical configuration include different geometric configurations of the steel core. The various configurations of the CYB performed well but highlighted the necessity to properly detail the geometry and properties (Higgins and Newell 2004). Various core geometries are sketched in Figure 2-16.

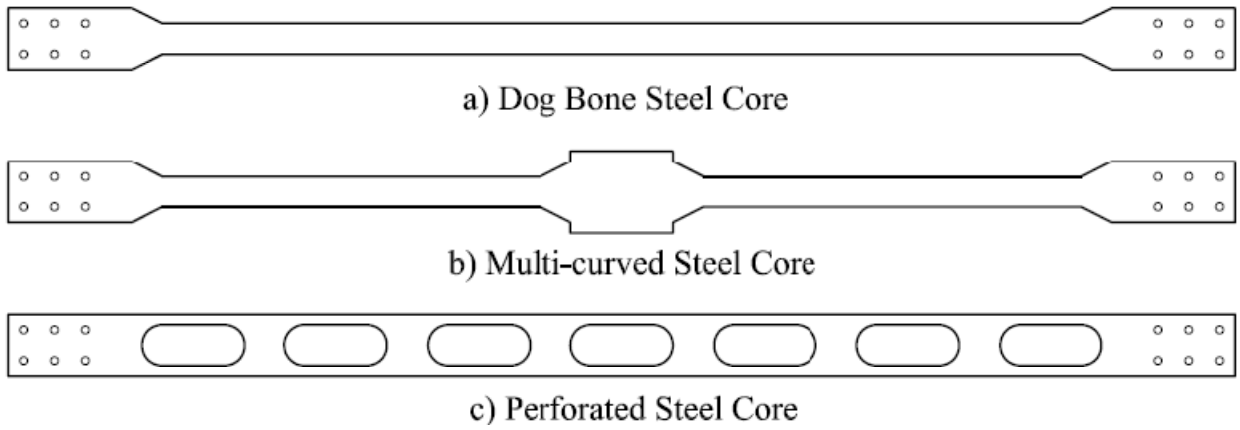

Figure 2 - 16 Steel Core Geometries for BRBs

Further shaking table testing of a reinforced BRB braced three-story structure shows that the braces performed well during simulated seismic events (Tsai et al. 2005a). A complete steel BRB system used both simplified (dog bone) and multi-curved cores. Instead of using mortar filler to confine the core, the pieces cut from the original full steel core are used. The remaining elements of the restraining member are structural tubes connected to either face to provide the overall buckling restraint. The all-steel system provides solutions for manufacturing quality control issues for standard BRBs with mortar fill and debonding material. The component tests proved that the advanced BRBs have stable behavior and outperform previous braces (Tsai et al. 2006). BRBs using two steel planks welded together around a steel core piece have also been evaluated. The manner of construction provides improved design options and on-site delivery of components for assembly and erection as two of multiple benefits. The physical tests verified that all the tested specimens had a stable hysteresis up to 1.0% strain. With the exception of specimens with a lower ratio of core yield force-to-Euler buckling load of the restraining member, the BRB specimens exhibited stable hysteresis up to 2.5% strain (Iwata and Murai 2006).

Another all-steel brace, the buckling-restraining mechanism (BRM), was tested and found to have good initial performance, although future work needs to be completed. Specifically, unbonding material, stiff restraining members, and closely spaced bolted connections were required to match the performance of concrete filled BRBs (Tremblay et al. 2006).

In addition to component tests and developments of new configurations of BRBs, research has also been concentrated on the performance of braces within a structural system. Kiggins and Uang (2006) reported that one of the drawbacks of a BRB-only system was residual deformation. To improve this behavior, they recommend installing BRBs with a special moment-resisting frame (SMRF) as a dual system. They analyzed three and six story frames and found that the ductility demand on the braces was not significantly reduced but the story drift and residual displacement were.

System level tests on a four-story scaled frame were done using BRBs with an unconventional brace connection which limits moments developed at beam-column joints. After tests of a design basis earthquake and maximum considered earthquake, no limit states other than yielding of the braces were found. The research concludes that properly detailed BRB frames can withstand

even the largest earthquakes (Fahnestock et al. 2006). Additional work on BRB detailing included research looking at the connection of the braces to the frame. The conclusions state that reduced stiffness of the gusset plate connection allowed the BRB to deform as designed and saved the frame from damaging deformations. The authors recommended that the bolted connections be slip critical at yield and bearing at ultimate strength of the core plate including strain hardening. The overall performance of the system with the connections detailed as recommended was excellent with large hysteretic energy loss (Roeder et al. 2006).

Scaled experimental tests of BRB frames with non-moment resisting connections were tested at Lehigh University during a comprehensive experimental and analytical project (Fahnestock et al. 2007a; Fahnestock et al. 2007b). The test results demonstrated that undesired failures due to cracks in the gusset plates and beam-column connections could be avoided with an appropriately detailed connection. The authors also stated that the testing demonstrated the viability of increasing the response modification factor, R, for a BRB frame with non-moment resisting connections. The response modification factor is a multiplier to account for the amount of reliable ductility in a structural system. A more ductile system can be designed for lower strength since the ductility of the system allows for energy dissipation through yielding. The current R value for a BRB system with non-moment resisting connections is 7. The recommendation is that it be made the same as a BRB and special moment frame dual system which has an R value of 8. The problem of BRB systems experiencing large residual drifts and causing problems for post-earthquake building occupation was highlighted, in addition to several recommendations for re-evaluation of current code provisions.

As can be seen from this sample of research, the opportunities for seismic protection by BRB systems are promising. Multiple brace configurations have been tested and have performed well. Several of these configurations are shown in Figure 2-17. The key elements include properly detailing the yielding core section, the buckling stiffness of the restraining member and the end connections to confine the plastic damage to the brace itself.

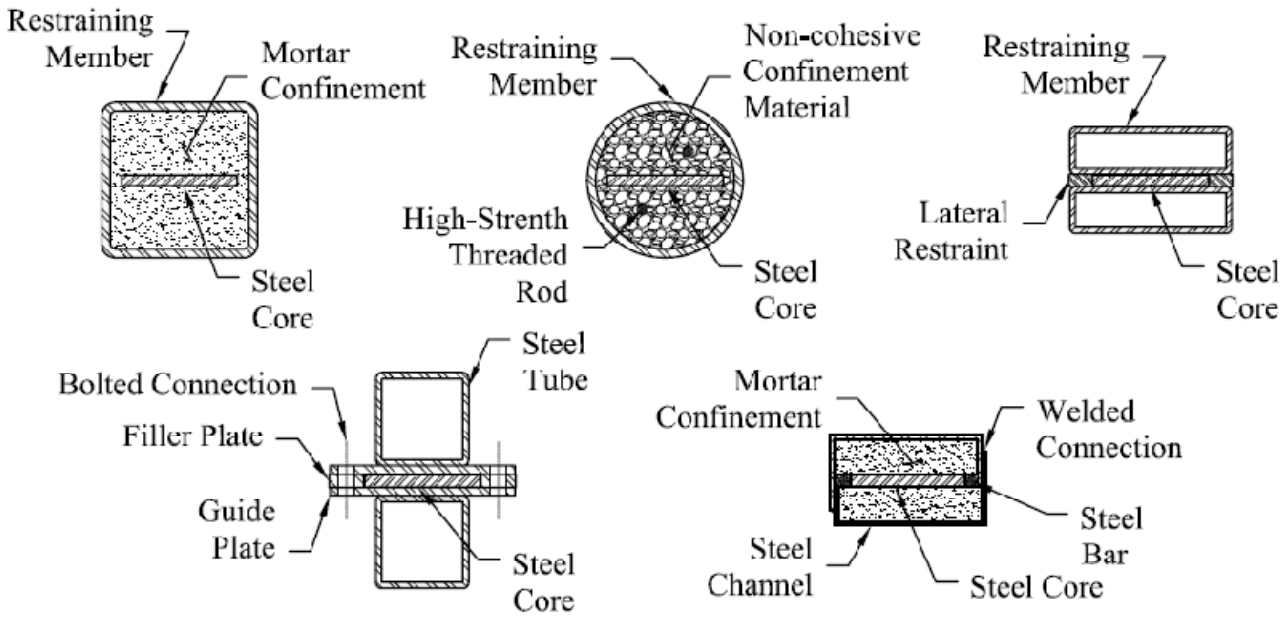

Figure 2 - 17 Various BRB Systems

2.3.2.1.4. Miscellaneous Metallic Devices

Because of the many possible configurations for metallic yielding dampers, numerous devices or systems using plastic deformation of metals have been developed and studied. A metallic yielding device for wood-frame structures was tested by Higgins (2001). This device is a simple diagonal bar with a unique anchorage. The anchorage slips in compression but grips instantly in tension. The unique anchorage produces a larger yield surface due to the catching at different locations along the bar. The testing of the device showed it to be as effective as an ADAS device at a lower cost for material and installation.

The multiple-direction damper is a short alloy column bonded to two steel plates. It is installed in structures between the bottom of a beam and the top of chevron bracing. The alloy chosen has a low yield point, high ductility and stable hysteresis. The device performed very well under 20 earthquake records (Tsai et al. 2002). Other work by Tsai and co-workers (2003b) includes the highly plastic material damper (HPMD) which is illustrated in Figure 2-18. The HPMD performs as a combination of rate-dependent and rate-independent devices. The principle is to extrude a highly plastic material which produces a highly nonlinear hysteresis. The device provides reliable resistance to wind and seismic loads with a combination of initial stiffness and energy dissipation.

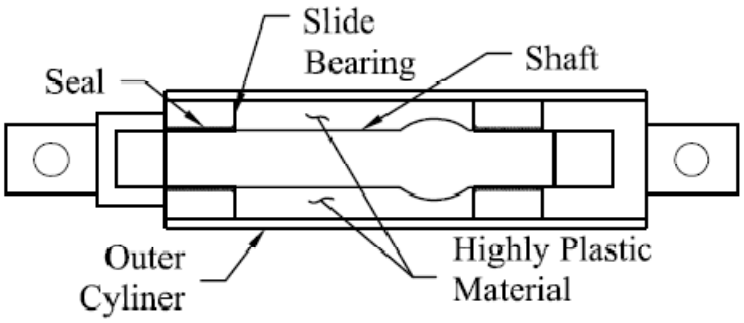

Figure 2 - 18 Highly Plastic Material Damper Schematic [after (Tsai et al. 2003b)]

The tube inversion device, sketched in Figure 2-19, is another way to use yielding to promote damping. This device operates by inverting a thin tube. Significant plastic deformation dissipates energy during inversion. Although regularly used for attenuation of shock in industrial applications, use in civil structures has been limited by buckling issues. A method of connection, as well as a restraining outer tube is employed to counteract buckling (Monir 2004).

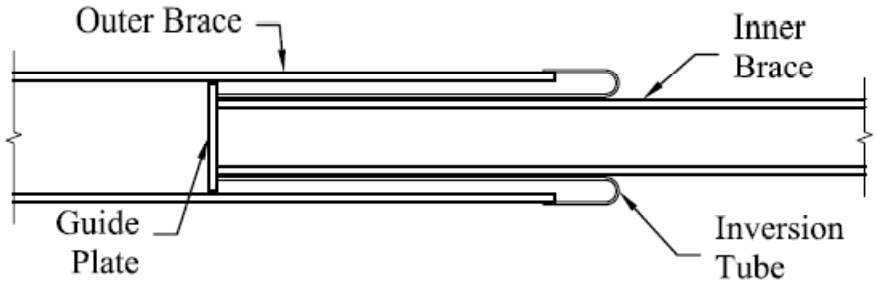

Figure 2 - 19 Inversion Tube Device Diagram [after (Monir 2004)]

The accordion metallic damper (AMD), shown in Figure 2-20, is another yielding device which has proved to be effective in dissipating energy. The resulting hysteresis loops are robust and of a similar shape to those of the ADAS or TPEA devices. During testing, the AMD tolerated 70 cycles at 7 cm (2.75 in) of deflection (Motamedi and Nateghi-A. 2006).

The dual function metallic damper (DFMD) is a damper that dissipates energy by yielding under in-plane loads. It is installed in a similar fashion to ADAS devices with the face of the plate parallel to the framing. Multiple shapes were tested, with the double X-shaped and single round-hole shapes performing the best (Li and Li 2006). DFMD plate shapes are drawn in Figure 2-21. A similar method using an HP section as a shear yielding element has been proposed as the efficient energy dissipating steel-brace frame (EEDBF). The device is implemented in a similar fashion to a TPEA or ADAS device with chevron bracing. The difference is that the energy

dissipation is through shear yielding. The HP section is used because the thickness of the web is larger providing a greater volume of material to be yielded resulting in greater energy dissipation. The proposed system is anticipated to confine the damage to the yielding element which could be replaced after a damaging seismic event. The analytical comparison of the EEDBF to moment resisting frames and concentrically braced frames showed that the EEDBF exhibited less damage and had greater capacity for lateral deformations (Dicleli and Mehta 2007a).

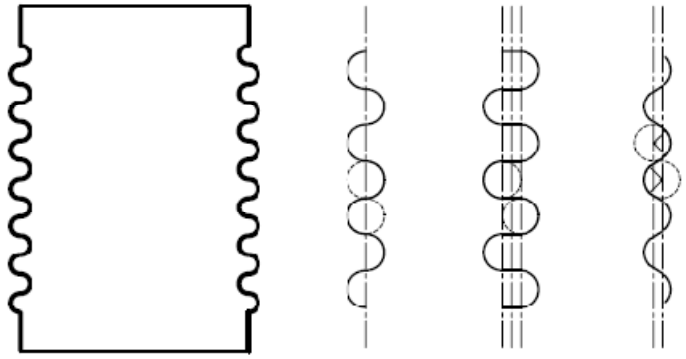

Figure 2 - 20 Accordion Damper [after (Motamedi and Nateghi-A. 2006)]

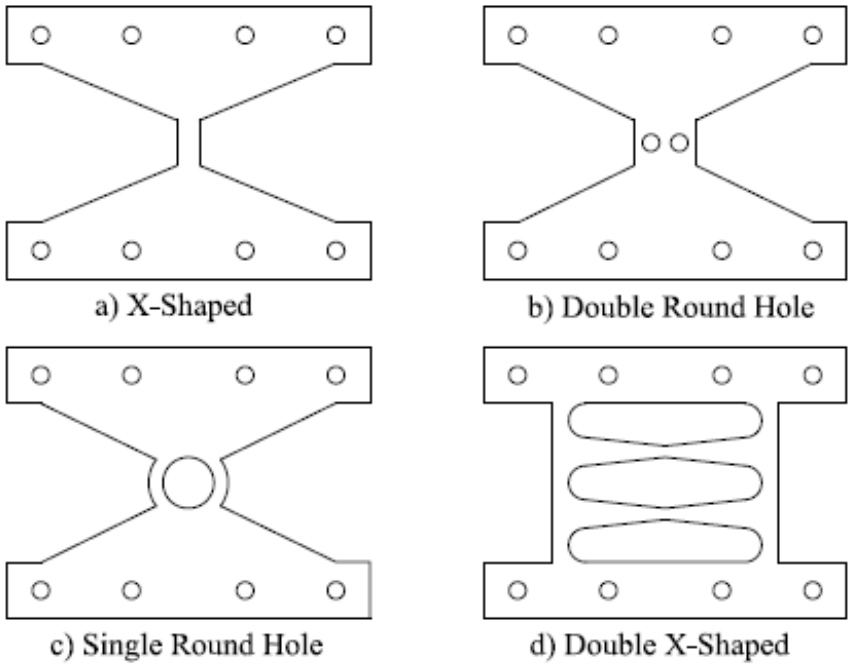

Figure 2 - 21 Dual Function Metallic Damper (DFMD) [after (Dicleli and Mehta 2007a)]

Recent work on an older concept is the J-damper. The dissipation of energy is through flexure of a curved plate. Kato et al. (2005) showed that the J-damper is effective in absorbing seismic energy in experimental and analytical tests.

Due to significant damage to fully welded moment connections in the 1994 Northridge and 1995 Kobe earthquakes, considerable effort has been put into better detailing for moment connections. This has included weld provisions as well as using bolted connections where possible. Due to this influence, work has been done on developing a mechanical joint which includes a hysteretic damping element, and is weld-free. A sketch of the weld-free system is shown in Figure 2-22. The development of this system required a new high strength bolt. The new bolt was required to reduce the number of bolts required for the connection. The only direct connection is between the top flange of the beam and the column. This point becomes the rotation point of the connection. The hysteretic element is a small buckling-restrained brace. The core of the brace is a flat plate and the restraining member is a tee-section. In experimental testing, stable hysteresis loops, considerably larger than for conventional steel moment resisting frames, were observed (Inoue et al. 2006; Suita et al. 2004).

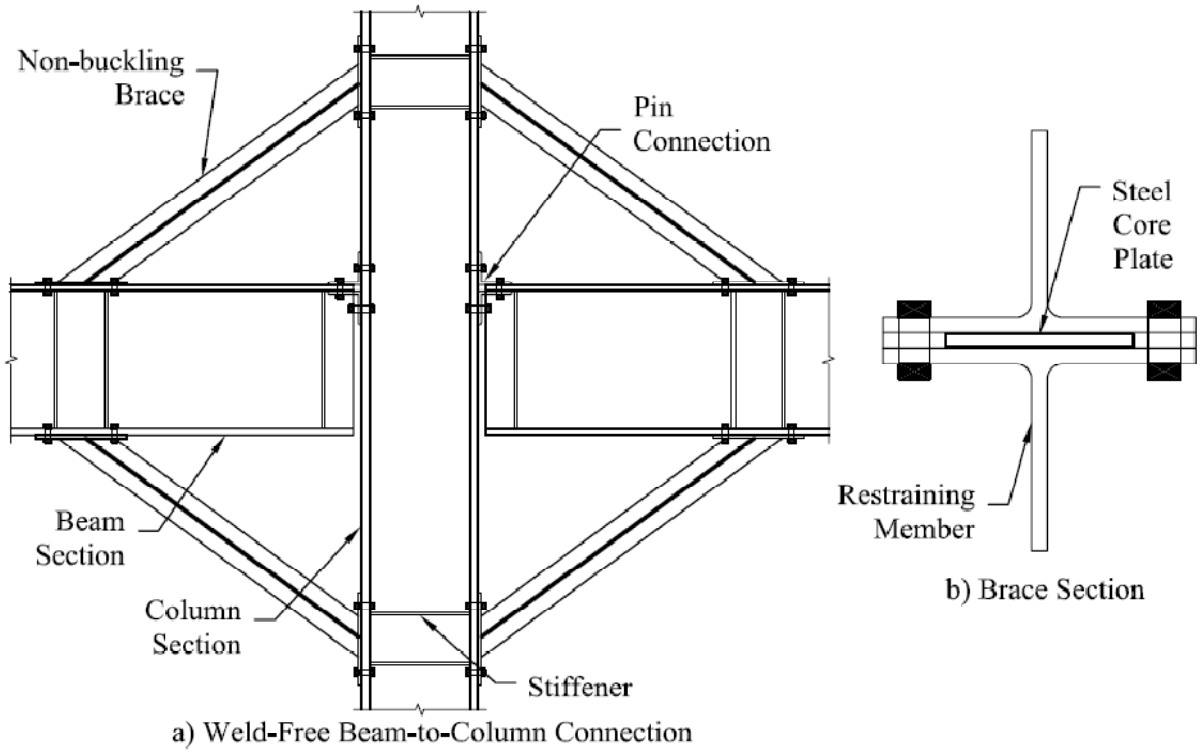

Figure 2 - 22 Weld-Free Beam-Column Connection [after (Inoue et al. 2006)]

As an add-on to the weld-free system, a hysteretic energy dissipating connection for the weak direction of columns was developed. Pi dampers, named because the shape resembles the Greek capital letter, are provided at the bottom flange connection. The shape of these cast steel connectors allows for yielding when the beam section rotates about the top flange connection. Experimental results demonstrate Pi dampers' ability to dissipate energy while the beam and column remain essentially elastic. The configuration with two pi dampers on the bottom flange, shown in Figure 2-23, is most effective according to Koetaka et al. (2005).

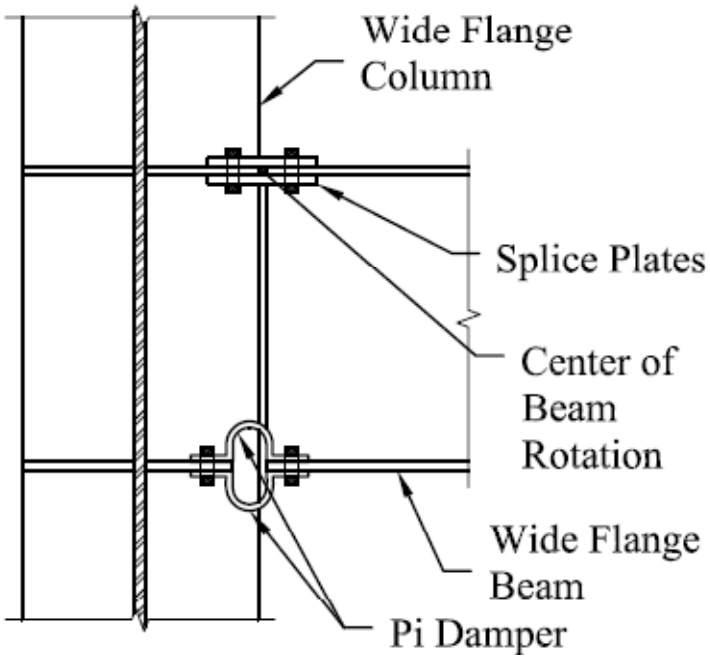

Figure 2 - 23 Pi Damper Connection [after (Koetaka et al. 2005)]

In addition to varying configurations of yielding devices, work has been done investigating other metals for energy dissipation applications. Aluminum alloys have already been used for structural retrofit of shear links in braced frames. The material properties including strength-to-weight ratio, wide range of available yield stress, significant strain hardening, ductility and ease of manufacture make aluminum a good selection for energy dissipation mechanisms (Di Sarno and Elnashai 2003). Recent work on pure aluminum shear panels (PASP) combined with a steel framing systems is an example of this. Two configurations of the shear panel, the full-bay and pillar type, were numerically analyzed. Preliminary experimental work has also been completed, showing large deformation capability. Some pinching of the hysteresis during testing demonstrates the need for future work (De Matteis et al. 2007).

Stainless steels (SS), metals containing a high percentage of chromium, have been investigated for use in energy dissipation. Of several types of SS, the austenitic-ferritic or duplex grade structural steel (AFSS) has been most successfully used in structures. One beneficial property of AFSS is a higher ultimate-to-yield stress ratio which produces larger yield surfaces. It also has a high value of elongation-to-fracture ratio and excellent post-buckling behavior (Di Sarno and Elnashai 2003).

From this review, we can see that metallic yielding devices are only limited by the imagination of the engineer and materials scientist. Various metals and geometric configurations that take advantage of the material properties, shape and loading condition can be effective energy dissipation elements.

2.3.2.1.5. Shape Memory Alloy (SMA) Devices

SMAs are special metal alloys which can deform up to large strain levels (up to 10%) with no residual deformation. This superelastic ability of SMA is due to a solid-to-solid phase change within the material. An austenite to martensite phase change can be initiated by either stress or temperature. The hysteresis comes from the unstable phase, martensite, changing to austenite at low stress levels (Di Sarno and Elnashai 2003). In some cases recovery from large strains comes from adding heat, also known as the shape memory effect (DesRoches and Smith 2004). Over the last 10 – 15 years, research on the behavior of SMAs and a reduction in cost has made them more attractive for civil structures. The qualities beneficial to seismic protection systems include energy dissipation, superelastic deformation, low-cycle fatigue resistance and re-centering capabilities. Various applications of SMAs include beam-column connections, diagonal braces, and as an element of an isolation system. SMAs are available in various alloys including copper, aluminum, nickel, titanium and zinc. The most commonly used alloy for seismic applications is nickel-titanium, NiTi, also called Nitinol. It is preferred because of the combination of physical properties and relative low cost (DesRoches and Smith 2004; Wilson and Wesolowsky 2005).

The following review cites research on SMAs used in seismic protection systems, but is only a sample of the body of work. State-of-the-art papers (DesRoches and Smith 2004; Wilson and Wesolowsky 2005) give more information about previous applications and a technically rigorous explanation of the mechanics of SMAs. Idealized hysteresis loops of the various states of SMAs are shown in Figure 2-24.

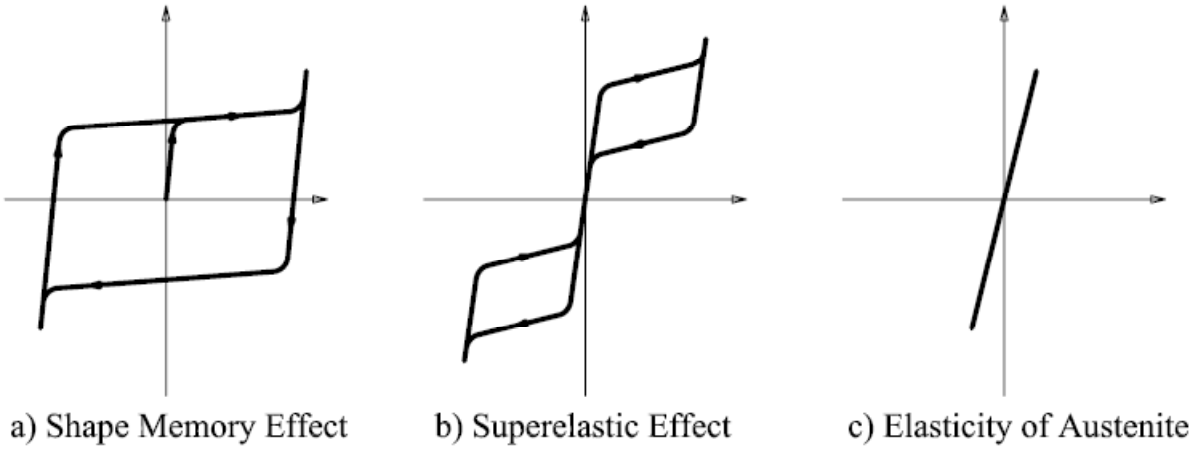

Figure 2 - 24 Hysteresis of SMA in Different States

As part of the MANSIDE (Memory Alloys for New Seismic Isolated Devices) project (Dolce et al. 2001), a prototype SMA isolation device was developed. The NiTi device provides high initial stiffness under low strains and flexibility during a large seismic event. A critical feature for this application is the re-centering capability. Full-scale devices were implemented and tested in a building, demonstrating the feasibility of the system. An innovative beam-column connection, shown if Figure 2-25, using Nitinol tendons as the tension and compression flanges was tested under cyclic loading. The results demonstrate stable and repeatable hysteresis for rotations up to 4% story drift. Following testing, the tendons were heated to recover most of the residual deformation. A second set of tests showed nearly identical results (Leon et al. 2001).

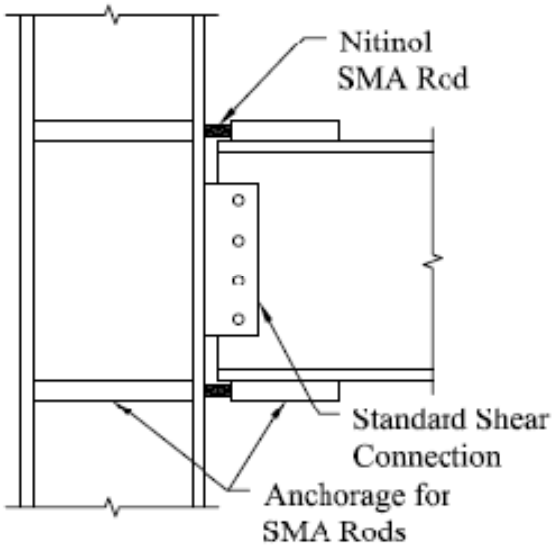

Figure 2 - 25 Beam-Column Connection with SMA Rods [after (Leon et al. 2001)]

An SMA brace was developed for a reinforced concrete (RC) building using austenite wires (Dolce et al. 2005). One set of wires was configured for energy dissipation. The other set was configured to provide a re-centering force. The performance of the SMA device was compared to a metallic yielding device. Due to a greater stiffness, the structure with the SMA device had a lower period and produced greater inelastic behavior in the frame. This disadvantage was somewhat offset by the re-centering behavior which recovered the frame to a near undeformed condition (Cardone et al. 2004). As a continuation, tests were done to compare an RC frame in a bare condition, with masonry infill and with either the metallic yielding or SMA device. The shaking table tests showed the braces' ability to resist seismic loads. The authors point out that to fully exploit the re-centering capabilities of the Nitinol wires, the design philosophy must be modified to allow inelastic deformation in the structural frame because of the re-centering behavior of the braces.

Reusable hysteretic damping braces (RHDB) were compared to a traditional BRB using analytical testing (Zhang and Erdman 2001). The RHDB uses NiTi wires for self-centering and dissipation properties. The dissipation property comes from non-pretensioned wires and the centering behavior comes from pretensioned wires. The analytical testing showed that the BRB frame had greater energy dissipation but significantly higher residual drift. The SMA structure experienced higher peak drifts due to lower damping but had less residual displacement due to re-centering. The pinching of the hysteresis loops is a shortcoming of the RHDB due to the self-centering behavior. The authors state that future work needs to investigate this trade-off. The issue of re-centering at the expense of damping was discussed in research on using superelastic SMA for seismic vibration control (McCormick et al. 2006). The results of the study showed that large-diameter bars as well as wires are applicable for vibration reduction provided methods to increase damping can be found.

Large-diameter superelastic Nitinol braces were employed as a brace for steel structures (Auricchio et al. 2006). The results showed the potential of the braces with the ability to reduce inter-story drift. Testing also highlighted potential problems, one being large forces in the SMA brace causing yielding in beams, columns and connections. In addition to their function as braces and isolation devices for buildings, SMAs are being investigated for use as tie-rods in masonry arches and vaults for in-service and seismic loadings (Dolce and Cardone 2006). This application is still under investigation and requires further research for full development.

SMAs are a unique material with beneficial properties for seismic protection. As is evidenced by the large amount of recent research, this is an actively developing area. With further studies and future inventive configurations and combinations, shape memory alloys will likely continue to grow in their applications for seismic protection of civil structures.

2.3.2.2. Friction Dampers

Friction devices rely on the same system as automobile brakes to dissipate energy. They are similar to metallic yielding devices in that they add only stiffness to the structure until the forces in the dampers reach the slip level. Upon slipping, they begin to dissipate energy through heat. A critical aspect to frictional dampers is the ability of the friction surface to maintain a constant frictional coefficient. When this occurs, the hysteresis loops are rectangular and stable. Friction is also a mechanism used in certain types of base-isolation systems as well as a connection between panels in precast or tilt-up concrete structures. This review will be specific to applications of friction dampers to frame systems.

Work in friction damped frames began in the early 1980s with the work of Pall and Marsh (1982). The proposed device for use in the middle of cross-bracing was shown through analytical means to effectively dissipate energy without damaging the structural frame (Aiken et al. 1988). A schematic of this device is shown in Figure 2-26. This friction damping system was later tested experimentally in a scaled nine-story structure. The results verified the benefit of the devices in providing significant energy dissipating capacity to the structure. The continued development and use of this type of device can be seen by the large number of projects and publications listed on the website of Pall Dynamics Limited in Montreal, Canada[1].

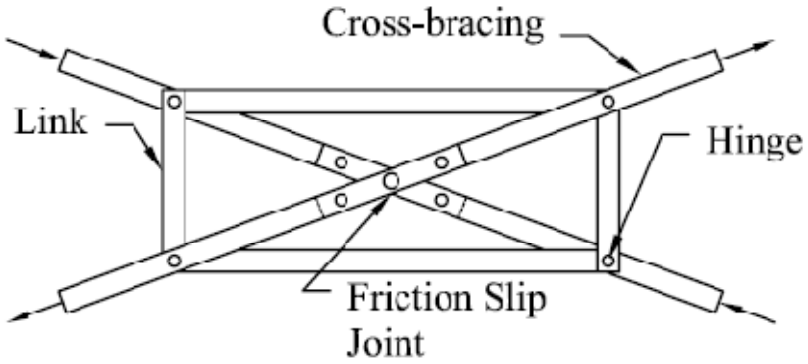

Figure 2 - 26 Friction Device for Frames

[1] www.palldynamics.com

The Sumitomo friction device is a cylindrical device with friction pads that slide on the inner steel surface (Aiken et al. 1993). It was developed by Sumitomo Metal Industries, Ltd., Japan. The device was tested on the same nine-story frame as the Pall device and demonstrated a reduction in structural response. The friction spring seismic damper is similar to the Sumitomo device (Filiatrault et al. 2000). The device consists of outer and inner rings with a tapered mating surface and friction springs. One beneficial property is a strongly self-centering behavior. The combination of damping and self-centering produce flag-shaped hysteresis loops. The experimental testing showed repeatable, stable and symmetric hysteresis loops which were nearly identical for all frequencies and independent of the earthquake records used. A sketch of the friction spring seismic damper is shown in Figure 2-27. The mechanical nature, required manufacturing precision and unique materials in these devices increase the cost.

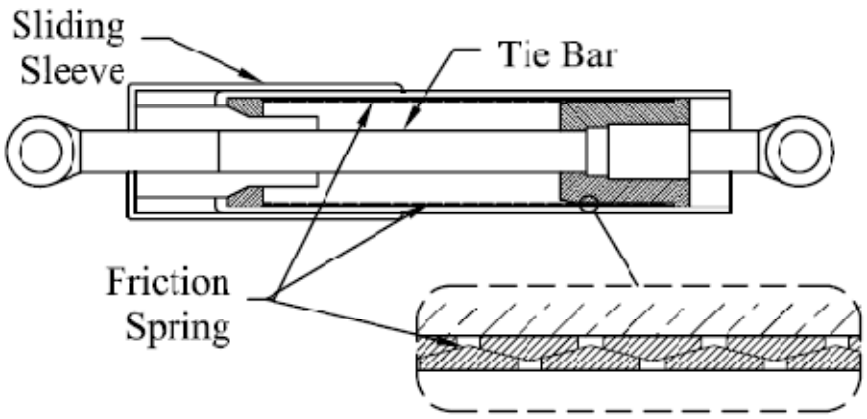

Figure 2 - 27 Friction-Spring Seismic Damper Schematic [after (Filiatrault et al. 2000)]

An inexpensive and simple device using friction is the slotted bolted connection (SBC) (Grigorian et al. 1993). A typical SBC is diagrammed in Figure 2-28. These connections are a modification to standard bolted connections. Slotted bolt holes are provided in the center plate, allowing it to slide relative to the outer plates. The compression force applied by the bolts and the coefficient of friction between the surfaces dissipates energy through heat. In connections where brass plates were inserted as slip surfaces against the mill scale steel, the friction forces were more reliable than steel on steel. Although not the earliest, this research on SBCs demonstrates the potential and simplicity of the concept. The key element is finding materials to achieve reliable and stable hysteresis. Recent work connects an SBC between chevron bracing and the bottom of a girder (Law et al. 2006). The numerical studies find significant response reduction for multiple stiffness and threshold slip levels.

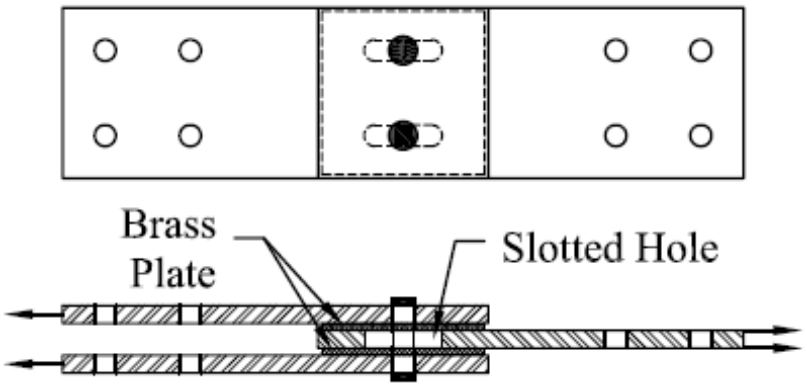

Figure 2 - 28 Typical Slotted Bolted Connection (SBC)

An innovative post-tensioned moment connection for steel frames integrating a friction damper has been developed in work by Rojas, Ricles and Sause (2005) and is illustrated in Figure 2-29. The post-tensioned friction damped connection (PFDC) uses high-strength tendons to apply a re-centering force and uses an SBC type friction damper at the top and bottom flanges to dissipate energy. The analytical model of the structure with the PFDC connections suggests that the performance is better than that of a fully welded special moment frame.

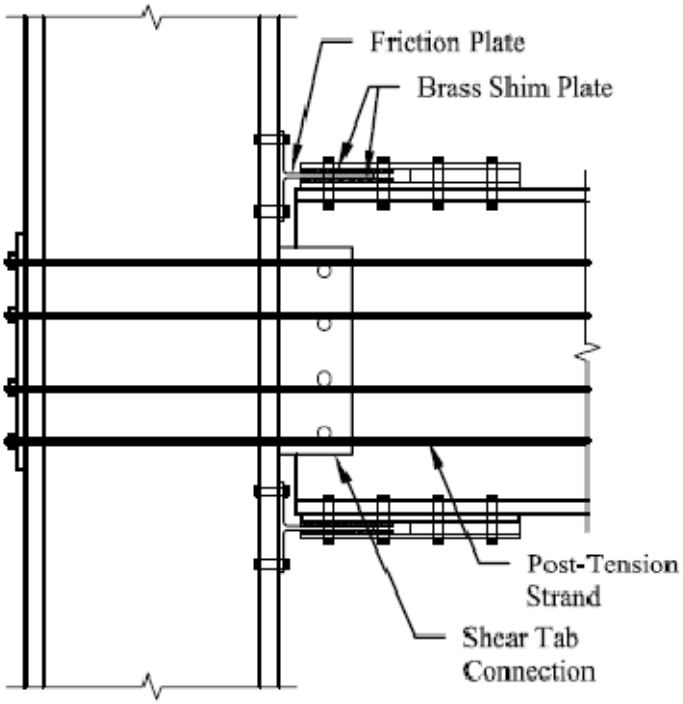

Figure 2 - 29 Post-tensioned Friction Damped Connection [after (Rojas et al. 2005)]

Recently, several new energy dissipation strategies have been developed which additionally add a self-centering feature to reduce residual displacements. A post-tensioned beam-column connection with a bolted web friction device was developed, analyzed and tested. The analysis was able to predict the experimental results. The results demonstrated consistent and repeatable hysteresis through large deformations. The drawbacks include beam buckling due to large post tension forces above 5% drift and possible interference with the friction device by the floor slab (Tsai et al. 2008). Another similar system, called the self-centering friction connection (SCFR), using post-tensioning and frictional dampers was developed and tested (Kim and Christopoulos 2008). The frictional dampers are located at the top and bottom flanges of the beam-column connection. The difference is that this friction device incorporates non-asbestos organic brake lining pads against stainless steel for energy dissipation. The results of the tests demonstrated stable energy dissipation and no residual drift within the limits of the self-centering system. The behavior was good even beyond the self-centering limits, although specific detailing is required to avoid buckling of the beams.

In addition to beam-column connections, self-centering friction damped braces have been investigated. The self-centering energy dissipative (SCED) device has been developed and tested analytically and experimentally (Christopoulos et al. 2008; Tremblay et al. 2008). The authors state that any type of energy dissipation device could be used in the brace, but the testing was done both quasi-statically and dynamically using a friction device. The SCED is a bracing member that can be used as any other brace. It consists of two bracing members, a tensioning system, an energy dissipation device and a series of guide blocks. After initial testing a structural fuse was included in series with the brace to prevent failure of the tension tendons. The results of the testing proved it to be a very attractive alternative to a BRB system with reduced story drifts and residual deformations. Another friction damping brace, the self-centering friction damping brace (SFDB), was developed for use in concentrically braced frame structures (Zhu and Zhang 2008). The SFDB consists of two blocks tied together using Nitinol shape memory alloy strands. The energy dissipation comes from friction between the surfaces of the blocks. The contact surfaces are carefully designed in conjunction with the clamping force due to the strands to produce a good hysteresis. The results of the response history analysis demonstrate comparable behavior to a BRB system with reduced residual story drifts. A slotted-bolted connection was

also included after initial analysis to prevent extreme axial forces due to the large strain capacity of the Nitinol strands.

In addition to being used in frames, a rotational friction damper consisting of two rigid plates and a frictional hinge has been used as the damping element of a base isolation system (Nielsen et al. 2004). For the application tested, the friction damping has been combined with a viscoelastic system. The friction device itself is simple to manufacture and due to the special friction pad at the joint the test results indicate stable performance over many cycles. A passive friction damper was planned for use in a three-story podium structure connected to a twelve-story structure (Ng and Xu 2006). The passive damper uses a slide plate clamped between two friction plates. To control the clamping force, an adjustable spring with a load cell provides the desired friction condition. Tests of the damper for the connection of the two buildings showed an enhanced performance under earthquake load. Another frictional damper with a rotational motion has been studied by Mualla and Belev (2002). The device includes two horizontal plates sandwiching one vertical plate with circular friction pads at the joint. The vertical device is connected to the beam with chevron-type braces connecting each end of the horizontal plates. All the connections of the bracing and devices are hinges. The two long braces are pre-tensioned to avoid compressive buckling. The device was analyzed in a one-bay frame and found to have excellent performance as well as being economical to build and install (Mualla and Belev 2002). Later tests of the same device on a shaking table in a three-story steel frame demonstrated the remarkable efficiency of the system (Liao et al. 2004). Figure 2-28 shows examples of rotational friction devices.

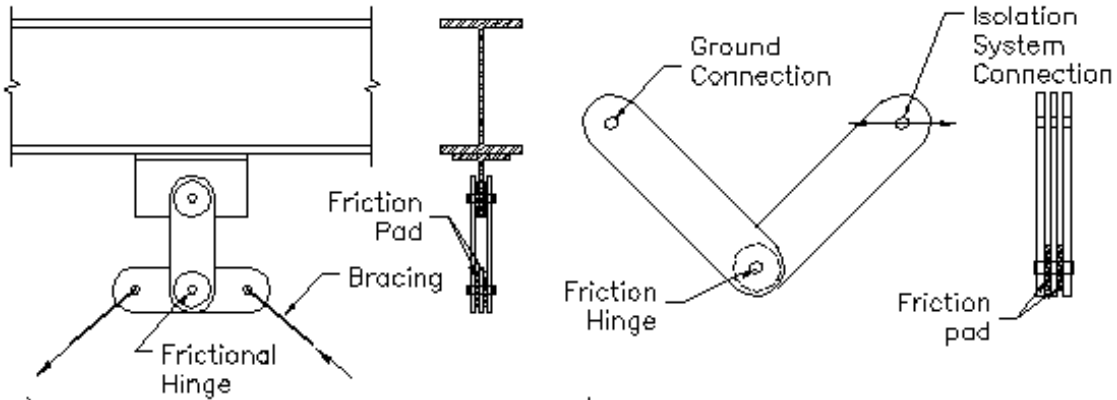

a) Rotational Friction Device in Chevron Bracing [after (Mualla and Belev 2002)]

b) Rotational Friction Device for Base Isolation System [after (Nielsen et al. 2004)]

Figure 2 - 30 Rotational Friction Damping Devices

The pseudo-viscous frictional energy dissipater (PVEDOR) is similar in many fashions to the Pall friction damper while making modifications to make the behavior more like viscous damping. Convex surfaces on the friction planes cause the maximum force in the damper to be out of phase with the displacement of the structure. This phase difference causes the damper to act in a pseudo-viscous manner which can reduce the design forces of the structure over a typical friction damper. In the undeformed condition the two convexities are aligned, which produces the greatest tensile force in the bolt and hence the greatest clamping force. As the slide plate moves, the clamping force is reduced. This produces a condition where the greatest force in the damper occurs when the displacement is zero. However, the hysteresis loops are not rectangular because the damping reduces as the clamping force is reduced. The shape of the hysteresis loop is roughly the shape of a viscous fluid damper with pointed ends. Component experimental testing and numerical structure modeling was done to evaluate the PVEDOR. Tests indicate that the device possesses the hysteretic features of viscous dampers. Some improvements are recommended to reduce local stresses (Wu and Ou 2003).

A unique application of friction damping using permanent magnets to reduce structural response in timber structures was investigated analytically (Patel 2005). The magnet provides the clamping force and the friction comes from the surfaces sliding. The device would be implemented as part of a timber shear wall. One wall would have a thin steel sheet attached to the face and be attached to the base of the structure. The second wall would have the magnet attached and would be attached to the top of the story. Energy dissipation would occur upon story drift. The analytical results reported that the magnetic friction damper was dissipating 60% to 80% of the energy and protecting the structure from damage. The structures also experienced reduction in base shear and displacement.

From this sample of research on friction dampers, it is apparent that these devices can be effective in many configurations. They can be very simple or very complex to construct. Friction devices can survive severe seismic events and require no repair or replacement. They are also independent of the frequency and velocity across the device. The key elements are the materials for the friction surface and the clamping force being able to apply a stable and repeatable hysteresis over time. Improper choice of materials can lead to the surfaces becoming pitted or sticking together, which would degrade the designed performance of the device. The clamping

force is also critical, since the damping is proportional to the force and loosening could decrease the energy dissipation.

2.3.3. Rate-Dependent Dampers

Rate-dependent dampers' performance depends on the velocity across the device or in some cases both velocity and displacement. Common devices in this class are viscous fluid dampers (VFD) and viscoelastic (VE) solid dampers. Idealized hysteresis loops are shown in Figure 2-31.

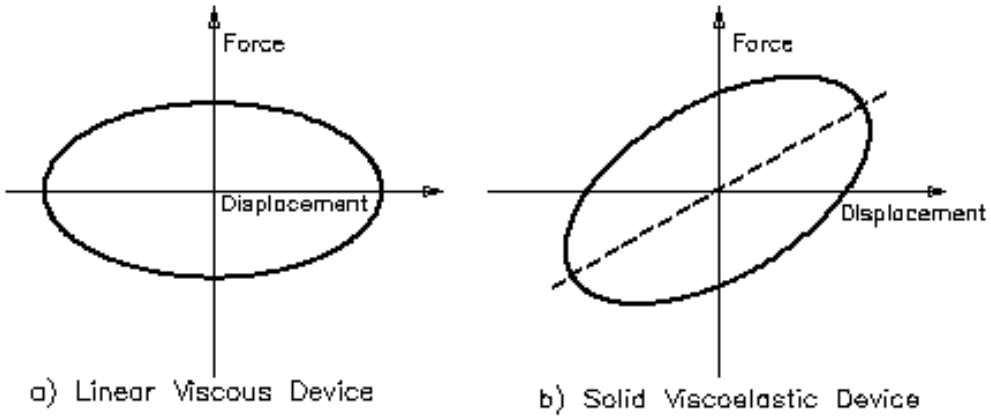

Figure 2 - 31 Idealized Rate-Dependent Hysteresis Loops

2.3.3.1. Viscous Fluid Dampers (VFD)

Viscous fluid dampers dissipate energy through deformation of viscous fluids. This is accomplished primarily in two ways. The first is a piston-type device with orifices in the face of the piston. As the piston head moves through the fluid inside the sealed cylinder, the deformations of the fluid dissipate energy. The configuration of the openings in the piston determines whether the device will be linear or nonlinear. Viscous walls are the other type of fluid damper. In this configuration a wall slides in a fluid filled chamber and causes damping through the deformation of the fluid. These devices typically add little or no stiffness to the structure at low frequency levels (below 4 Hz) and do not modify the fundamental modes of the structure. A true viscous damper does not add significant additional base shear to the structure while it remains elastic because the force in the damper is out of phase with the structure. The phase difference means that the maximum damping force occurs at maximum velocity, not at maximum displacement when the elastic base shear is at a maximum. The damping properties of VFDs are typically dependent upon the temperature and frequency as well as the velocity across the device.

Viscous damping walls as a passive control device were a concept of Japanese engineer Mitsuo Miyazaki in the 1980s (Yeung and Pan 1998). An inner wall is attached to the floor above. The outer walls, attached to the floor below, sandwich the inner wall and are filled with a viscous fluid as shown in Figure 2-32. When the structure experiences inter-story drift, the inner wall moves through the fluid and damps vibrations through the fluid deformation (Yeung and Pan 1998). Numerical simulations of a 20-story benchmark building with damping walls further illustrate a reduced response (Fukukita et al. 2002).

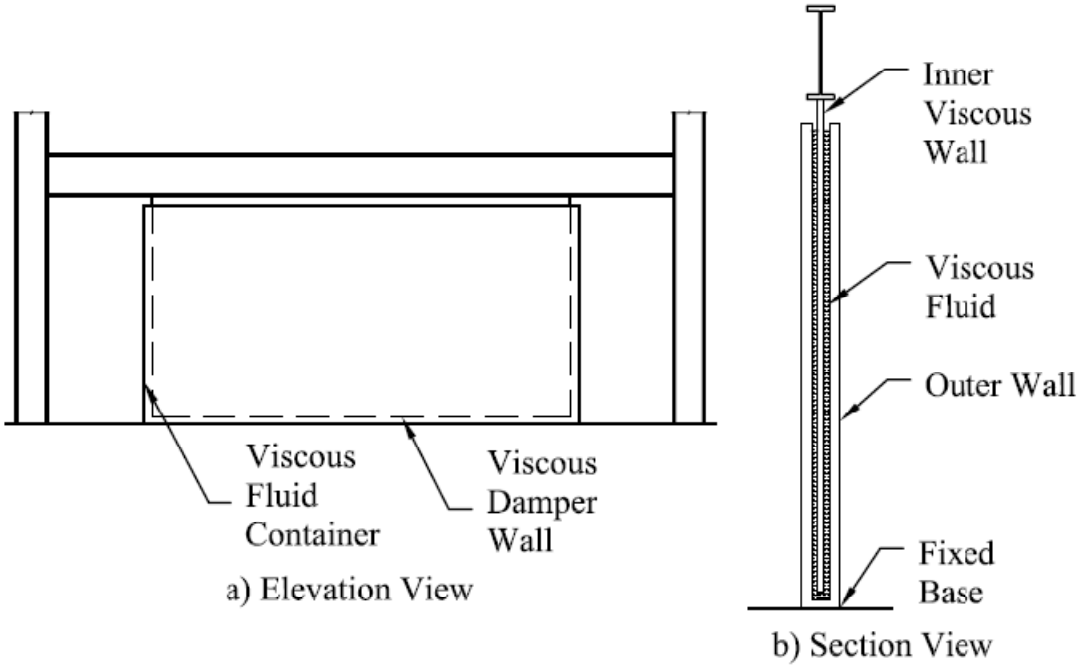

Figure 2 - 32 Viscous Damping Wall

VFDs have been used for many years in aerospace and military applications for shock attenuation and vibration isolation. In the early 1990s significant research began to study implementation of these devices in civil structures for earthquake protection. See Figure 2-33 for a schematic of a VFD. A combined experimental and analytical study using linear VFDs to absorb earthquake energy was undertaken by Constantinou and Symans (1993). The conclusions of the study report 30% to 70% reductions in story drifts, which are comparable to other types of dissipation systems. However, they also reported reductions in story shear which are not seen in other types of dissipation devices. Viscous dampers can also be designed to be either linera or nonlinear. A linear damper, meaning the force in the damper is proportional to the velocity,

produces an elliptical hysteresis loop. A nonlinear VFD with an exponent of 0.3 produces a nearly rectangular hysteresis loop.

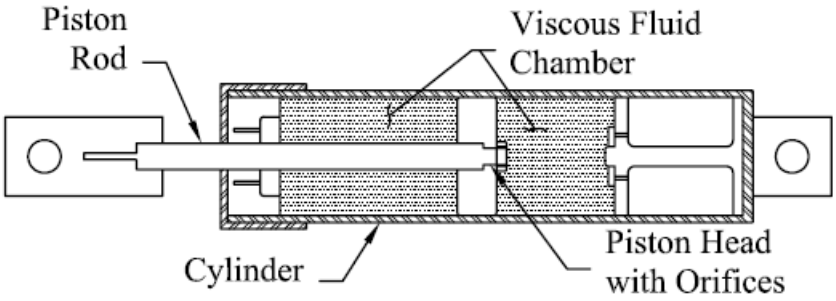

Figure 2 - 33 Schematic Diagram of Viscous Fluid Damper

A simple form of the damping law is (Lee and Taylor 2001):

$$F = C * Sign(V) * |V|^{N} \qquad \textbf{Equation 2 - 2}$$

In the above equation, F is the force in the damper, C is a damping constant specific to the device, V is the velocity across the device and N is an exponent that ranges from 0.3 to 1.95. The sign function represents the Signum function and returns the sign of the velocity. Structural dampers typically use values of N between 0.3 and 1.0. Lower exponent values are preferred in earthquake applications since the maximum force is limited by the reduced exponent. An analytical study of a four-story frame using both metallic yielding and viscous dampers was done to compare the responses. The results concluded that in most cases, viscous dampers were somewhat more effective. It was also noted that metallic dampers are suited for applications where large amounts of seismic energy must be absorbed. Vilcheck and Pong (2001) recommend future work in combination systems of viscous and metallic devices for better performance from minor wind events up to extreme earthquakes. Further studies also proved the capabilities of protecting not only the structural frame, both steel and concrete, but providing the benefit of protecting secondary and non-structural elements (Dicleli and Mehta 2007b; Pavlou and Constantinou 2006; Sinha 2004).

Pseudo-dynamic tests were performed on a frame with a pressurized fluid-viscous spring device. The difference between this device and a standard VFD is an initially pressurized condition. Due to the preload on the fluid, a self-centering pressure is exerted by the damper on the structure. The experimental test set-up used a pair of these single acting devices. The pressurized dampers

used in this work only work in compression, although double acting (tension-compression) devices can be manufactured. For both steel and concrete structures the dampers were effective at reducing the seismic response (Molina et al. 2004). Pressurized silicone fluid viscous devices were used in scaled testing on a steel structure and for a full-scale retrofit of a three-story reinforced concrete frame structure. The dampers were used with a chevron brace and installed adjacent and parallel to the floor beam. The studies demonstrated a benefit in reduced interstory drift levels from the application of the pressurized dampers (Sorace and Terenzi 2008).

Viscous dampers have also been used to benefit wood-framed structures. A damper was placed in a diagonal brace inside a sheathed timber shear wall and subjected to multiple near and far-field ground motions. The results verified the benefits of viscous dampers for single and three-story symmetric and asymmetric timber structures through experimental and numerical studies (Symans et al. 2004).

In addition to diagonal or chevron pattern configurations, viscous dampers have been used in unique configurations to amplify their effect on the structure by increasing the displacement and velocity across the device. Figure 2-34 illustrates several configurations of viscous dampers in structural frames. The toggle-brace-damper was studied initially by Constantinou et al. (2001). These configurations use a viscous damper connected to two additional stiff braces at various angles within a single bay. The three configurations provide magnification factors in the range of 2.5 to 3.0. The magnification factor is a measure of the velocity across the device divided by the velocity of the frame. What this means is that for a given relative velocity of the story (velocity of the upper floor relative to the lower floor), the velocity across the device will be magnified and hence the damping will be increased. The effectiveness of the system was proven by a half-scale shaking table test in which substantial increases in the damping ratio were observed. Further shaking table tests with a scaled three-story steel structure found that the toggle-brace system was more effective than a diagonal viscous damper. Careful attention to the swivel connections is required for practical applications (Hwang et al. 2005). Additional work found that the toggle system works well in concrete buildings with lightly reinforced shear walls. The amplification of damping overcomes the reduced story drift to provide sufficient energy dissipation (Hwang et al. 2006). Charney and McNamara (2008) also found that the stiffness of the braces has a significant effect on the effectiveness of the dampers.

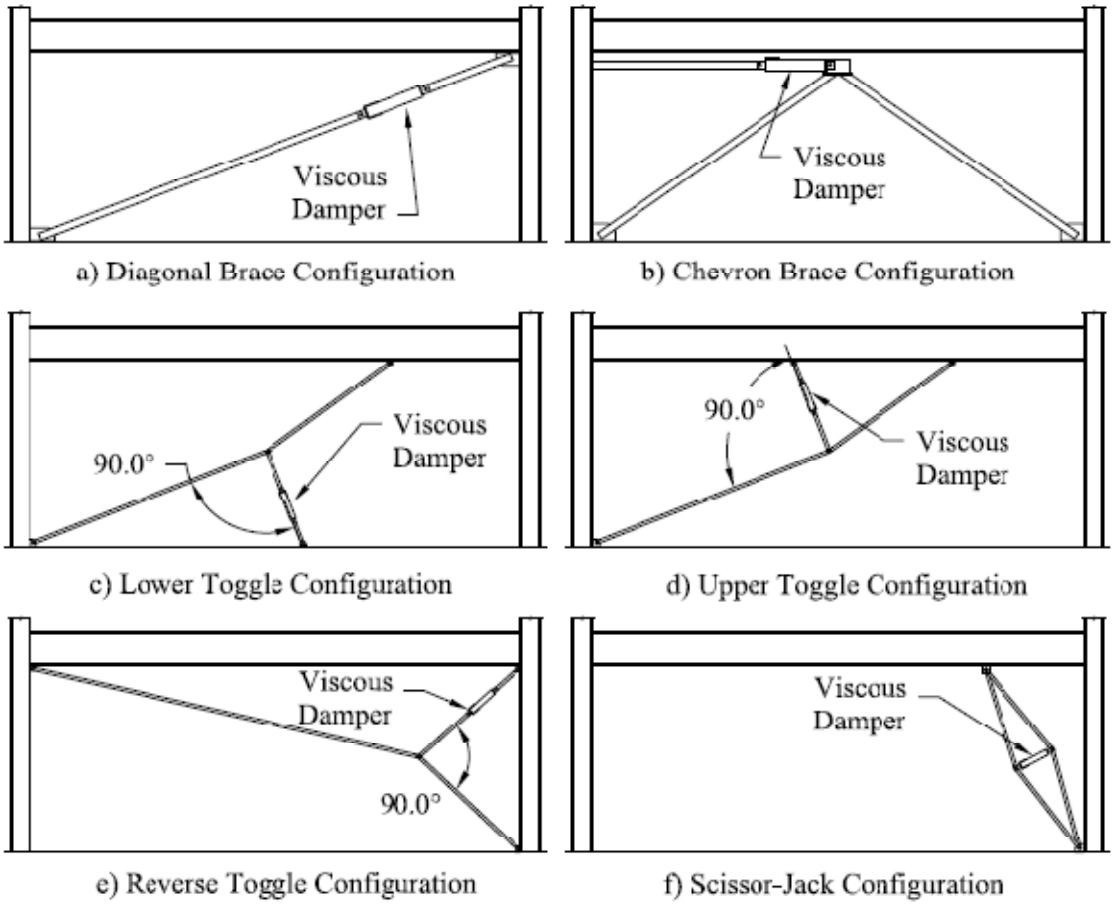

Figure 2 - 34 Various Configurations for Viscous Fluid Dampers

The scissor-jack-damper was developed as a variation of the toggle-brace-damper system. In this system, four hinge-connected stiff braces form a stretched diamond shape. The damper is connected across the short diagonal and the whole system is connected into a structural bay. When the structure deforms, the scissor-jack magnifies the displacement across the viscous damper. The research confirms that this type of system can be applied to structures with high stiffness under seismic loads and minor wind forces (Sigaher and Constantinou 2003). In another example of amplification, a scissor-jack type device is installed through connection to a chevron brace. A numerical analysis of an eight-story structure verified that the damper system is effective (Ribakov and Dancyoier 2006).

From the representative sample of research presented on viscous fluid damping it can be seen that VFDs and viscous damping walls are effective energy dissipating devices. They can be used in a variety of configurations and have multiple parameters that can be controlled to yield

specific hysteretic and force-displacement behavior. For a recent list of actual building applications of fluid viscous dampers, see Symans et al. (2008).

2.3.3.2. Viscoelastic (VE) Solid Dampers

Viscoelastic solid devices are dampers which use VE materials sandwiched between steel plates. Two typical configurations of VE dampers (VED) are shown in Figure 2-35. VE materials dissipate energy when they are deformed in shear. Unlike viscous dampers, VEDs add stiffness to the structure initially, although not to the same degree as metallic yielding devices. Unlike metallic or friction dampers, VE materials dissipate energy for all deformation levels. One problem with viscoelastic dampers is the variation of the properties, sometimes dramatically, with temperature. This effect can cause problems for long events such as a hurricane due to heat build-up. Earthquakes typically do not have a long enough duration for this effect to become a problem for high damping rubber materials, but this could be an issue for other materials like the 3M material ISD-110 which has also been used in building structures (Lee et al. 2004).

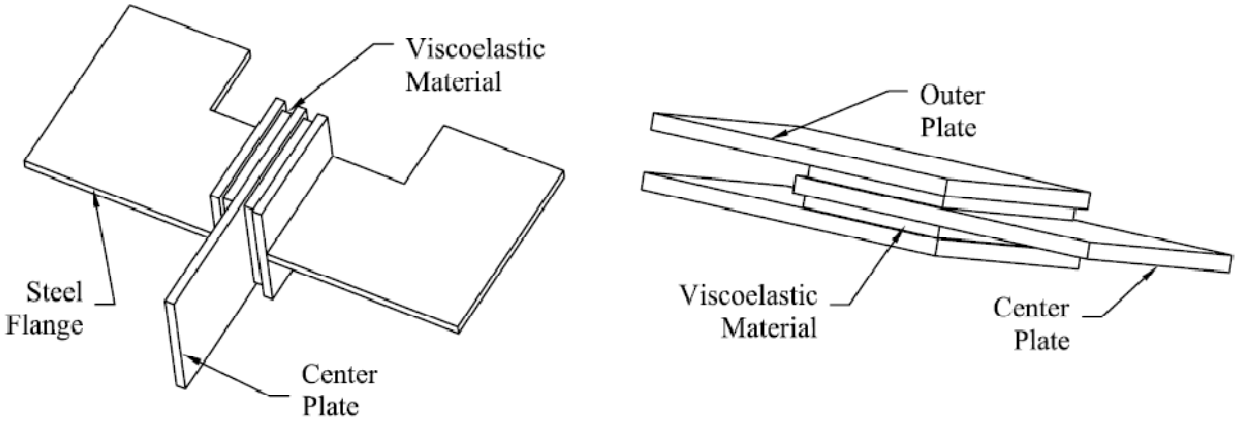

Figure 2 - 35 Typical Configurations for VE Devices

More recently, high-damping natural rubber (HDNR) has been used in these devices, many of which will be cited later. HDNR is composed of natural rubber (isoprene) filled with carbon-black during the vulcanization process. These dampers show less dependence on both temperature and frequency and have high energy dissipation capabilities. Additionally, the force-deformation relationship of these materials experiences a hyperelastic effect as the strain increases above 200%. An additional benefit is the ability to reach strains of up to 500% or more without failure, depending upon the rubber compound and amount of filler.

Performance under small deformation of VEDs paved the way for installation in four tall buildings in the United States prior to 1999 and multiple buildings in Japan (Kareem et al. 1999). VE dampers were also used to reduce vibration under wind loading for the World Trade Center buildings in New York City. Studies on buildings using VE materials for dampers demonstrate the benefit of reduced vibration under wind excitation (Higgins and Kasai 1998; Tan et al. 1997). VE dampers were recently used to meet wind serviceability requirements for a 46-story RC residential structure in Korea. The primary lateral resisting system is a core concrete shear wall. The devices were used in place of an outrigger to control deformations. The dampers were placed in a unique location to reduce the architectural impact. Steel stub beams were connected to adjacent columns just below the structural slab. The damper was the connection between the two beams. As the columns rotated, the rubber damper was deformed in shear, adding both stiffness and damping to the structure (Ahn et al. 2008). A sketch of the VE damper with the stub beams in the reinforced concrete frame is shown in Figure 2-36.

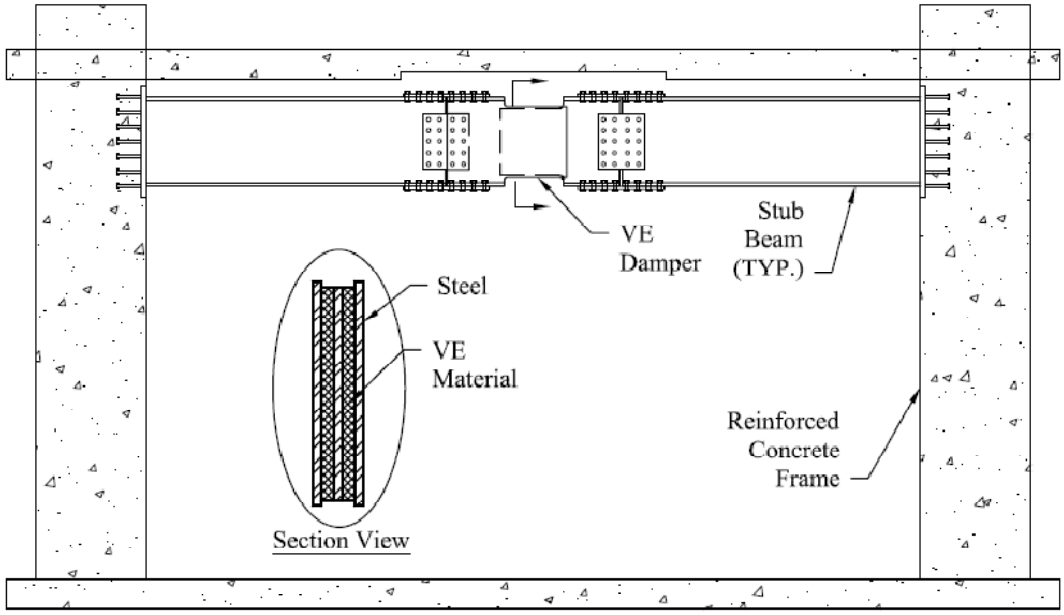

Figure 2 - 36 VE Damper in Reinforced Concrete Frame [after (Ahn et al. 2008)]

Although viscoelastic dampers have been previously used for wind vibrations, research on using VEDs for seismic protection began in the mid to late 1980s (Constantinou et al. 1998). Studies by Tsai and Lee (1993) using VEDs subjected to seismic loads at varying temperatures found reduced stresses and displacement of the structure. A parametric numerical study of minimum weight seismically designed structures showed that elastic structures could be obtained by using

VEDs (Chang and El-natur 1993). An experimental study added VEDs to a damaged 1/3 scale RC frame. The results indicate that even with significant inherent damping from the damaged frame, the devices were effective in reducing seismic response (Shen et al. 1995). As reported in a series of articles, experimental shaking table tests of a 2/5 scale three-story steel frame with VEDs demonstrated effective energy dissipation over the frame tested without supplemental dissipation (Chang et al. 1996; Chang et al. 1995; Lai et al. 1995). In addition to experimental testing, numerical modeling of VE damped structures also indicates the benefit of the dampers to both steel and reinforced concrete frames by reducing ductility demand on the frames (Fu and Kasai 1998; Munshi 1997; Tezcan and Uluca 2003).

Experimental testing on five-story steel frames illustrates the benefit of the VEDs but also demonstrates that increased temperatures adversely affect the performance of the dampers. The negative effect is the reduced stiffness and damping as the material heats up and the mechanical properties are modified (Chang and Lin 2004; Min et al. 2004). VEDs have also been studied for use in connecting adjacent structures or across seismic joints. The results of the numerical analyses demonstrated significant reduction of the connected structures, especially in the case where the natural frequencies differ significantly (Kim et al. 2006). The application of a vibration prevention system to a 13-story structure found VE dampers to be most effective at reducing response. The reasoning is the performance of the VE materials across all levels of vibration including both small mechanical vibrations and seismic events. A long-term monitoring program is in place to study the building response (Lin et al. 2006).

Research has been done implementing unique configurations and placement of VE materials. Connection dampers with elastomeric pads or VE layers in shear at the tension and compression flanges of bolted connections, shown in Figure 2-37, were studied numerically. The configuration is highly controllable in the damping value and connection fixity. The studies showed significant structural response reduction under certain fixity conditions (Xu and Zhang 2001). Another configuration used at column bases is a VE material wrapped around the RC column and then covered with a composite wrap which is then anchored into the foundation. This damping-enhanced strengthening methodology illustrated in Figure 2-38 provided approximately 50% reduction in displacement and acceleration (Wang and Chen 2006).

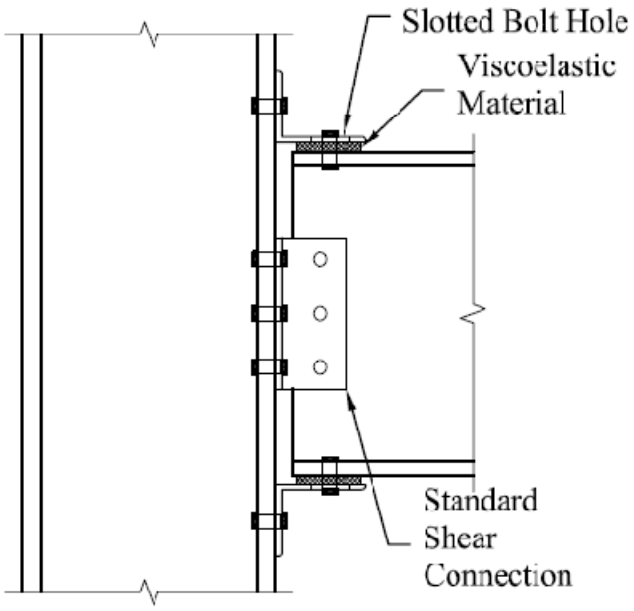

Figure 2 - 37 Beam-Column Connection with VE Dampers

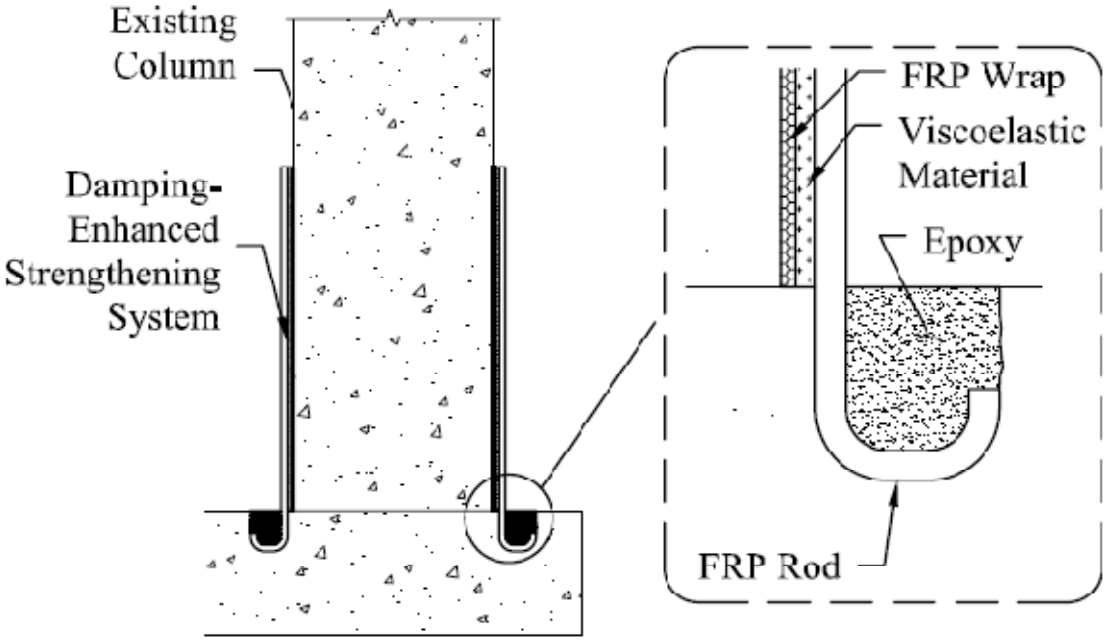

Figure 2 - 38 Damping-Enhanced Strengthening System [after (Wang and Chen 2006)]

Conventional wood-frame shear walls have also been tested with VE materials applied to absorb energy. The tests focused on the performance of shear walls with VE materials. Five different damper configurations were tested with results as high as a 59% increase in energy dissipation (Dinehart et al. 1999). A later study focused more on the 3M VE materials used. The research used combinations of various materials either in parallel or series. The results demonstrate that

the combination of polymers provided a better result than individually. The combination still failed to provide effective energy dissipation over a broad range of temperatures and frequencies (Joye and Dinehart 2007).

High-damping rubber (HDR), similar to that used in base isolation bearing pads, has also been used as an elastomeric damping material. In most cases the addition of carbon black to different types of rubber, natural or synthetic, creates a material with high energy dissipating capacity. Styrene-Ethyrene-Butadiene-Styrene (SEBS) rubber was used in both a sandwich type and cylinder type damper for vibration attenuation of high-rise buildings. The study found little dependence on temperature and good energy dissipation from vibrations on the order of μm to 200% strains (Fujita et al. 1992; Fujita et al. 1995). Further research on a cylinder type rubber damper used in an 11-story building showed significant reduction in response (Furuya et al. 1999). A schematic of the cylindrical high damping rubber damper is shown in Figure 2-39.

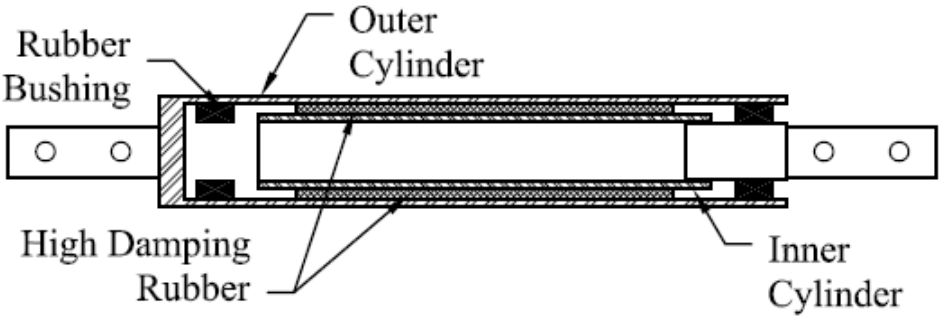

Figure 2 - 39 Cylinder Type High Damping Rubber Damper

The remainder of the articles cited in this review study natural rubber, isoprene, filled with carbon black. Work done at Lehigh University on Ultra-high Damping Natural Rubber (UHDNR) structural dampers includes development of hysteresis models and behavior of frames with installed dampers. UHDNR structural dampers have a loss factor between 0.35 and 0.40. The loss factor is the ratio of the loss modulus of a material to the storage modulus. It represents the amount of energy dissipated to the amount of elastic strain energy stored and released for a given cycle. In development of nonlinear hysteresis models it was found that a dependence on strain level, temperature and frequency exist but the dependence is much less than for standard VE materials used in structural dampers (Lee et al. 2004; Sause et al. 2001). In the work on the behavior of a steel moment resisting frame, the UHDNR damped system outperforms 3M

ISD110 when the range of temperature is considered in the design. Both materials reduced the structural response of the frame under seven different ground motions (Lee et al. 2003).

Experimental research on application of high damping rubber devices (HDRD) to a reinforced concrete frame was conducted to analyze the response of structures with dampers. The research showed the ability of the HDRD to provide an increase of up to 120% of the inherent damping in the frames. The rubber dampers showed a stable performance if the stress is applied in simple shear (Bartera et al. 2004; Bartera and Giacchetti 2004). The rubber used in the studies at Lehigh and by Bartera and co-workers was provided by, and the research supported by, the Tun Abdul Razak Research Centre (TARRC) and Malaysian Rubber Board. It should be again noted that the behavior and modeling of the filled rubber in these dampers has been extensively studied and a review of that research is presented in a later chapter.

Viscous and VE dampers are both effective in vibration reduction of structures. The benefit of these devices is that they can be used for all levels of vibrations. Viscous walls, viscous dampers and VE dampers have been effectively used for wind and seismic response reduction throughout the world and will continue to be used. VFDs can be especially effective if used in a unique configuration such as a scissor-jack or toggle brace system. VEDs have also demonstrated effective energy dissipation and response reduction for multiple levels of vibration. They are simple mechanically and provide flexibility in the way they are implemented in structures.

2.4. Hybrid Passive Control Devices

Hybrid damping devices consist of two different types of passive damping systems used together. Typically, a hybrid combination consists of a rate-dependent device paired with a rate-independent device. One example is using a VED combined with a metallic yielding device. The VED will perform well under low level vibrations while the hysteretic devices provide only stiffness. Taking this further, the hysteretic device has significant energy absorption capacity which can augment the VED under large-scale seismic events. Limited research has been carried out using combinations of rate-dependent and rate-independent devices.

One combination damper, shown in Figure 2-40, is a metallic yielding device in parallel with a VE damper. A TPEA device is used as the hysteretic element. The analytical models show that the combination of velocity-dependent and velocity-independent devices on the same structure is a potent tool to enhance seismic protection (Tsai et al. 1998). A further parametric study with

similar combination devices was completed using a four-story six-bay frame. The results confirm the benefit of the strengths of the different devices offsetting the weaknesses (Chen et al. 2002).

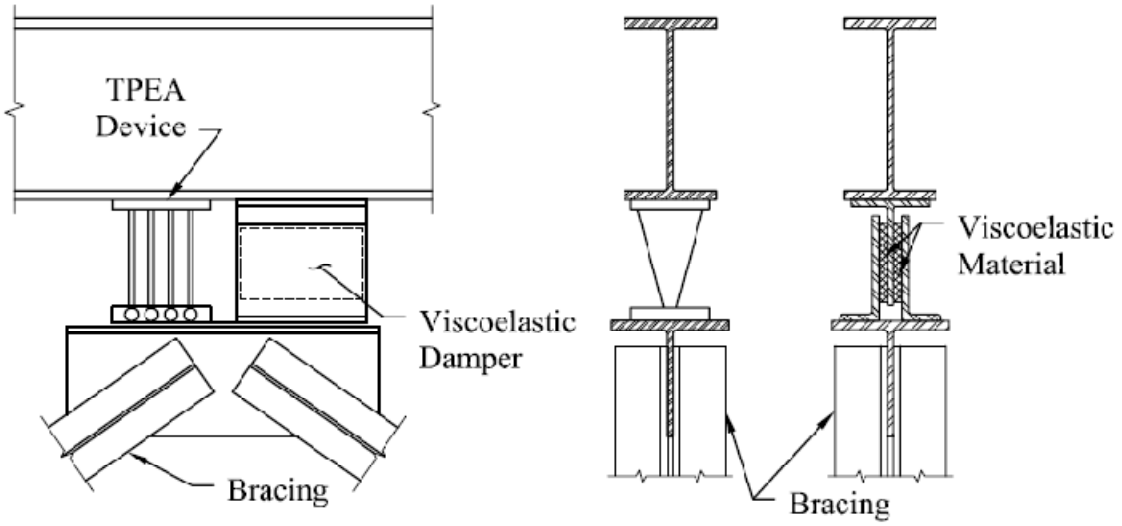

Figure 2 - 40 Combination TPEA & VE Device

The Visco-Plastic Device (VPD), illustrated in Figure 2-41, uses two bent channels or plates with an elastomeric damping material sandwiched between. The VPD takes advantage of an amplification of displacements across the rubber to increase damping. Additionally, upon reaching the axial-flexural yield of the steel elements, the energy absorbing capacity is augmented by steel yielding. The geometry of the damper has a hyperelastic effect when it undergoes large displacements. The increase in stiffness aids in collapse prevention by stiffening the structure during significant seismic events (Ibrahim 2005; Ibrahim et al. 2007).

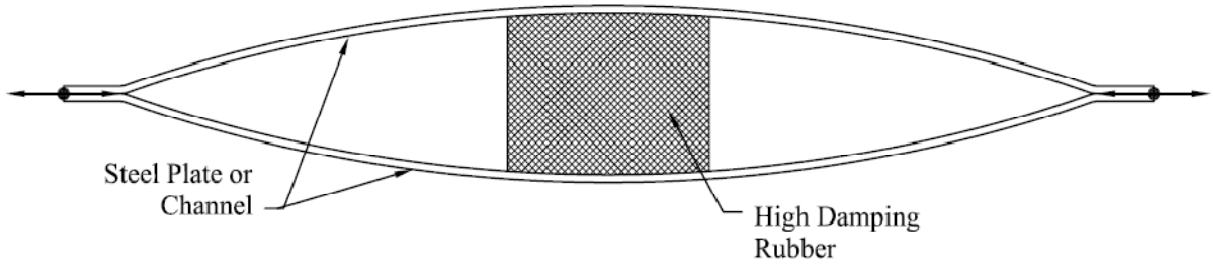

Figure 2 - 41 Visco-Plastic Device (VPD) [after (Ibrahim et al. 2007)]

Concentric steel rings with a dissipative material sandwiched between is a brief description of the visco-hyperelastic device (VHD), illustrated in Figure 2-42. This device is connected in the center of a structural bay using four braces or in a toggle-brace configuration. The device is a multi-stage device as is the VPD. Due to steel yielding and the geometry of the device, it has a

large capacity to dissipate energy as well as a stiffening effect (Murthy 2005). Another benefit of both the VPD and VHD is the many parameters that can be modified to control response.

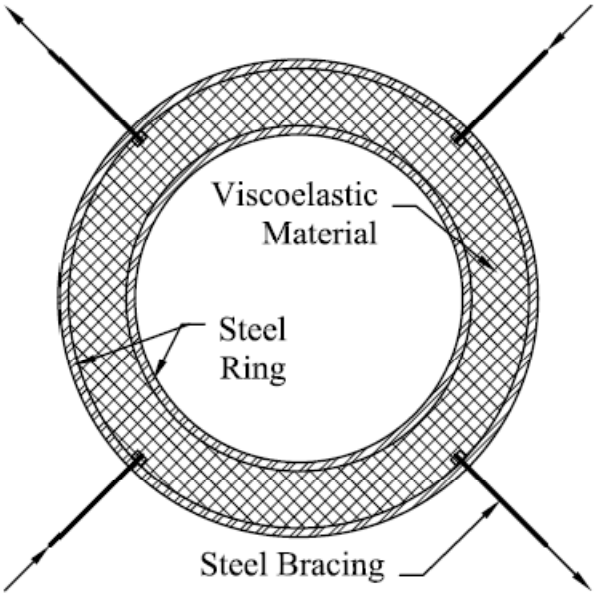

Figure 2 - 42 Visco-Hyperelastic Device (VHD) [after (Murthy 2005)]

More recent work in combination or hybrid devices includes adding viscous dampers to a lateral resisting system with metallic dampers. The goal of adding the dampers was to maintain the low displacements while also reducing non-structural damage and reducing accelerations. The analytical single degree of freedom study found that the viscous dampers reduce the effectiveness of the metallic dampers. The authors also found that floor accelerations are likely to increase for systems with a small strain hardening ratio (Vargas and Bruneau 2007).

A hybrid system using partially restrained (PR) moment connections coupled with viscoelastic dampers was explored analytically and experimentally. The benefit of the PR connection is minimal damage to the structural frame with the hysteresis of the connection. The viscoelastic dampers were used with chevron braces. The results of the testing demonstrated a considerable reduction in displacement demand and structural damage. This type of system is also able to satisfy performance-based design criteria. The analysis demonstrates that the best performance with least cost was achieved with damping ratios of 10% or less (Amadio et al. 2008).

Combination or hybrid devices contain significant potential for the future. Little research has been completed in this area, but the possibilities for combining rate-dependent devices for their

small vibration reduction capacity with metallic or friction devices for their large energy absorption capacity provides a significant opportunity for effective earthquake protection.

2.5. Summary

This review of passive structural control systems demonstrates the large array of possibilities available for protection of structures from wind and seismic loads. The multiple types of devices and various configurations within each type are innumerable. Each type of energy dissipation system has its own strengths and weaknesses. The possibilities for combining devices to more fully protect structures are endless. The challenge is to continue moving forward, creating more effective devices and improving their effect on structural performance. The realm where this is directly applicable is in performance-based earthquake engineering (PBEE). The goal of PBEE is to create a performance specification for a structure and then design the structure to meet those criteria versus a simple strength or serviceability based design. It requires greater understanding of structural behavior and more in-depth analysis, with the end result being a more efficient structure tailored to the owner's specific needs.

Hybrid passive devices blend well with PBEE. Developing hybrid passive devices requires an understanding of the current condition of passive control methods. Knowing the strengths and weaknesses of the individual devices as well as their effect on structural behavior is critical. As an example, consider the BRB system. The increased stiffness results in reduced displacements and significant energy dissipation once the braces yield. The cost of this improved performance is increased base shears, large accelerations and possible residual deformations. The same comparison could be made for any other type of passive control system. The key to development of an effective hybrid system is combining devices in a manner that the strengths are maximized and the weaknesses are offset.

Semi-active control devices can be used as a model for the concept being developed in this research. In semi-active systems, the device properties can be modified by the controller monitoring the structural response. Creating a completely passive device that can be essentially preprogrammed based on the understanding of both the structure and the device has great potential. It would possess the benefits of passive control while including the power of properties tailored to the expected structural response. The body of information generated by this literature review is critical to developing an innovative, practical, effective and controllable hybrid device.

The research in hybrid passive control devices or even hybrid passive configurations to this point has been limited. Multiple options and significant potential exist for combinations of passive energy dissipation elements that provide the characteristics desired for the hybrid device proposed in this research. The first challenge of this research is to find an effective combination that can be economically fabricated. The inclusion of these devices in structures requires significant experimental testing and analytical research. This research takes an initial step, both analytically and experimentally, in the right direction. Using a combination of experimental and analytical tools, a unique hybrid passive control device is developed, analyzed and tested to verify that the device design functions as designed and that the response of structures subjected to seismic loading is reduced. This type of device could significantly change the way structures are designed to resist seismic loads. Not only could the structure be designed for a collapse prevention or immediate occupancy limit state following a large-scale event, response under a small-scale or mid-range event could be reduced to the point where a structure could remain linear elastic and have reduced accelerations. Based on the current state-of-the art, these performance measures could only be met through active or semi-active control. A properly designed hybrid device could meet these performance specifications. This research can provide significant progression towards such a goal.

Chapter 3. Mechanics of High Damping Rubber

3.1. Introduction

Natural rubber is obtained in the form of latex from the Hevea Braziliensis tree. However, in modern language the term rubber can also include synthetic materials with similar mechanical properties. The term elastomer is a more general term for this family of materials. In this document, the term rubber will be used interchangeably with the term elastomer. If the reference is to natural rubber, it will be specified or obvious from context. There are many varieties of synthetic elastomeric materials created to have specific properties. In this research, two rubber compounds were studied, highly damped Natural Rubber (NR) and highly damped Butyl Rubber (BR). Both were chosen because of their unique combination of engineering properties.

In its natural or raw state, rubber is highly deformable, highly elastic and very soft. To create an efficient engineering material, compounding of the raw materials with other materials including sulfur and carbon black is required. Producing a useful engineering material from raw rubber requires appropriate additives as part of the compounding process.

3.2. Rubber Properties

3.2.1. Molecular Structure

Rubber materials are an amorphous network solid of long chain molecules. Natural rubber is a hydrocarbon polymer with the chemical formulation $(C_5H_8)_n$. The subscript "n" in the chemical formula represents the fact that it is a repeating chain of the molecule in parentheses. The chain molecules with freely rotating bonds are entangled with adjacent chains. This gives rise to some weak ties between chains. Without vulcanization, these weak intermolecular forces can be easily overcome. The large-deformation capacity comes from the fact that these chains are irregularly kinked. As the polymer chains are pulled, the kinked shape straightens out. Due to the chains having significant capacity to extend, many rubbers are able to elastically deform to greater than 500% strain (Treloar 2005). The weak intermolecular forces are the reason that raw rubber is very soft.

3.2.2. Rubber Compounding

The process of turning raw rubber into a useful engineering material is termed compounding or formulating. The process typically involves vulcanization and the addition of reinforcement and anti-degradants, both of which will be discussed more later in this chapter.

3.2.2.1. Vulcanization Process

The vulcanization process is typically carried out using sulfur as the agent. The process creates chemical links between adjacent polymer chains. These links transform the nearly liquid state of raw rubber into a tough elastic solid. Accelerators are also used to achieve a greater efficiency and rate of cross-linking. The mechanical properties of a vulcanized rubber are highly dependent upon the density of cross-link sites. The modulus and hardness of a rubber compound increase as the number of cross-links increase. The vulcanization process also removes to a degree the dependence of the physical properties on temperature (Freakley and Payne 1978).

3.2.2.2. Addition of Reinforcement

Addition of reinforcement or fillers is another part of the compounding process. The most common filler materials for improving the properties of rubber are carbon black and silica. These particulates, with a size on the order of 100 to 200 Å, can increase the strength of the amorphous rubber more than ten times (Gent 2001). The fillers also increase the inherent material damping. The properties which comprise good fillers are high specific surface area, structure and surface chemistry. Carbon black is an effective filler for increasing the strength and damping of rubber compounds. The increase in damping with the addition of carbon black is due to the concept of strain amplification. The simple explanation is that the filler is much stiffer than the surrounding rubber. Because of the decreased rubber volume, the rubber undergoes greater strain under the same deformation as would an unfilled rubber sample. This increased strain in the rubber is the source of the increase in the material loss factor (Freakley and Payne 1978). Some increase in damping can also be attributed to the softening of filled rubbers in the early cycles. This stress softening is termed the Mullins effect.

3.2.2.3. Mullins Effect

The Mullins effect is evident in the behavior of filled rubbers under repeated loading. As initial rubber-filler bonds break, the stiffness of the rubber is reduced. The effect is more pronounced as the filler loading increases, although the reduced stiffness is still greater than for unfilled rubber. The effect only occurs when the strain level has not been previously reached by the material. The modulus will continue to degrade at and below the maximum strain level until it reaches a steady state value. This occurs anywhere between five and 20 loading cycles depending upon the amount of filler and the type of rubber. However, each time the maximum previous strain is exceeded, a reduction in stiffness will occur. To compensate for this effect, rubber elements are

mechanically cycled (preconditioned) to remove this effect prior to being placed in service (Mullins 1969). Some recovery of the stiffness is apparent in retesting of rubber samples, however full recovery has not been observed. This type of behavior can be seen in stress-strain plots from materials tested in any state of deformation. Figure 3-1 shows uncorrected test data from uniaxial testing of the 60 hardness high damping butyl rubber specimen. It can be seen that the stiffness decreases between the first and second cycle. This decrease continues for several cycles until a steady state behavior is developed. An additional aspect to this behavior is that the higher strength initial cycle is present every time the rubber is allowed to rest before being loaded. In short, if the test specimen is tested one day and then tested again the next day, the stress softening would be apparent in the data from both tests.

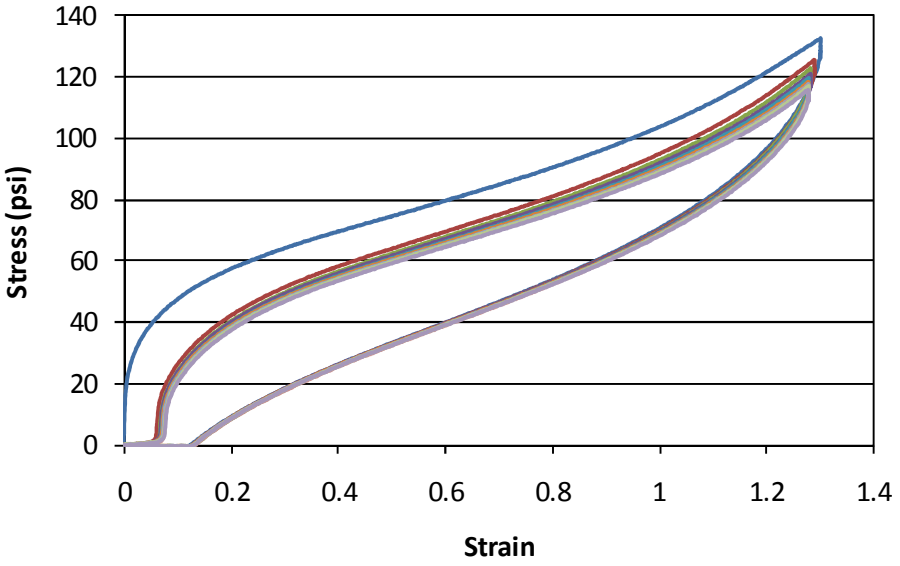

Figure 3 - 1 Stress-Strain Plot for Uniaxial Tension Test of BR60 Specimen

3.2.2.4. Anti-Degradants

Oxygen and Ozone react with elastomers and cause degradation. Ozone readily cleaves carbon-carbon double bonds. The result of this is the development of surface cracking. This can lead to quick degradation of strength and stiffness, especially over a long period of time. This is one of the primary reasons rubber is not used significantly in tension. Oxygen can cut molecular chains and cause additional cross-linking. In most elastomers the additional cross-linking causes them to harden and become brittle. To overcome this problem, chemical protectants such as aromatic amines, phenolics and phosphites are added during the compounding process (Gent 2001).

3.2.3. Incompressibility of Rubber

Unlike standard materials, rubber is nearly incompressible. This near incompressibility means that rubber has a very high bulk modulus of elasticity. In very simple terms, rubber has a very high resistance to volume change under load. Rubber materials tend to have a low shear modulus, G, and a very high bulk compression modulus, K. These behaviors approach a purely incompressible material which would have a Poisson's ratio of exactly 0.5. The approximate value for rubber is typically taken as 0.4999 (Gent 2001). For applications where rubber is not highly confined, the assumption of incompressibility is very reasonable. The incompressibility assumption is an important element of many mathematical models developed for rubber.

3.2.4. Rubber Material Properties

Due to the highly nonlinear nature of rubber, there is not a constant modulus of elasticity or shear modulus. When these terms are used with elastomers, they refer to the stress at a given strain. The typical values that are reported are either at 100% or 300% strain or the strain at rupture. In this work a modulus value if given can be assumed to be at 100% strain or shear strain, unless otherwise specified. The shear modulus for typical rubbers at 100% strain is generally between 75 and 700 psi (Gent 2001). Rubber hardness values are often reported in place of a modulus. On the Shore A hardness scale, typical rubber values fall between 30 and 80. There is a correlation between the hardness and modulus, although it is not direct. Typically, a higher hardness is indicative of a higher stiffness.

3.2.5. High Damping Rubber

High damping natural rubber (HDNR) is a vulcanized natural rubber compound with added carbon black and other fillers to enhance the engineering properties. The addition of carbon black has the effect of increasing the stiffness and the loss factor. These fillers also reduce the dependence of the material properties on temperature, loading and frequency. The same principles apply to creating a high-damping butyl rubber. Raw butyl rubber has a higher loss factor than raw natural rubber. Because of this, the addition of the carbon black to butyl rubber creates a compounded material with higher damping than a filled natural rubber. The rubber compounds used in this research are specifically formulated to have a high loss factor.

3.3. Mechanical Behavior of Filled Rubber

Mathematically modeling the behavior of filled rubbers is highly complex. Rubbers are classified as isotropic materials. The primary complexity is that rubbers are also classified as a viscoelastic solid. Metals can be treated as an elastic solid because the inherent damping is so small. Conversely, HDR has the capability to dissipate significant energy. Because of this, rubber has two aspects to its behavior, one portion being time independent, the other being time dependent. The time independent element is the static force-deformation relationship. The time dependent nature is represented by the loss modulus. These two elements can be seen in the stress-strain equation for viscoelastic materials shown in Figure 3-1. *E**, the complex modulus, is represented mathematically by the real part, *E*', and the imaginary part, *E*". This mathematical representation can be explained in the physical world by noting that the storage or real part of the modulus is in phase with the strain. The imaginary part, the loss modulus, is 90 degrees out of phase with the strain. What this means is that due to the viscoelasticity, the maximum stress and maximum strain do not occur at the same time and have to be represented mathematically as being out of phase. Typically, *E*' is termed the storage or elastic modulus and *E*" is termed the loss modulus. The storage modulus is the amount of strain energy stored and released elastically per unit volume. The loss modulus corresponds to the energy lost per unit volume. This equation can also be written as in Equation 3-2 with the loss factor, η, in place of the loss modulus. The loss modulus can also be represented as the tangent of the phase angle between the stress and strain, commonly referred to as tanδ. These relationships are shown in Equation 3-3. The variable δ represents the time lag between the stress and strain.

$$\sigma_o = E^* \varepsilon_o = (E' + iE'')\varepsilon_o \qquad \textbf{Equation 3 - 1}$$

$$\sigma_o = E'(1 + i\eta)\varepsilon_o \qquad \textbf{Equation 3 - 2}$$

$$\eta = {}^{E''}\!/_{E'} = \tan(\delta) \qquad \textbf{Equation 3 - 3}$$

These equations are based on an applied strain of $\varepsilon_o \sin(\omega t)$. These same equations can also be written for simple shear deformation with *E** being replaced by *G** and using shear stress, τ, and shear strain, γ. It would also be necessary to use the loss factor determined for simple shear deformation versus axial tension (Nashif et al. 1985). Generally the loss factor is approximately

the same in tension and shear for filled rubbers. For this work the principal deformation of the rubber will be in simple shear, so the loss factor will be determined in shear.

Figure 3-2 shows the plot of stress and strain versus time. The two stress traces are differentiated based on the loss factor which is indicated in parentheses in the legend. The phase angle, δ, for a loss factor of 0.4 can be seen as the difference between where the stress and strain cross the horizontal axis. The time lag in seconds between the stress and strain can then be transformed to an angle in radians. This is done by dividing the time lag by the period of the motion and multiplying by 2π. The tangent of that angle is the loss factor, η, which is equivalent to the ratio of the loss modulus to the storage modulus. The stress plot with the greater loss factor has a larger lag between the stress and strain. The larger loss factor also has a higher maximum stress. This is because both traces have the same storage stiffness but the dynamic stiffness is larger with a larger loss modulus.

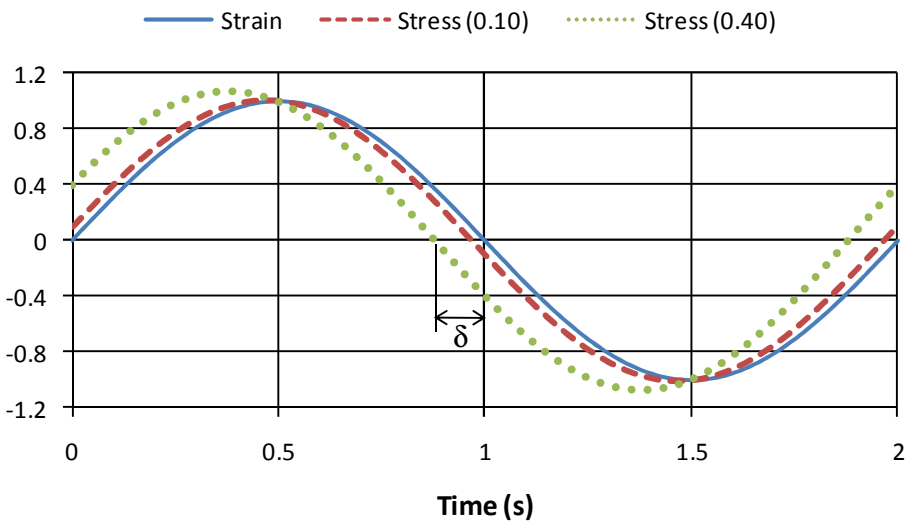

Figure 3 - 2 Stress and Strain versus Time for Sinusoidal Strain (ε_o = 1, E' = 1 psi)

Another way to see the amount of energy dissipation under a cyclic deformation pattern is a hysteresis loop. Figure 3-3 shows a hysteresis loop for the same loading as in Figure 3-2. In a hysteresis plot, the loss factor can be determined from a ratio of the area of the loop divided by the elastic strain energy stored and released during a single cycle. The case where the loss factor is equal to zero is shown as the line in the middle of the plot. Another way of saying this is the loss modulus is equal to zero. This results in a purely elastic response with no energy dissipated.

An example of this would be steel. There is a very small amount of energy loss during cyclic loading, but it is generally negligible. The more robust loop is, the higher the material loss factor.

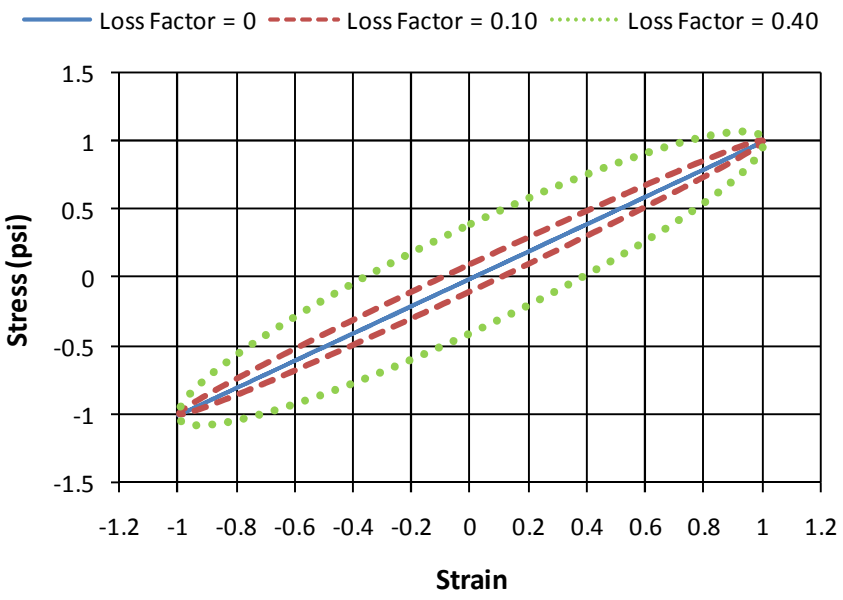

Figure 3 - 3 Hysteresis Plot for Sinusoidal Strain (ε_o = 1, E' = 1 psi)

Due to the dual nature of HDR, the physical testing of the material requires determination of the stress-strain properties corresponding to *E*' under static loading conditions. Additionally, the loss factor or loss modulus must be determined from dynamic testing. These two properties can be determined independently through appropriate testing. The development of the behavioral models for HDR is also broken into two areas, the first being the elasticity and the second being the viscoelasticity. It should be noted that typical viscoelastic materials have a dependence on temperature and frequency for many properties. One of the benefits of filled rubbers is a lessened degree of dependence. The temperature dependence can be very significant if the material is used near the glass transition temperature. For the HDR compounds used in this research, the glass transition temperatures are well below 0º C.

3.3.1. Elasticity Material Models

The elasticity of rubbers is complex. At small strains, less than 15%, the material behaves almost according to Hooke's law. Above this strain level, the behavior becomes highly nonlinear. Because of the nonlinearity of the stress-strain relationship and a large capacity for elastic deformation, these materials are termed hyperelastic materials. Instead of modeling behavior

with a stress-strain curve, a strain-energy density function, *W*, is used to describe their behavior (Muhr 2005). The hyperelastic curve can then be differentiated with respect to strain to determine stress. There have been two general approaches to determining the appropriate mathematical models for these hyperelastic functions. The first is the statistical or physically based method and the second is the phenomenological theory.

3.3.1.1. Statistical Theory

The statistical theory attempts to use the properties of the long-chain molecules and the application of their characteristics to the entire amorphous network to derive a formula. The mathematics involved is highly complex, even in the range of small strains. The experimental verification has shown that although it is a good first approximation, the statistical theory has problems matching the actual behavior (Treloar 2005). This discrepancy becomes more significant with large-deformation problems.

3.3.1.2. Phenomenological Theory

The second approach to mathematically modeling elastomers' stress-strain behavior is a phenomenological approach. This method is not based upon the actual molecular make-up but on a purely mathematical approach to matching the experimental behavior. These treatments have had greater success matching the test data and have found significant use in commercial finite element programs. The work on phenomenological functions was initiated by Mooney and further developed by Rivlin in the 1940s (Freakley and Payne 1978). Mooney's original strain energy equation is shown as Equation 3-4 (Treloar 2005).

$$W = C_1(\lambda_1^2 + \lambda_2^2 + \lambda_3^2) + C_2(\,1/\lambda_1^2 + 1/\lambda_2^2 + 1/\lambda_3^2) \qquad \textbf{Equation 3 - 4}$$

The terms C_1 and C_2 represent elastic material constants. The λ terms are the extension ratios for the three principal directions. The extension ratio is a measure of the axial deformation from the original length. For an unstrained sample, the extension ratio is equal to 1. An extension ratio of 2 would be equivalent to a 100% strain.

For an example of how these functions work, take the case of simple shear for the Mooney equation. For simple shear, λ_3 is equal to $1/\lambda_1$ and λ_2 is equal to 1. For this case, Equation 3-4 becomes Equation 3-5. Plugging in the shear strain, γ, being equal to the quantity λ_1-$1/\lambda_1$ leads to the second part of Equation 3-5. The next step involves taking the derivative of *W* with respect to

shear strain. This results in Equation 3-6. From this equation it is evident that $2*(C_1+C_2)$ is equivalent to the shear modulus G. Using the fact that the Mooney formulation assumes incompressibility, the modulus of elasticity, E, is calculated by multiplying G times 3.

$$W = (C_1 + C_2) * (\lambda_1^2 + {}^{1}\!/\!_{\lambda_1^2} - 2) = (C_1 + C_2) * \gamma^2 \qquad \textbf{Equation 3 - 5}$$

$$\tau = \frac{dW}{d\gamma} = 2 * (C_1 + C_2) * \gamma \qquad \textbf{Equation 3 - 6}$$

For the case of the Mooney formulation the constants can be shown to be related to mechanical properties structural engineers can understand in a simple fashion. The other hyperelastic material models function in the same manner, although determining the correlation of the hyperelastic constants to typical isotropic material properties is not as simple. The way to generate these constants for hyperelastic material models is based on using test data obtained in pure homogeneous states of strain. This concept is discussed further in a later chapter.

Rivlin's further development of Mooney's model maintains the assumption of incompressibility but adds three strain invariants. The strain invariants were developed based on the fact that an isotropic material must be symmetric with respect to the three orthogonal principal strains. The updated mathematical model includes the use of these invariants, shown as Equation 3-7. The third invariant, I_3, is equal to 1 when incompressibility is assumed. Because of that fact, only the first two invariants are actually independent of each other. The Mooney-Rivlin formulation is shown as Equation 3-8 (Treloar 2005). Creating the number of constants required for the equation summed to infinity has mathematical meaning but none physically. In typical use, the formulation uses values of *i* and *j* of no more than 1 or 2 with the term C_{00} being equal to zero to maintain consistency at zero strain. It should also be mentioned that the Mooney equation is a special case of the Mooney-Rivlin formulation. This model has been shown to be effective at predicting behavior up to strains of 100% but is not able to represent the increasing stiffness at higher strains (>200%). Many versions and modifications to these equations have been developed in attempts to provide simpler or better fits to the physical behavior. The number of these is too great to consider here and well beyond the scope of this work.

$$I_1 = \lambda_1^2 + \lambda_2^2 + \lambda_3^2$$
$$I_2 = \lambda_1^2\lambda_2^2 + \lambda_2^2\lambda_3^2 + \lambda_3^2\lambda_1^2 \qquad \textbf{Equation 3 - 7}$$
$$I_3 = \lambda_1^2\lambda_2^2\lambda_3^2$$

$$W = \sum_{i=0,j=0}^{\infty} C_{ij}(I_1 - 3)^i (I_2 - 3)^j \qquad \textbf{Equation 3 - 8}$$

The Ogden model is mentioned here because of its departure from the standard set by Rivlin. It has stood the test of time and still provides one of the better models available in commercial finite element software today for modeling large-strain behavior of rubber. The work by Rivlin held to the theory that even powers of the extension ratios were desired. This was apparent in Equation 3-7 for the strain invariants. Ogden developed his equation by going back to the extension ratios and allowing the exponents, α_n, to have any value, positive or negative, integer or not. The Ogden strain-energy function is shown in Equation 3-9 (Treloar 2005). This model creates even more terms that must be generated since both the μ_n and α_n terms must be determined based on test data from homogeneous states of strain. The strength of the Ogden function is the ability to tailor the number of terms to the amount of data. If there is a large amount of data, a greater number of terms can be used to fit the data. The converse is true, that with a smaller amount of data, fewer terms can be used to achieve a good fit. It is also effective at modeling the upturn of the stress-strain curve in the high strain range.

$$W = \sum_n \frac{\mu_n}{\alpha_n}(\lambda_1^{\alpha_n} + \lambda_2^{\alpha_n} + \lambda_3^{\alpha_n} - 3) \qquad \textbf{Equation 3 - 9}$$

This discussion includes only a few of the numerous models available for modeling the elastic behavior of HDR. In addition to the Ogden and Mooney-Rivlin models, several strain-energy or hyperelastic models are available in ABAQUS (ABAQUS 2007) to model rubber elastic behavior. For a further discussion and ranking of multiple strain-energy density functions, see the work by Marckman and Verron (2006). It should be noted that although the Ogden function falls fourth in the Marckman and Verron ranking, the three models ranked higher are not yet available in commercial FEA packages. The other models applicable to this research will be further discussed in the section on finite element analysis of HDR.

3.3.2. Viscoelastic Material Behavior

The viscoelastic nature of rubber provides the inherent damping properties. Rubber behaves in an approximately linear viscoelastic behavior in simple shear for the typical deformation range (Freakley and Payne 1978). This implies that the viscoelastic behavior is not a function of the stress level for the normal range of usage. In simple terms, the viscoelastic properties of rubber can be represented by a single stress relaxation curve no matter what the strain level.

The numerical values for material damping can be determined in several fashions. Under cyclic testing, there are two ways to determine the loss modulus. If the stress and strain are both plotted against time, the phase angle can be determined from the lag between stress and strain. This can be seen from the equations for stress and strain under forced harmonic loading, shown in Equation 3-10. This is the simpler of the two methods. The phase angle, δ, is determined from the lag in seconds multiplied by the radial frequency, ω. This calculation is shown in Figure 3-4.

$$\sigma = \sigma_o \sin(\omega t + \delta)$$
$$\varepsilon = \varepsilon_o \sin(\omega t)$$

Equation 3 - 10

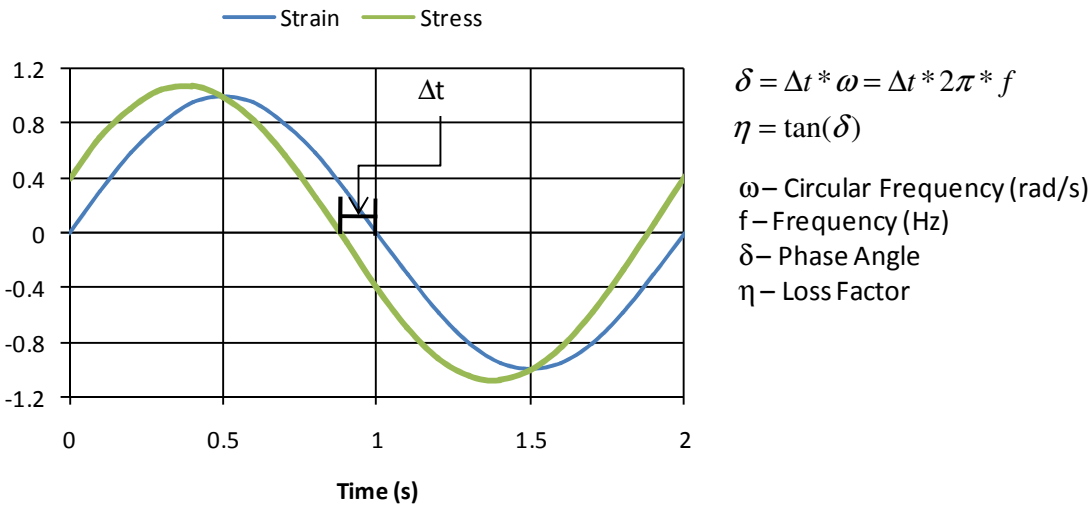

Figure 3 - 4 Calculation of Loss Factor from Cyclic Stress and Strain Data

The other way to determine the required properties from the same forced vibration experiment is by plotting strain on the horizontal axis and stress on the vertical. This will create an elliptical hysteresis plot. The loss factor can be calculated by the ratio of the area of the ellipse, which is the energy dissipated, to the quantity 2π multiplied by the strain energy stored during that loop.

In short, it is the energy dissipated divided by the elastic strain energy. An example of this calculation is shown in Figure 3-5. For both methods, the testing should be done throughout the frequency range and strain levels applicable, to determine the variation.

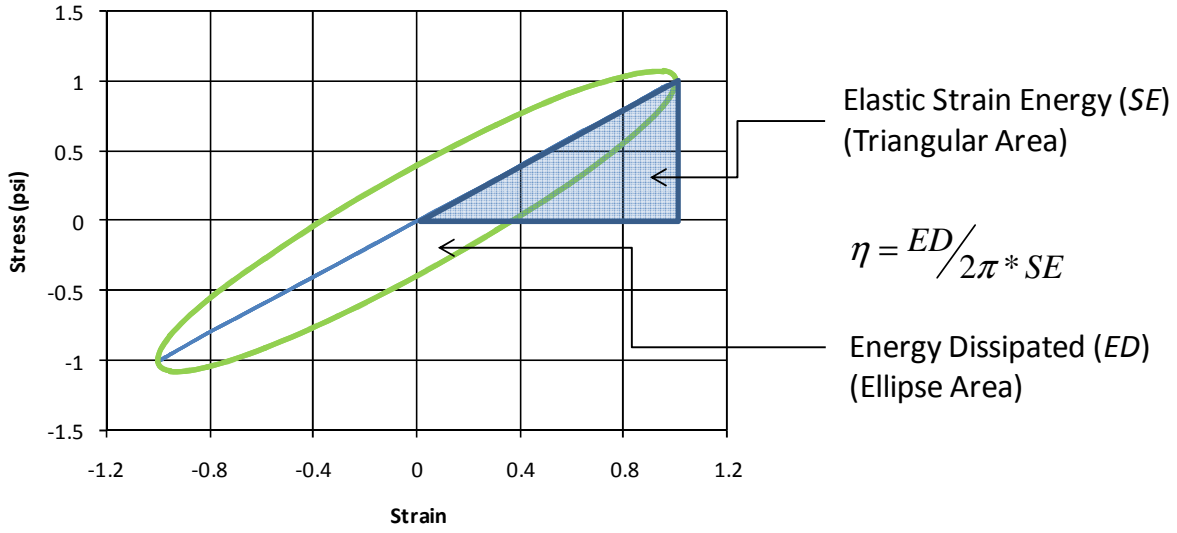

Figure 3 - 5 Loss Factor Determination from Hysteresis Loop

Another method of quantifying the time dependent properties of HDR is through a creep or stress relaxation test. The creep test consists of applying a specified stress and holding it while measuring the strain over a period of time. Stress relaxation consists of imposing a specified strain and monitoring the stress. To verify the assumption of linear viscoelasticity, the tests should be carried out at varying stress or deformation levels.

3.4. Experimental High Damping Rubber Models

Modeling rubber by using both a strain-energy function and the appropriate viscoelastic behavior is highly complex. Significant work has been done to generate rubber material models based on experimental data. A portion of this work is reviewed and discussed in this section. The largest part of this work has been done for seismic isolation pads since the earliest use of HDR in seismic applications was for base isolation systems.

An energy based model using a power function of the shear displacement was developed to model HDNR bearing pads. The basic premise of the model is a combination of linear, viscous and hysteretic elements along with a gap element to provide the stiffening effect at higher strain levels. Because of its makeup of basic elements, it was developed for use in typical nonlinear

analysis programs (Clark and Kelly 1996). Other work on HDR isolation bearings developed two analysis models. The first model was based on the system identification method. The second model was a fractional derivative Kelvin model. Both models demonstrated accurate modeling of experimental shaking table tests up to a shear strain of 100% (Hwang and Ku 1997).

Constitutive models have also been developed and tested based on developing specific applications of HDR. A visco-hyperelastic approach was developed for applications where rubber acts as an impact absorbing device. The main deviation from typical models for this case was the strain rate sensitivity of the properties. Typical rubbers show a significant increase in stiffness at high strain rates. The testing shows that the constitutive relationship, which has been implemented in an FEA code called DYNA3D, exhibits good agreement with experimental results (Yang et al. 2000). A hyperelastic relation was developed to improve the modeling of HDR in compression. Experimental testing including constant-rate monotonic compression and multi-step relaxation tests was used to calibrate the model. The model performed better than previous hyperelastic models for HDNR under compression (Amin et al. 2002).

A unique constitutive model was developed which combines hyperelasticity in parallel with elasto-plasticity. Several experimental tests of HDR were conducted to calibrate the material model. The constitutive relationship performed well in simulations and was able to predict the behavior of HDNR and natural rubbers (Yoshida et al. 2004a).

The Wen model has been used to model base isolation devices and buckling-restrained braces. By modifying the Wen model to include a rate-dependent term, another analytical model was developed for HDNR bearings. The model uses seven parameters and was found to accurately predict the nonlinear behavior of high damping rubber bearings. This model was also implemented in finite element software for analysis of base-isolated structures (Tsai et al. 2003a). Another rate-dependent model developed by testing three different types of HDR bearings includes a nonlinear spring-dashpot element. The calibration of the model was completed using least-squares curve-fitting based on the test results for three samples. The correlation between the model and experiment was good over a wide range of shear strains (Jankowski 2003).

An effort was undertaken to produce a constitutive model of an HDR bearing including the steel plates. The rubber portion of the model contained a hyperelastic damage model in parallel with

an elasto-plasticity element with a strain-dependent hardening law. This model is implemented in finite element software. The results of the modeling exhibit good agreement with experimental data (Yoshida et al. 2004b).

A bidirectional model was proposed including the degradation due to stress-softening of HDR bearings. The model included an elastic spring parallel to the deformation and a hysteretic spring parallel to the velocity vector. The specific purpose was to create a model that could be used for design rather than a constitutive relationship for FEA. The calibration of the model to experimental results showed promise in the low strain-rate tests but had up to 30% error in high strain-rate tests (Grant et al. 2004).

Several hyperelastic models, most based on the work of past models, have also been proposed to further the ability to accurately model the behavior of HDR (Amin et al. 2006a; Amin et al. 2006b). Some models have also attempted to include the compressibility of rubber in the model and implement it into a finite element code (Ghaemi et al. 2006a; Ghaemi et al. 2006b).

The prior studies have been focused on applications of HDR in shear and compression for seismic isolation. Other studies have begun to use HDR as a dissipative element in a damping brace. Rate-independent models for ultra-high damping natural rubber (UHDNR) dampers were developed based on experimental tests of sandwich dampers up to 100% strain. The most effective was found to be a fourth-order polynomial function combined with a sequential asymptote model (Sause et al. 2001). A different model was later developed by adding a dashpot in parallel with the rate-dependent model from the earlier work by Sause et al. The modified model provided good agreement at various loading frequencies and ambient temperatures (Lee et al. 2004). Another constitutive model based on a thermodynamically compatible rheological model using internal models was developed and compared to experimental testing. This model used the internal variables to describe the dependence on strain-rate and the Mullins effect (Dall'Asta and Ragni 2006). Further work by the same authors defined equivalent linear models for the complex behavior of HDR. The model includes two parts. The first represents the first cycle properties of the material prior to the reduction in stiffness due to the Mullins effect. The second portion represents the steady state response. The results show that the two models can be used to bracket the actual response and provide approximate force and displacement values for nonlinear response histories (Dall'Asta and Ragni 2008).

A series of work has developed a unique model for elastomeric materials that breaks the behavior into a perfect equilibrium response in parallel with a time-dependent element responsible for the damping. The perfect network can consist of any hyperelastic strain-energy function. The Arruda-Boyce 8-chain model was used throughout the research. Experimental tests on filled and unfilled vulcanized elastomers showed good correlation (Bergstrom and Boyce 1998). The extension of this work was aimed at including the effects of strain amplification due to fillers. The modified constitutive model displays effective modeling of the behavior of filled elastomers up to 25% volume fraction of carbon black (Bergstrom and Boyce 2000). Further improvement of the model expanded it to include soft biological tissues in addition to filled elastomers. The modifications made to the previous work include easier numerical implementation and the addition of another term which results in improved accounting for rate-dependence and hysteresis for filled rubber and soft biological tissues (Bergstrom and Boyce 2001).

3.5. Finite Element Analysis of High Damping Rubber

Based on the brief review of the significant volume of work on modeling HDR, it can be seen that the mechanical behavior can be highly complex. The elastic behavior alone is highly nonlinear. The number of hyperelastic models that exist provides multiple options depending on the deformation range and the material itself. The viscoelastic behavior is complex, even if linear viscoelasticity is an appropriate assumption. When stress-softening and the ability to recover a portion of the softening upon rest are included, the combination seems a significant obstacle. Fortunately, the commercial finite element software ABAQUS (ABAQUS 2007) has many of these complex abilities implemented. The following sections present available options for modeling rubber and viscoelasticity.

3.5.1. Hyperelastic Functions

The hyperelastic functions in ABAQUS include several models previously mentioned. They are sorted into the physically based models and phenomenological models. The implementation of the models is done through providing static test data and using curve fitting routines within the program to determine which of the models best fits the data. Uniaxial, planar and biaxial tension deformation states are the options available for test data input. Generally, the more test data input, the better the fit of the hyperelastic function. In the discussion below, the strengths and weaknesses of the various models are discussed.

3.5.1.1. Physically Motivated Models

3.5.1.1.1. Arruda-Boyce Model

The Arruda-Boyce 8-chain model is based on I_1 only and includes two material parameters. The hyperelastic equation, *W*, is shown in Equation 3-11. Because of the small number of coefficients, the ability to change shape is limited. However, because of only having two coefficients, fitting with limited test data works well. For this model, μ represents the shear modulus and *D* is equal to 2 times *1/K*, where *K* is the bulk modulus. The parameter λ_m, the locking stretch, is typically set to a value of 7. J_{el} is the elastic volume ratio which is only important when thermal strains are significant.

$$W = \mu\{\frac{1}{2}(I_1-3)+\frac{1}{20\lambda_m^2}(I_1^2-9)+\frac{11}{1050\lambda_m^4}(I_1^3-27)+\frac{19}{7000\lambda_m^6}(I_1^4-81) + \frac{519}{673750\lambda_m^8}(I_1^5-243)\}+\frac{1}{D}(\frac{J_{el}^2-1}{2}-\ln(J_{el}))$$

Equation 3 - 11

3.5.1.1.2. Van der Waals Model

The Van der Waals model includes four parameters, allowing a greater ability to fit data. Modeling the upturn in the stress-strain curve is possible. This model has dependence on both I_1 and I_2. The dependence on I_2 can be removed by setting $\beta = 0$, where β is the invariant mix parameter. The initial shear modulus is represented by μ, with *D* governing the compressibility as in the Arruda-Boyce model. The other parameters, *a* and λ_m, are the global interaction parameter and the locking stretch, respectively. J_{el} is the same as for Arruda-Boyce. The Van der Waals strain-energy function is shown in Equation 3-12.

$$W = \mu\{-(\lambda_m^2-3)[\ln(1-\eta)+\eta]-\frac{2}{3}a(\frac{\tilde{I}-3}{2})^{\frac{3}{2}}\}+\frac{1}{D}(\frac{J_{el}^2-1}{2}-\ln(J_{el}))$$

$$\tilde{I} = (1-\beta)\overline{I_1}+\beta\overline{I_2}$$

Equation 3 - 12

$$\eta = \sqrt{\frac{\tilde{I}-3}{\lambda_m^2-3}}$$

3.5.1.2. Phenomenological Models

3.5.1.2.1. Full Polynomial Model

Polynomial models can be classified as full or reduced polynomial models. Full polynomial models include the generalized form of the Mooney-Rivlin equation and include a dependence

on I_1 and I_2. The full polynomial model is shown in Equation 3-13. ABAQUS allows for up to N=2. Setting N = 1 gives the standard Mooney-Rivlin model, which is good for below 100% strain but cannot capture the upturn in higher strain ranges. Using a larger value of N in the full polynomial requires a larger body of test data. Setting N=2 requires fitting of 5 coefficients. The initial shear modulus for this model is represented by $2*(C_{10} + C_{01})$ with the initial compressibility being represented by $2/D_1$. J_{el} is the same as for the other forms.

$$W = \sum_{i+j=1}^{N} C_{ij}(\overline{I}_1 - 3)^i (\overline{I}_2 - 3)^j + \sum_{i=1}^{N} \frac{1}{D_i}(J_{el} - 1)^{2i} \qquad \textbf{Equation 3 - 13}$$

3.5.1.2.2. Reduced Polynomial Model

Reduced polynomial models remove the dependence on I_2. The first-order reduced polynomial is called the Neo-Hookean Model. It is one of the earliest models, developed in the 1930s. Because of the limitations, it is simple to use and can be effective at small strains. The Neo-Hookean formulation is shown in Equation 3-14. For this model the initial shear modulus is C_{10} and the initial bulk modulus is $2/D_1$.

$$W = C_{10}(\overline{I}_1 - 3) + \frac{1}{D_1}(J_{el} - 1)^2 \qquad \textbf{Equation 3 - 14}$$

A third-order, N=3, reduced polynomial model is called the Yeoh model. This function can fit data over a large strain range, be used with limited data and will represent the other modes not present in the supplied data. This model can capture the upturn at higher strains. The Yeoh model is presented in Equation 3-15. For the Yeoh model the initial shear modulus is $2*C_{10}$ and the initial bulk modulus is $2/D_1$. J_{el} is the same as for the other forms. Reduced polynomial models can be used with up to N=6.

$$W = \sum_{i=1}^{3} C_{i0}(\overline{I}_1 - 3)^i + \sum_{i=1}^{3} \frac{1}{D_i}(J_{el} - 1)^{2i} \qquad \textbf{Equation 3 - 15}$$

3.5.1.2.3. Ogden Model

The Ogden model uses the principal stretch ratios, λ, rather than the stress invariants, I. It is also unique in that the exponents are not required to be integers. Up to N=6 terms are allowed, although up to N=3 is common. This model can provide a good fit of data in large-deformation problems including the upturn. The problem with this model is that it should not be used with

one type of test data, especially if using multiple terms. The generalized Ogden model is shown in Equation 3-14. The initial bulk compressibility is again $2/D_1$. The initial shear modulus is shown in Equation 3-17. The J_{el} term is the same as all the previous models.

$$W = \sum_{i=1}^{N} \frac{2\mu_i}{\alpha_i^2}(\overline{\lambda_1^{\alpha_i}} + \overline{\lambda_2^{\alpha_i}} + \overline{\lambda_3^{\alpha_i}} - 3) + \sum_{i=1}^{N} \frac{1}{D_i}(J_{el} - 1)^{2i} \qquad \textbf{Equation 3 - 16}$$

$$\mu_o = \sum_{i=1}^{N} \mu_i \qquad \textbf{Equation 3 - 17}$$

3.5.1.2.4. Marlow Model

The Marlow model is a general first invariant model with the ability to exactly capture the behavior from one test mode. No curve fitting is required for this model. The representation of the other modes is reasonably good. This model is ideal when only one type of test data is available. The general form additively splits the strain energy into the deviatoric and volumetric parts. The deviatoric term is generated from inputting test data in uniaxial, planar or biaxial tension. The volumetric term is based on the input test data from volumetric tests or specifying the Poisson's ratio. The formulation of the Marlow model is shown in Equation 3-15.

$$W = W_{dev}(\overline{I}_1) + W_{vol}(J_{el}) \qquad \textbf{Equation 3 - 18}$$

3.5.1.2.5. Mullins Effect

The Mullins effect can be accounted for when using the hyperelastic functions provided in ABAQUS (ABAQUS 2007). The implemented model provides a damage type model which is developed based on input test data. The problem is that if the Mullins effect is used, the viscoelastic nature of the material cannot be modeled.

3.5.2. Viscoelastic Behavior

Accounting for the time-dependent behavior of HDR in ABAQUS can be accomplished in two ways. For both options, a hyperelastic function must be defined. The viscoelastic function and the hysteresis functions are the two methods implemented for viscoelastic solids.

3.5.2.1. Viscoelasticity

Finite strain viscoelasticity is the way to account for the time dependent properties of rubberlike materials. A Prony series is generated that modifies the hyperelastic material properties as a non-

dimensionalized multiplier. The Prony series can be evaluated with up to 13 terms. Definition of the series is through input of normalized creep or stress relaxation data. This representation only works for linear-viscoelasticity. Only one curve can be input. Because HDR does not behave as a perfect linear viscoelastic material, two options are available. The first is to average the stress relaxation or creep curves over the strain range. The second option is to use the hysteresis option.

3.5.2.2. Hysteresis

The hysteresis option for rubbers is based on the work by Bergstrom and Boyce (1998; 2000; 2001). The model in ABAQUS includes the perfect elastic spring, a hyperelastic material definition, in parallel with the time-dependent element. The effective creep strain in the time-dependent element is shown in Equation 3-19.

$$\dot{\varepsilon}^{cr} = A(\lambda^{cr} - 1)^{C}\sigma^{m} \qquad \textbf{Equation 3 - 19}$$

The positive exponent, *m*, characterizes the effective stress dependence on the effective creep strain. *C*, restricted to values between -1 and 0, characterizes the creep strain dependence on the creep strain rate. The constant *A* must be greater than 0 and maintains dimensional consistency. In addition to the terms in Equation 3-19, there is a stress scaling factor, *S*, defining the ratio of stress carried by the time-dependent spring-dashpot to the elastic spring. The typical values suggested in the development are illustrated in Equation 3-20. Unfortunately, there are no curve fitting options for this model. Fitting in ABAQUS requires a trial and error approach beginning with the numbers provided in the paper (Bergstrom and Boyce 2001).

$$\begin{aligned} S &= 1.6 \\ m &= 4 \\ C &= -1.0 \\ A &= \frac{5}{(\sqrt{3})^{m}}(\sec)^{-1}(MPa)^{-m} \end{aligned} \qquad \textbf{Equation 3 - 20}$$

3.5.3. Modeling Issues

There are several issues that should be discussed about finite element modeling of rubber materials and viscoelasticity. One of the first issues is the incompressibility of rubber. In general, if the material is not highly confined, incompressibility is a reasonable assumption. Hybrid elements are recommended for compressible hyperelasticity and required for incompressible

hyperelasticity. Hyperelastic materials can be used with solid, truss, beam and finite strain shell elements. They cannot be used with small-strain shell elements.

For an application where the rubber is highly confined, in addition to the tension test data, volumetric test data must also be input to accurately model behavior. For most elastomers, a bulk modulus of 290 ksi is a reasonable value. When using hyperelastic materials and the automatic material evaluation, the stability of the strain energy function must be verified. This information is output by ABAQUS at the end of the process. FEA is a very powerful tool for analyzing the dual nature of HDR, provided that the user understands the assumptions and models associated with hyperelastic and viscoelastic or hysteretic behavior. Critical to the process is verifying that the material properties generated match the test data with unit cube tests.

3.6. Summary

This chapter is a primer for structural engineers on the behavior and modeling of high damping rubber materials. It also presents the capabilities of finite element software to model the viscoelastic nature of rubber. Creation of a device utilizing rubber materials requires an understanding of rubber behavior. To analytically model the hybrid device, the material properties of the rubber must be created using the appropriate models and assumptions. The information presented in this chapter provides the basic knowledge necessary to test, design and analyze high damping rubber materials as part of development of the hybrid device concept.

Chapter 4. High Damping Rubber Material Testing and Finite Element Modeling

4.1. Introduction

Due to the complexities of analyzing rubber and the lack of a standard set of engineering constants, the material properties used for analysis and design must be developed from physical testing. The focus of the testing program is on generating the required data for ABAQUS. In the absence of test data, approximations could be used by finding test data from prior publications or contacting rubber manufacturers for their quality control test data.

4.2. Rubber Compounds

The high damping rubber compounds used in this research were donated and fabricated by Corry Rubber Corporation, Corry, Pennsylvania. A matrix of the six tested compounds is presented in Table 4-1. Four of the compounds are carbon-black filled natural rubber (NR). Within the four NR samples, there are two levels of Shore hardness and two levels of damping. The remaining two samples are butyl rubber (BR) with higher inherent damping and two levels of hardness. Each of the compounds represents a unique combination of stiffness and damping properties. All compounds will be generally referred to as high damping rubber (HDR). Specific reference to natural or butyl rubber will be understood from the context.

Table 4 - 1 High Damping Rubber Compounds

Compound Name	Rubber	Hardness (Shore A)	Damping Level
NR-40L	Natural	40	Low
NR-60L	Natural	60	Low
NR-40H	Natural	40	High
NR-60H	Natural	60	High
BR-40H	Butyl	40	High
BR-60H	Butyl	60	High

4.2.1. Natural Rubber (NR)

Isoprene is the chemical name for raw natural rubber. It is one of the most versatile general purpose elastomers. The benefits of NR include higher relative tensile strength, extensibility and high elasticity. It also has good resistance to tearing, flexure and abrasion. However, it has a low resistance to oxidation and ozone attack as well as being seriously affected by industrially used

oils including petrol, benzene and lubricating oils. The resistance to oxidation and ozone can be improved with additives. The natural rubber samples used in the testing are carbon black filled natural rubber specifically designed to dissipate energy during straining.

4.2.2. Butyl Rubber (BR)

Butyl rubber is a synthetic rubber which is a copolymer of isobutylene and a small percentage of isoprene. BR has very good resilience properties for a rubber with a low glass transition temperature (about -70º C). Other highly desirable properties of BR include resistance to ozone, weather, heat and chemicals, low gas permeability and good abrasion resistance. It also has excellent damping qualities. Some typical uses include inner tubes, bladders of inflatable balls, dock fenders and motor mounts (*Rubber Engineering* 2000). The high damping butyl rubbers tested are specifically formulated to have a high loss factor.

4.3. Material Testing

Material characterization testing was used to generate the required data for FEA models. The test matrix included static, dynamic and time-dependent tests. Static testing included uniaxial tension, planar tension or pure shear, and simple shear. Dynamic testing consisted of uniaxial tension specimens cycled from 25% strain to 50% strain and simple shear specimens cycled at four frequencies and three displacement levels. Multi-step stress-relaxation testing was completed for all of the loading conditions at various strain levels.

4.3.1. Testing Equipment

The testing machine used was an MTS 244 Series Servo-hydraulic testing machine with Test Star Classic software for data acquisition. The maximum stroke capability is 6 in. with maximum force capacity of 10 kips. The force during testing was measured with a 500 lb load cell for the planar and uniaxial tension testing. The strain for uniaxial and planar tension was measured with a non-contact laser extensometer having a beam width of 2.5 in. A 5000 lb load cell was needed for the simple shear testing. The crosshead measurement with compensation for the test set-up was used for the simple shear tests.

Use of the laser extensometer required applying contrasting color strips to the rubber samples. White strips have the greatest contrast and after trying labels provided by the extensometer manufacturer, a white marker and a white-out pen, the best option was found to be white electrical tape. The spacing between the strips on the uniaxial tension specimens was the width

of the uniaxial specimen, approximately 0.375 in. The minimum distance from the grip was determined through finite element analysis. A simple model with approximate properties was analyzed to determine the minimum distance from the edge to be outside the influence of edge effects. This distance was determined to be twice the width of the specimen. To be conservative, 0.125 in. was added for a distance of 0.875 in. from the grips. For the planar tension specimens, the strips were placed approximately 0.125 in. apart, centered between the grips.

The grips for the uniaxial and planar tension samples had medium grit sandpaper glued to both sides to reduce slippage. Both of the grips were made of steel angles back-to-back with 1/4 in. diameter bolts to close the grips. For the planar tension samples, holes were punched in the samples with the same pattern as the grips.

4.3.2. Sample Preparation

The materials for the uniaxial and planar tension samples were shipped as 6 in. x 6 in. x 0.08 in. flat sheets. Six sheets of each compound were provided. The sheets were cut into the appropriate sized test specimens using a rotary cutter to avoid scalloping. The planar tension specimens were then marked with the appropriate hole pattern. The holes were cut using a punch. The simple shear specimens were shipped in the as-tested configuration. The shear specimens consist of two rubber pads sandwiched between three pieces of steel. The rubber was bonded to the steel during the curing process for the rubber. All specimens were measured using a Vernier caliper to determine the cross-sectional area of the specimens.

4.3.3. Uniaxial Tension Testing

Uniaxial strip test specimens 0.375 in. wide by 0.08 in. thick by 6 in. long were tested in static tension, cyclic tension and tensile stress relaxation. The length and width were chosen to ensure that the width of the specimen was approximately 1/10 of the length between the grips (approximately 4 in.), ensuring a state of pure tension in the sample (Gent 2001). Five specimens of each rubber compound were tested. To determine the steady state properties in static tension, the sample was tested to the ultimate strain level 10 times. A large number of static cycles is required to remove the Mullins effect and determine the steady-state properties. Because of the viscoelastic properties of the rubber, a rest period of 5 minutes was allowed between strain cycles for the specimen to return to the undeformed length. The crosshead speed was maintained at a constant rate of 50 mm/min (2 in./min) to stay in the static range (Brown 1996). Cyclic

tension was conducted following the last static uniaxial strain cycle. The specimen was ramped up to a 50% strain level and then cycled down to 25% in a sinusoidal wave. The frequencies used were 0.5, 2.0 and 4.0 Hz for 50 cycles each. Stress relaxation tests were run at 50% and 100% strain and held for 1000 seconds. A schematic and photo of the test set-up is shown in Figures 4-1 and 4-2 respectively. Table 4-2 shows the testing protocols.

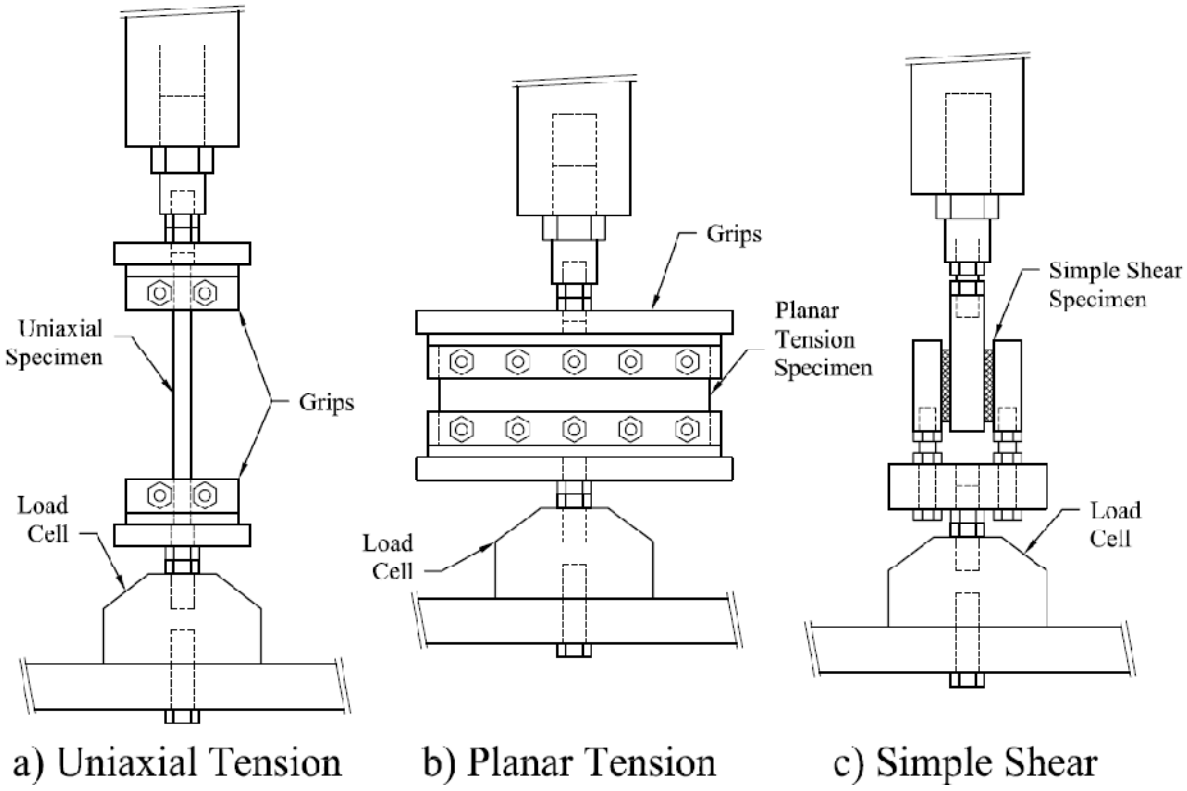

Figure 4 - 1 Schematic Drawing of Test Set-ups

4.3.4. Planar Tension Testing

A planar tension specimen of the same thickness as the uniaxial specimen was tested. The specimens had a width at least 10 times more than the length (Gent 2001). The width of the specimen is 6 in. and the distance between the grips was 0.5 in. Neglecting the edge effects puts the central part of the specimen into a pure shear condition (Treloar 2005). These specimens, five of each compound, were tested in a similar manner to the uniaxial tension samples. The static tension testing was done in the same fashion as for uniaxial tension but they were strained to 300%. Stress relaxation tests were run at strain levels of 50%, 100% and 150% and held for 1000 seconds at each strain level. Cyclic tests were not run for the planar tension specimens. The uniaxial tension cyclic tests were only run in case there was a problem with the cyclic shear data.

The value attributed to the planar tension cyclic data was not worth the time to complete the tests.

Table 4 - 2 Material Testing Protocol

Uniaxial Tension Testing Protocol	Planar Tension Testing Protocol	Simple Shear Testing Protocol
Static Tension Step (Repeat 10 Times)	**Static Tension Step (Repeat 10 Times)**	**Static Shear Step (Repeat 10 Times)**
1) Ramp Up -Elongation Rate - 50 mm/min -Maximum Strain - 130% 2) Ramp Down 3) Hold Period - 250 seconds	1) Ramp Up -Elongation Rate - 25 mm/min -Maximum Strain - 300% 2) Ramp Down 3) Hold Period - 250 seconds	1) Ramp Up -Elongation Rate - 25 mm/min -Maximum Shear Strain - 115% 2) Ramp Down -Elongation Rate - 25 mm/min -Maximum Shear Strain - (-115%) 3) Hold Period - 120 seconds
Cyclic Tension Step	**Tensile Stress Relaxation Step**	**Cyclic Shear Step**
1)Initial Step Up -50% Strain level 2) 0.5 Hz Frequency Cycles -Upper Level - 50% Strain -Lower Level - 25% Strain -50 Cycles 3) 2.0 Hz Frequency Cycles -Upper Level - 50% Strain -Lower Level - 25% Strain -50 Cycles 3) 4.0 Hz Frequency Cycles -Upper Level - 50% Strain -Lower Level - 25% Strain -50 Cycles 4) Ramp Down 5) Hold Period - 300 seconds	1) Initial Step Up -50% Strain Level 2) Hold at Constant Strain - 1000 seconds 3) Second Step Up -100% Strain Level 4) Hold at Constant Strain - 1000 seconds 3) Third Step Up -150% Strain Level 4) Hold at Constant Strain - 1000 seconds 5) Step Down	1) 0.5 Hz Cycles -Displacement Levels - 25%, 50%, 100% -50 Cycles/ Displacement Level 2) 1.0 Hz Cycles -Displacement Levels - 25%, 50%, 100% -50 Cycles/ Displacement Level 3) 2.0 Hz Cycles -Displacement Levels - 25%, 50%, 100% -50 Cycles/ Displacement Level 4) 4.0 Hz Cycles -Displacement Levels - 25%, 50%, 100% -50 Cycles/ Displacement Level
Tensile Stress Relaxation Step		**Shear Stress Relaxation Step**
1) Initial Step Up -50% Strain Level 2) Hold at Constant Strain - 1000 seconds 3) Second Step Up -100% Strain Level 4) Hold at Constant Strain - 1000 seconds 5) Step Down		1) Initial Step Up -25% Displacement Level 2) Hold at Constant Strain - 250 seconds 3) Second Step Up -50% Displacement Level 4) Hold at Constant Strain - 250 seconds 3) Third Step Up -75% Displacement Level 4) Hold at Constant Strain - 250 seconds 5) Fourth Step Up -100% Displacement Level 6) Hold at Constant Strain - 250 seconds 7) Step Down

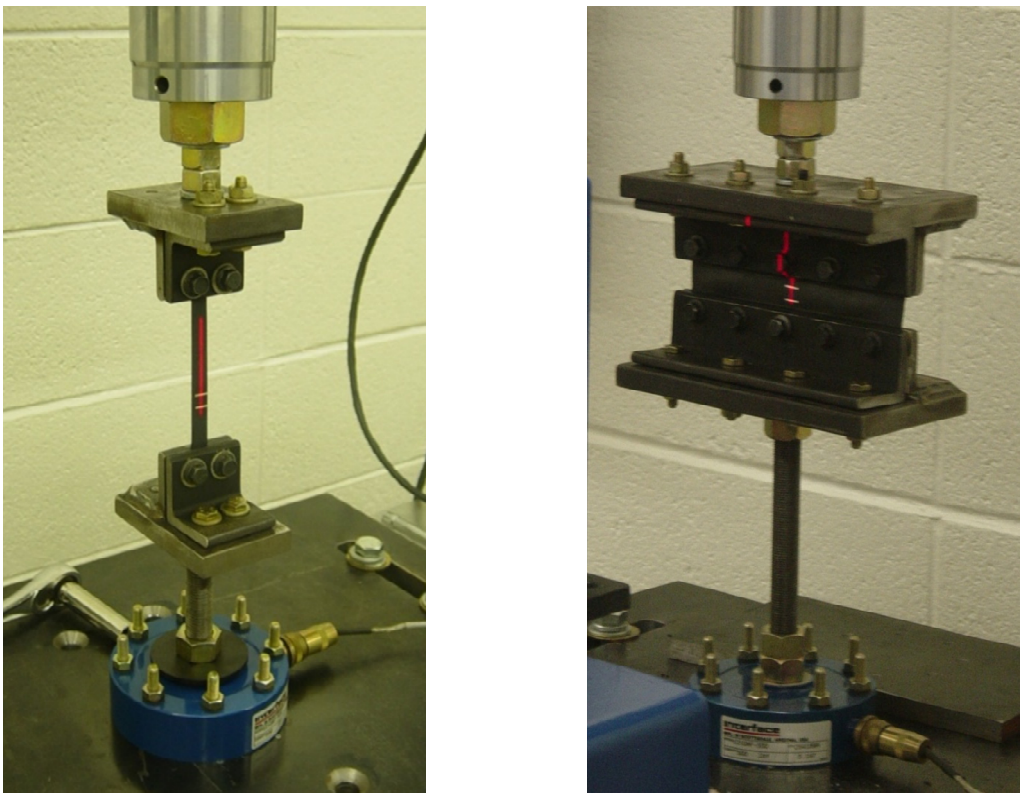

a) Uniaxial Tension Test Set-up b) Planar Tension Test Set-up

Figure 4 - 2 Uniaxial and Planar Tension Test Set-up

4.3.5. Simple Shear Testing

The simple shear specimens used in this research were standard double sandwich specimens with dimensions shown in Figure 4-3. The shear area for each layer of rubber was 1.0 in.^{2} and the thickness of the rubber pad was 0.2 in. The rubber was bonded to the steel during the vulcanization process. The bond in this case is considered stronger than the rubber. The specimens were tested in static shear up to a strain of 115% which corresponds to a displacement of 2.5 times the thickness of the rubber pad. The static testing started at the zero displacement level and ramped up to a positive displacement and then back through zero to a negative displacement, and then back to zero. This cycle was repeated 10 times to find the steady-state material properties. Displacement was measured using the crosshead displacement while compensating for the test apparatus flexibility.

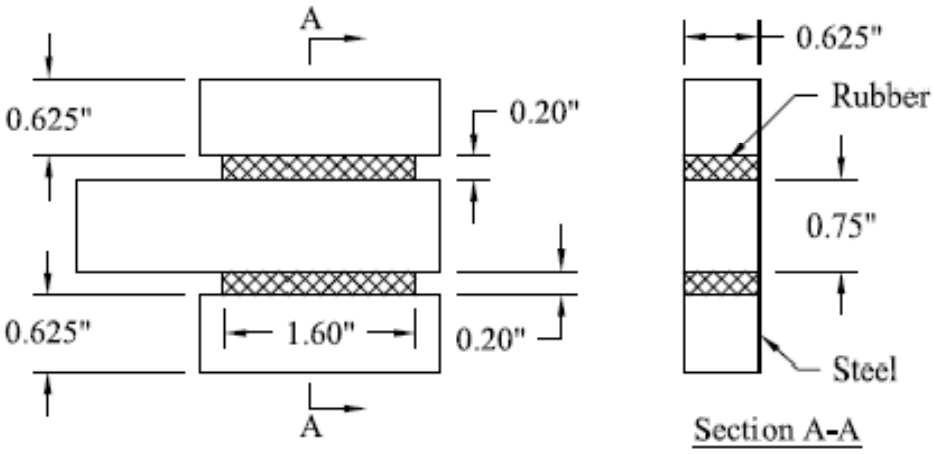

Figure 4 - 3 Simple Shear Specimen Dimensions

Dynamic simple shear tests were carried out at four displacement levels. Displacement percentages of 25%, 50%, 75% and 100% of the rubber thickness were used. The displacement percentage is the displacement of the outer block divided by the thickness of the rubber pad. The frequencies used in the tests were 0.5, 1.0, 2.0 and 4.0 Hz. Tests were carried out for 50 complete sinusoidal cycles which is the preferred waveform (Brown 1996). The number of cycles was chosen to determine if a loss in stiffness or damping levels was observed due to a long event. The frequencies and strain levels were selected to simulate periods of vibration and strain levels in actual applications.

Multi-step stress relaxation tests were carried out using simple shear specimens at the same displacement levels as the cyclic tests. The specimen was held at the prescribed strain for 250 seconds. This was reduced from 1000 seconds due to the negligible change past 250 seconds. A test schematic and photo are shown in Figures 4-1 and 4-4. Table 4-2 shows the testing protocols.

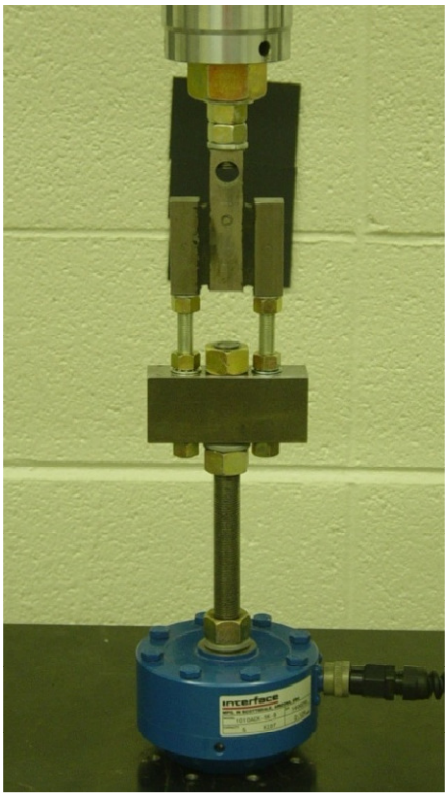

Figure 4 - 4 Simple Shear Test Set-up

4.4. Material Testing Results

The experimental results are presented for each of the three deformation states. Both rough and reduced data are presented along with a discussion of the methods for data reduction and test results. A representative sample of the raw and reduced data is presented. Data for all the specimens is presented in Appendix A.

4.4.1. Uniaxial Tension Results

The testing carried out in the uniaxial tension state included static tension, cyclic tension and multi-step stress relaxation. The cyclic tension and stress relaxation tests were not required for the generation material properties in the finite element analysis program. They were carried so the data would be available if needed.

Static tension tests are essential for input into ABAQUS to define the hyperelastic function. It was hoped that strains up to 150% could be achieved in tension. Due to the length of the laser extensometer beam, a maximum strain of 130% was possible. In some cases, due to differences in the distance between the strips of electrical tape of the specimens and slippage in the grips, 130% was not reached. For all the specimens, a minimum of 120% strain was achieved. The tests

were run under displacement control. In some cases, the white strips went outside the limits of the laser beam. When this occurred, the strain reading remained at its last good reading so this could be easily located in the raw data.

The raw tension data clearly illustrates the Mullins effect (see Figures 4-6 through 4-8). The difference between the first and second cycle is the most significant. The stiffness change between successive cycles diminishes to the point that after the fifth or sixth cycle a steady-state curve is present. Even though the tests are carried out in a static manner, the difference in the loading and unloading path demonstrates the capacity to dissipate energy. The difference in damping level can be seen graphically on the stress-strain plots of the various materials. Permanent set is also visible for the cycles following the first cycle. The amount of set differed depending on the compound. One other observation made during testing was that for the natural rubber samples a white film was apparent on the samples after testing. This is due to anti-oxidants additive in the natural rubber samples. The anti-oxidant is used to reduce tension cracking in the rubber, so the film demonstrates the additive working. The same film did not appear on the butyl samples. This makes sense as BR has a greater resistance to ozone attack so the additive is not required. Raw data is shown for several representative uniaxial tension samples in Figures 4-5 through 4-7.

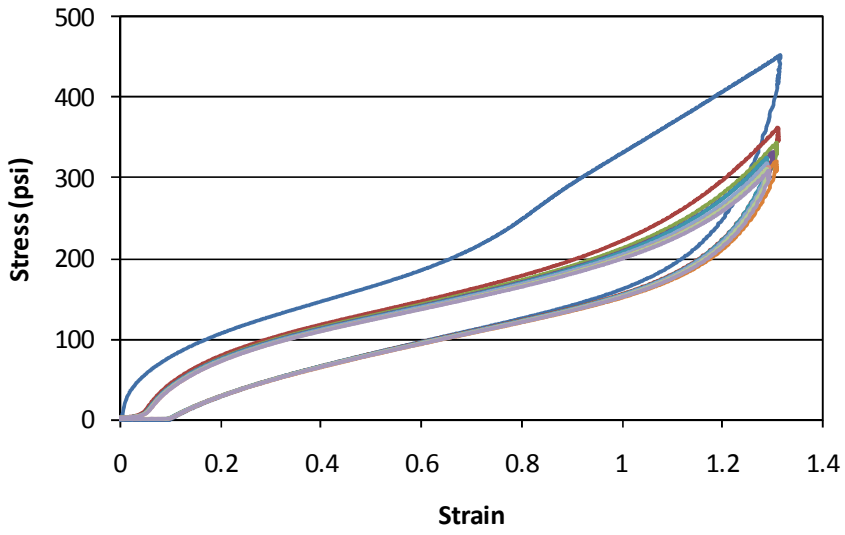

Figure 4 - 5 NR60H-5 Uniaxial Tension Raw Data

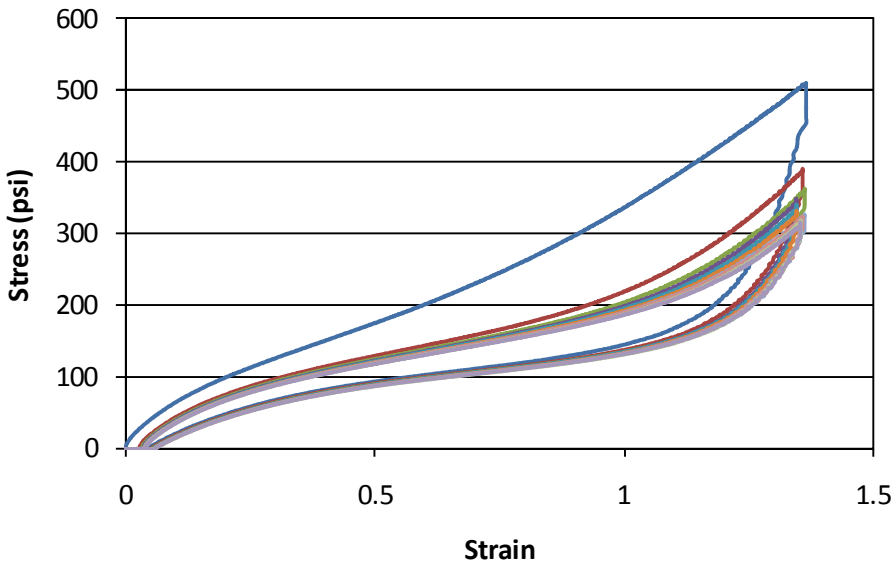

Figure 4 - 6 NR60L-5 Uniaxial Tension Raw Data

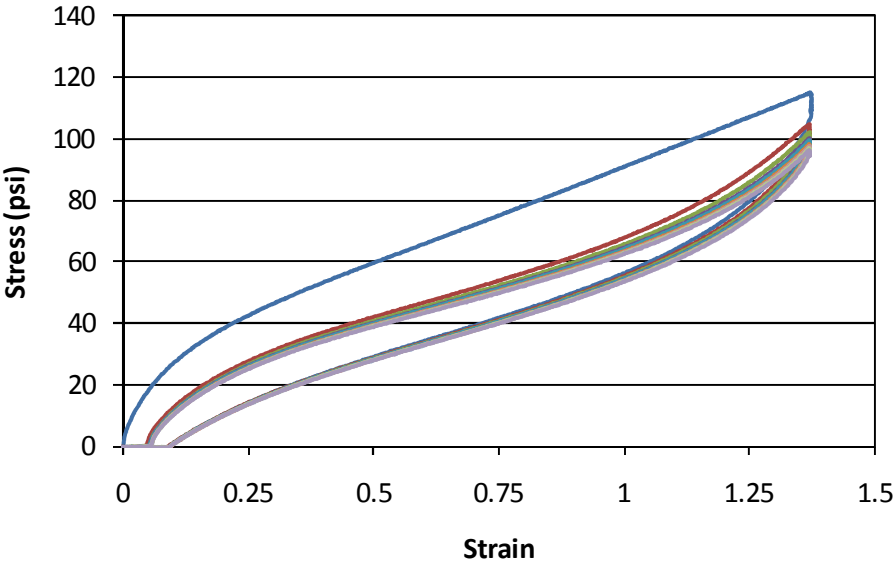

Figure 4 - 7 BR40H-2 Uniaxial Tension Raw Data

Determining the representative stress-strain curve for each rubber compound required an average of the data from the five specimens. Data from each of the five specimens, for the 8^{th}, 9^{th} and 10^{th} cycles was used for a total of 15 representative curves. The first step in data reduction included cutting off the unloading portion at the top. Secondly, the permanent set was removed by adjusting both the strain and the stress so the curve started at the origin. Determining the permanent set required finding the point where slack due to the increased specimen length is

removed and the steady state stress-strain curve began. The slope of this early portion of the curve was used to extrapolate the location of the x-intercept. The x-intercept is the value used for the permanent set. Once the amount of permanent set is determined, all the strains are modified for the new initial length and the stress is modified for the new area. The modified area was based on the assumption of a Poisson ratio of 0.5. The equations are shown as Equation 4-1. In the equations, ε and σ are the modified stress and strain. Stress and strain before accounting for permanent set are ε_o and σ_o. The permanent set is represented by ε_{ps}.

$$\varepsilon = \frac{\varepsilon_o}{1+\varepsilon_{ps}}$$

$$\sigma = \frac{\sigma_o}{(1-\upsilon\varepsilon_{ps})^2}$$

Equation 4 - 1

Averaging the 15 curves required determining a curve fit for the reduced stress-strain curves. Due to the nonlinearity of the curves, a sixth-order curve fit was used. The lowest R value was 0.991 with the typical value being 0.997, indicating that the curve fits were a good representation. Averaging was done in a table with all 15 trend line functions evaluated at specific strains. The values were averaged at each strain to generate the average curve. The average curves would only extend as high as the lowest strain of the five samples. The curve for input into ABAQUS was generated using a fourth-order curve fit on the average curve to remove any discontinuities from averaging as well as to reduce the order for better stability during analysis. An example of reduced data with the trendline is shown in Figure 4-8 including the R value. The dotted line represents the data and the solid line is the trendline.

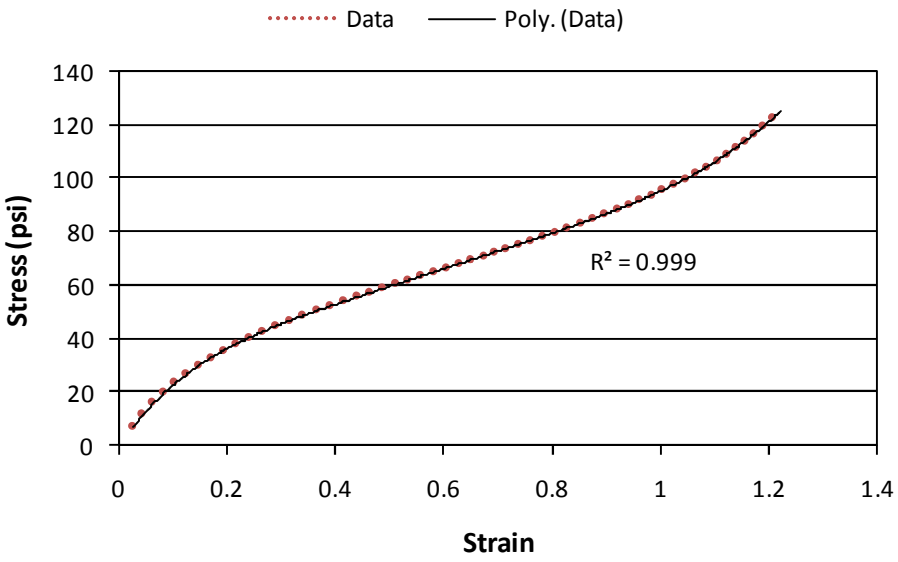

Figure 4 - 8 Reduced Uniaxial Tension Data with Curve Fit (NR40H-2-Cycle 10)

Average curves and modified curves of two compounds are shown in Figures 4-9 and 4-10. The dotted lines represent the curve fits of the various steady state stress-strain curves with the permanent set removed. The thick solid line represents the average.

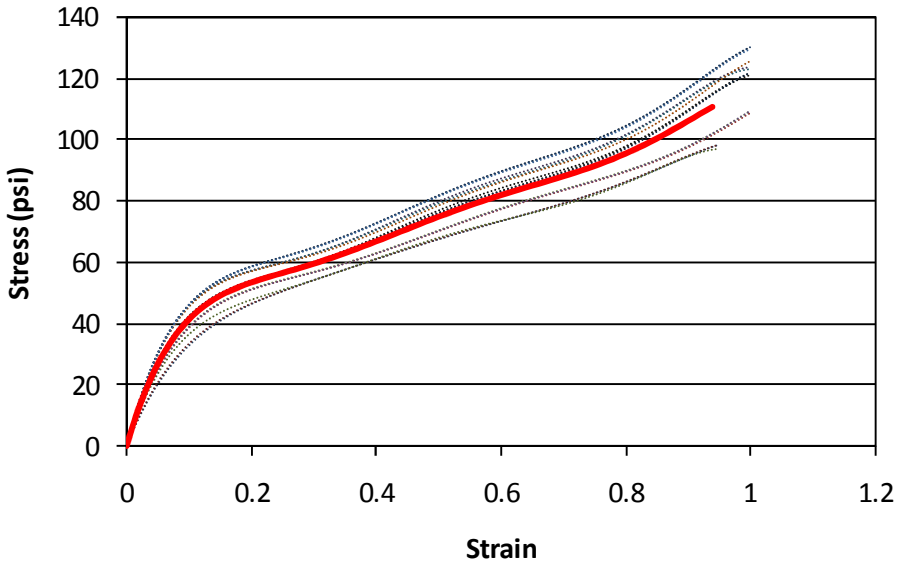

Figure 4 - 9 BR60H Uniaxial Tension Representative Curves

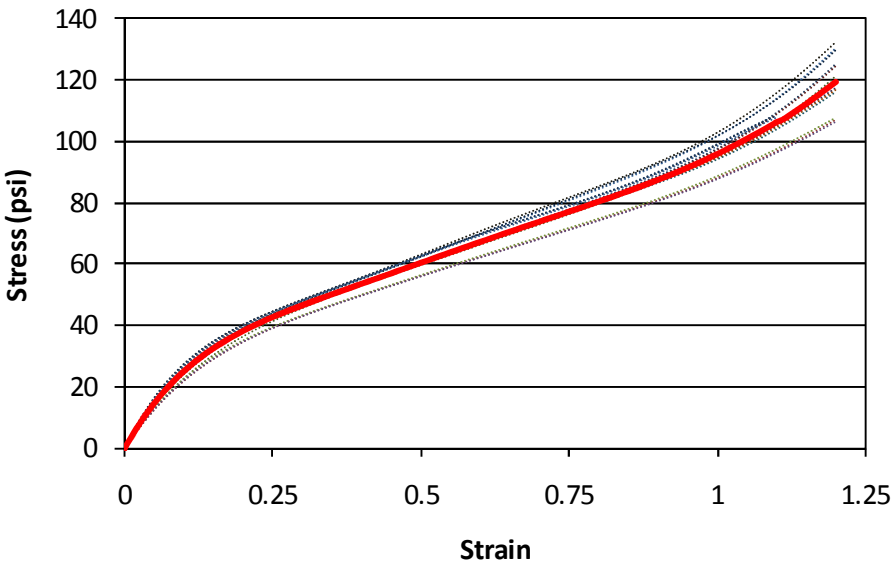

Figure 4 - 10 NR40H Uniaxial Tension Representative Curves

4.4.2. Planar Tension Results

Planar tension samples were tested in static tension and stress relaxation. The static tension results are used for input into ABAQUS. The planar tension samples were tested in displacement control up to 250% strain. Because of the larger forces, strains between the white strips were not always up to the desired level because of larger slip occurring at the grips and around the holes in the specimen. Many observations from uniaxial testing apply to the planar specimens. The Mullins effect is very apparent in the first couple of cycles, and by the 5^{th} or 6^{th} cycle a steady-state behavior is evident. The white film on the specimens after testing appeared on natural rubber specimens but was not observed on the butyl rubber specimens.

Determining the average curve for each compound followed the same procedure as for the uniaxial specimens. The 8^{th}, 9^{th} and 10^{th} cycles for each specimen were modified for permanent set and then averaged with the other samples. Typical R values of 0.996 for the trend lines were observed for planar tension specimens. The modified curve had maximum strains of around 170%. Before being input into ABAQUS, a fourth-order curve fit was used for the average data. This was done to remove any discontinuities as well create a more stable curve for use in analysis. This procedure was used for the uniaxial and simple shear data as well. Raw data for three samples are presented in Figures 4-11 through 4.13. The average curves with the modified specimen curves are shown in Figures 4-14 and 4-15.

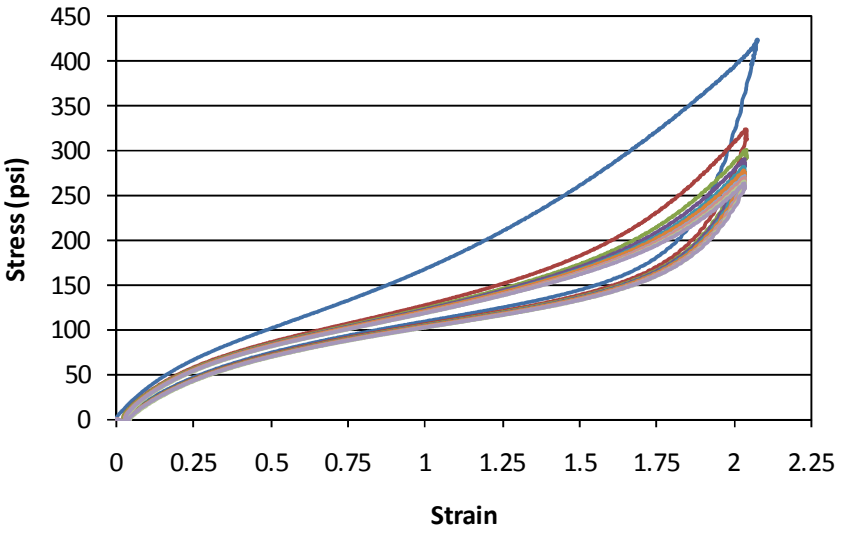

Figure 4 - 11 NR40L-1 Planar Tension Raw Data

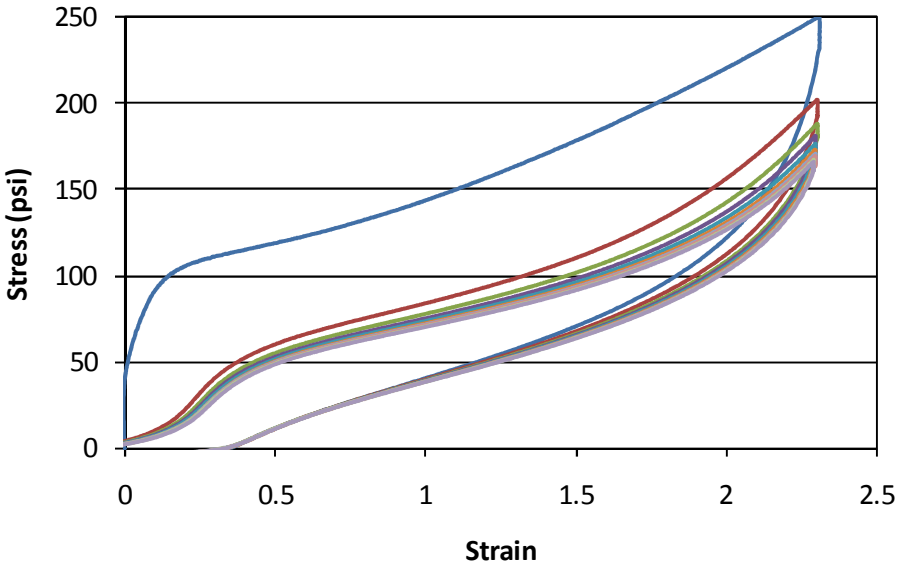

Figure 4 - 12 BR60H-3 Planar Tension Raw Data

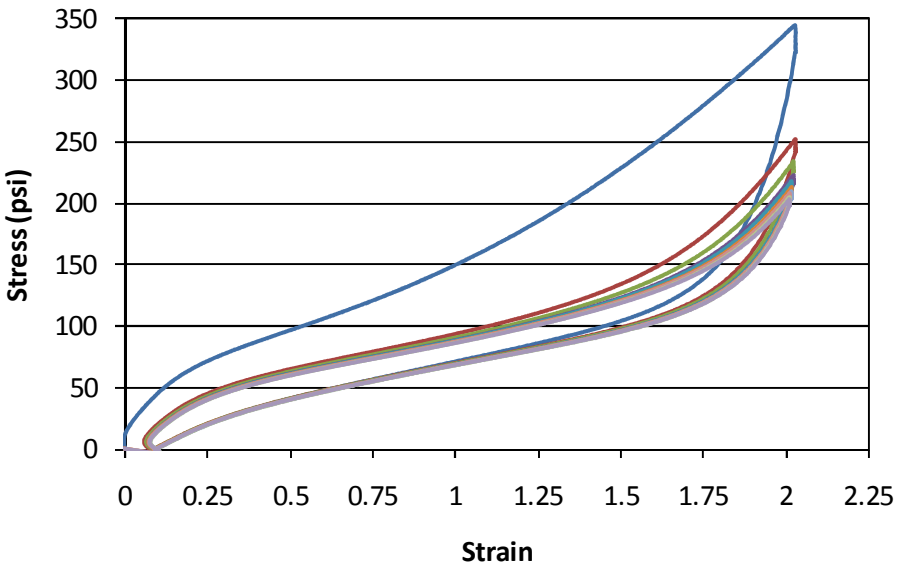

Figure 4 - 13 NR40H-4 Planar Tension Raw Data

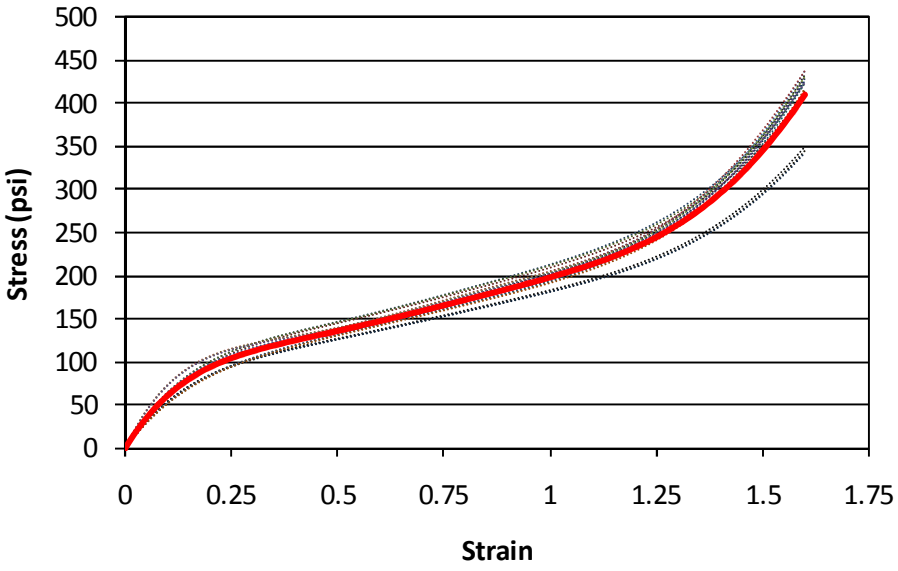

Figure 4 - 14 NR60L Planar Tension Representative Curves

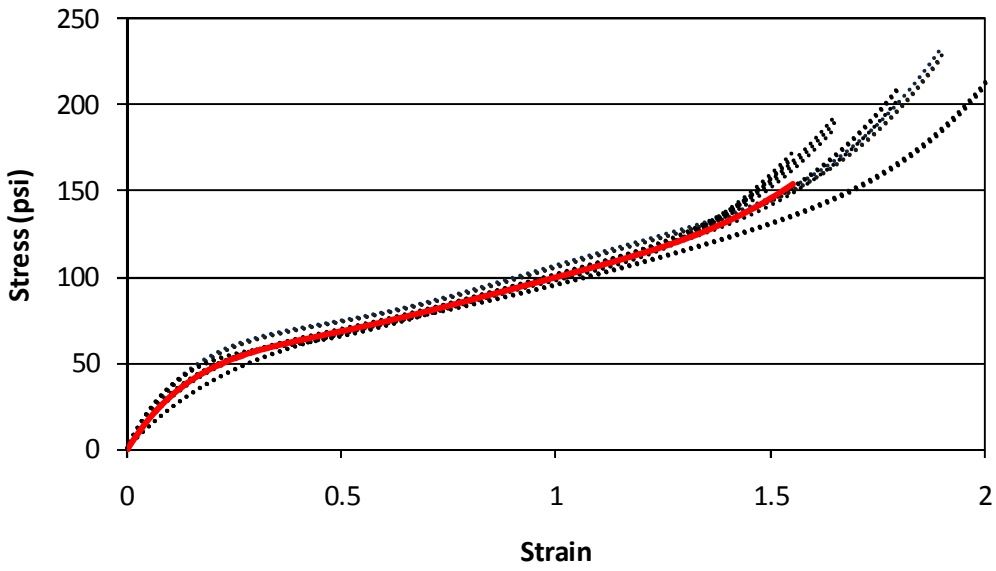

Figure 4 - 15 NR40H Planar Tension Representative Curves

4.4.3. Simple Shear Results

Simple shear specimens were tested in static, cyclic and simple shear stress relaxation. The stress relaxation results are the only results that will be directly input into ABAQUS. The static and cyclic tests, however, were used to measure the accuracy of the material models generated from the experimental input. All three types of test results are presented. There were only three simple shear samples of each compound.

4.4.3.1. Static Simple Shear

Only tension inputs are used to determine the hyperelastic function in ABAQUS. However, since the likely deformation state for the damper will be simple shear, the ability to accurately model the static simple shear behavior is critical. The automatic material evaluation in ABAQUS has the option to output the shear stress-strain curve for the hyperelastic models selected.

Ten cycles of static shear were run for each specimen. The maximum and minimum displacements of the cycle were determined by the thickness of the rubber pad. The displacement was 200% of the thickness of the pad in both directions. The reason the samples were tested to both extremes was to determine whether or not the stress-softening had to occur in both directions. The results demonstrate that the strain in the positive direction also had a softening effect in the negative direction. This can be seen in the raw data shown in Figures 4-16 and 4-17. The first cycle in the negative direction is lower than the corresponding positive cycle. The

reduction of the shear data was much simpler because of the deformation state. The only modification to the data was for the small stress present prior to beginning the cycling, typically on the order of 3 to 5 psi. The same procedure of using a trend line for averaging the positive 8th, 9th and 10th cycle of each specimen was again used to determine the average shear stress-strain curve. The unique shape typical of HDR stress-strain data is readily apparent in the raw data. Figures 4-18 and 4-19 present average curves for two compounds.

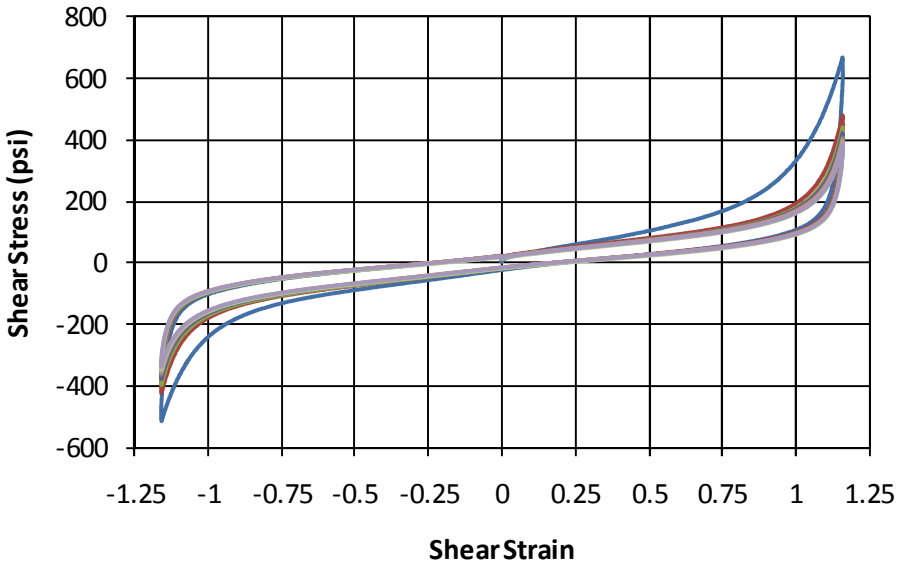

Figure 4 - 16 NR60H-3 Simple Shear Raw Data

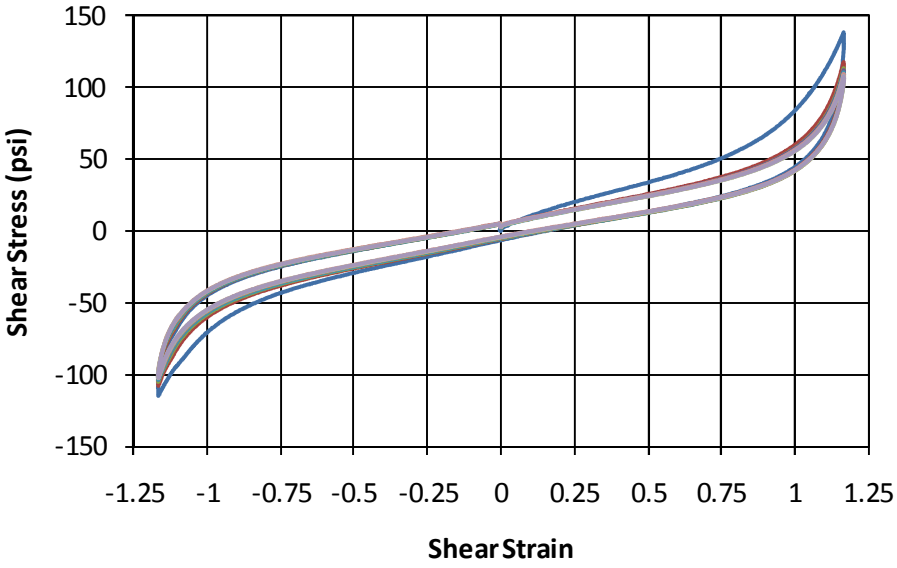

Figure 4 - 17 BR40H-2 Simple Shear Raw Data

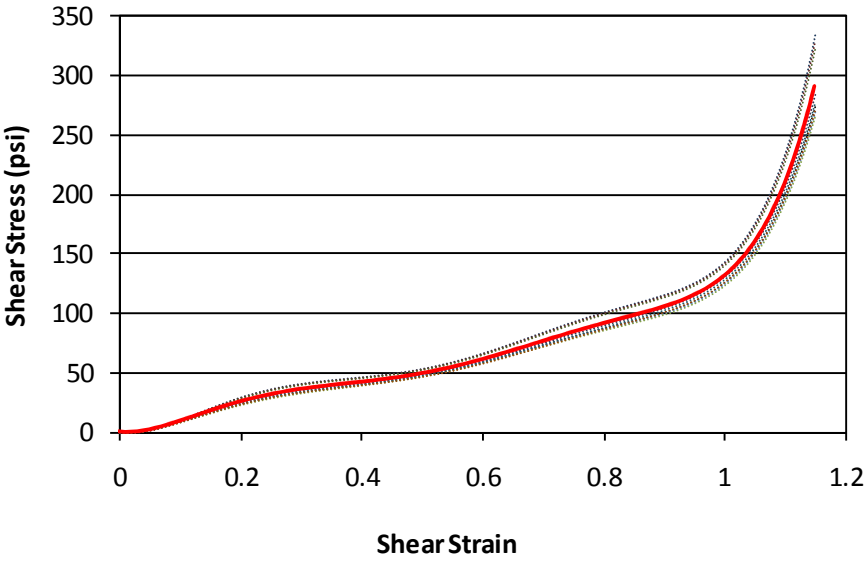

Figure 4 - 18 NR60L Static Simple Shear Representative Curves

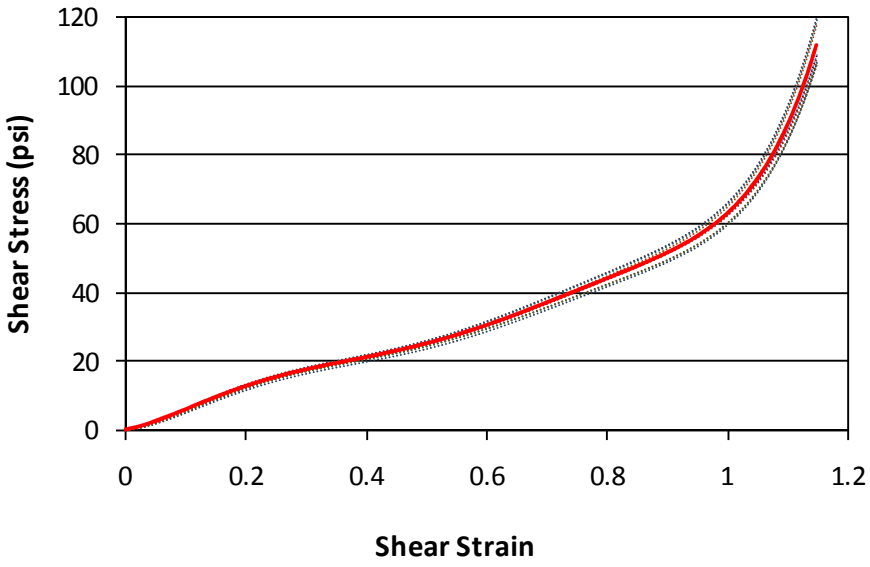

Figure 4 - 19 NR40H Static Simple Shear Representative Curves

4.4.3.2. Cyclic Simple Shear

Cyclic simple shear tests were carried out at three strain levels and four frequencies. The strain levels correspond to displacement levels of 25%, 50% and 100% of the thickness of the rubber pad. The frequencies, 0.5, 1.0, 2.0 and 4.0 Hz, correspond to typical modal frequencies of buildings and frequencies contained in earthquake records. Although this data was not directly used in ABAQUS, determining the adequacy of the finite element model is done by comparison of the analytical and experimental hysteretic and cyclic plots. Several hysteretic and stress and strain versus time plots are shown in Figures 4-20 through 4-22. In Figure 4-21 the plot shows the phase difference between the stress and the strain. It is easiest to see when the traces cross the horizontal axis. The change in the damping can also be seen as the difference between the 25% and 100% displacement levels. For the stress and strain plot versus time, the vertical axis is normalized for both stress and strain relative to the maximum values. The hysteresis plot in Figure 4-22 shows that for the same strain level and different frequencies, the loops are similar. The minor differences can be seen in the change in loss factor as the frequency increases. This dependence on frequency and strain is typical for filled rubbers.

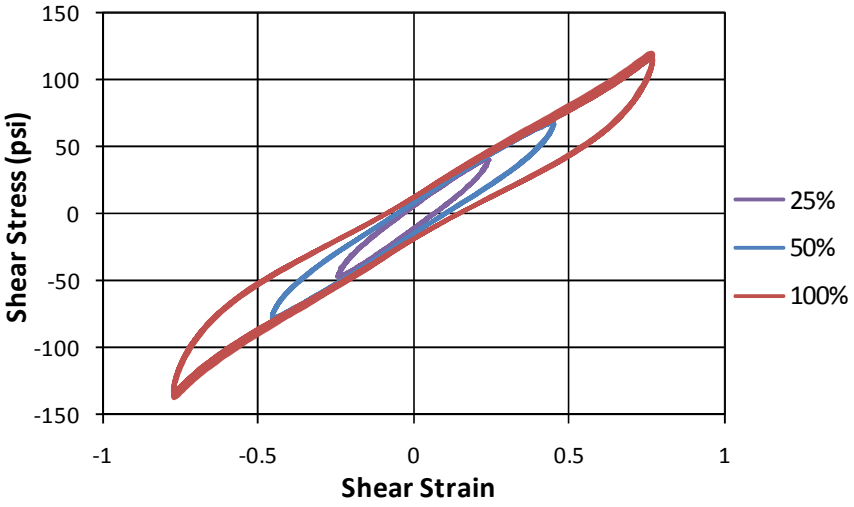

Figure 4 - 20 Hysteresis Loops NR60H-2 (1.0 Hz)

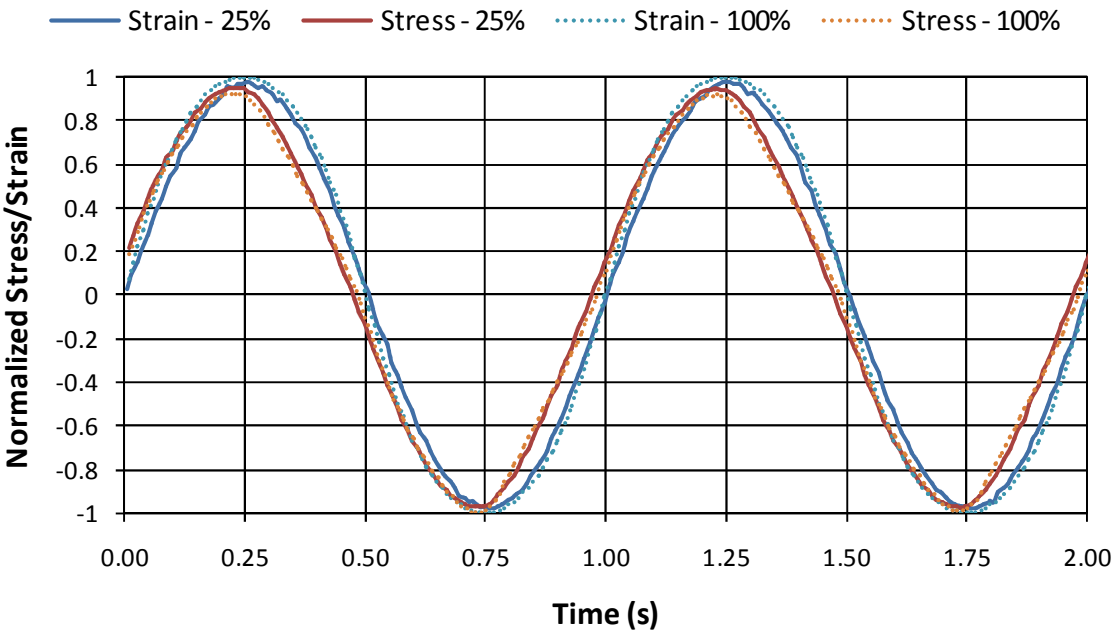

Figure 4 - 21 Cyclic Stress and Strain Plot NR60H-2 (1.0 Hz)

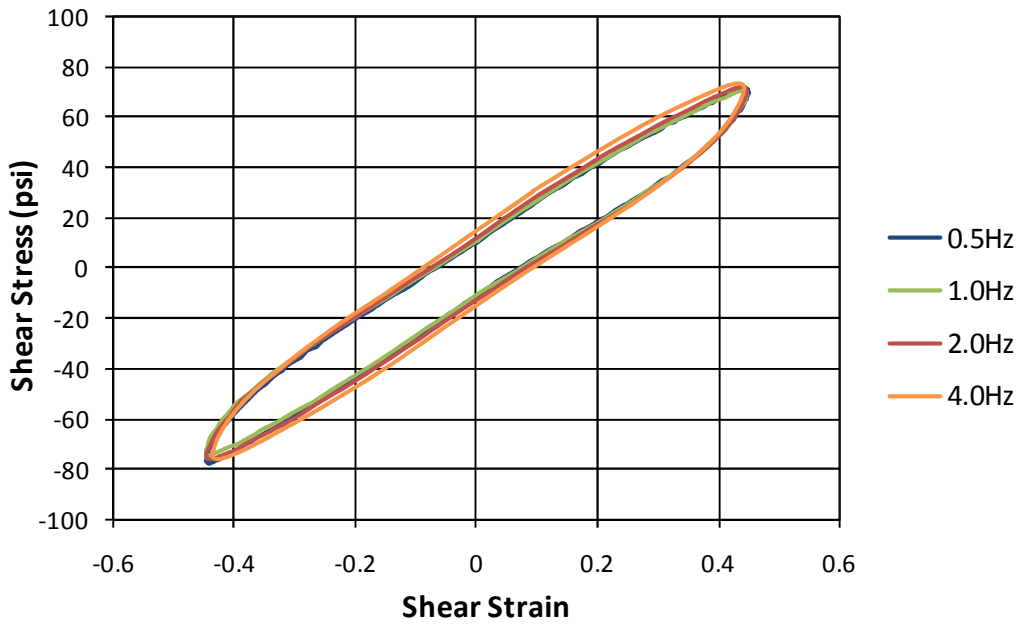

Figure 4 - 22 Hysteresis Plot NR60H-3

As an approximation, the plots of the stress and strain versus time were used to calculate the approximate loss factor based on the phase angle. This was done by determining the time lag of the shear strain. The time lag is then converted to a phase angle by multiplying by 2π times the frequency. The loss factor is equivalent to the tangent of the phase angle. The loss factor was also calculated by using the area of the hysteresis loops divided by the product of the elastic strain energy and 2π. The results from the two methods were equivalent. The sample with the highest loss factor is BR60H with a loss factor as high as 0.40. The lowest damping material is the NR40L which had an average loss factor of about 0.03. The values for 100% displacement and 4.0 Hz are excluded, because the time interval for recording data was not small enough to capture the curves. Figures 4-23 and 4-24 show the loss factors at the various frequencies and displacement percentages for two of the higher damping materials. It should be noted that the horizontal axis is displacement percentage and not shear strain. Table 4-3 shows the data for all the compounds. The general trend is that with increased displacement, the damping decreases and increased damping occurs at higher frequencies.

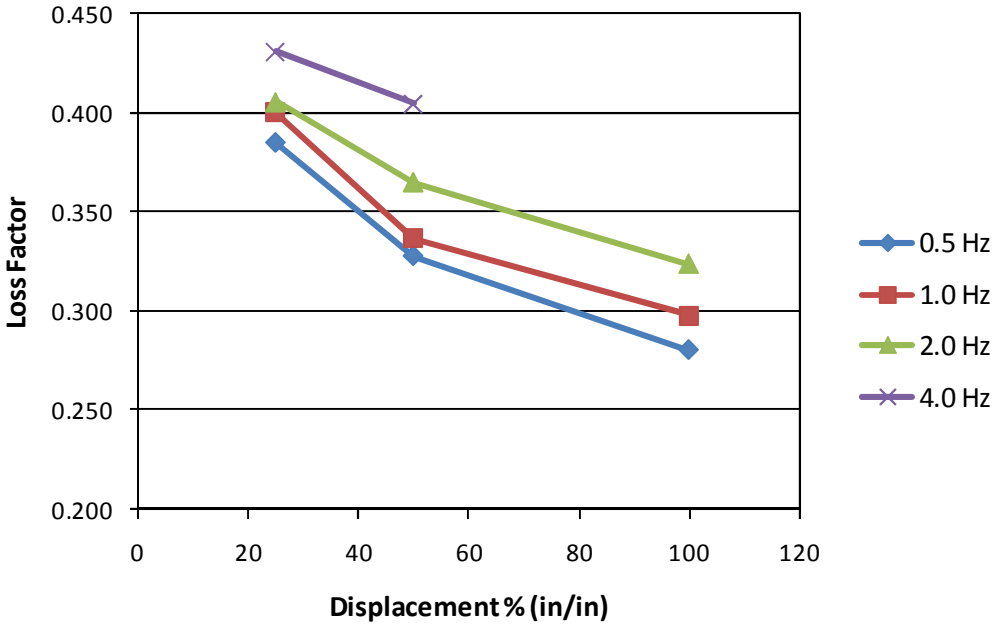

Figure 4 - 23 BR60H Loss Factor

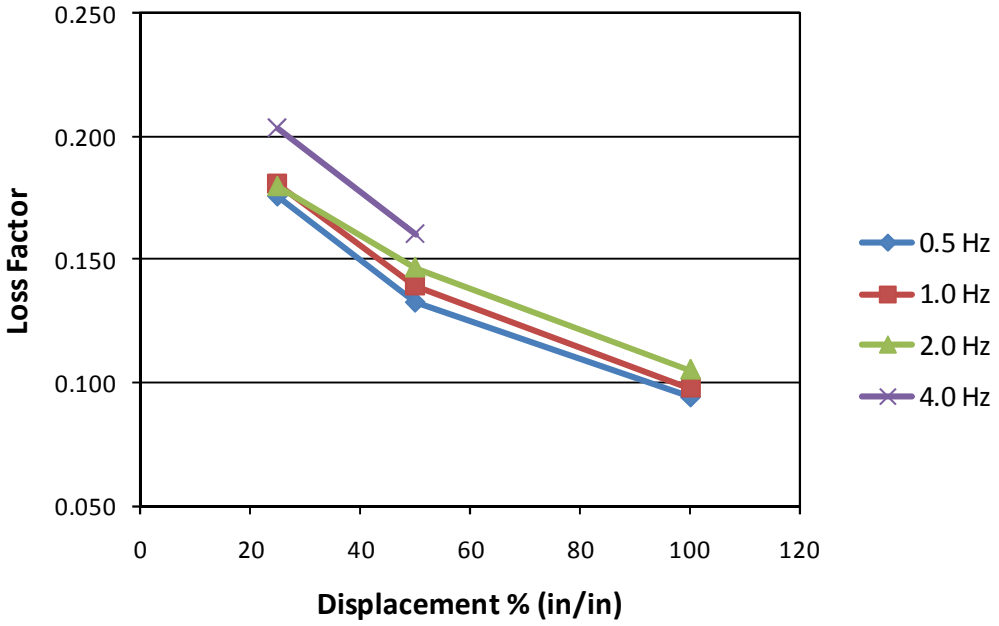

Figure 4 - 24 NR40H Loss Factor

Table 4 - 3 HDR Material Loss Factor

Frequency (Hz)	Displacement % (in/in)	Material Loss Factor					
		BR40H	BR60H	NR40H	NR40L	NR60H	NR60L
0.50	25	0.18	0.38	0.18	0.02	0.17	0.09
0.50	50	0.17	0.33	0.13	0.03	0.14	0.08
0.50	100	0.14	0.28	0.09	0.03	0.11	0.06
1.00	25	0.21	0.40	0.18	0.04	0.17	0.11
1.00	50	0.19	0.34	0.14	0.04	0.13	0.08
1.00	100	0.16	0.30	0.10	0.03	0.11	0.07
2.00	25	0.21	0.41	0.18	0.04	0.18	0.11
2.00	50	0.20	0.36	0.15	0.04	0.14	0.09
2.00	100	0.17	0.32	0.11	0.03	0.12	0.07
4.00	25	0.23	0.43	0.20	0.04	0.19	0.11
4.00	50	0.22	0.40	0.16	0.05	0.16	0.10

4.4.3.3. Simple Shear Stress Relaxation

Simple shear multi-step stress relaxation tests were carried out at four different strain levels, 25%, 50% 75% and 100%. The specimens were held at constant strain for a period of 250 seconds. The first set of tests was run for 1000 seconds but had to be rerun due to having too long of a time increment on data capture. The time was reduced since the data beyond 250 seconds was constant and beyond the time frame for the analyses. Based on the results of these tests, it was determined that the rubber samples do not behave in a linear viscoelastic behavior. The samples show different levels of stress relaxation at each strain level. The greatest relaxation occurs at the lower strain levels, which matches the data shown in the hysteresis loops with decreasing damping at increased strain levels. Figures 4-25 and 4-26 illustrate stress relaxation curves for two rubber compounds. The graphs show the average for the three specimens at each strain level and the overall average of all the curves.

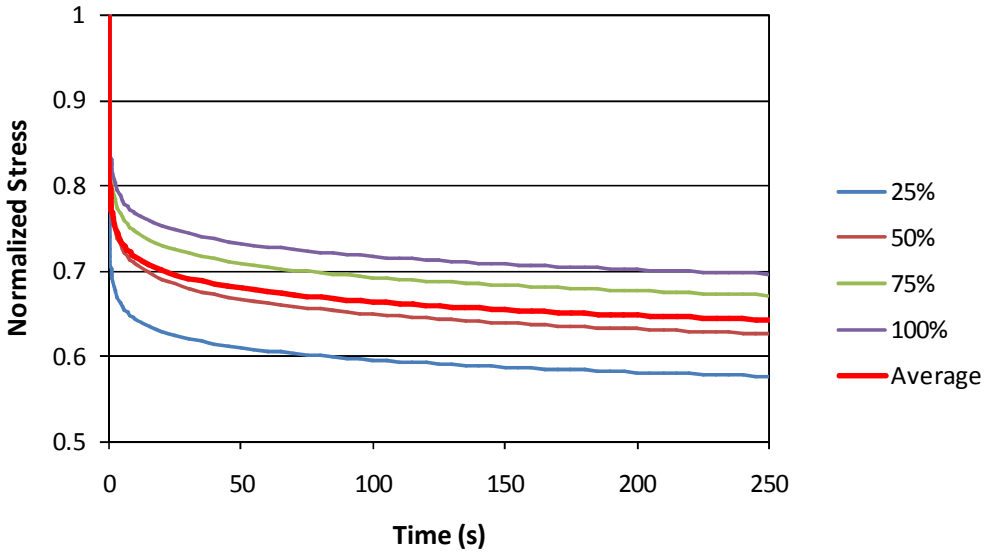

Figure 4 - 25 BR60H Stress Relaxation Curves

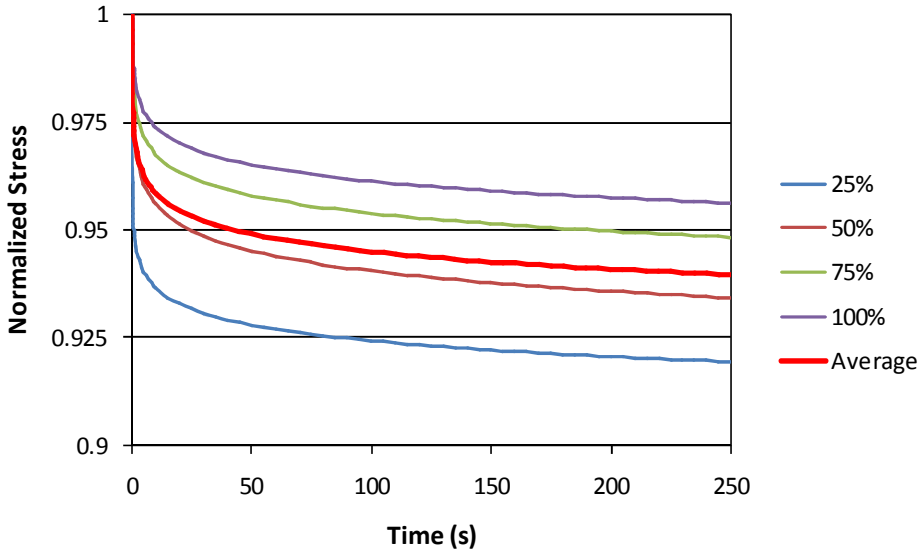

Figure 4 - 26 NR40L Stress Relaxation Curves

4.4.4. Results for ABAQUS Input

The data required for input into ABAQUS includes the uniaxial and planar tension and the average stress relaxation curve. The simple shear data is also included, as it was used to determine which of the hyperelastic material models best fits the static shear behavior. The average stress relaxation curve was input to define the linear viscoelastic response. The stress-strain and stress relaxation plots are shown in Figures 4-27 and 4-28 for NR60H. Figure 4-29 shows the static test data for BR60H material. What is interesting to note on this plot is that the

planar tension testing is more compliant than the uniaxial data. (The test data was re-examined and no problem with the data could be found.) This inconsistency was looked at in more detail during the generation of analytical material models in ABAQUS.

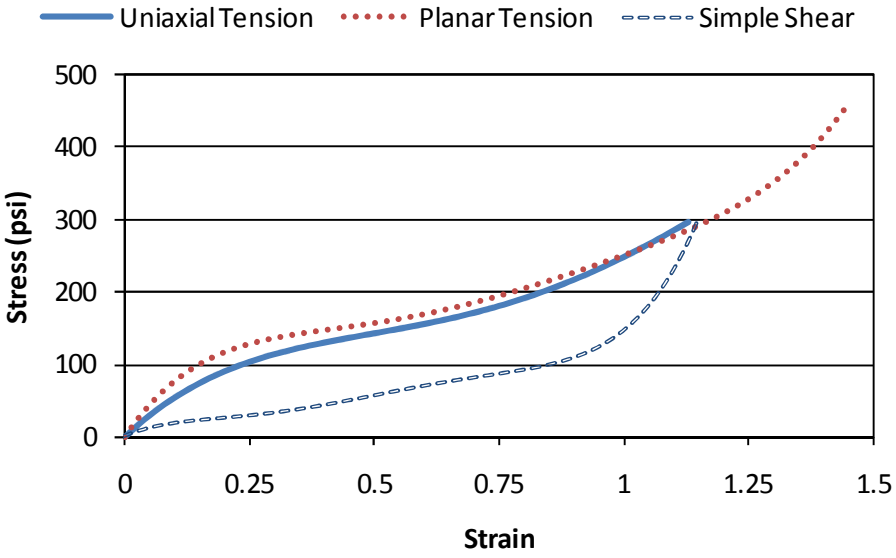

Figure 4 - 27 NR60H Static Stress-Strain Data

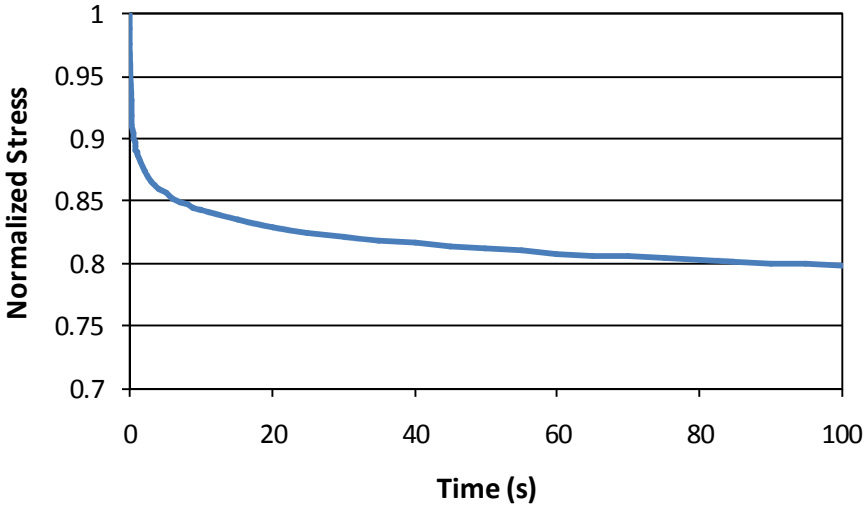

Figure 4 - 28 NR60H Stress Relaxation Curve

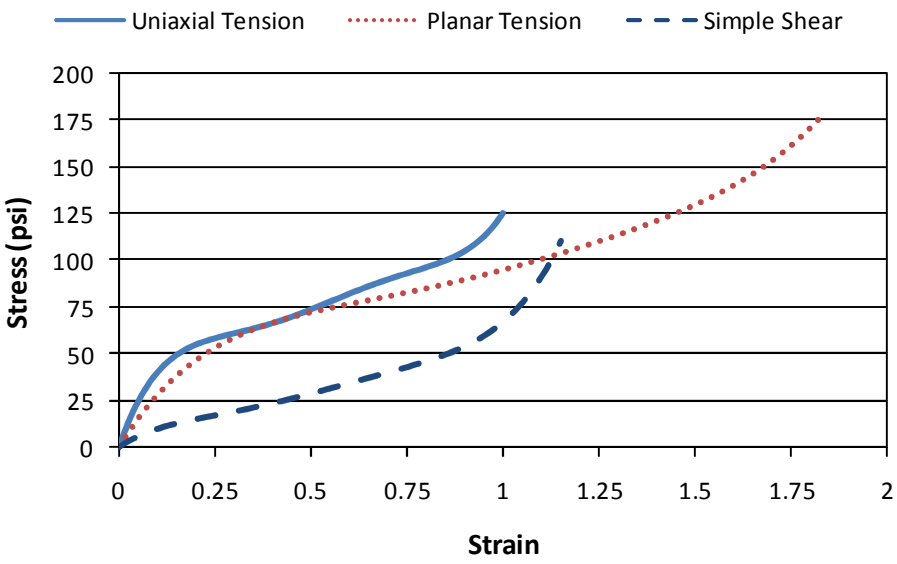

Figure 4 - 29 BR60H Static Stress-Strain Data

4.5. Discussion of Test Results

4.5.1. Uniaxial Tension and Planar Tension

Uniaxial and planar tension results match with the expected results except for the case of BR60H which can be seen in Figure 4-29. The general trend in elastomers is that the stiffness of the planar tension tests should be slightly above the uniaxial curve, which is the case in Figure 4-27 and for the remainder of the compounds. The stiffest materials are the NR60 compounds. The most flexible rubber is BR40H. Although the strain levels originally planned during testing were not reached, the results extend to large enough strains to generate the hyperelastic functions in ABAQUS. It is also apparent that the Mullins effect occurs during the early cycles of all the materials. The data also has shown that after the first five or six cycles the behavior becomes steady state. The most significant stiffness drop is between the first two cycles. After a recovery period, some of the loss is recovered, but the actual amount was not measured in this work.

The natural rubber samples showed evidence of oxidation resistance during the planar and uniaxial tension tests, whereas the butyl samples did not. Oxidation results in microcracks and breaking down of the network of the rubber when under tension. This phenomenon is one of the primary reasons that rubber is typically not used in tension applications. The white film that appeared on the natural rubber samples is the visible proof of the anti-ozonant additive working

while the sample is under tension. Because butyl rubber is inherently stronger in resisting oxidation, the additive is typically not needed.

4.5.2. Simple Shear

The simple shear results show that the area with the most uncertainty was in the viscoelastic properties. The hysteresis loops show a consistent behavior over the range of frequencies and strain levels with minor differences in the width of the hysteresis loops. The slope of the loops is the same, which shows that the stiffness properties are not dependent on the strain rate in the applicable range. However, there is a dependency on both strain level and frequency on the loss factor. The data that was used for finite element analysis is the average stress relaxation curve. The problem with that data is that the viscoelastic model can only handle a linear viscoelastic material and the behavior is clearly not linear based on the stress relaxation tests. Because of that fact, the use of the hysteresis option versus the viscoelastic option will likely be a better representation of the dynamic behavior. Both options will be examined in ABAQUS to determine the better option.

Because of the low damping values of the NR60L and NR40L, these compounds will not be analyzed for use in the damping device. The other materials have an average loss factor of at least 0.15. NR60L has an average around 0.08 and NR40L has a loss factor around 0.03. Because of the similar stiffness of the higher loss factor NR materials, there is no loss of performance options in excluding these materials from further consideration.

4.5.3. Overall Results

The high damping rubber test data provides several options for use in the device. The BR60H material provides the highest loss factor of around 0.40 but has roughly half the stiffness of NR60H. The NR60H compound provides the greatest stiffness with an equivalent linear shear modulus of 140 psi but has significantly lower damping properties than the BR60H. The 40 hardness samples, BR40H and NR40H, both provide around the same amount of damping as the NR60H but with stiffness corresponding to the BR60H material. The priority for developing analytical models in ABAQUS was given to the BR60H and NR60H compounds, as they represented the extremes of the stiffness and damping spectrum for the four compounds still under consideration.

4.6. Finite Element Modeling Procedures

4.6.1. Automatic Material Evaluation

The automatic material evaluation available in ABAQUS was used to calibrate the analytical model for both the hyperelastic material properties and the viscoelastic material properties. The evaluation is based on input test data with subsequent curve fitting or the appropriate constants being directly specified.

4.6.1.1. Hyperelastic Material Models

The first step in evaluating a hyperelastic material model is inputting the test data from the homogeneous states of strain. ABAQUS uses engineering stress and strain for the input in either uniaxial, planar or biaxial tension or any combination of the three. This work included both the uniaxial and planar tension. The data entered into the tables represented the steady-state static properties of the various compounds. The data was also adjusted for the initial set that occurred during the testing of the samples so that the input curves started from the origin, which is required by definition for the strain energy density functions.

The next step in the process was to determine which models to include in the evaluation procedure. The hyperelastic models evaluated for all the rubber compounds include Arruda-Boyce, Van Der Waals, Ogden with N=2 and N=3, Marlow for both the planar and uniaxial tension, the Polynomial model with N=2 and the Yeoh model also known as the Reduced Polynomial model with N=3. The input for the models was typically both the uniaxial and the planar tension data with the exception of the Marlow model. The Marlow model creates an exact replica of the input data and creates an approximate fit to the other models. However, in cases where it is specifically noted, some models were evaluated with only one set of data in an attempt to produce a better fit to the results. The automatic material evaluation would then display graphically and numerically the results of each of the models. Although it is not supplied as part of the input data, the option is available to view the results of the various models in a simple shear state of strain. This was the main factor in selection of the model, as the rubber in the hybrid device is in a state of simple shear. Another factor was the stability of the model. In addition to the coefficients, a description of the stability of each model based on the strain range is given. This procedure provides a very simple procedure for identifying which hyperelastic formulation best suits the various rubber compounds.

4.6.1.2. Finite Strain Viscoelastic Model

The finite strain viscoelasticity model is one of the ways to include the inherent material damping of the rubber compounds in the time domain. There are four different ways to generate the required constants. The constants are used to define a Prony series which acts as a non-dimensional multiplier on the stiffness of the material. The Prony series defines a curve with the same shape as a stress relaxation curve. The reduction in the stress under constant strain or the increase in displacement under constant load is the mechanism which creates energy dissipation.

The first method available is to directly input the Prony series coefficients in tabular form. The second method is to input test data from cyclic testing which includes the storage and loss modulus at a given frequency for the range of frequencies for which data is available. The other two methods include test data for stress relaxation or creep tests. For the last three methods, after inputting the test data, a material evaluation procedure is run to determine the number of terms needed to fit a Prony series to the test data. The maximum number of terms allowed in the series is 13. For the evaluation, a maximum number of terms used to fit the data can be specified along with the minimum variance between the test data and the calculated coefficients.

The viscoelastic model was tested for both the BR60H and NR60H compounds. In both cases stress relaxation data was used to generate the Prony coefficients. The material evaluation provided the requisite tolerance of 0.005 on the fit for 5 terms. The analytical testing of the material model matched very well under a stress relaxation test. The problem came when attempting to correlate the model with the simple shear cyclic tests. The damping values from the analysis were much too low. Many attempts were made to determine why this was occurring, but none succeeded. In conjunction with another researcher, a study is ongoing as to why this is occurring, but the reason for the poor performance of the viscoelastic model is not clear. Because of this problem, the viscoelastic model was not be used as the time-dependent portion of the material model.

4.6.2. Hysteresis Model

The Hysteresis model implemented in ABAQUS is based on the work by Bergstrom and Boyce at MIT (1998; 2000; 2001). It must be used in conjunction with any hyperelastic material model. The model creates a parallel spring network with the hyperelastic material being the perfect nonlinear elastic spring. The other leg of the network models the time-dependent nature of the

rubber, which gives rise to the damping. The four parameters that control this model were explained earlier in the chapter. Unfortunately, there is no easy way to determine the values needed to match the various compounds. The work by Bergstrom and Boyce prescribes an initial starting point and then uses a trial and error approach to determine the actual values that match the observed behavior.

Determining the value of four parameters required significant analytical testing to establish the effect of each. The analytical model consisted of a single rubber pad with the top and bottom surfaces constrained to behave as if they were perfectly bonded to a steel block. A prescribed sinusoidal simple shear strain pattern was applied at each of the displacement levels and frequencies corresponding to the test data. This data was then compared to the values from the test data to correlate the dynamic stiffness and loss factor for the analytical model.

The original goal was to determine the material damping properties and match them as a function of frequency and displacement for the range of 0.5 – 4.0 Hz and at 25%, 50% and 100% displacement. Because of the interdependence of the parameters, this goal was not achievable. Because of this limitation, the goal was modified with an aim to achieve the best fit at a specified frequency and then using the variation of parameters to get a good fit over the three levels of displacement at the specified frequency. The first priority was placed on the 50% displacement level. The second priority was given to the fit at the 25% displacement. The parameters were adjusted until the stiffness and damping values achieved a good fit. The results of the analytical and experimental correlation are shown in the following sections for each material.

4.7. BR60H Material Model

4.7.1. Hyperelastic Material Model

The material models that were investigated for the BR60H material included the Arruda-Boyce, Arruda-Boyce with only uniaxial data, Marlow with uniaxial data, Marlow with planar tension data and the Yeoh model. The Ogden model with N=2 was also attempted, but due to stability issues it was not considered further. The best fit initially chosen for the material was the Arruda-Boyce model. The chosen model generated an essentially linear response in simple shear. Although the behavior of this material is not linear, it provided the best fit overall. The shape of the Marlow model using the uniaxial tension data provided a similar shape, but the static stiffness was significantly higher. The Arruda-Boyce with only uniaxial data was not part of the

initial evaluation. Because the hysteresis option uses the hyperelastic function as an integral part, the hyperelastic material model selection for BR60H was modified to create a better match for the dynamic stiffness. The final selection for this compound was the Arruda-Boyce model with only uniaxial data. This material provided the best fit for the combination of the hyperelastic and hysteresis model. A graph showing the simple shear stress-strain plot produced from the hyperelastic automatic material evaluation is shown in Figure 4-30.

4.7.2. Hysteresis Model

The hysteresis model for BR60H resulted in a good fit for cyclic loading at 1 Hz and 50% displacement. The fits at the 25% and 100% level were reasonable, with the biggest discrepancy being the dynamic stiffness. This can be easily explained by the fact that the stiffness of the hyperelastic model is a roughly linear fit which correlates best with the stiffness at 50%. The 100% loops show the worst correlation. Figures 4-31 through 4-33 show the comparison of the analytical hysteresis loop to the experimental test data. From these figures it is evident that the 100% displacement level will not have the level of correlation needed for analysis. This will be accounted for in the device design through the avenue that the damper will lock out prior to reaching this level of displacement. The value for each parameter in the hysteresis model is shown in Table 4-4.

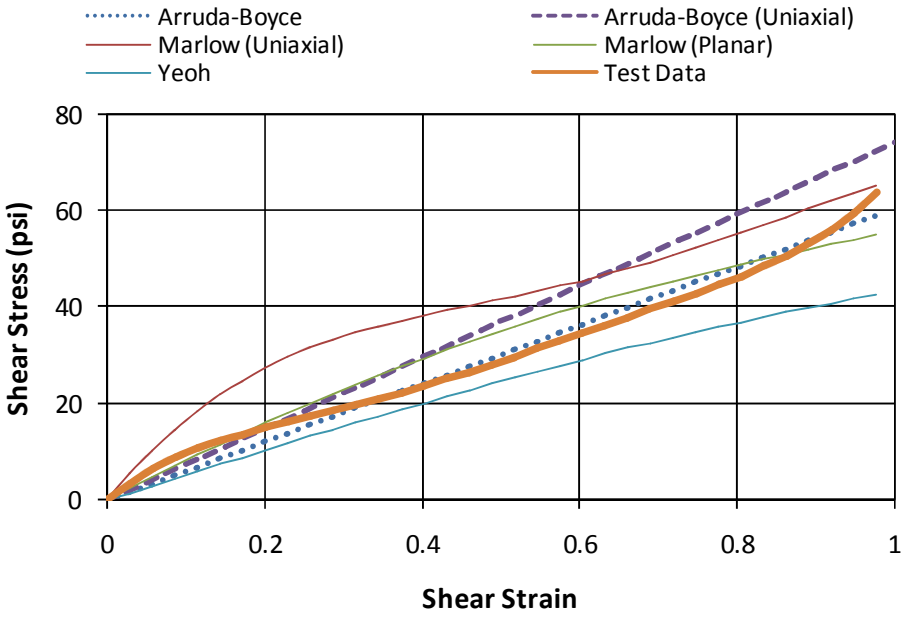

Figure 4 - 30 BR60H Hyperelastic Models – Static Simple Shear

Table 4 - 4 Hysteresis Model Parameters for BR60H

S	A	m	C
1.6	0.00005	2.3	-1

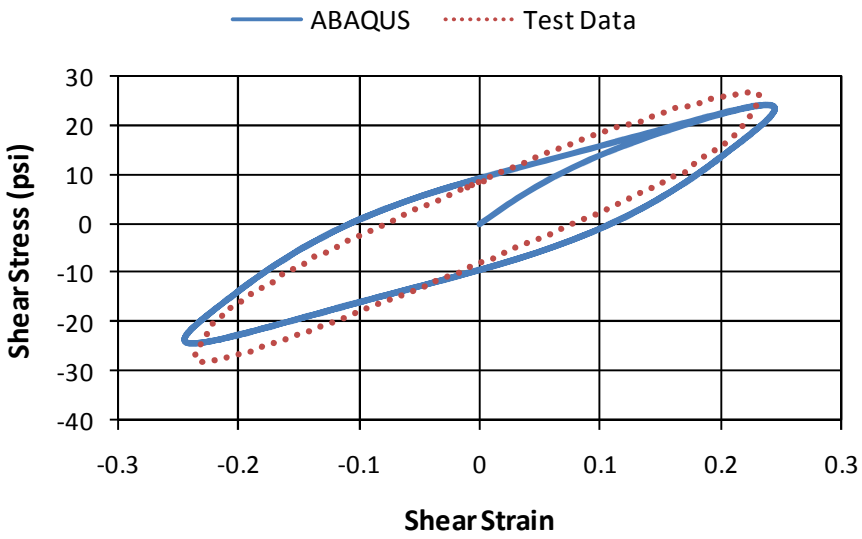

Figure 4 - 31 Hysteresis Loops – BR60H – 1 Hz

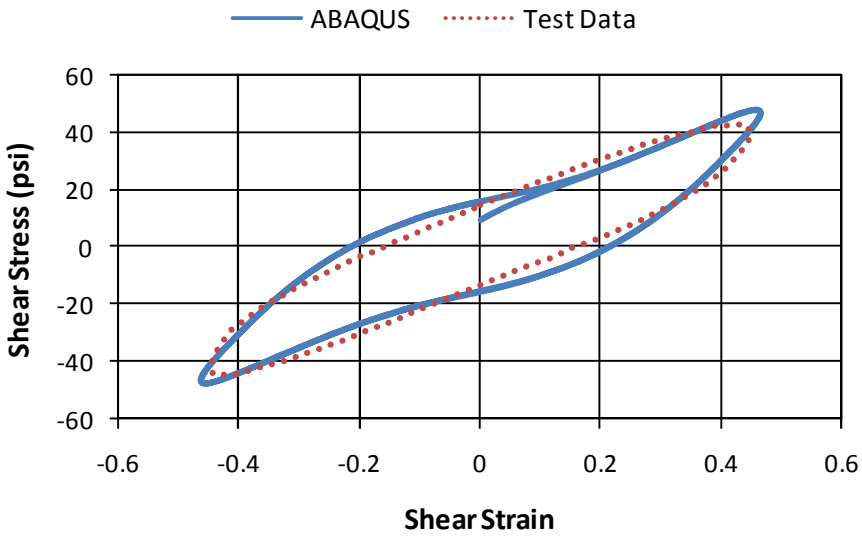

Figure 4 - 32 Hysteresis Loop – BR60H – 1 Hz

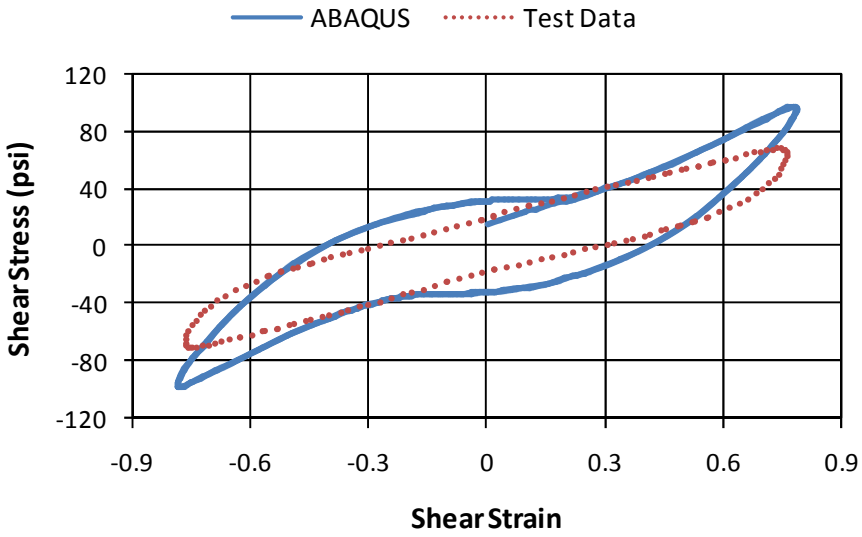

Figure 4 - 33 Hysteresis Loop – BR60H – 1 Hz

4.8. NR60H Material Model

4.8.1. Hyperelastic Material Model

The same models were used for the 60 hardness natural rubber material as for the butyl rubber with the exception that only the Marlow model was used with only uniaxial test data. The results of the initial material evaluation of the NR60H sample were maintained when generating the Hysteresis model. The Arruda-Boyce mode was also chosen because it provided the best fit of the hyperelastic models which did not have stability problems. It again provided an essentially linear fit. The results of the hyperelastic material evaluation are shown in Figure 4-34.

4.8.2. Hysteresis Model

The Hysteresis model for the NR60H compound exhibited the same pattern as the BR60H. The fit for the hysteresis loop is best at the 50% displacement level and 1 Hz. The 25% and 100% behavior deviates more from the test data with the difference being the greatest for the 100% displacement level. The hysteresis loops for NR60H are shown in Figures 4-35 through 4-37. The values of each of the parameters of the hysteresis model are shown in Table 4-5.

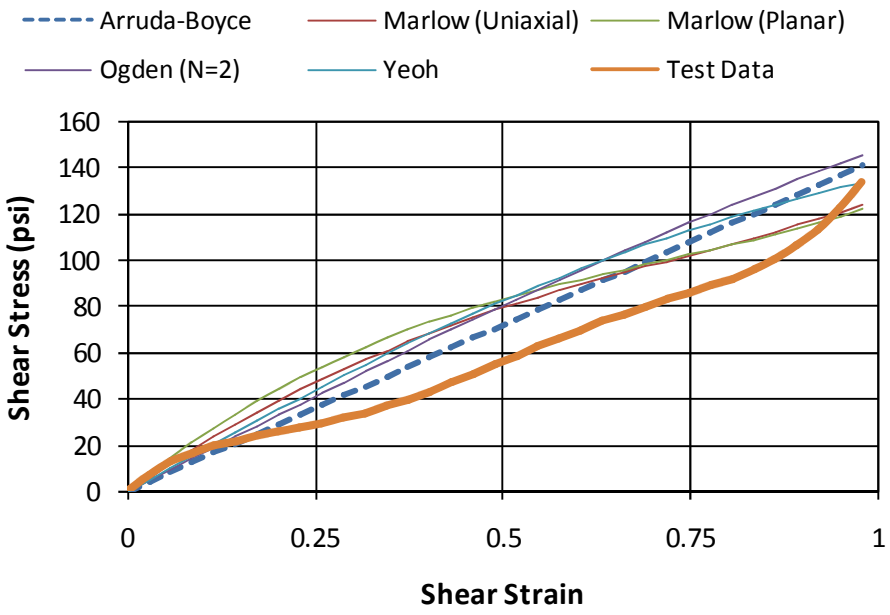

Figure 4 - 34 NR60H Hyperelastic Models – Static Simple Shear

Table 4 - 5 Hysteresis Model Parameters for NR60H

S	A	m	C
1.6	0.00022	1.79	-1

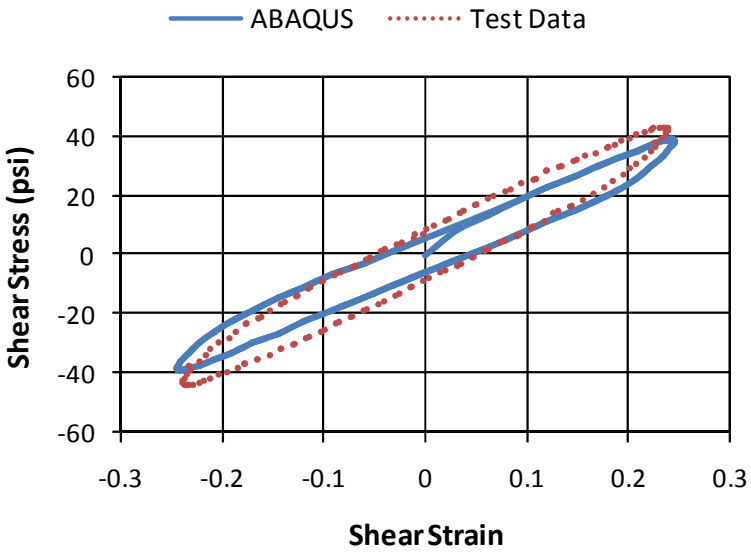

Figure 4 - 35 Hysteresis Loop – NR60H – 1 Hz

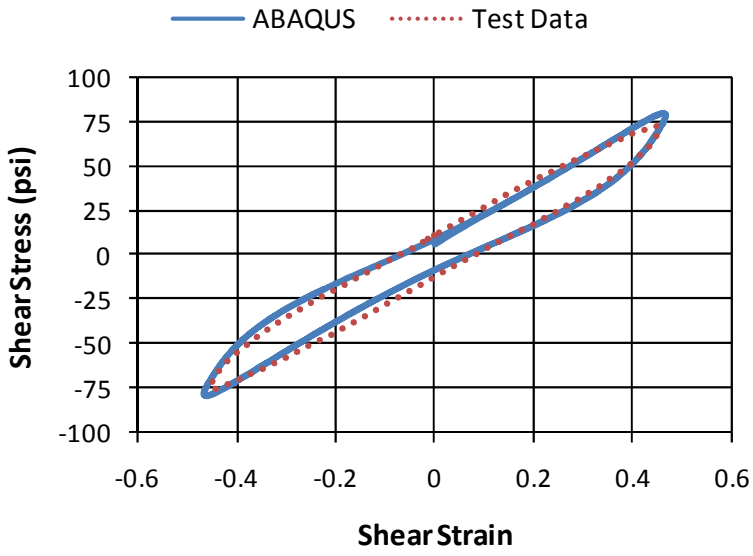

Figure 4 - 36 Hysteresis Loop – NR60H – 1 Hz

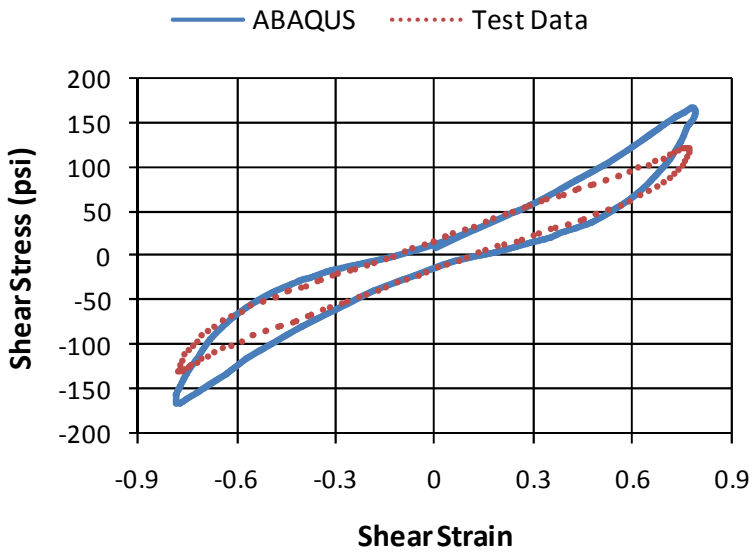

Figure 4 - 37 Hysteresis Loop – NR60H – 1Hz

4.9. Summary

The analytical material models provide reasonable correlation to the experimental data. These material models are used in the upcoming analytical model to verify the concept of the HPCD. Both the BR60H and the NR60H material models were used to create a model of the hybrid device. Because of the limitation of the hysteresis model to capture the loss factor dependence on frequency, a frequency of 1 Hz was used for all the initial analytical tests.

Chapter 5. Hybrid Passive Control Device Description and Finite Element Modeling

5.1. Introduction

The purpose of this chapter is to describe the initial concept of the hybrid passive control device and present results of analytical models. The analytical models were simple finite element models used to study the concept of a multi-phase device. The models are considered simple, because some elements of the device are not explicitly modeled. The essential elements of the device including the rubber damper and hysteretic element were fully modeled in 3-D including material nonlinearity and hysteresis effects in both the steel and rubber. The secondary elements such as the buckling restraining mechanism for the BRB and the lockout mechanism for the damper were not physically part of the model. They were simulated in the analysis which is discussed later. The reasons for the simpler analysis are explained in more detail later in the chapter. The goal of this analysis is to prove that the device performs as predicted. The model was created with both the BR60H and NR60H compounds to investigate the difference between the two materials.

5.2. Preliminary Device Description

The hybrid passive control device (HPCD) concept combines two typical passive control devices in a fashion that the benefits are increased and the negative aspects offset. There is also a priority to include an increasing stiffness to the device to help reduce the chance of collapse due to second-order load effects. The benefits of hyperelastic braces were studied and found to benefit structures by preventing collapse and increasing the predictability of response under extreme loading (Saunders 2004). The initial concept for this device is based on the Visco-Plastic Device (VPD) which is made of two curved plates sandwiching a rubber dissipative element (see Figure 2-40). The VPD provides damping for all ranges of displacement. It also amplifies the strains in the rubber due to the unique geometry, creating a more effective damper. Upon yielding of the outer plates, it provides hysteretic energy dissipation for significant seismic events. The stiffening effect is present due to the hyperelastic nature of the rubber and the geometry of the device. Analytical evaluation of the device verified that the concept of the device in structures reduces structural response (Ibrahim et al. 2007). The drawback discovered with this device is the manufacturing. In conversations with rubber manufacturers, it was determined that the size of

the rubber block required for the device would be difficult and very expensive to produce. An additional drawback is that the device is not symmetric as designed. Rubber is an isotropic material, but the geometry of the device creates a stiffer force deformation relationship in compression. This problem could be overcome through pre-compressing the block or using the device in pairs. Although there is still promise for the VPD, this work has taken a different direction.

Several configurations were generated and considered as part of the development of the HPCD. The concept requires two phases. In the first phase the hybrid device acts like a viscoelastic solid damper. The second phase engages either a friction or a metallic yielding device. The second phase should also include a hyperelastic or stiffening effect. Other considerations used to rate the initial configurations include the ability to tailor the device to multiple situations, the yielding component (if included) being easily replaceable, symmetric behavior in tension and compression and inexpensive fabrication and installation.

A high-damping rubber sandwich damper has been selected for use as the viscoelastic damper. The only other element considered was a tube-in-tube rubber damper. The tube option for the damper provides greater stability under compressive loads. This benefit was outweighed by the difficulty in fabrication which includes both production of the damper as well as design of a method to lock out the damper. A sandwich damper is easier to manufacture, especially when trying to design and manufacture a lockout mechanism.

Two types of hysteretic dampers were considered for the second stage of the device. The first one considered was a buckling restrained brace (BRB). The device is very simple and is being used in many buildings because of the large capacity for ductility and energy dissipation. The second option that was investigated was a friction damper. The friction device has also been successfully implemented in structures and has many of the same benefits of a BRB. Friction devices tend to be more difficult to manufacture. In the end, the best choice for this work is to utilize an all-steel BRB for the hysteretic element. A simple schematic of the device with the restraining member removed from the BRB steel core is shown in Figure 5-1. The lockout mechanism in the damper is not shown.

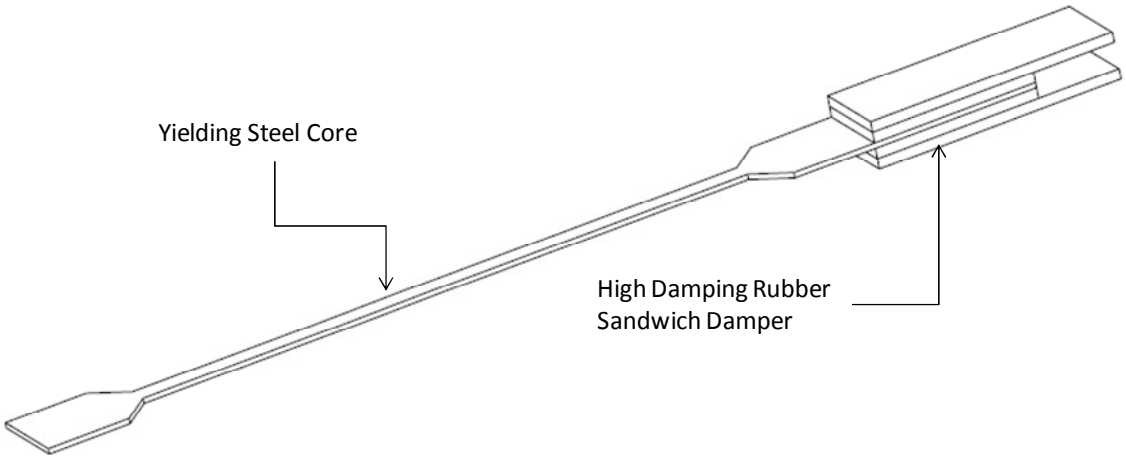

Figure 5 - 1 Simple Schematic of HPCD

5.2.1. Viscoelastic Solid Element

The benefit of the first phase of the device being a high-damping rubber damper is that energy dissipation is provided for all levels of vibration. It reduces wind excited vibrations and structural response under minor seismic events without causing permanent structural damage. Unlike the VPD, the HPCD will not have amplified strains across the energy dissipating material. This difference should be somewhat offset by the high loss factor of the high damping rubber material. It is also theorized that it is only necessary to provide structural damping on the order of 10% to achieve the desired reduction in response.

Another aspect of the rubber element is the ability to engage the yielding device. The low shear stiffness of rubber relative to steel requires the sandwich damper to lock out to transfer enough force to cause yielding. Ideally, the mechanism chosen to lock the rubber damper should not have a sharp transition. A sharp transition could cause problems with increased accelerations during significant events. Several mechanisms were developed and investigated to lock out the damper. For the sake of simplicity, the idea of slotted bolt holes in the outer steel plates was chosen. To lessen the sharpness of the transition, rubber pads could be bonded into the edge of the slots to soften the transition from the rubber damper to the locked out position. A sketch of the damper element is shown in Figure 5-2.

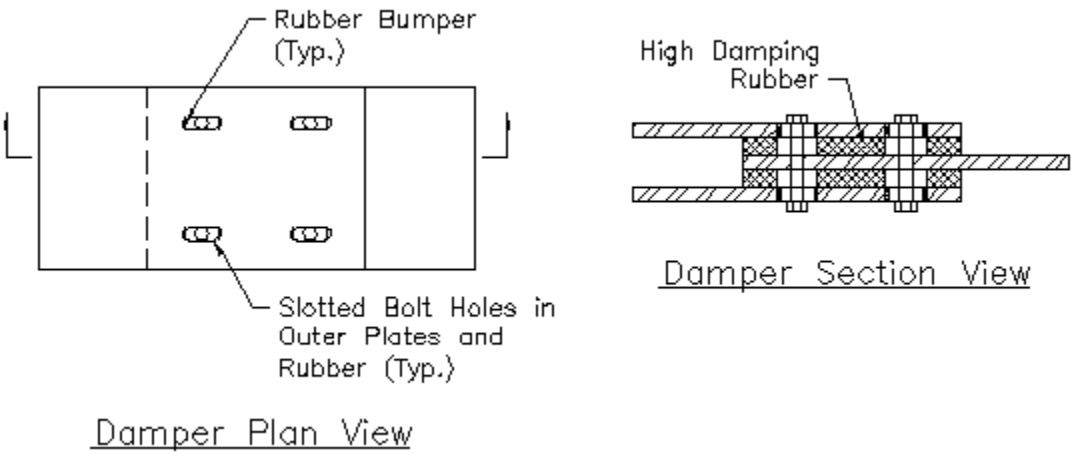

Figure 5 - 2 High Damping Rubber Sandwich Damper

5.2.2. Hysteretic Yield Element

A BRB has the benefit of being a simple but effective option for dissipating significant amounts of energy without the problem of buckling. This device is a small BRB compared to typical braces used in construction. The yielding core length is shorter than a typical device due to the space required by the rubber damper in series. The restraining member is a built-up steel member composed of structural channel and plate material. The channels sandwich the yielding core and are bolted through plates on either side of the core. This concept is similar to other systems that have been successful. The reasoning behind choosing this option is the ease of fabrication and the ability to inspect the yielding core following testing. A sketch of the BRB element of the device is shown in Figure 5-3.

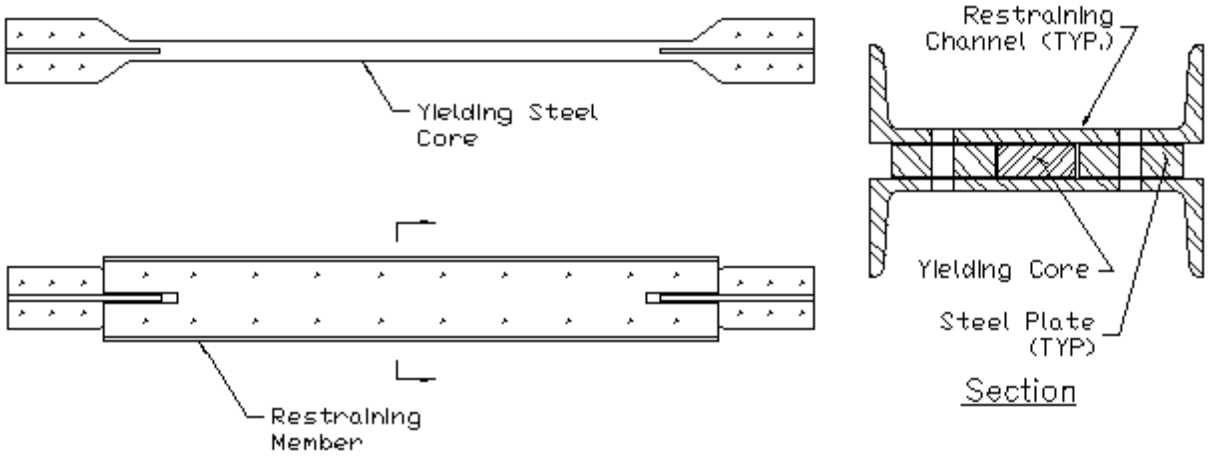

Figure 5 - 3 BRB Element of HPCD

5.3. Finite Element Analysis of Device

Initial finite element analyses of the device were completed to provide tentative verification that the device behaves in the expected manner. The steel elements were modeled using a 36 ksi yield stress with an ultimate strength of 58 ksi at a plastic strain of 0.2. Kinematic strain hardening defined the behavior between yield and ultimate. Both the rubber and steel were meshed using C3D8R elements in ABAQUS. These elements are 3-D solid first-order reduced integration elements. The elements were smaller for the rubber materials because of the large amount of shear strain.

Typically rubber is considered incompressible. The only situation where this is not a good assumption is when the material is restrained. Because of excessive restraint of the rubber by the bonding to plates on both sides, a Poisson's ratio of 0.495 was used to model the near incompressibility of rubber. The behavior of the hyperelastic and hysteresis material models had better correlation with the test data using this assumption. Nonlinear springs were used to lock out the damper in the initial models. The nonlinear springs were nearly perfectly compliant prior to lockout and were set up to have an equivalent stiffness to the bolts in slotted holes after locking out. The nonlinear springs were attached between ground and the free edge of the center plate. The model was run with a prescribed sinusoidal displacement pattern applied to the face of the BRB element away from the damper. The two outer plates of the damper were restrained in all three principal directions. The buckling restraint was provided by restraining the surfaces of the yielding core. The restraints were only applied to one face in each direction. This was done so that the material would have room to expand and contract without external restraint. To save computational effort, symmetry was exploited in one direction of the damper. A screen capture from ABAQUS shows the meshed model of the device in Figure 5-4.

The goal of these analyses was to verify that the concept of the hybrid device performed as expected. ABAQUS is a very powerful program which is capable of explicitly modeling the HPCD including all the elements. There are several reasons the full capabilities were not exploited. The simple model already included a significant number of nonlinear elements. These include the yielding steel elements, the hyperelastic rubber elements and the nonlinear springs used to simulate the locking mechanism. Explicitly modeling the buckling restraining member and the lockout mechanism would add a significant number of elements. In addition to the additional elements, the model would include a significant number of contact surfaces. The

computational and development cost of a model of that magnitude would be significant. The benefit would be a greater understanding of the interaction of the various elements. As the focus of this analysis is a proof of concept, the cost-benefit ratio was too large to justify the effort.

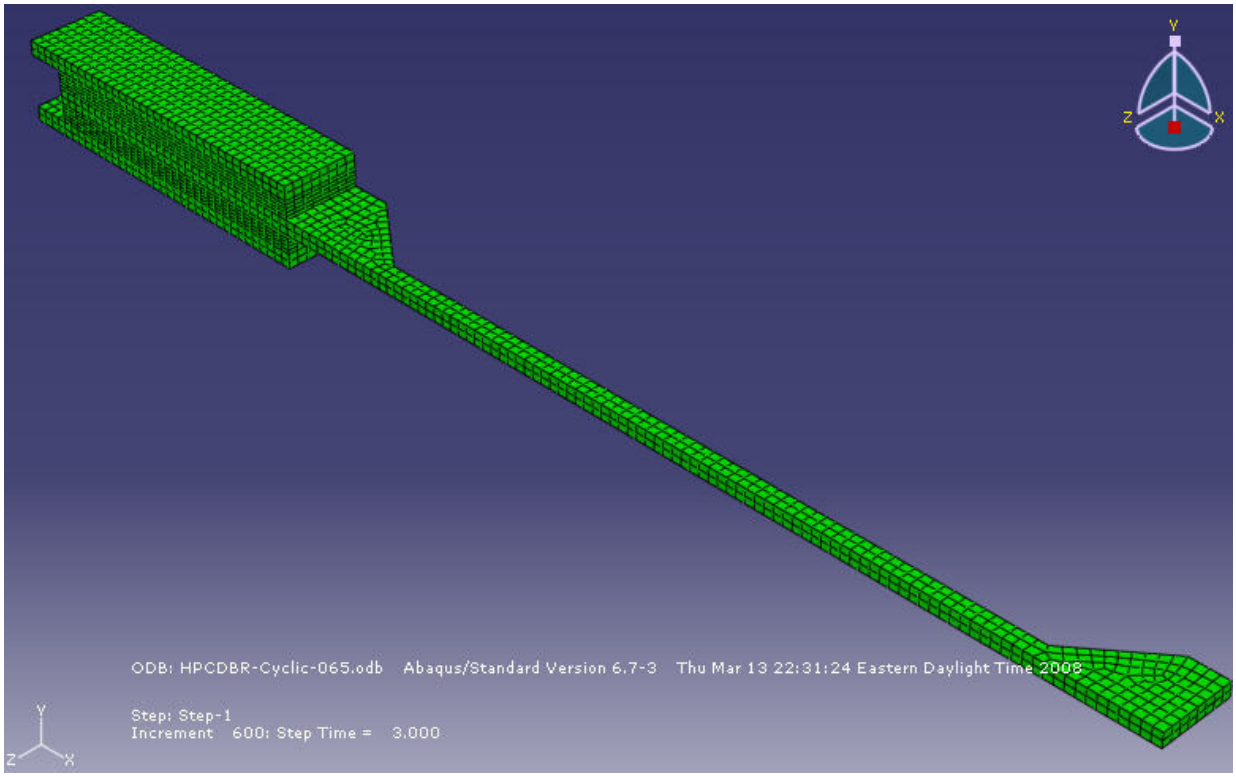

Figure 5 - 4 ABAQUS Model of HPCD

5.4. Analytical Results

The choice of rubber material is based on the performance of the initial HPCD models. The butyl rubber compound has a higher loss factor and was specifically designed by Corry Rubber for use in energy dissipation applications. The greater stiffness of the material is the primary reason that the NR60H compound may be better suited. The stiffer material, although it has a reduced loss factor, may perform better due to a smaller change in stiffness between the damper phase and the BRB phase. The increased stiffness could lead to greater energy dissipation, as the hysteresis loops will be longer, although not as robust as for the BR60H.

The size of the rubber blocks for the initial analyses is 1 in. x 8 in. x 16 in. This is a reasonable size for a damper, although the actual specimens may be smaller in plan due to manufacturing issues. A 36 ksi steel yielding element was used with a gross area of 1.31 in.^{2}, resulting in a yield

force of 47.5 k. The yield length of the device is 36 in. The nonlinear springs used to lock out the damper in the analytical model engaged at a displacement of 0.625 in.

The initial results of the BR60H model damper show that the device is performing analytically as expected. Three different displacement levels are shown for the butyl rubber HPCD in Figure 5-5. This figure shows that for the inner loop, the device is acting as a viscoelastic solid device with an oval hysteresis loop. Upon increasing the cyclic displacement, the second curve shows the increasing stiffness occurring as the damper is locked out followed by yielding of the steel element. The final level includes significant yielding in the element where the strain hardening is apparent. For both the outside loops, it is apparent that the energy loss for the BRB greatly exceeds that of the rubber device.

Initial results for the natural rubber also validate the performance theory. The geometry and loading protocol of the NR60H model are exactly the same as the BR60H model. The only difference is in the rubber properties. The NR60H rubber is approximately twice as stiff as the butyl rubber but has a much lower loss factor. The results for two analyses of the HPCD with NR60H are shown in Figure 5-6. The increased stiffness of the rubber damper is apparent from the smaller differences between the stiffness of the two phases and the height of the yielding plateau.

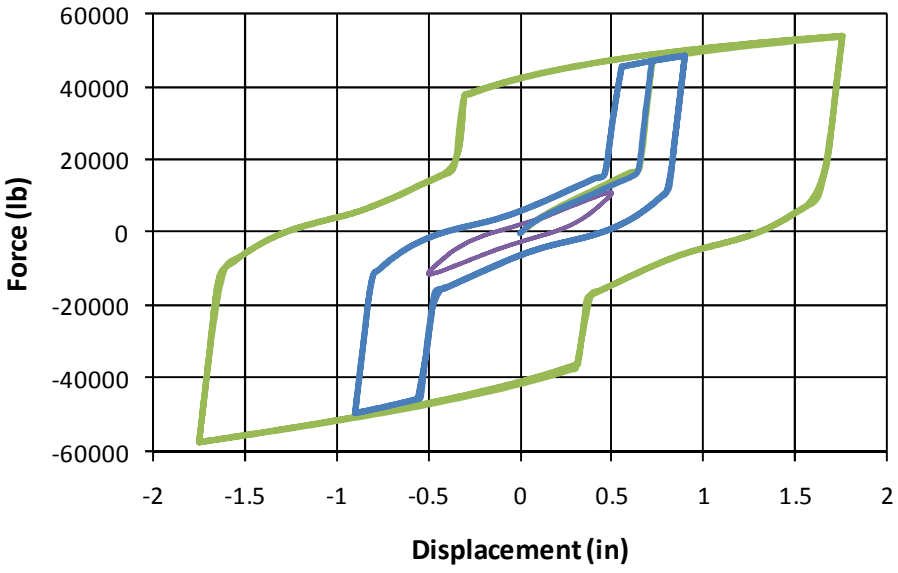

Figure 5 - 5 Analysis of HPCD with BR60H Rubber

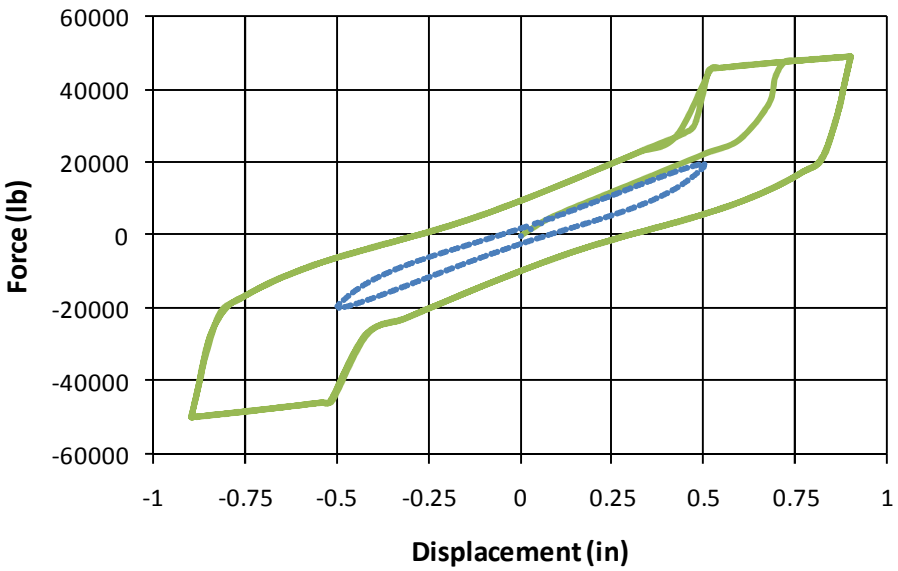

Figure 5 - 6 Analysis of HPCD with NR60H Rubber

The behavior of the damper for the BR HPCD can be seen in Figure 5-7. The behavior of the damper during the initial phase of the damper resembles the hysteresis loop for the entire device. The difference is that the displacement for the damper is less than for the device due to the displacement across the core. The inner circle represents the device subjected to a cyclic amplitude of 0.50 in. The outer loop represents an amplitude of 1.75 in.

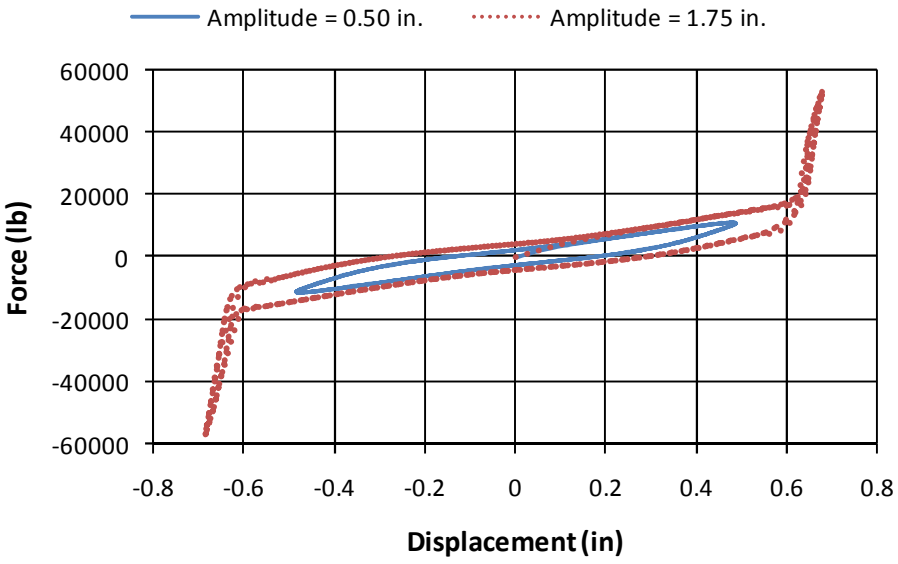

Figure 5 - 7 HPCD BR Damper Hysteresis Loops

One drawback of the HPCD is the reduced effectiveness of the damper. The displacement across the damper is reduced relative to an HDR damper with stiff elastic braces. The reduced effectiveness can be seen in Figures 5-8 and 5-9. Figure 5-8 shows the hysteresis loops for the BR HPCD for the HPCD and the damper element. Figure 5-9 shows the hysteresis plot with the HPCD and the damper for the NR device. The reduction in energy dissipation is more significant for the NR specimen because of the higher stiffness of the NR damper. The larger stiffness causes an increase in deformations across the steel core for the same device displacement.

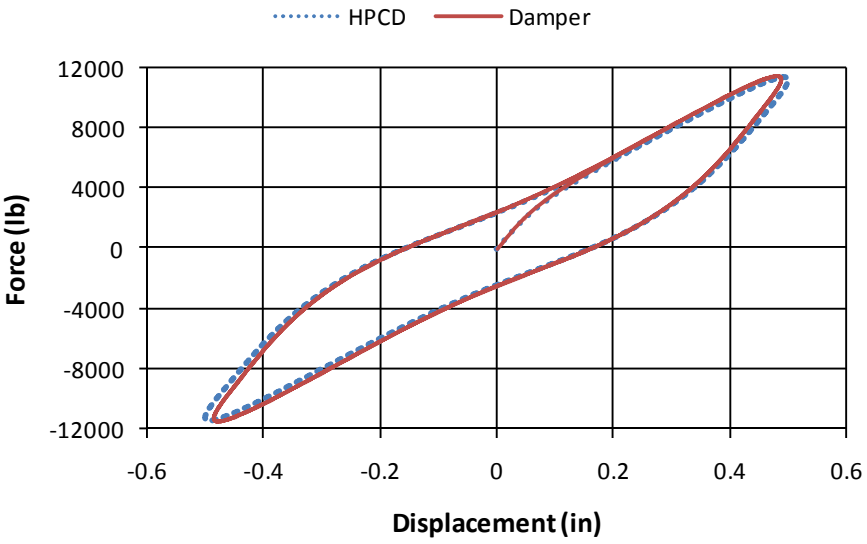

Figure 5 - 8 Device and Damper Hysteresis Loops for HPCD BR

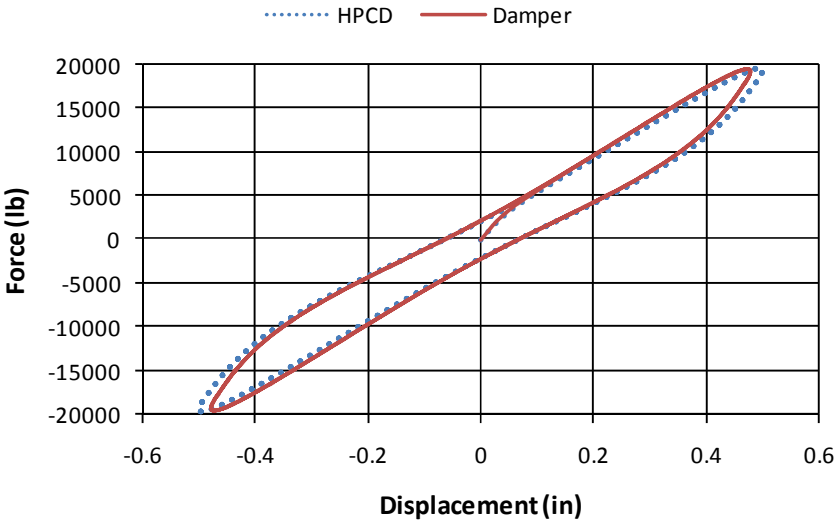

Figure 5 - 9 Device and Damper Hysteresis for HPCD NR

The amount of energy dissipated during the damper only phase for both materials appears to be very similar. The difference between the two inner loops is plotted in Figure 5-10. Both loops are undergoing the same displacement protocol. The NR device is stiffer and the thickness of the hysteresis loops appears similar. Based on the material tests, the BR damper should have almost twice the loss factor of the NR. The loss factor is a ratio of the energy dissipated to the elastic strain energy. If the loops in the figure have approximately the same area, then due to the reduced strain energy, the BR damper would result in a higher loss factor.

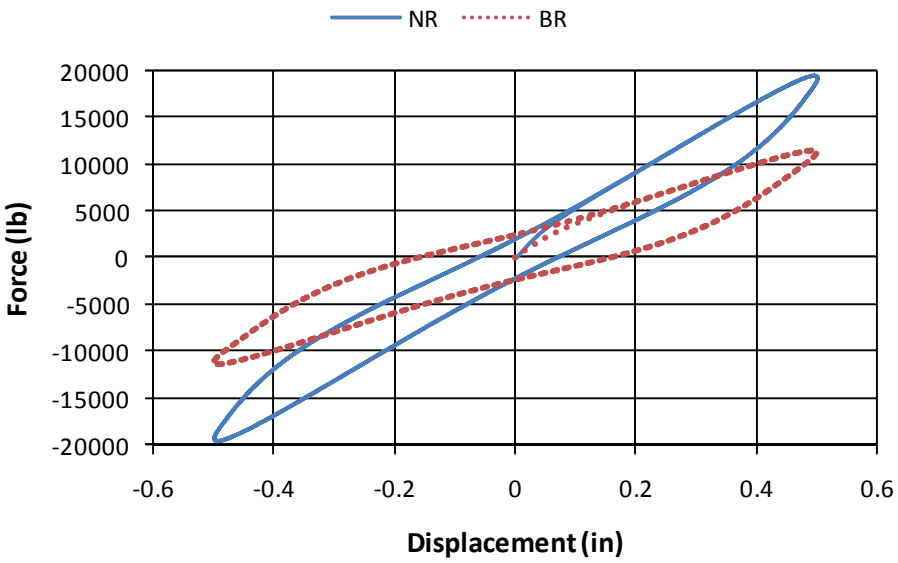

Figure 5 - 10 HPCD – First Phase Hysteresis Loops

A comparison of the post-yield behavior of the NR and BR devices is shown in Figure 5-11. The displacement amplitude for the plot is 0.90 in. The difference in the two hysteresis plots is primarily in the early phase of the device. The initial stiffness of the BR model is less stiff than the NR model. The NR model yields at a smaller device displacement because of the increased strain of the BRB core prior to the damper locking mechanism engaging.

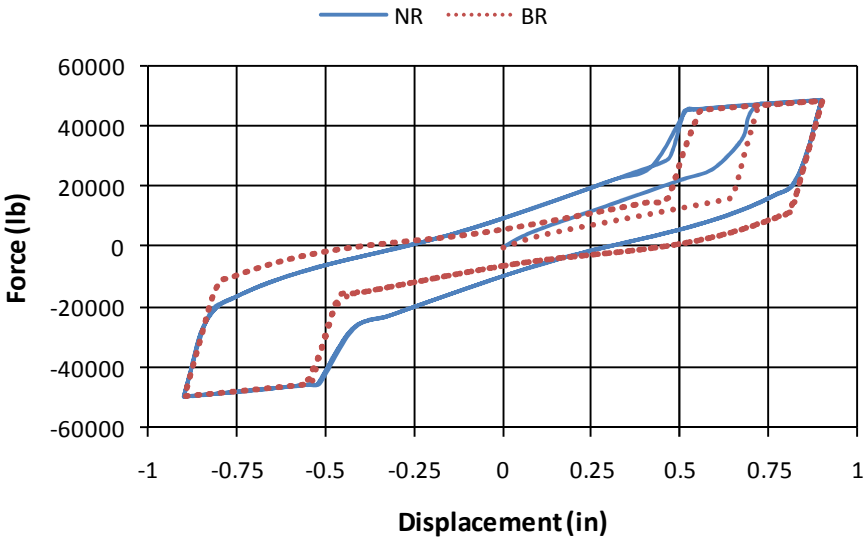

Figure 5 - 11 HPCD – Post-Yield Hysteresis Loops

5.5. Discussion of Analysis Results

The analytical model demonstrates the multi-phase behavior of the HPCD concept. The initial phase with the stiffness and damping of the rubber is shown to transition into the higher stiffness when the damper is locked out. This second phase prior to yielding has a very interesting hysteresis loop. The loading outside the initial oval and prior to the yield of the BRB would be a line with no additional energy dissipation. The final phase of the device when the brace is yielded is also demonstrated. The unique shape of the hysteresis loops resembles a pinched hysteresis loop for a typical hysteretic damper or plastic hinge in a moment frame. However, what is occurring is a changing of phase each time the locking mechanism engages or disengages. The difference between this loop and a yielding steel hysteretic loop is two-fold. The first is a reduced initial stiffness. The reduced stiffness provides the benefit of reducing the seismic loading as the period of the structure is lengthened. The second is energy dissipation occurring prior to yield. This is beneficial as it provides seismic protection in the form of energy dissipation for small seismic events without damage to the structure. Additionally, a re-centering force is applied by the rubber damper to help with residual displacements. Based on the results of this simple analytic model, the feasibility of the HPCD concept has been demonstrated. A simple analytical model was sufficient to show the energy dissipation capability of the HPCD. Further proof of the concept of the hybrid device is presented in Chapter 6 as part of an experimental test program.

Chapter 6. Experimental Testing of Scaled Hybrid Passive Control Device

6.1. Introduction

The first portion of this chapter is the detailed description of the hybrid passive control device (HPCD). The preliminary concept from previous chapters has been developed and fabricated into a prototype for testing. The experimental testing is designed to prove that the concept of the HPCD is viable. The critical elements are the buckling restraint for the BRB element, the HDR damper, and the lockout mechanism for the damper. The testing included one HPCD specimen built at a 1/2 scale. The testing protocol included cyclic tests on the damper alone and static testing for the device. The test protocol for the hybrid device conforms to the standard set forth in the AISC Seismic Specification (AISC 2005) and the NEHRP Recommended Provisions (FEMA 2003) for buckling restrained braces.

6.2. Full Scale Device Description

The HPCD test specimen is a 1/2 scale version of a device designed for the lower stories of a 9-story structure in Los Angeles, CA. The damper is designed to provide approximately 10% total damping, including 2% inherent damping, in the first mode of vibration. The BRB element of the device is designed to yield at the equivalent lateral force loads specified in ASCE 7-05 Minimum Design Loads for Buildings and Other Structures (ASCE 2006). Another primary design variable is the gap prior to the lockout of the damper. A gap of 1 in. was selected for this device. For a typical story height, the maximum story displacement is approximately 3 in., corresponding to a 2% drift. This leaves a total of 2 in. of drift that must be accounted for by inelastic deformation in the BRB element. Assuming a steel yield of 36 ksi and a length of 96 in., the yield deformation is 0.12 in. If the design displacement is divided by the yield displacement, the result is a ductility demand at the design displacement of 16.8. This value is higher than typical BRBs because of the reduced length of the core.

The rubber slabs in the full size damper are 3/4 in. thick by 48 in. long by 15 in. wide. The rubber used for the device is 60 hardness high damping butyl rubber. The properties developed during the mechanical testing and used for device design and structural analysis are a shear storage modulus (G') of 87 psi and a shear loss modulus of 31 psi (G''), which corresponds to a loss factor of 0.36. The resulting stiffness of the spring (K) and viscous damper coefficient (C)

for the sandwich damper are 167 k/in and 23.7 k-s/in respectively. The equations used to calculate these damper properties are shown as Equations 6-1 and 6-2. In the equations, A is the area of the rubber slab, t is the thickness of the rubber slab and ω is the circular frequency which for this case is the primary frequency of vibration of the 9-story Los Angeles structure. Due to the geometry of the damper, the area, A, is twice the area of a single rubber slab. The area of a single rubber slab is the shear area, which is the width multiplied by the length of the rubber.

$$K = G' A/t \qquad \textbf{Equation 6 - 1}$$

$$C = G'' A/t\omega \qquad \textbf{Equation 6 - 2}$$

The BRB element has a 200 k yield based on a 36 ksi material. The length of the yielding core is 8 ft. The geometry of the core is a simple dog bone shape. The buckling restraining mechanism is made of two channels separated by plates and bolted along the length. It should be noted that the tested device required a connection between the damper and the BRB. This was only done for testing purposes and may not be done if the device were implemented in a structure. Providing a connection reduces the length of the BRB core. The longer the core, the lower the ductility demand on the steel core. A greater length reduces the chances of getting into the strain hardening range of the steel. The benefit of the connection is that the BRB element could be removed and replaced after an event without replacing the HDRD.

6.3. 1/2 Scale Device Description

The 1/2 scaling was selected as the largest scaling that could be accommodated by the testing facilities in the Structures and Materials Research Lab at Virginia Tech. The dimensions of the rubber were reduced to 3/8 in. thick by 24 in. long by 7.5 in. wide. The scaling reduced the stiffness and damping coefficients of the half scale rubber damper to 83.5 kip/in. and 11.8 kip-s/in. respectively. The yield force of the BRB was reduced by 75% to 50 kips and the yielding length reduced to 4 ft. The gap and total displacement required of the device were reduced to 0.5 in. and 1.5 in. respectively. Detailed sketches of the various elements of the scaled HPCD are shown in Figures 6-1 through 6-3. The connections between the device and test frame were fabricated using (4)-L3x3x3/8. These connection angles are not shown in the sketches.

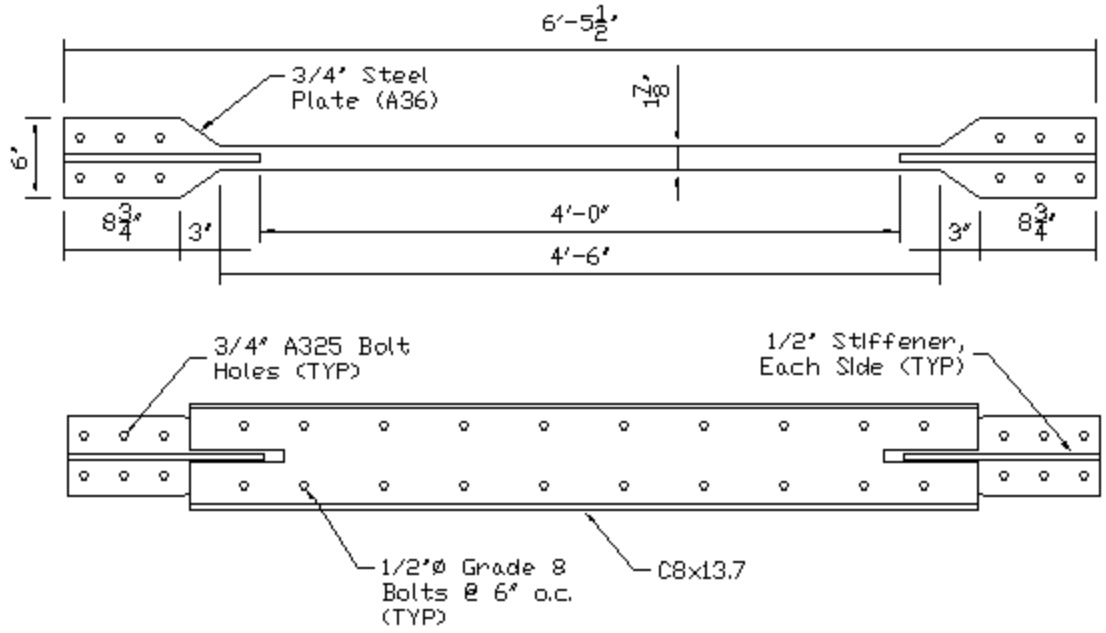

Figure 6 - 1 Detailed Sketch of 1/2 Scale BRB Element of HPCD

The connections and the test frame were designed prior to the coupon tests on the BRB steel, which required providing an adequate margin for a yield and ultimate stress of the steel significantly greater than 36 ksi and 58 ksi. To account for this event, the connections and frame were designed for an ultimate stress of 75 ksi multiplied by a 1.25 load factor. This results in a design load of 130 kips. The bolted connections were designed as slip critical with 3/4 in. diameter A325 bolts. Larger bolts (1¼ in. diameter A325 bolts) were required for the damper locking mechanism. The eccentricity due to the rubber thickness required designing for combined shear and bending.

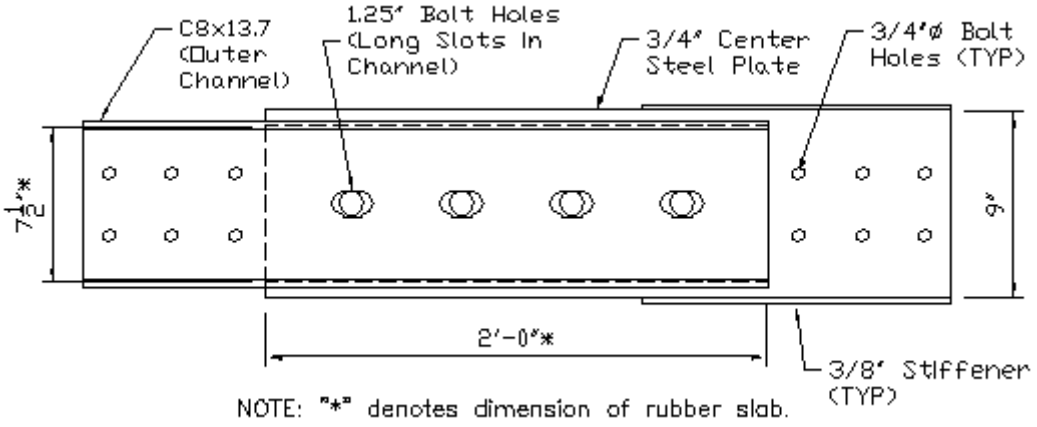

Figure 6 - 2 Detailed Sketch of 1/2 Scale Rubber Damper of HPCD

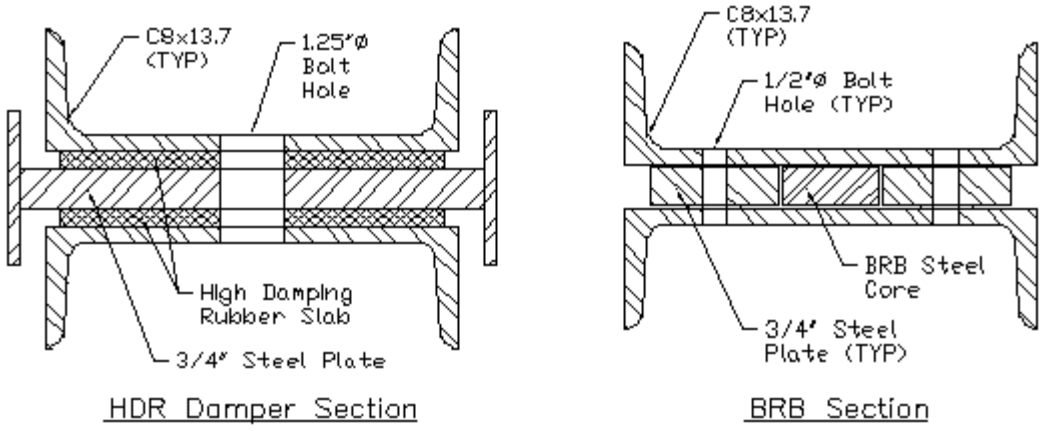

Figure 6 - 3 Section Sketches of 1/2 Scale HDR Damper and BRB

6.4. Scaled Prototype Fabrication

Both the BRB and HDR test specimens were fabricated from standard pieces. The 3/8 in. thick rubber slabs were provided as 12 in. squares by Corry Rubber Corporation. The square samples were trimmed to 7.5 in. wide and then bonded to the outer channels and center plate. CA40H adhesive by 3M was used to bond the rubber to the steel. Both surfaces were prepared by sanding with fine grit sandpaper and then thoroughly cleaning with isopropyl alcohol. The CA40H is a slow setting cyanoacrylate adhesive (also known as superglue) which allowed for 5 - 40 seconds for placing the specimens prior to setting. The adhesive technical data sheet lists the shear strength at 1500 psi, which is greater than for the rubber itself.

The BRB was fabricated from standard channel and plate sections. The yielding core section was machined on a CNC mill from a 3/4 in. thick by 6 in. wide plate. The remaining fabrication, other than the cutting of the slotted holes, was performed by the author using the tools available in the lab. All the welding was done by a certified welder. Initially, the spacer plate was supposed to be 1/8 in. thicker than the BRB core. Due to steel availability, 3/4 in. plate was used for both and washers were used to provide a gap around the yielding section to account for Poisson's effect and to reduce friction in compression. Figures 6-4 is a photo of the rubber damper attached to the reaction beam. The projecting steel piece on the damper is used to attach equipment for monitoring displacements.

Figure 6 - 4 Rubber Damper Attached to Reaction Beam

Figure 6-5 is a photograph of the BRB prior to assembly. Three of the six strain gages are visible. The two channels and the side plates are also visible. The large-diameter holes in the channel are provided for the strain gages. The series of holes in the side plates and channels are for the 1/2 in. diameter Grade 8 bolts used to assemble the BRB. Washers are used between the side plates and the channels to provide the gap around the core for expansion and contraction. Figure 6-6 is a photograph of an assembled BRB.

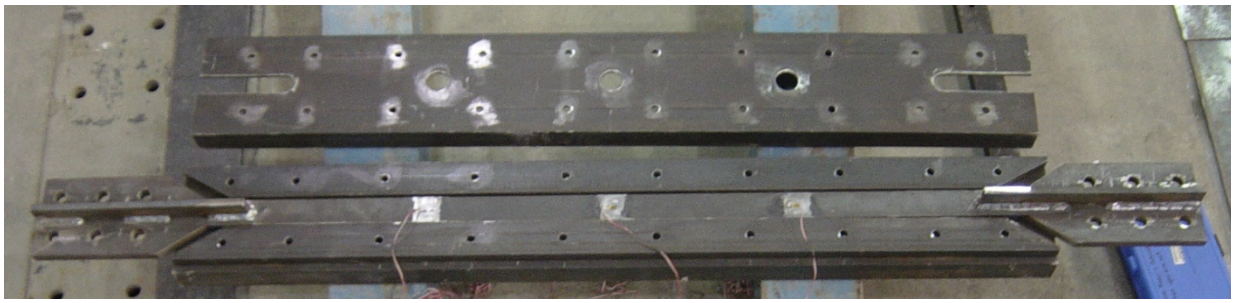

Figure 6 - 5 Disassembled BRB Element

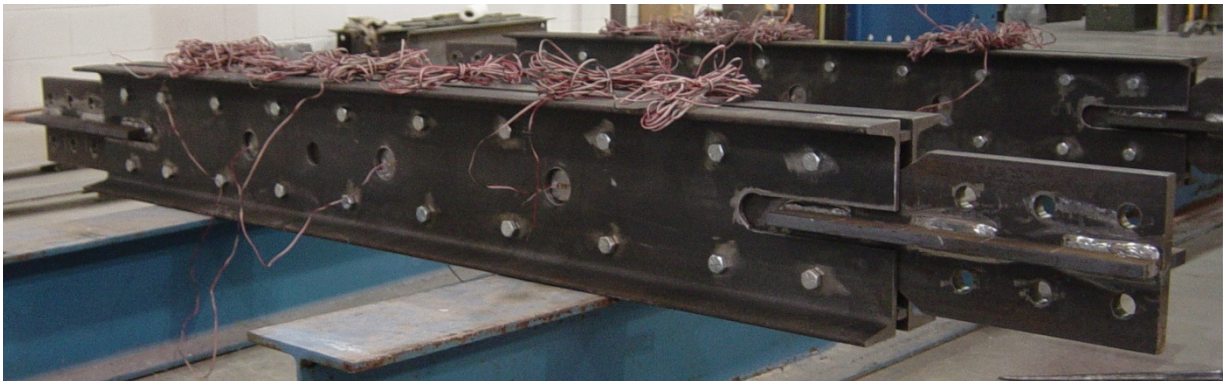

Figure 6 - 6 Assembled BRB Element

6.5. Test Frame and Data Acquisition System

A layout of the test frame including the location of data acquisition equipment is shown in Figure 6-7. The W24 reaction beams were bolted to the strong floor beams using triangular stiffeners welded to thick plates. The actuator was bolted to a reaction beam on one end and connected to the BRB on the other end. The MTS Actuator, model 243.60, has a compression capacity of 235 kips, a tension capacity of 150 kips and 20 in. of travel. The actuator and the hydraulic system are controlled by an MTS 407 controller. The controller drives the actuator and is capable of either force or displacement control. The actuator has an internal linear variable displacement transducer (LVDT) and 220 k load cell in line with the cylinder.

StrainSmart by Vishay Micro-Measurements was used for data acquisition. The hardware interface was the System 5000 Model 5100 B scanner also manufactured by Vishay. The location of measurement devices is shown in Figure 6-7. Locations 1 and 7 are barrel LVDTs used to monitor the displacement at the midspan of the W24 reaction beams. The LVDTs have a total travel of 2 in. The other numbered locations are cable-extension position transducers with a total travel of 10 in. Transducer 2 is attached to the outer channel of the damper. It is used to measure slip in the connection of the damper to the reaction beam. Slip in other connections can be calculated from the difference in displacement of other transducers. The transducer at location 3 measures the deflection at the center of the damper. The transducers in locations 4 and 5 are used to measure the deflection at each end of the BRB core. These locations were used to calculate the deflection across the BRB core. The final displacement transducer measures the deflection of the end of the actuator. This is a verification and back-up of the actuator LVDT. The overall deformation of the BRB core was calculated based on the transducers at each end.

To monitor the behavior of the BRB core, strain gages were used. Six gages were used on each specimen. They were located on both sides of the steel core at the mid-point and quarter points. The EP-08-250BG-120 strain gages are made for cyclic and inelastic behavior. They are rated by the manufacturer, Vishay Micro-Measurements, for strains up to 10%. To access the strain gages, large holes were drilled in the outer channels of the BRB. The strain gages allowed determination of the distribution of inelastic strain along the length.

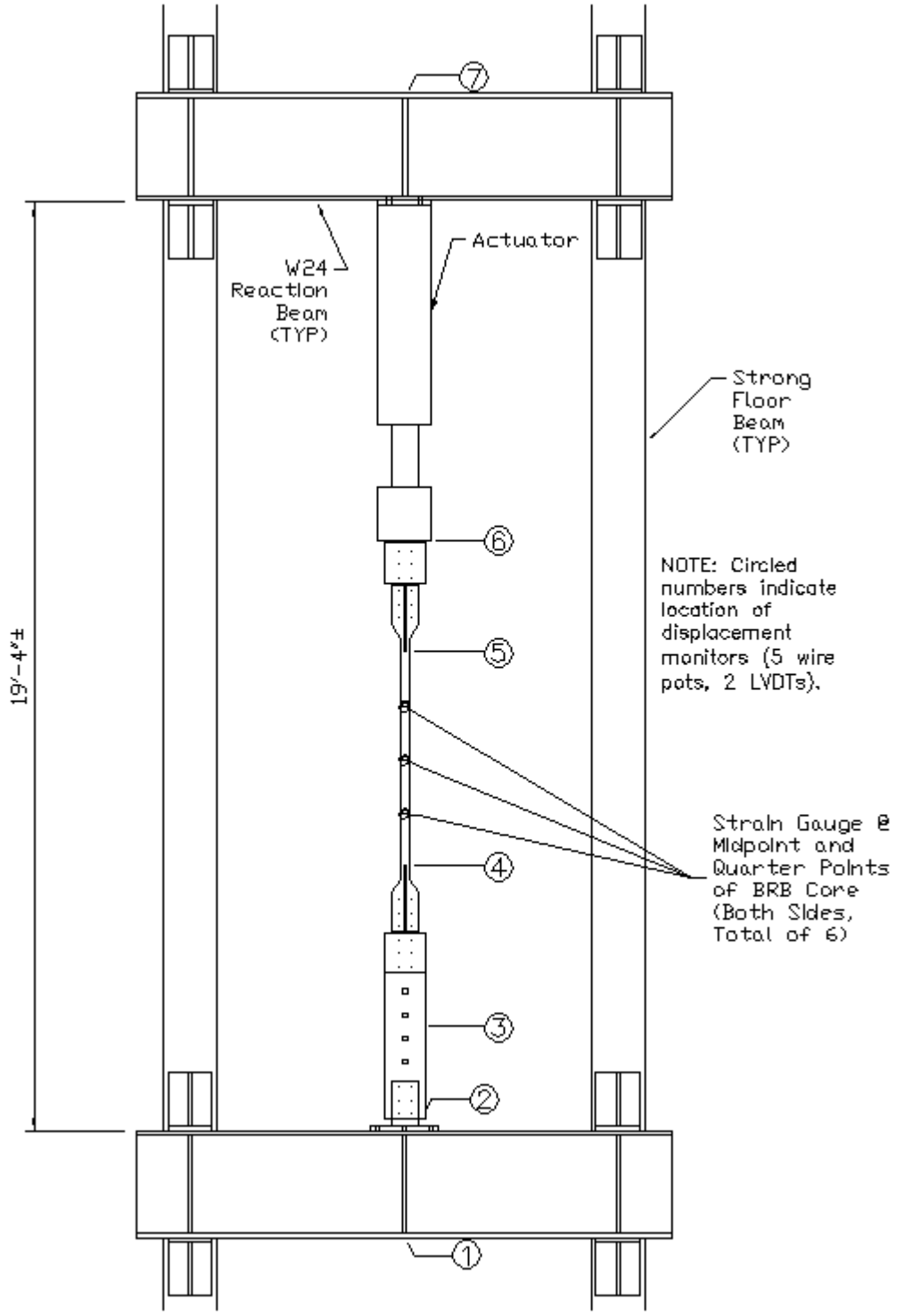

Figure 6 - 7 Test Frame and Data Acquisition Plan

The bracing scheme for the test setup is based on providing similar bracing to what would be used in an actual structure. In a structure, the device as designed would be connected from the

top of a chevron brace into the beam-to-column joint. Based on this configuration, the HPCD would be braced against rotation and displacement at each end. To achieve this, a kicker brace would be used from the top of the chevron brace back to the floor system. For testing at the damper end, the damper was braced by a steel beam under the damper. Steel shims were installed to achieve a tight fit. The damper is only braced against downward movement, because the self-weight of the HPCD deflects it downwards. Having an initial deflection towards the ground makes the most probable direction of buckling was toward the ground. The steel section bracing the damper is shown in Figure 6-8. The steel shims are visible on the flanges of the steel section.

Figure 6 - 8 Vertical Bracing at Rubber Damper

To complete the bracing scheme, the actuator was braced against displacement and rotation at both ends. Initially, mounted channels were used to guide the plate at the end of the actuator so the hinge would not rotate. These channels were not effective during the initial testing. In the end, it was discovered that the actuator was allowing for rotations in both directions. To overcome this problem, a beam was used to brace the back end of the actuator both vertically and horizontally. It was attached to the strong floor beams using high-strength rod. The horizontal

bracing stems from a rubber bearing pad between the beam and the actuator. This bracing prevents rotation of the hinge attached to the reaction beam, and is shown in Figure 6-9.

Figure 6 - 9 Hydraulic Actuator Braced with Beam Attached to Strong Floor

The other hinge on the actuator was also rotating in both directions. It is designed to rotate in one direction but the rotation in the other direction was due to too much play in the joint. This joint was restrained against rotation by locking out the joint. The play in the joint was removed by using steel shims. In the other direction, the hinge was locked out using steel blocks in two locations, as shown in Figure 6-10. These measures prevented any rotation in the actuator and provided a test condition similar to the service condition for the HPCD.

Figure 6 - 10 Actuator Joint with Blocks and Shims to Eliminate Rotations

6.6. Experimental Testing Procedure

The experimental testing includes both cyclic and static tests of the HPCD. The cyclic tests show the behavior of the first phase of the device when the rubber damper is active. The cyclic tests are all run at displacements below the lockout of the damper. The static tests are used to exercise the lockout mechanism of the damper and the BRB element.

6.6.1. Rubber Damper Tests

The damper cyclic testing was completed at reduced scale displacement levels of 0.09 in., 0.19 in., 0.28 in, 0.38 in. and 0.45 in. These levels correspond to displacements of 25%, 50%, 75%, 100% and 120% of the rubber thickness. The levels in this testing were selected so the damper would not lock out during the testing. The frequencies were selected based on the typical structure that would benefit from these devices, that has a first mode period in the range of 1 – 5 s. This corresponds to a range of frequencies from 0.2 – 1.0 Hz. Due to the limitations of the hydraulic system, the frequency is limited to a maximum of 0.5 Hz. Because of the scaling of the test specimen, the frequencies must be scaled appropriately. The time scaling factor is the square

root of the length scale factor. Using a scale factor of two and recognizing that the time unit is in the denominator, the scaled frequencies were multiplied by $\sqrt{2}$. The scaled frequency range for the reduced scale testing is then 0.283 – 0.707 Hz. Cyclic testing using 30 cycles of a sinusoidal displacement protocol was run at frequencies of 0.283, 0.354, 0.471, and 0.707 Hz. Due to the previously mentioned limitations of the actuator, not all the frequencies could be run at the higher displacement levels. For displacements of 0.38 in. and 0.45 in. the valve on the actuator does not have the flow capacity to run the tests at 0.707 Hz. The initial damper testing was done with the bolts installed and the damper connected to the BRB. Table 6-1 shows the range of displacement amplitude and frequencies for the damper cyclic testing.

Table 6 - 1 Range of Frequency and Amplitude for Damper Cyclic Testing

Displacement Amplitude (in)	0.09	0.19	0.28	0.38	0.45
Frequency (Hz)	0.283	0.283	0.283	0.283	0.283
	0.354	0.354	0.354	0.354	0.354
	0.471	0.471	0.471	0.471	NT*
	0.707	0.707	0.707	NT*	NT*

NT* - Not Tested due to limitations of the hydraulic actuator.

6.6.2. HPCD Tests

The protocol for the testing of the hybrid device is based on the requirements for BRBs. The two sources referenced are the AISC Seismic Specification (AISC 2005) and the NEHRP Seismic Provisions (FEMA 2003). The requirements of the AISC Seismic Manual are more severe than NEHRP and were used to develop the protocol. Two specific requirements are set forth for testing BRBs. The first is that the test must be carried out to twice the design displacement. For these tests, that means a maximum displacement of 3 in., referred to as $2.0\Delta_{bm}$, was used. The second requirement is that a cumulative inelastic deformation of 200 is achieved. Using the assumption that the initial gap is 1/2 in. prior to having the capacity to yield the BRB, the yield deformation of the HPCD was determined. The approximate yield strain of the brace is 0.075 based on a 29,000 ksi modulus of elasticity and 45.5 ksi tested yield strength. When the brace yield is added to the lockout dimension, this produces a total displacement of 0.575 in. To be sure that the specimen has reached yield, the displacement used in the protocol for the yield of the specimen was 0.6 in. The static testing protocol including the expected summary of

cumulative inelastic deformation is shown in Table 6-2. The cycle and cumulative inelastic deformations are measures of the inelastic deformation divided by the yield deformation of the steel core.

Table 6 - 2 Static Testing Protocol for HPCD

Displacement Level	# Cycles	Cycle Displacement (in)	Cycle Inelastic Deformation	Cumulative Inelastic Deformation
Δ_y	2	0.6	0	0
$0.5\Delta_{bm}$	2	0.75	2.0	8.0
$1.0\Delta_{bm}$	2	1.5	12.0	56.0
$1.5\Delta_{bm}$	2	2.25	22.0	144.0
$2.0\Delta_{bm}$	2	3	32.0	272.0
$1.5\Delta_{bm}$	2	2.25	22.0	360.0

6.7. Test Results

6.7.1. Tensile Coupons

Two tensile coupons conforming to ASTM specifications from the same steel plate as the BRB core were tested to determine the actual yield stress and ultimate strength of the A36 steel. The average yield stress for the two specimens is 45.5 ksi. The average ultimate strength of the two specimens is 65.5 ksi. Both specimens elongated approximately 50% prior to fracture, demonstrating significant ductility.

6.7.2. Modifications to HPCD Prototype

After the HPCD specimen was fabricated, preliminary testing and further analysis revealed a possible problem with the device and a minor error in the design calculations. Investigation of the buckling-restraining mechanism highlighted the possibility for buckling of the core member in an undesirable fashion. In order to prevent this failure, side plates were added to the spacer plates. A photograph of this modification to the restraining member is shown in Figure 6-11.

A review of the design calculations for the HPCD prototype highlighted the fact that the stiffener on the BRB core was undersized. The reinforcing of the stiffener was completed by welding an additional stiffener of the same size onto the existing stiffener. The existing piece was a 1.5 in. by 0.5 in. stiffener. The total height of the new stiffener was 3 in. by 0.5 in. The height of the stiffener to meet design requirements was 2.0 in. A photograph of the modified stiffener is shown in Figure 6-12.

Figure 6 - 11 Design Modification to Prevent Lateral Buckling

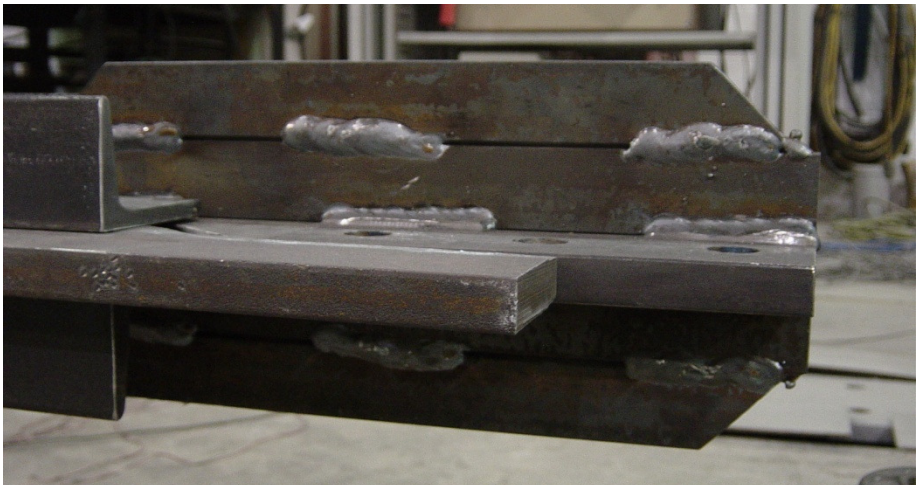

Figure 6 - 12 Design Modification to BRB Stiffener

6.7.3. HPCD Specimen

The testing of the HPCD included three series of tests. The first set of cyclic tests was only half completed before it was determined that the rubber had debonded from the steel channels. Data from these tests is presented to show the results. Following reassembly of the damper, the second set of cyclic tests was run. These tests were completed for all levels of displacement and frequency set forth in the test protocol. Some debonding of the rubber was experienced during the cyclic tests, but was not as significant as in the first cyclic tests. The static tests were run to test the lockout mechanism and the BRB according to the AISC Seismic Specification (AISC 2005). In addition to tests on the prototype device itself, two separate studies were completed on bonding rubber to steel, as the problems with bonding occurred during testing.

6.7.3.1. Cyclic Testing #1

The test data for this set of cyclic tests shows the behavior of the damper but at a reduced strength and stiffness. The reason for the failure of the damper was that the surfaces were not properly prepared prior to bonding. The surfaces had been sanded but the mill scale was not completely removed. The mill scale adhered to the rubber but pulled off the steel channel. The testing was completed for 30 cycles at amplitudes of 0.09 in. and 0.19 in. for the four frequencies specified earlier. Tests were also run at an amplitude of 0.28 in. and a frequency of 0.283 Hz.

Figure 6-13 shows tests at 0.283 Hz at the three different amplitudes. At this frequency the Mullins effect is evident with the first loop being of higher stiffness than the following loops. The other trend apparent here is that for larger displacements, the maximum force increased from the smallest to the middle amplitude but not from the second to the third. This is the result of the rubber detaching from the steel. The trend of increased displacement with little increase in force is apparent in Figure 6-14. Figure 6-15 is a photo of the disassembled damper. On the left of the photo the mill scale is attached to the rubber slab which is still bonded to the center plate. The channel section on the right has lost the mill scale where the rubber was previously bonded. This failure indicates that the problem with the bond may be with the channel section. The bond failure of the center plate did not occur until after the channel bond failed. Because of this failure, small damper tests were run to verify that a good bond could be achieved with proper surface preparation. These tests are discussed in Sections 6.7.3.4 and 6.7.3.5.

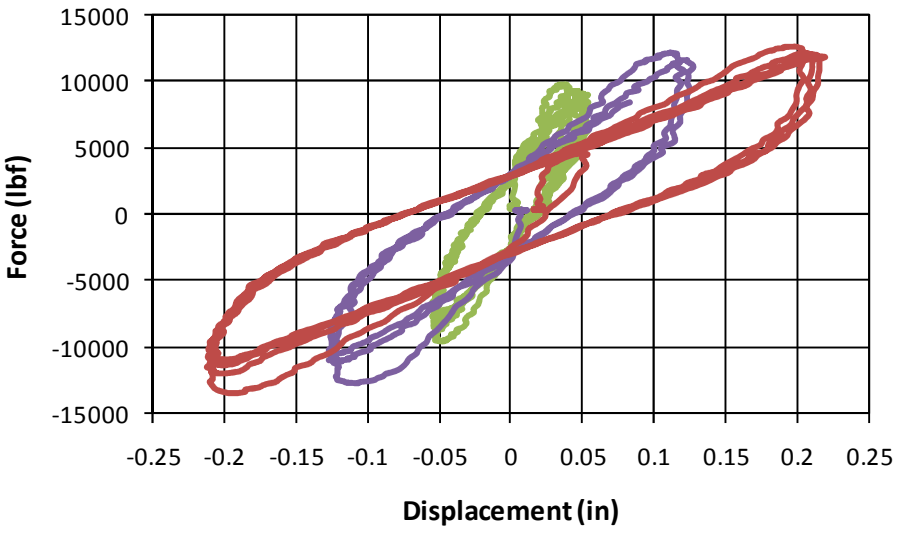

Figure 6 - 13 Damper Hysteresis Loop at 0.283 Hz

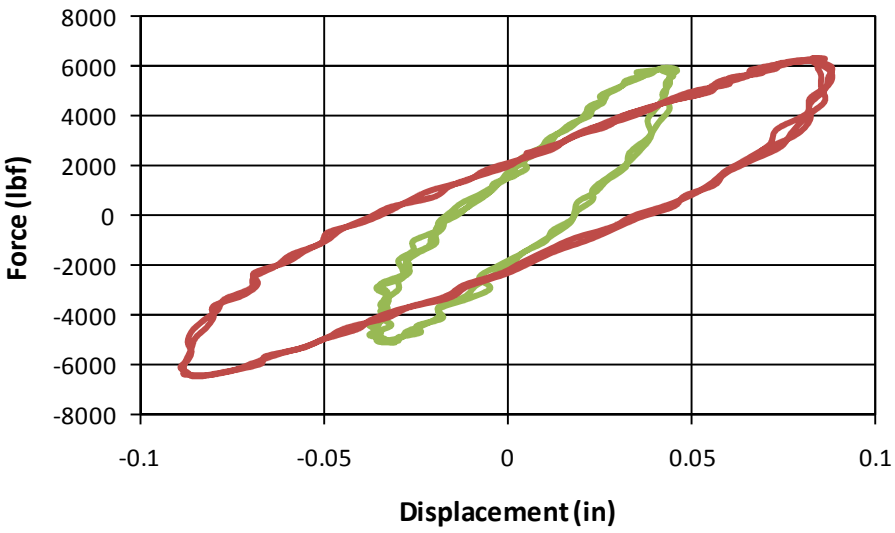

Figure 6 - 14 Damper Hysteresis Loop at 0.707 Hz

Figure 6 - 15 Photograph of Debonded Damper

6.7.3.2. Cyclic Testing #2

After the initial failure of the rubber-steel bond, the damper was rebuilt. The second set of cyclic tests for HPCD was run at all displacement amplitudes and frequencies specified in the protocol in Table 6-1. The damper experienced problems with the bond between the channel section and

the rubber slab. The extent of the debonding was not as severe as during the first cyclic tests. The results are somewhat compromised because of the unknown amount of rubber that is fully adhered to the steel. The results demonstrate proof that the device has merit. More discussion about the rubber-steel bond is presented in Sections 6.7.3.4 and 6.7.3.5.

Hysteresis loops of two types are presented. The HPCD response represents the force-displacement relationship at the end of the BRB element including the deformation of the damper and the BRB. The hysteresis loops for the damper alone are also presented. The reason for showing these two sets of data is to explore the reduced effectiveness of the HDRD due to deformation in the BRB. The difference is shown in Figures 6-16 and 6-17. The HPCD experiences a greater deformation for the same force. The hysteresis loops for the damper are slightly larger, showing the reduced effectiveness of the damper in series with the BRB. However, the programmed displacement amplitudes do not correspond with the graphs, because reaction displacements were accounted for in data reduction. Also, the hydraulics did not have the capacity to meet the velocity requirements.

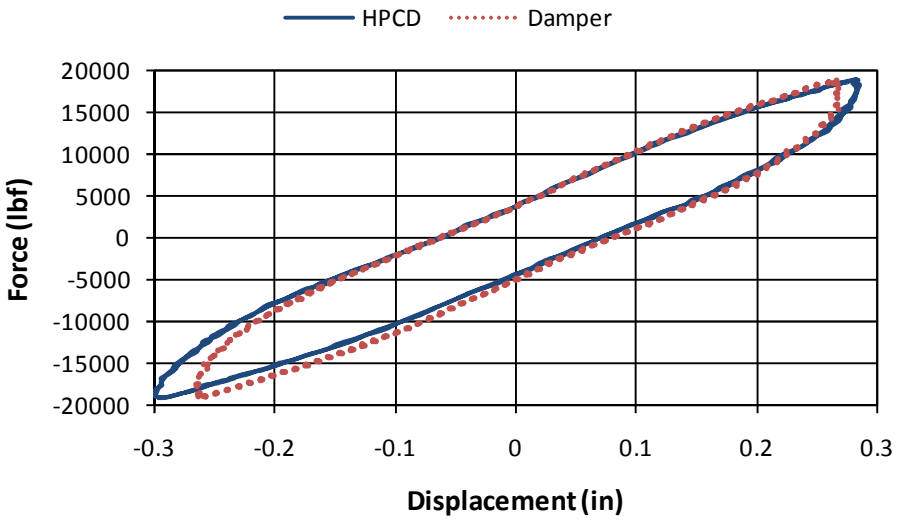

Figure 6 - 16 Hysteresis Loops for HPCD and Damper Only (0.283 Hz)

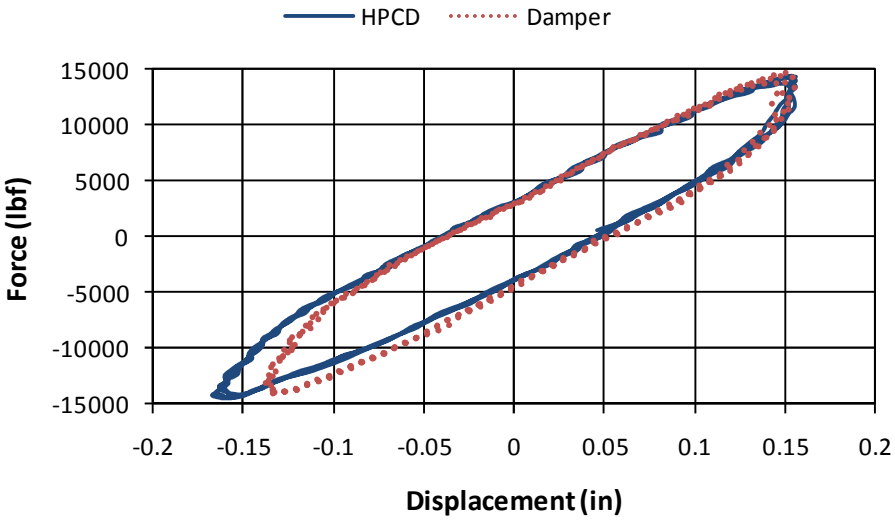

Figure 6 - 17 Hysteresis Loops for HPCD and Damper Only (0.471 Hz)

Table 6-3 shows the results of the equivalent loss factor calculated for each of the loops. The effectiveness of the damper in the HPCD was also calculated. The effectiveness of the damper ranges from a low of 0.701 at 0.283 Hz and an amplitude of 0.09 in. to a high of 0.857 at the same frequency with an amplitude of 0.38 in. The average effectiveness of the damper is 0.795, indicating a reduction of about 20% due to the flexibility of the brace.

The results of the damper tests show typical properties of a high damping rubber. The Mullins effect is present in the first cycle at a previously unattained displacement. This is illustrated in Figure 6-18. The first loop at each increment of amplitude is higher than the subsequent loops. After the first loop, the stiffness is reduced until the material reaches a steady state. This process can be seen in Figure 6-19 which are hysteresis loops of the damper at a frequency of 0.283 Hz.

Table 6 - 3 Loss Factor and Effectiveness of Rubber Damper and HPCD

Amplitude (in)		Frequency (Hz)			
		0.283	0.354	0.471	0.707
0.09	Damper	0.398	0.374	0.404	0.383
	HPCD	0.279	0.265	0.293	0.288
	% Effective	0.701	0.709	0.725	0.753
0.19	Damper	0.343	0.334	0.368	0.369
	HPCD	0.270	0.270	0.287	0.287
	% Effective	0.787	0.809	0.782	0.776
0.28	Damper	0.329	0.331	0.332	0.365
	HPCD	0.261	0.273	0.281	0.285
	% Effective	0.791	0.826	0.846	0.780
0.38	Damper	0.302	0.307	0.322	NT*
	HPCD	0.259	0.261	0.266	NT*
	% Effective	0.857	0.850	0.825	NT*
0.45	Damper	0.289	0.302	NT*	NT*
	HPCD	0.245	0.255	NT*	NT*
	% Effective	0.847	0.843	NT*	NT*

NT* - Not Tested due to limitations of the hydraulic system.

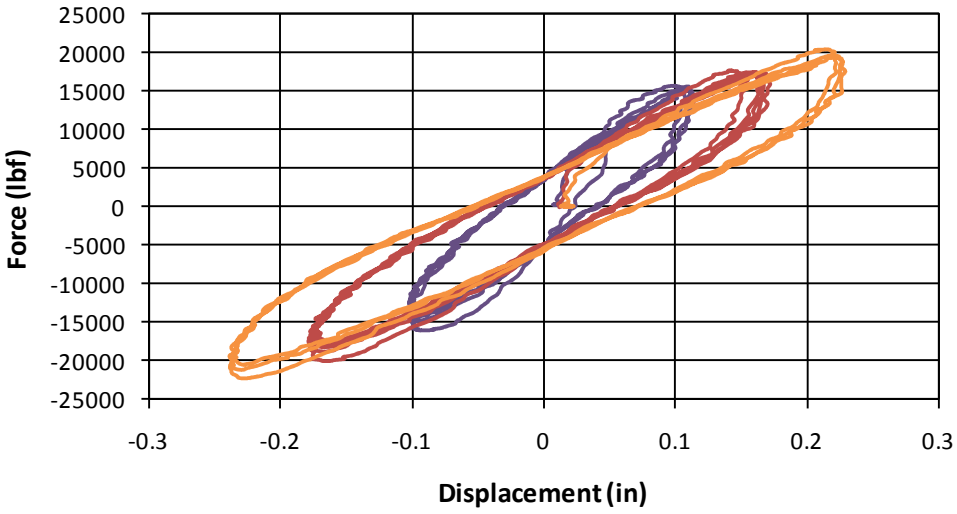

Figure 6 - 18 Hysteresis Loops for HPCD (0.283 Hz)

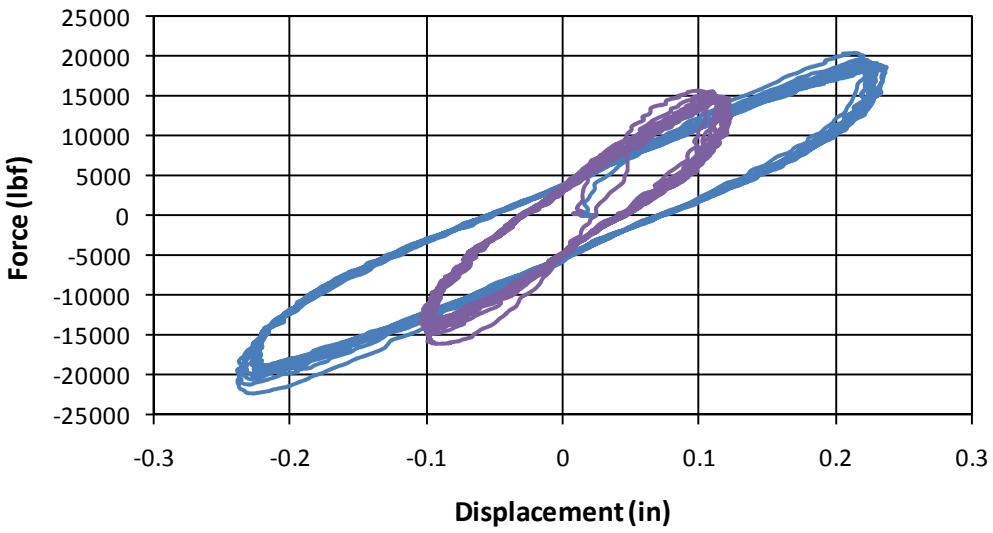

Figure 6 - 19 Hysteresis Loops for Damper in HPCD (0.283 Hz)

The nonlinear stress-strain behavior of the rubber is apparent in Figure 6-20. Although some of the decreasing stiffness of the hysteresis loops may be due to debonded rubber, the initial high stiffness of the rubber followed by a decreasing stiffness is typical of the shear stress-strain curves from the static testing done to characterize the rubber materials.

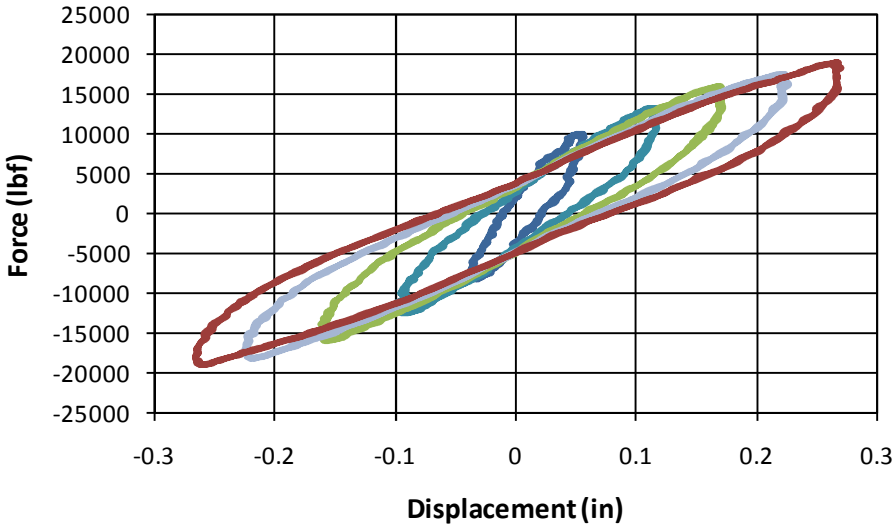

Figure 6 - 20 Hysteresis Loops for Damper in HPCD (0.354 Hz)

The effect of frequency on the damper over the range tested is shown in Figures 6-21 and 6-22. The figures show the results at two different amplitudes. The aforementioned inability of the hydraulic system to meet the velocity demands is apparent in both plots. As the frequency

increases, the maximum displacement decreases as a result of the inability of the actuator to maintain the displacement protocol. The lowest frequency plots are the outside loops, with the highest frequency loop being the most interior. Typically, the properties of high-damping rubber change with frequency. The range of frequencies tested here is small enough that both the stiffness and damping properties are relatively constant. Even with the change in deformation due to the actuator, the constant stiffness and width of the loops verify the limited variation in properties. This can also be seen in Table 6-3 by comparing the equivalent loss factors.

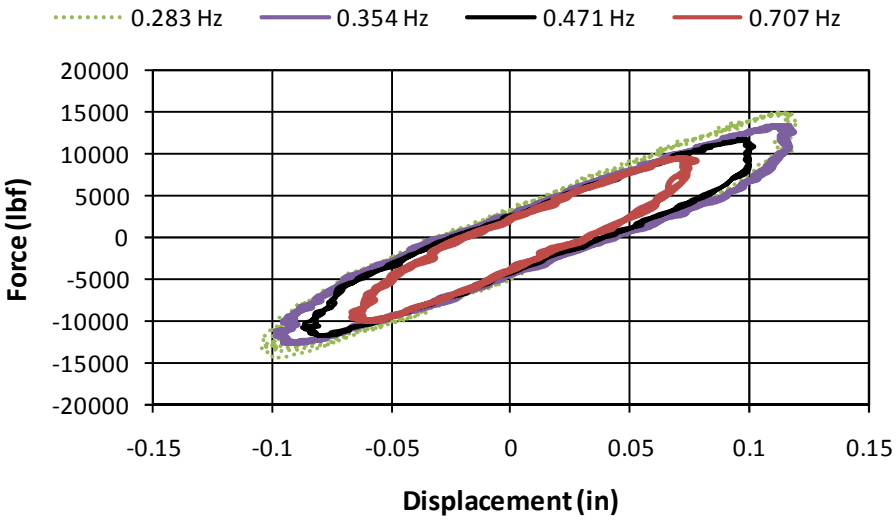

Figure 6 - 21 Hysteresis Loops for Damper in HPCD (0.19 in.)

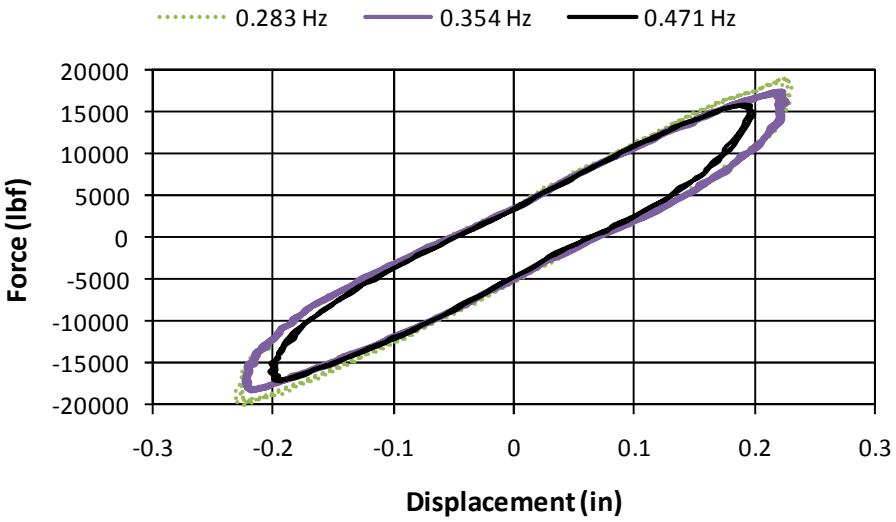

Figure 6 - 22 Hysteresis Loops for Damper in HPCD (0.38 in.)

The behavior of the BRB core during the cyclic tests was monitored by the six strain gages. Stress-strain plots for the core are shown in Figure 6-23 and 6-24. The bending in the core was removed by averaging the strain gages on each side of the core. SG1 and SG2 represent the strain gages at the quarter points and SGCL represents the gages at the center line of the core. The results show that for the cyclic tests, the strain was uniform over the length of the BRB core. Figure 6-24 shows an interesting response for the smallest displacement amplitude. A small hysteresis loss is apparent in the stress-strain plot. This hysteresis is likely due to friction between the core and the restraining member. This small energy dissipation occurs for all of the tests but is only visible in Figure 6-24 due to the scale of the vertical axis.

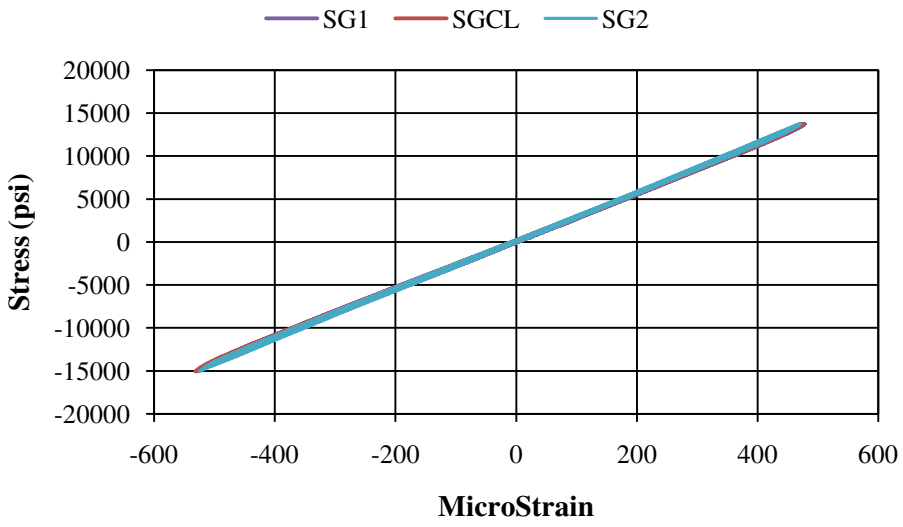

Figure 6 - 23 Stress-Strain Plot for BRB Core (0.45 in., 0.354 Hz)

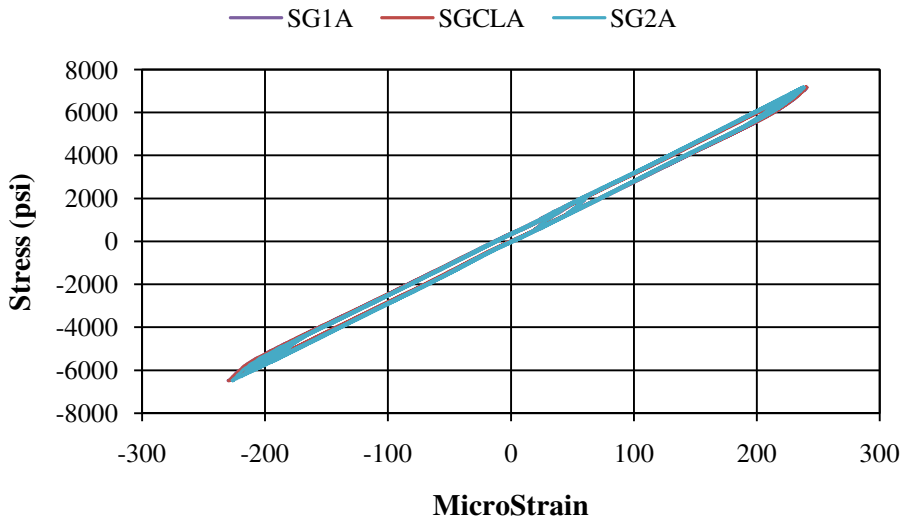

Figure 6 - 24 Stress-Strain Plot for BRB Core (0.09 in., 0.354 Hz)

The cyclic tests of the dampers demonstrate behavior typical for a high-damping rubber and a reduction in damper effectiveness in series with a BRB. Due to the unknown loss in strength and stiffness, the design values for the stiffness and loss factor of the damper cannot be verified as expected. With the exception of minor issues with the rubber-steel bond, the HDR damper performed well during the cyclic testing.

6.7.3.3. Static Testing

Static testing was used to test the HPCD prototype according to the AISC Seismic Specification (AISC 2005). The device did not reach the full requirements. Table 6-4 shows the results of the testing. The first three displacement levels were completed, although the target displacements were not exactly met. The controller was programmed with displacements that should have accounted for support displacements, but the reduced data shows that the design values were not achieved. The fourth displacement level was not completed. The first cycle and the tension half of the second cycle were completed at 150% of the design displacement. The second compression cycle was not completed due to a local buckling of the core and the buckling restraining member. The lockout mechanism of the damper performed well, as the damper locked out at a displacement of 0.44 in. in tension and 0.53 in. on the compression side. These values increased to 0.45 in. and 0.56 in. in the last cycle prior to failure, indicating deformation of the bolt holes.

Figure 6-25 shows the force-displacement plot of HPCD for the first displacement level. Figure 6-26 shows the stress-strain plot for the BRB core for the same segment of loading. The phased behavior of the HPCD is readily apparent from the hysteresis plot. The lockout of the dampers is followed by the increase in stiffness with the subsequent yielding of the BRB. The stress-strain plot shows a typical hysteresis loop for an axially loaded member. The yield load is higher on the compression side due to friction between the core and the restraining member. The traces are jagged due to the measurement device. The wire pots are used to measure large deformations, and the initial cycles of the BRB core represent small increments. The strain gages provided much better measurement but were damaged during the initial inelastic cycles.

Table 6 - 4 Results of Static Test Protocol

Displacement Level	# Cycles Completed	Expected Cycle Displacement (in)	Actual Cycle Displacement (in)	Cycle Inelastic Deformation	Cumulative Inelastic Deformation
Δ_y	2	0.6	0.61	1.5	6
$0.5\Delta_{bm}$	2	0.75	0.71	2.5	15.9
$1.0\Delta_{bm}$	2	1.5	1.39	9.2	52.6
$1.5\Delta_{bm}$	1.5	2.25	1.98	15.3	98.4
$2.0\Delta_{bm}$	0	3	NC*	NC*	NC*
$1.5\Delta_{bm}$	0	2.25	NC*	NC*	NC*

NC* - Not Completed

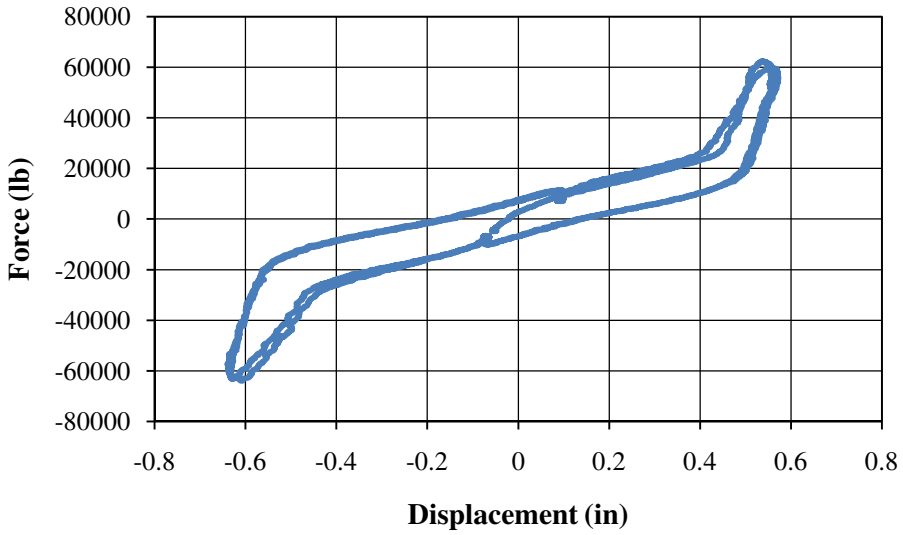

Figure 6 - 25 HPCD Force-Displacement Plot – Cycle 1

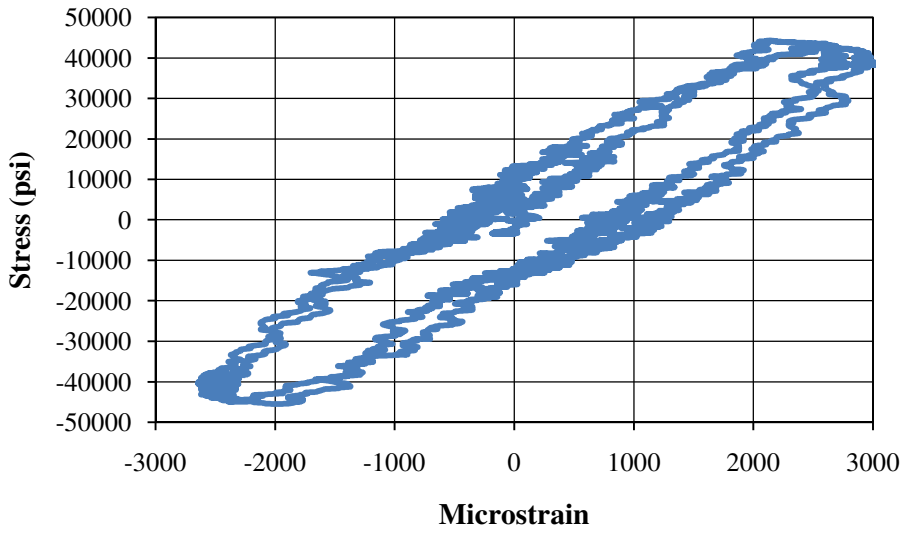

Figure 6 - 26 BRB Core Stress-Strain Plot – Cycle 1

Figure 6-27 shows the displacement of the damper for the first cycle of static testing. The lockout of the damper is evident by the increase in stiffness. Note that the damper lockout is slightly larger in compression than in tension.

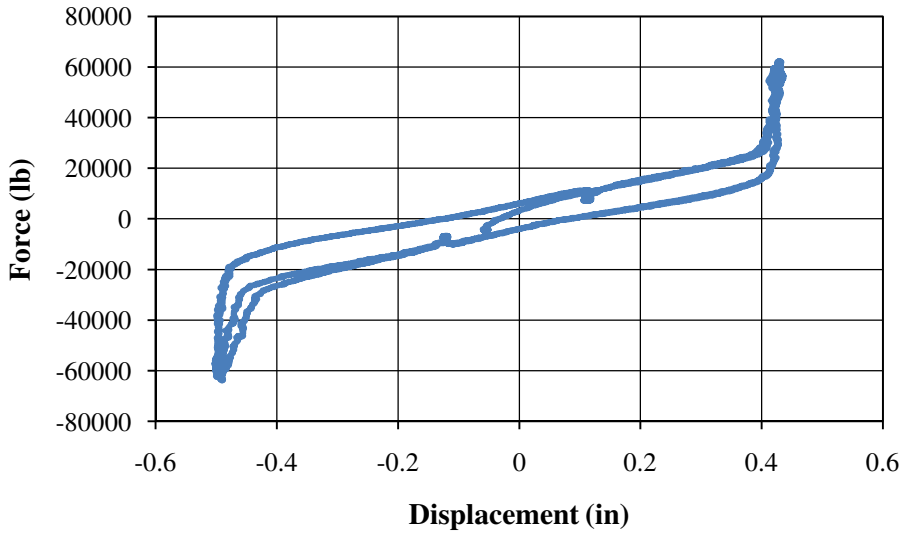

Figure 6 - 27 HDR Damper Force-Deformation Plot – Cycle 1

Figures 6-28 and 6-29 show the force-displacement and stress-strain plots for the second cycle the protocol. The plots are similar to the previous plots, with increased inelastic deformation.

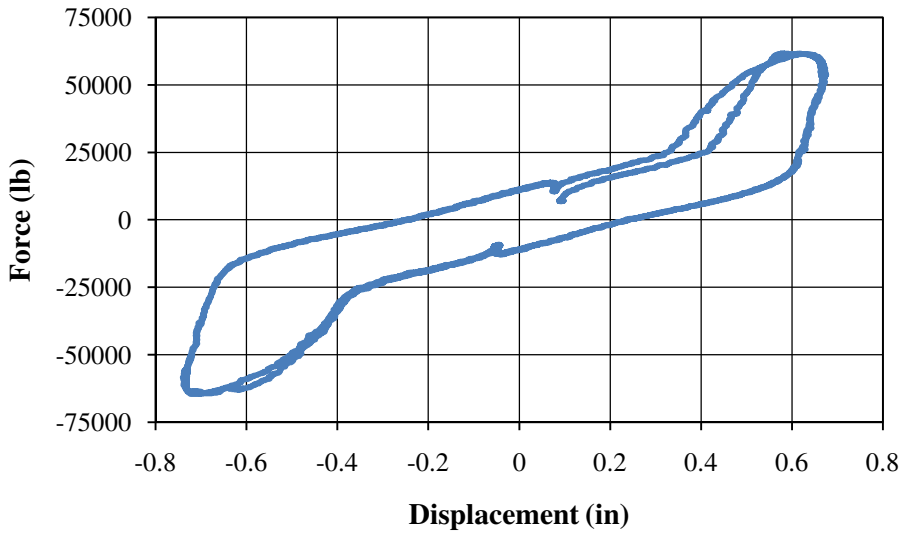

Figure 6 - 28 HPCD Force-Displacement Plot – Cycle 2

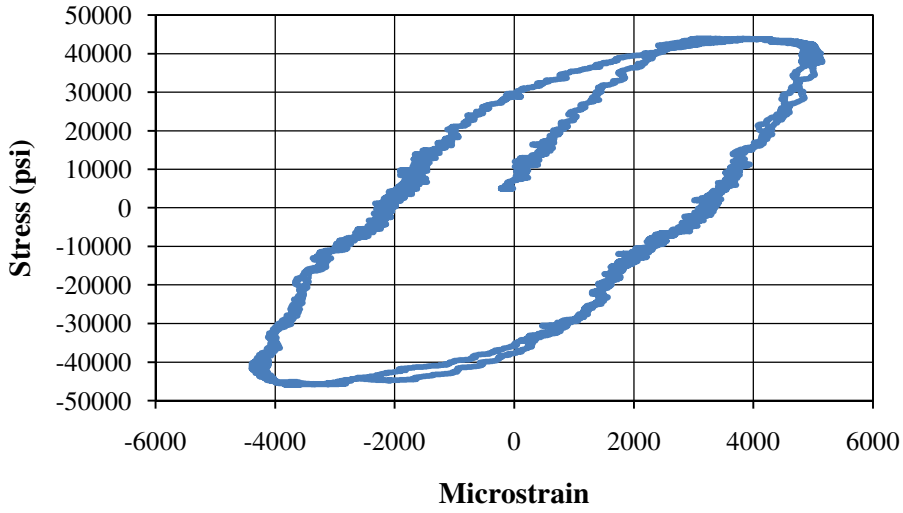

Figure 6 - 29 BRB Core Stress-Strain Plot – Cycle 2

Figures 6-30 through 6-31 are the force-displacement and stress-strain plots for the third cycle of displacement. This is the level of the design displacement. During these cycles, the compressive load exceeded the load limits set on the controller, so the hydraulics shut down. The data acquisition did not stop, so the re-start of the hydraulics is visible. The hysteresis loops show that significant ductility in compression and tension has been achieved. The larger force in compression indicates continuing friction between the core and the buckling restraint.

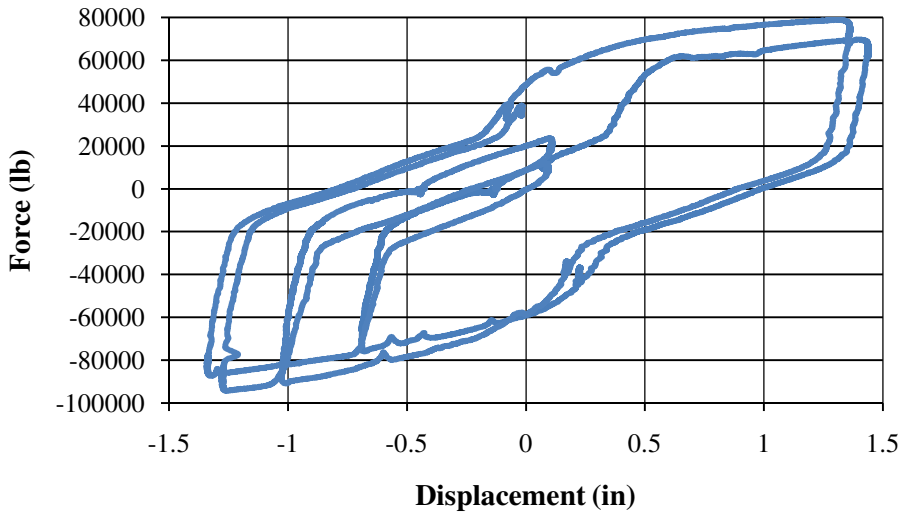

Figure 6 - 30 HPCD Force-Displacement Plot – Cycle 3

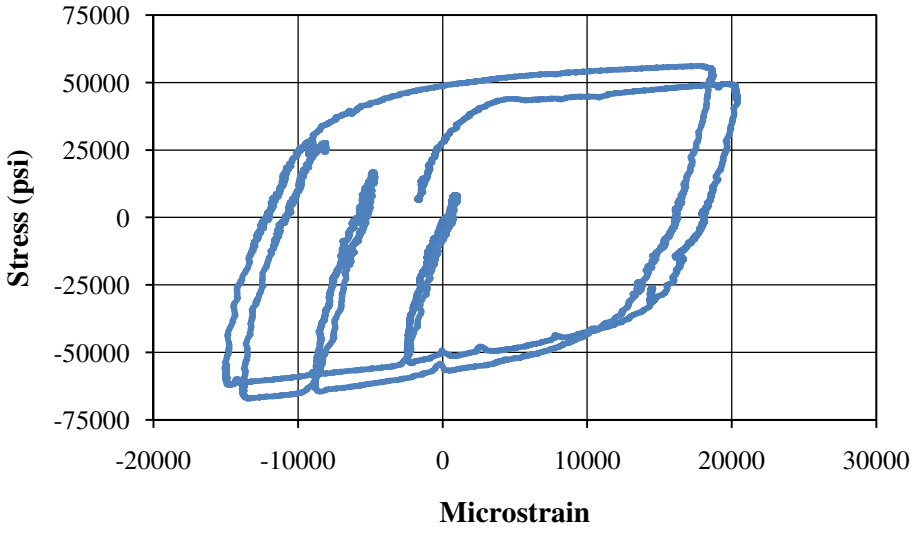

Figure 6 - 31 BRB Core Stress-Strain Plot – Cycle 3

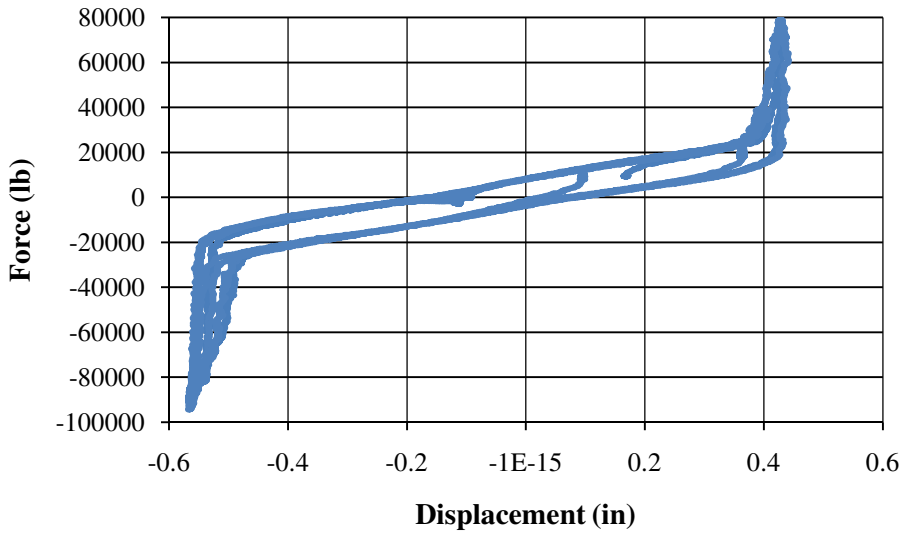

Figure 6 - 32 HDR Damper Force-Deformation Plot – Cycle 3

Figures 6-33 and 6-34 show the force-displacement and stress-strain plots for the fourth and final displacement level. The tension cycles show the expected performance. The first compression cycle again exceeded the force limits and was restarted after the hydraulics shut down. The first compression cycle shows evidence of the beginning of the local buckling failure. At the bottom of the loop in both plots, the magnitude of the force is decreasing as the deformation increases. When the device was returned to the zero displacement point after the final tension cycle, the first visible proof of the buckling occurred. This can be seen in the jagged line just prior to the failure of the device. The device failed due to a local buckling in the BRB core. The apparent initiator of the failure was that the restraining channel web thickness was not sufficient. The inadequate thickness is particularly critical around the slot for the BRB core stiffener. The core plate buckled in an S-shape with circular web buckles in an alternating pattern occurring in the channels. The resulting eccentricity caused buckling of the side plates added to the restraining mechanism. Figure 6-35 shows a photograph of the position of the HPCD when the testing was terminated. The buckling occurred in the weak direction of the core.

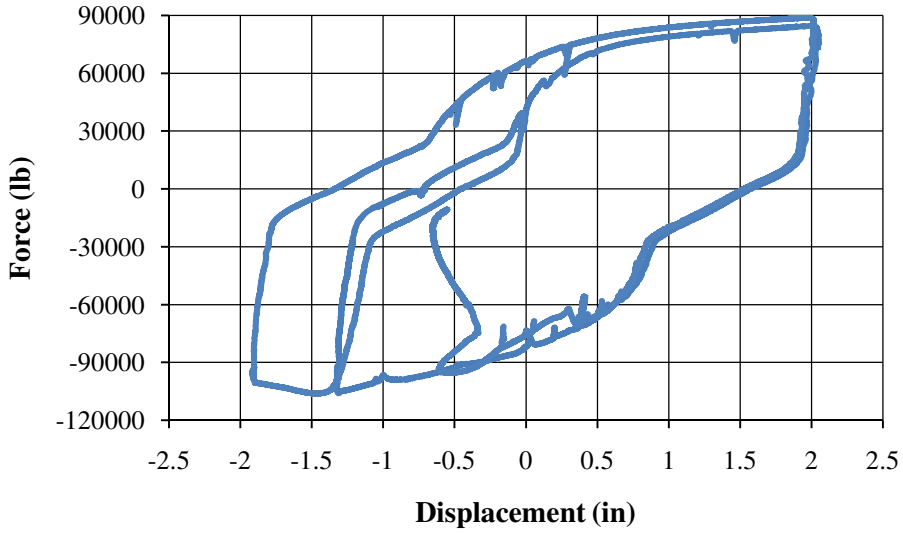

Figure 6 - 33 HPCD Force-Displacement Plot – Cycle 4

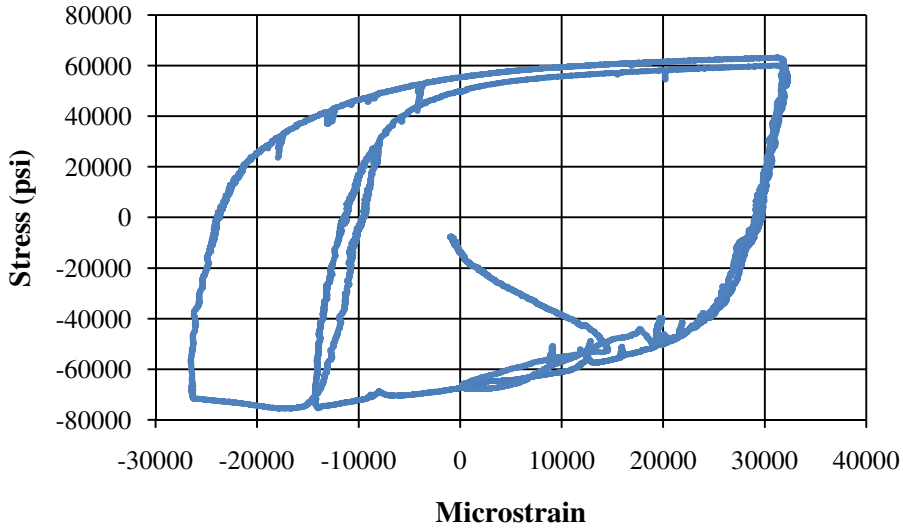

Figure 6 - 34 BRB Core Stress-Strain Plot – Cycle 4

Figure 6 - 35 Photograph of Buckled HPCD

Figure 6-36 shows the BRB disassembled after testing. The S-shaped buckling of the core is clearly visible. The upward wave created a circular shaped deformation in the web of the top channel not shown in the photo. The two downward waves of the core created similar deformations in the lower channel. Figure 6-37 shows a closer view of the buckled core and the matching deformations in the web of the channel. The two deformations occurred at web penetrations. One occurred at the end of the slot for the stiffener, the other occurred at the site of a strain gage access hole.

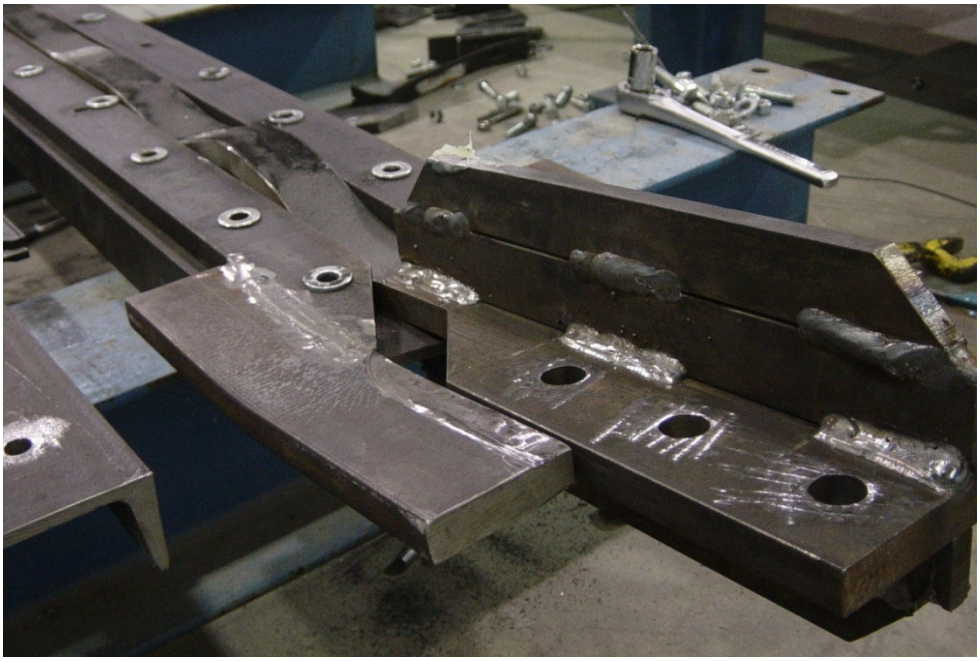

Figure 6 - 36 Photograph of Disassembled BRB After Testing

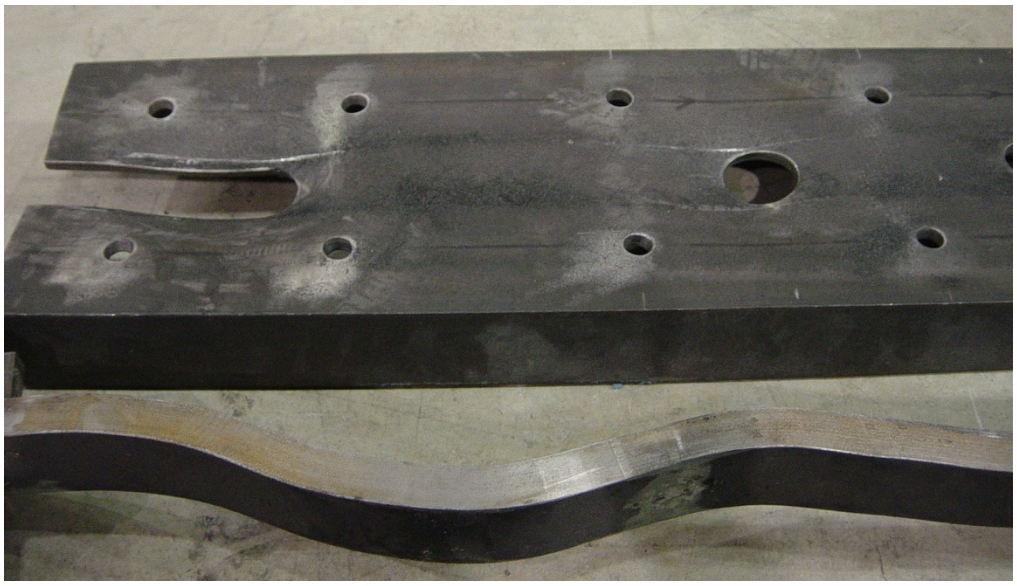

Figure 6 - 37 Photograph of Buckled BRB Elements

The static testing of the HPCD prototype highlighted an unexpected failure mechanism in the BRB restraining mechanism. The device did not complete the required protocol for BRB elements. The local buckling initiated an undesirable failure after significant inelastic deformation. The tests did show that the lockout mechanism functioned excellently, which demonstrated the feasibility of the phased behavior required for the hybrid device.

6.7.3.4. Rubber-Steel Bond Tests #1

Bonding of the rubber slabs to the steel for the damper is a critical aspect. During testing of the HPCD prototypes, debonding of the rubber occurred. The mill scale detached from the steel channels. The bond to the center steel plate remained intact for the most part. The initial preparation included sanding and thorough cleaning of the specimen but not total removal of the mill scale. The failure due to the mill scale demonstrated the need to completely remove the mill scale as part of the surface preparation. To verify that the removal of the mill scale would provide the needed strength, a small experimental study was completed using shear sandwich specimens. The dimensions of the shear specimens are shown in Figure 6-38.

Three separate surface preparations of the steel plate were used for six different test specimens. The surface preparation for the rubber was the same for all specimens. The rubber was abraded with fine grade sandpaper and cleaned thoroughly using isopropyl alcohol. The three different surface preparations for the steel plate are listed in Table 6-5. Figure 6-39 shows a picture of specimens after surface preparation. The top plates have surface preparation #2. The bottom

plates have the mill scale removed in accordance with surface preparation #3. The right side of the plates shows the surface prepared for bonding. The left half of the specimens is the unprepared surface.

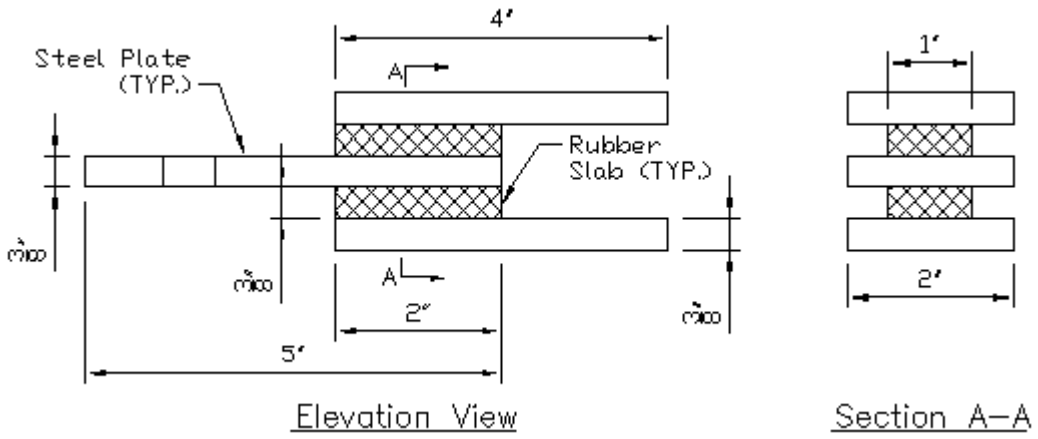

Figure 6 - 38 Sketch of Sandwich Shear Specimen for Bond Tests

Table 6 - 5 Description of Steel Surface Preparation

Surface Preparation	Description
1	Surface is thoroughly cleaned with isopropyl alcohol
2	Surface is sanded to remove loose mill scale and thoroughly cleaned with isopropyl alcohol
3	Mill scale is completely removed, surface is sanded and thoroughly cleaned with isopropyl alcohol

Figure 6 - 39 Surface Preparation of Steel Plates for Shear Sandwich Specimens

The specimens were tested statically in an MTS Insight electromechanical testing machine with a 30k capacity and load cell. The data acquisition was done with Testworks 4 software by MTS. The testing was completed under displacement control at a rate of 1 in/min. The slip in the grips was not critical, as only the maximum load at failure is reported. Figure 6-18 shows a specimen ready to be tested.

The test results are summarized in Table 6-6. The first number in the specimen number refers to the surface preparation. The second number is the number of the specimen within that group. The values for specimens 1-1 and 1-2 are shown as not tested (NT), as the specimen debonded while being placed into the testing machine. The failure was a result of the adhesive removing the mill scale from the steel sample. Figure 6-41 is a photograph of specimen 1-1 after failure. The adhesive and the mill scale can be seen on the rubber pad, showing that the mill scale was detached from the steel plate. This was not an unexpected result as this surface preparation did not comply with the manufacturer's specifications, but were done to see if the failure was similar to what occurred during the first HPCD cyclic tests. It should be noted that the mill scale for these steel plates was much easier to remove than for the center plate and the channels used for the HPCD specimens.

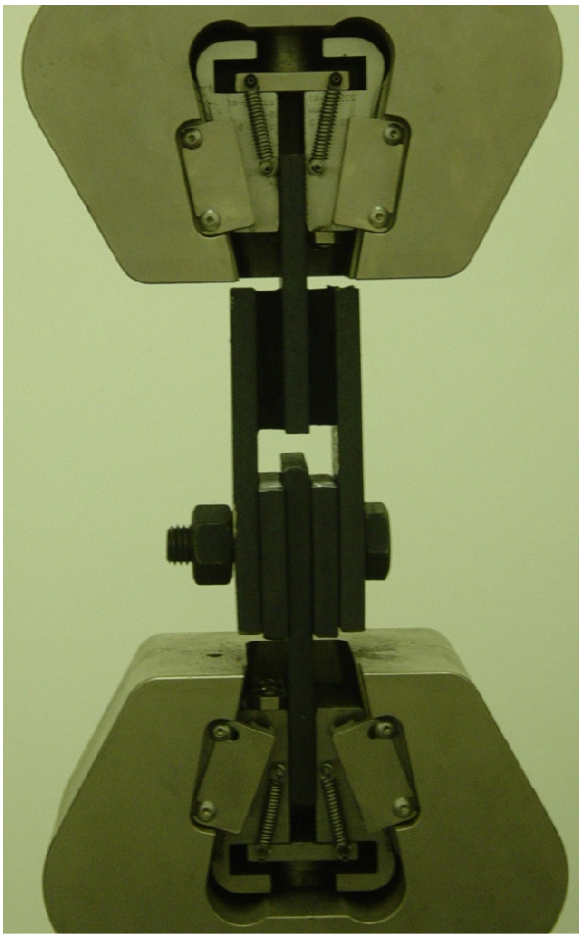

Figure 6 - 40 Sandwich Shear Specimen in Test Machine

Figure 6 - 41 Failure of Rubber-Steel Bond for Specimen 1-1

Table 6 - 6 Test Results for Shear Sandwich Specimens

Specimen Number	Maximum Load (lb)	Maximum Shear Stress (psi)
1-1	NT*	NT*
1-2	NT*	NT*
2-1	880.5	220.1
2-2	1187.6	296.9
3-1	1249.0	312.3
3-2	1249.1	312.3
* NT - Not Tested		

The other simple shear specimen test results demonstrate the necessity for complete removal of mill scale prior to bonding. Specimen 2-1 failed primarily through the mill scale debonding from the steel. Specimen 2-2 failed at a much higher load and showed some rubber failure. Figure 6-42 shows specimen 2-2 after testing. The bottom right portion of the bonded section of the center piece shows rubber residue, indicating that the failure in that region was the rubber tearing. The difference in the values between 2-1 and 2-2 shows that although the bond to the mill scale can achieve significant strength, it is also unpredictable.

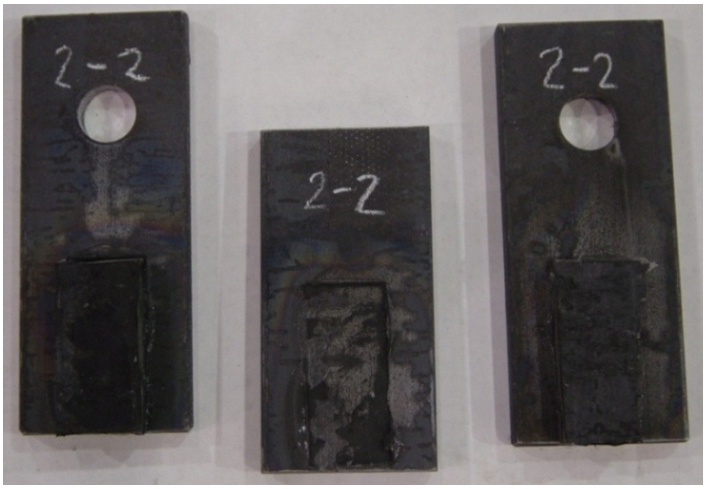

Figure 6 - 42 Failure of Rubber-Steel Bond for Specimen 2-2

The maximum force reported for specimens 3-1 and 3-2 are remarkably similar. They are not significantly increased above specimen 2-2, but the method of bond failure is different from previous specimens and consistent for the two similar specimens. Figure 6-43 is a photograph of specimen 3-1 after testing. Both surfaces where the bond was broken show evidence of rubber failure. The left and center pieces show a large percentage of the bond surface with rubber

residue. The fact that the samples both achieved a very similar strength and the significant amount of rubber residue present in the bonding area is proof that the adhesive is stronger than the inteerface with proper surface preparation. The result of this testing is that for HPCD specimen #2, the damper was disassembled and rebuilt after experiencing nearly total debonding of the channel sections. During the rebuilding process, all of the steel surfaces had the mill scale removed and were thoroughly cleaned prior to bonding.

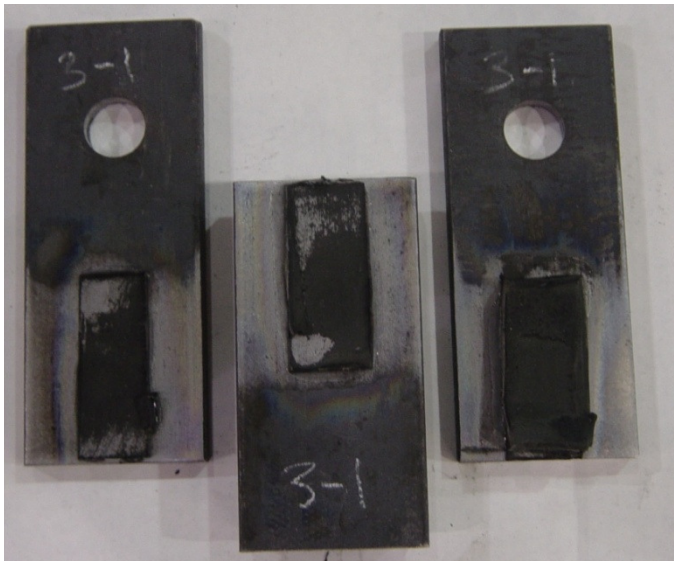

Figure 6 - 43 Failure of Bond for Specimen 3-1

6.7.3.5. Rubber-Steel Bond Tests #2

After experiencing a minor failure of the bond for the damper during cyclic tests, a short study of smaller dampers was completed to increase confidence in the ability to create a reliable bond between rubber and steel. After consulting with Corry Rubber, one recommendation was to try a different adhesive system. The alternate system is an epoxy adhesive with an additional surface treatment for the rubber. Lord Corporation's 310A/B system is a two-part, thixotropic epoxy adhesive system for use with metals, rubber, urethane and plastics. Chemlok 7701, also by Lord Corporation, is a surface treatment for vulcanized, thermoset and thermoplastic polymers. The surface treatment improves adhesion of the epoxy to the rubber.

The study was carried out with surplus materials from the HPCD prototype. The remaining stock allowed for 3 specimens with 4 in. square rubber slabs. Two specimens were constructed using the 310A/B epoxy adhesive. Specimen #3 was constructed using the same adhesive, 3M CA40H, used for the HPCD specimens. The geometry of the small damper specimens is shown in Figure

6-44. The previous mini dampers were only tested statically. The small dampers were designed to fit into the HPCD test frame with the BRB element replaced by back to back channels so they could be tested cyclically. Static tests following the cyclic tests were run at a displacement of three times the rubber thickness. Table 6-7 shows the displacement and frequency range of cyclic and static tests for the dampers. Figure 6-45 is a photo of the damper installed in the test frame.

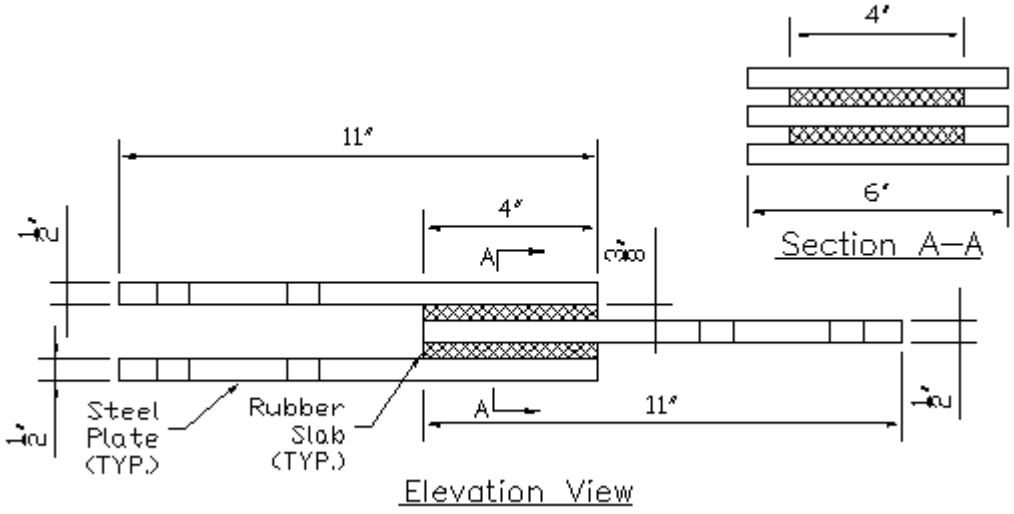

Figure 6 - 44 Sketch of Small Damper Specimens

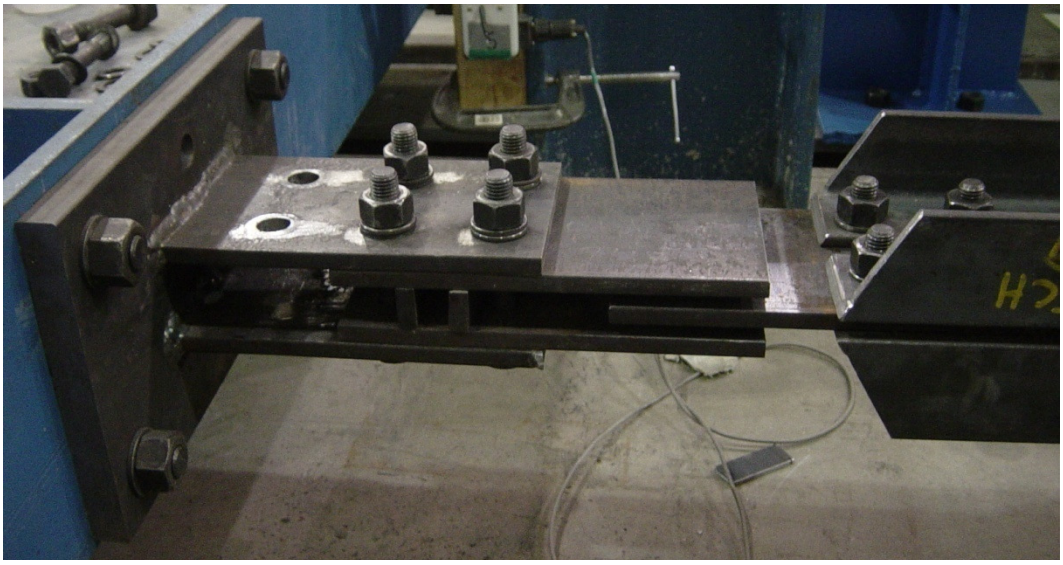

Figure 6 - 45 Photograph of Small Damper in Test Frame

Table 6 - 7 Range of Cyclic and Static Tests for Small Dampers

Displacement Amplitude (in)	0.09	0.19	0.38	0.56	0.75	1.13
Frequency (Hz)	0.25	0.25	0.25	0.1	0.1	Static Tension
	0.75	0.5	0.5	0.25		

The goal of this small experimental study was to successfully manufacture a rubber-steel damper and to investigate the reasons behind the failure of the HPCD dampers. Possible explanations for the premature bond failure are: The set time of 5-40 seconds for the CA40H is not sufficient with the large surface that had to be covered. Another possibility was that the surface of the channel was not flat. The undulations on the surface of the steel could cause some of the bond to be in tension once the pressure from the clamping was removed. The clamps were used during the curing process to ensure good contact between the surfaces. A third possibility was that because the rubber had been previously bonded, detached and the surface prepared again, the second bond may not have been as good.

The three specimens all had the same surface preparation. The mill scale was completely removed from the steel. The surface was then roughened with a palm sander and fine grit sandpaper. The surface was then thoroughly cleaned with isopropyl alcohol to remove any grease or particles. The rubber surfaces were cleaned and sanded with fine grit sandpaper. Just prior to bonding, both surfaces were cleaned again with alcohol. Both adhesive systems were applied according to the manufacturer specifications. The CA40H was quicker to apply and to set. The problem with the CA40H is that the set time does not allow for large applications easily. The 4 in. square dampers were not large enough to cause any problems. The 24 in. by 7.5 in. HPCD dampers were pushing the limits to cover the surface with adhesive and then place it within the short set time. The epoxy adhesive has a 30 min working time at room temperature. More work is required to measure the components, mix them together and apply the Chemlok 7701. However, the additional time before setting allows for precise placement and resetting if necessary. The drawback with the Chemlok is the long cure time at room temperature. The samples did not set-up for several hours. The process was shortened by adding heat, as the manufacturer's specifications recommended a high temperature cure for better bond properties and shorter cure time.

The results of the testing showed a similar performance for the three specimens. Figures 6-46 and 6-47 show hysteresis loops at 50% and 100% displacement and at a frequency of 0.25 Hz.

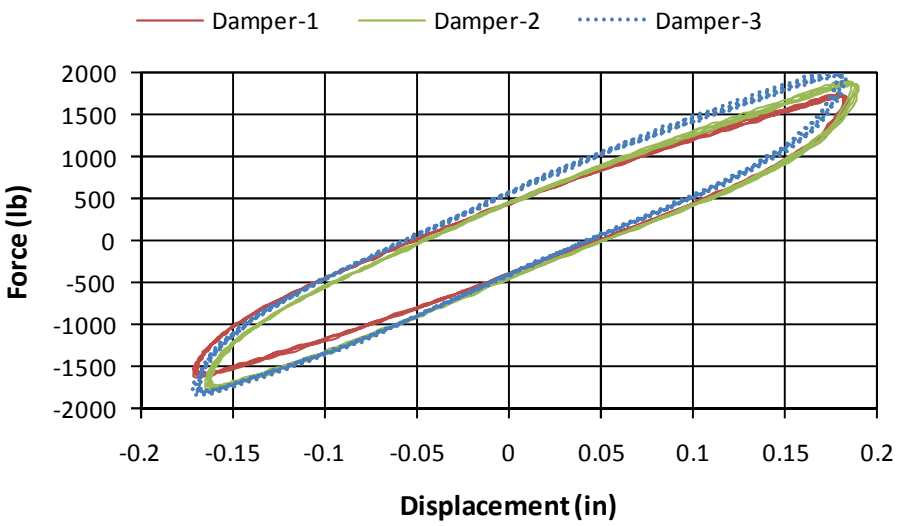

Figure 6 - 46 Hysteresis Loop for Small Dampers (0.25 Hz)

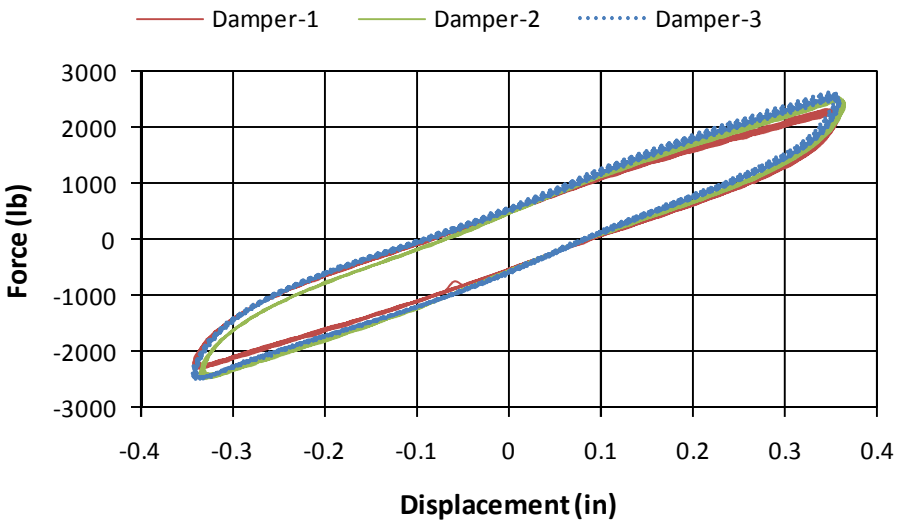

Figure 6 - 47 Hysteresis Loops for Small Dampers (0.25 Hz)

Each of the specimens performed well up to a displacement of 100% of the thickness or 0.38 in. At this level the samples all experienced some form of debonding. The initiation of the bond failure typically occurred where the edge of the plate and the rubber were aligned. It appears that this location is a weak point and a poor detail. This was not the only location of debonding, but it was the first location in all three samples. Figures 6-48 and 6-49 are photographs of this type of

bond failure. These photos were taken at larger displacements, but the locations of failure all initiated where the end of the plate and the rubber are aligned.

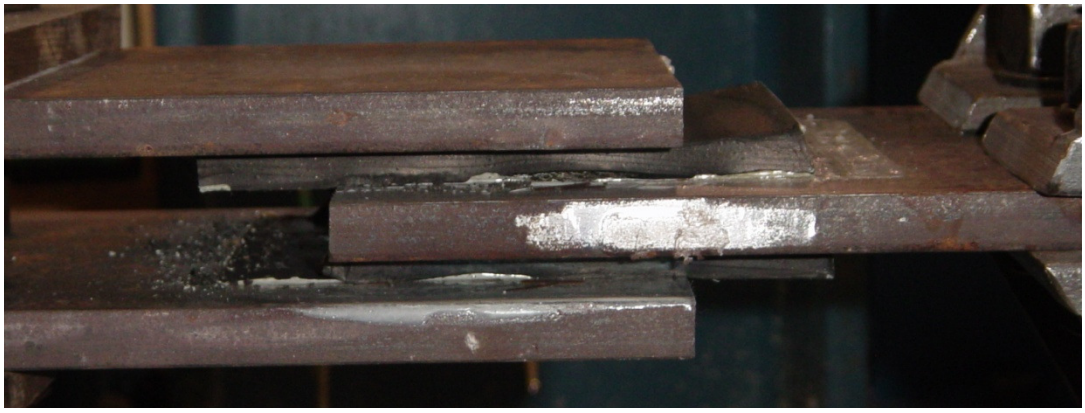

Figure 6 - 48 Photograph of Bond Failure of Small Damper #1

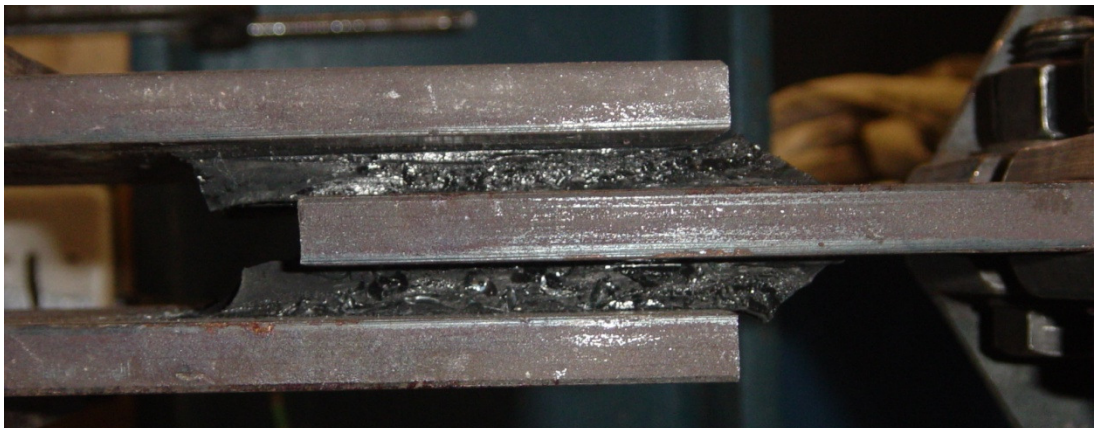

Figure 6 - 49 Photograph of Bond Failure of Small Damper #3

The degradation of the rubber-steel bond was most apparent at the level of 200% of the thickness of the rubber. Figure 6-50 shows the hysteresis loops for specimen #2 at increasing displacement and 0.25 Hz. There is an increase in force as the displacement increases and the hysteresis loops remain constant. The maximum level of displacement shown on this plot is 0.56 in., corresponding to 150% of the rubber thickness.

At a displacement of 0.75 in., the degradation of the bond becomes apparent. Figure 6-51 is a plot of specimen #2 at 0.75 in. Note the Mullins effect followed by continually decreasing stiffness. A steady state behavior was not reached after the first couple of cycles, as is typical. This indicates a continued degradation of the bond. The displacement amplitude is shown for specimen #3 in Figure 6-52. The degradation is not as severe for the compression side of the

loop. The reason is the location of the bond failure and the loading. Large simple shear displacement causes normal forces at the interface. If the area of bond failure is under compression, then the degradation is not as severe due to friction at the bond line which creates a weak bond. The degradation is more severe for the epoxy adhesive (specimen #2).

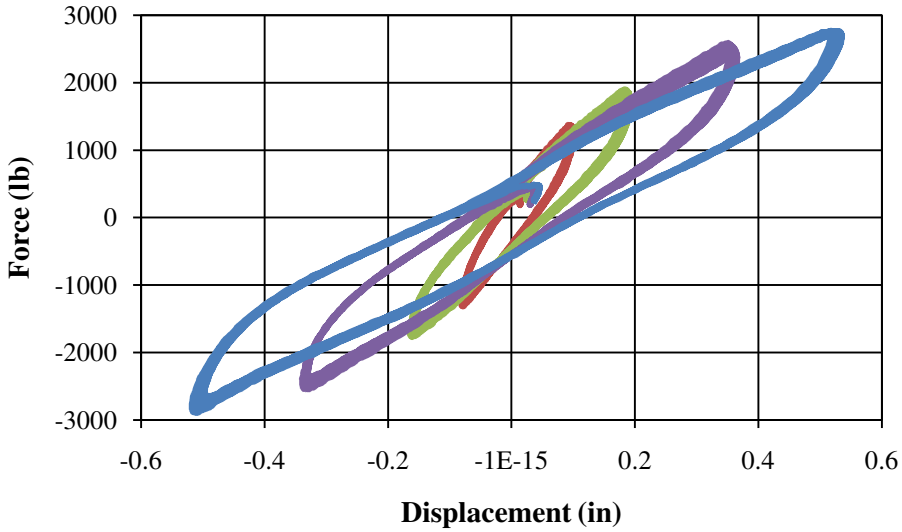

Figure 6 - 50 Hysteresis Loops for Small Damper #2 (0.25 Hz)

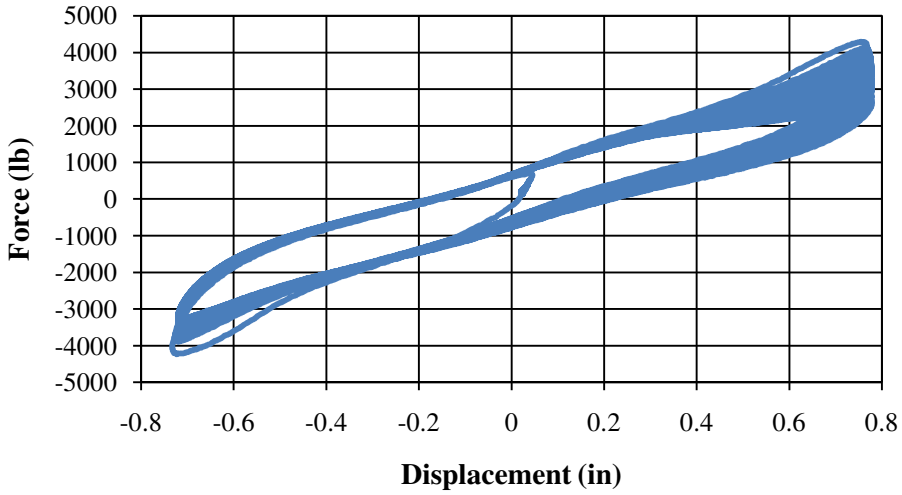

Figure 6 - 51 Hysteresis Loops for Small Damper #2 (0.10 Hz)

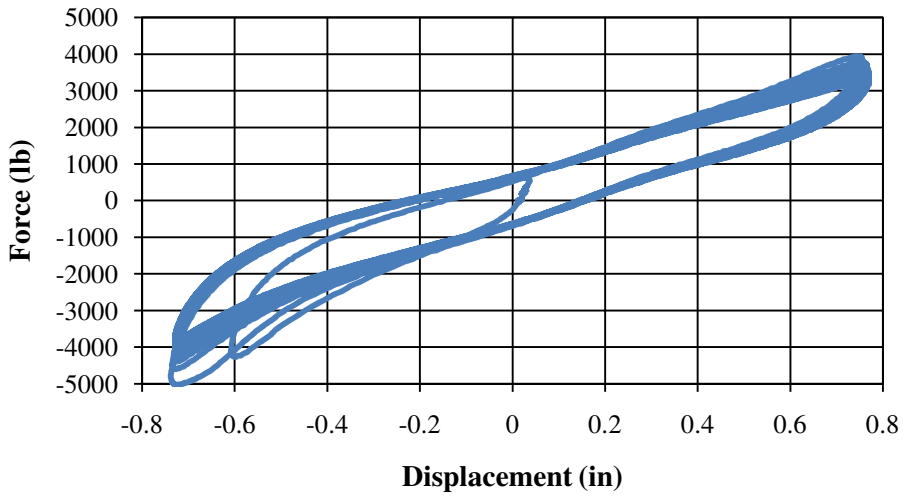

Figure 6 - 52 Hysteresis Loops for Small Damper #3 (0.10 Hz)

One constant for all the small dampers was the failure mechanism. The initial failures at the edges were followed by failure of the rubber. The surfaces of the steel after testing were covered with rubber residue, indicating failure of the rubber versus failure of the adhesive.

The tests on the small dampers indicate that there were minor problems with the bond at displacement levels expected of the HPCD dampers. However, the performance was much more reliable with both adhesive systems than for the HPCD tests, indicating that the adhesive was not the issue. One detail that should be modified based on observations made during this small study is that the rubber should be set back from the edge of the steel. Another observation was that the excess adhesive needs to be removed from the edge of the rubber. When a line of adhesive remains and hardens, it causes a stress concentration. The thickness of the rubber at the end of the slab is essentially reduced because it has to deform around a more rigid substance. The study showed that a better bond is possible with the CA40H adhesive. It also demonstrated that more study is required to determine the problems with the bonding of the damper for the HPCD.

6.8. Discussion of Results and Recommendations for Future Work

The purpose of the work in this chapter was to experimentally test an HPCD prototype and determine the viability of the concept. The critical components include the rubber damper, the damper lockout mechanism and the BRB element. Of the three critical elements, the damper lockout mechanism performed as expected. The rubber damper had minor problems with bond failure between the rubber and steel. Two small studies were run to ascertain the reason for the

bond failure. The studies did illustrate that some problems were present in the manufacturing process. Had trial dampers been constructed prior to manufacturing the HPCD damper, the bond issue may have been eliminated. The tests were not conducted earlier, as the rubber manufacturer did not indicate that problems were typical for this type of application. Future work is required to create a more reliable bond for these devices to be used in structures. The key will be inclusion of a rubber manufacturer to a greater degree to create a manufacturing process that creates a reliable bond. Another option would be to design a device that could have the rubber bonded to the steel during the rubber cure process. This type of bond is more reliable and stronger than a post-cured adhesive system.

The performance of the BRB element illustrated a design flaw and an unexpected failure mode in the prototype. These were prevented through addition of side plates and increasing the size of the BRB core stiffener. Failure of the HPCD specimen pointed out problems with the channel web. The problems were penetrations and an insufficient thickness of the web. The circular penetration would not be present in a typical design as it was only for the strain gages, however the buckling was present in an area without penetration. The channel web with the penetration was not strong enough to prevent formation of a buckling mechanism inside the restraint. The proposed solution for this problem is to increase the thickness of the web and provide stiffeners around the penetrations. A study to determine a minimum ratio of channel web to BRB core thickness should be done using FEA to prevent this failure in the future. Had the initial analysis of the device included all the elements of the HPCD, this failure could have been prevented. In addition to the failure of the web, the side plates added to the HPCD buckled, as it was the weak point in the buckling restraint system. The repair proposed for this problem is to lengthen the restraining channel so it continues past the transition to the full width of the core specimen. A sketch of proposed modifications to the restraining mechanism is shown in Figure 6-53. The modifications include a wider channel with a thicker web so the side plates can be attached to the channel. Another consideration would be to use a core with a larger ratio of the width to the thickness, which would require less stiffness to resist the buckling of the core. The thickness of the core plate was selected based on the thickness of the center plate for the damper. All these issues could be included in an analytical study to determine appropriate ratios for the member thicknesses.

The ultimate goal of this research is to create, analyze and test a prototype hybrid device. The design of the prototype device was tested successfully. The lockout mechanism performed well. The damper element had some problems with bond failure at the rubber-steel interface, but otherwise performed as expected. The BRB experienced a premature failure due to localized buckling in the core after achieving significant ductility in compression and tension. This failure was initiated by a localized buckling failure of the restraining mechanism. The experimental tests demonstrated that the device had the properties and behavior expected. As a first prototype, it also showed that the device prototype is in need of modification. The damper phase of the HPCD demonstrated the ability to dissipate energy under small levels of deformation. The second phase of the device demonstrated the ability of the BRB element to engage and dissipate large amounts of energy. Although further work is required in development, the potential to create a single hybrid device with existing passive control technology has been demonstrated.

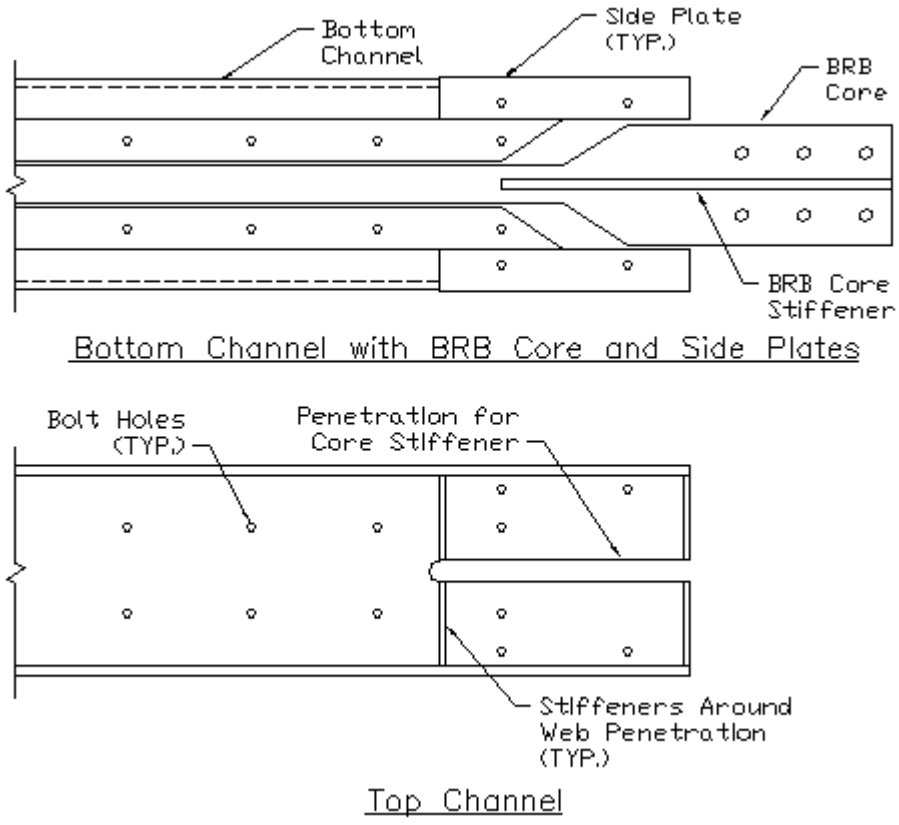

Figure 6 - 53 Sketch of Proposed Modifications to BRB Element

Chapter 7. Nonlinear Dynamic Response History of Steel Moment Frame Structures with Hybrid Passive Energy Dissipation Systems

7.1. Introduction

The concept of a hybrid device includes the previously described hybrid passive control device (HPCD). In addition to the HPCD, multiple options for hybrid combinations of passive dampers have been generated for this study. This chapter presents the results of an analytical study aimed at investigating the seismic response of steel moment frame structures with various standard and hybrid passive control systems. Nonlinear dynamic response history was completed using the Computers and Structures, Inc. (CSI) program SAP 2000 (CSI 2007). The performance of a steel moment frame with various hybrid damping systems is compared to a bare steel moment frame and a moment frame with typical passive control systems. The goal of the study is to highlight and compare the benefits and possible drawbacks of employing hybrid passive control systems. It is also an initial investigation into the effect of the variables associated with these systems.

7.2. Analysis Plan

A special steel moment frame was designed to meet current code requirements for both strength and displacement including second-order effects. The frame had 9-stories above grade and was 5 bays wide. The codes used for design are ASCE Standard 7-05 (ASCE 2006) and the AISC Seismic Provisions for Structural Steel Buildings (AISC 2005). The lateral system design was controlled by drift limitations. This code compliant moment frame was then altered to create a modified frame to which the various earthquake protection devices were added. The modified frame was created by reducing the column and beam stiffnesses by approximately 30% and 45%, respectively. The reduction in stiffness also reduced the strength of the modified structure. The modified frame met the strength requirements of the code including p-delta but exceeded code specified drift limits. The columns were not decreased in size as much as the beam sections. This was done to account for increased axial force demands from the energy dissipation devices and to maintain strong column-weak beam requirements. The reduced-strength structure was developed to demonstrate the performance of the hybrid devices. Initially the devices were added to a drift controlled structure. In this structure, the hybrid devices were not experiencing adequate deformation due to the stiffness of the code compliant moment frame.

The analyses were run in the form of an incremental dynamic analysis (IDA) (Vamvatsikos and Cornell 2002) using two earthquake records. An IDA is a method used in earthquake engineering for running a series of analyses to investigate the performance of a structure. The ground motion records are selected and appropriately scaled for application to the seismic hazard required. The scaled ground motion is then run at multiple scale factors to see the effect of the increasing ground accelerations. A scale factor of 1.0 in this IDA is equivalent to the design basis earthquake (DBE), with 1.5 being the maximum credible earthquake (MCE). The ground motion records were run at scale factors of 0.2, 0.4, 0.6, 0.8, 1.0, 1.2, 1.4 and 1.5. A damage measure such as maximum displacement, drift, or base shear is selected and plotted on the x-axis with the scale factor plotted on the y-axis. This curve is sometimes termed a dynamic pushover curve, as the curve will become horizontal when the structure begins to fail. Several damage measures were calculated, including maximum roof drift, maximum base shear and maximum total roof acceleration. This mix of results allowed for the best overall performance analysis of the various seismic protection strategies. Although not presented as an IDA, results of maximum story drifts and residual displacements along the height of the building were investigated at the DBE level.

The first record is the East-West component of the Sylmar County Hospital record of the 1994 Northridge earthquake. The second ground motion is the East-West component of the El Centro record of the 1940 Imperial Valley earthquake. These were chosen to include two different types of events. The Northridge (NR) event consists of a large initial pulse followed by smaller accelerations for a short duration. The Imperial Valley (IV) record has a strong initial stage followed by a longer duration of significant ground acceleration. In addition to dynamic analyses, nonlinear static pushover (SPO) analyses with p-delta effects were run. The unscaled Northridge and Imperial Valley acceleration records are shown in Figures 7-1 and 7-2, respectively.

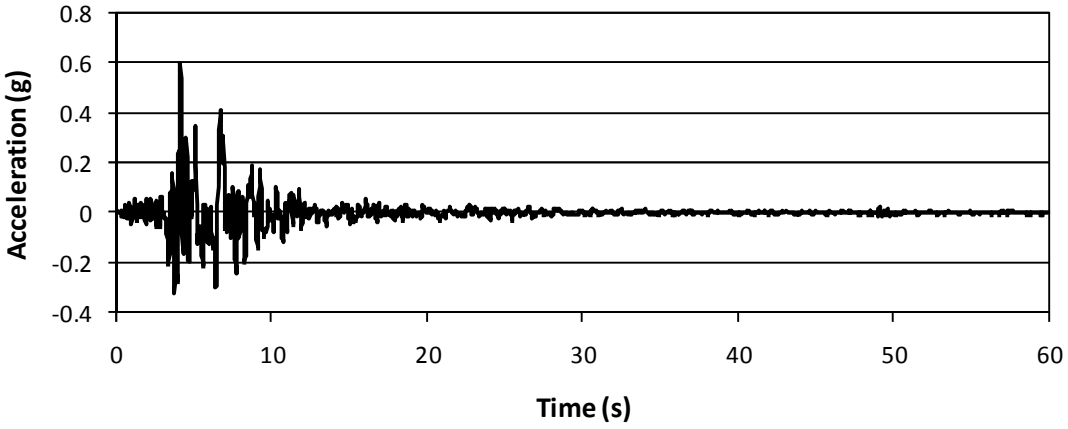

Figure 7 - 1 Sylmar County Hospital Earthquake Record (Northridge 1994)

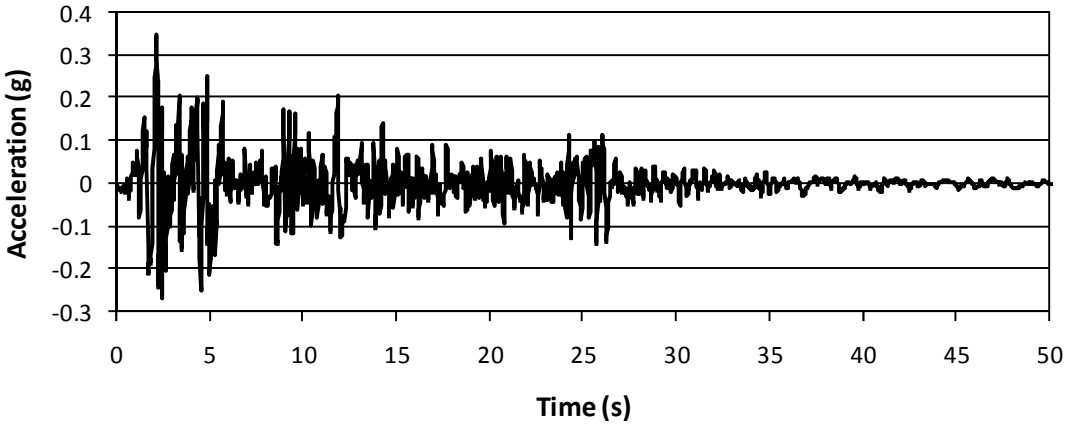

Figure 7 - 2 El Centro Earthquake Record (Imperial Valley 1940)

7.3. Model Description

The following section provides a description of the analytical models. It includes the modeling of the frame elements, second-order effects and hybrid devices. It describes the various passive energy dissipation systems and the elements used in SAP 2000 to model them.

7.3.1. Modeling Steel Moment Frame Elements and P-Delta Effects

The steel moment frame elements were modeled using frame elements with yielding plastic hinges. The frame elements are modeled using ASTM A992 steel. Each beam has a plastic hinge including strain hardening about the strong axis at each end. The columns were not expected to yield but were modeled with an interacting axial load-bending moment plastic hinge at each end. The only exceptions to this were the spliced columns which were modeled as two frame elements per story. Each spliced column element had an interacting hinge at the end closest to the beam column joint. A centerline analysis was used with respect to deformations of the beam-

column joint. Research has shown that the centerline analysis can be a reasonable approximation of beam-column joint deformation without explicitly modeling the panel zone (Charney and Marshall 2006). For this analysis, the focus is on the behavior of the added hybrid and standard energy dissipation systems and the relative performance during seismic events. When the beam-column joint is designed according to the AISC Specification, yielding of the panel zone is prevented by minimum required thicknesses so the deformation is minimal and can be approximated by the centerline model.

P-delta effects were implemented using a slaved ghost column. The ghost column is made of rigid truss elements with moment releases at each end. The lateral displacement at each floor level is tied to the displacement of the frame at the same level through nodal slaving. The gravity loads for the leaner columns tributary to the frame are applied to nodes of the ghost column.

7.3.2. Seismic Resisting System Configurations

The analyses include eight different seismic resisting systems. The first is a special steel moment resisting frame (SMRF). This configuration is a bare steel frame with no added energy dissipation. The seismic energy is dissipated as the beams reach yield and plastic hinges are formed. All of the other systems are created by adding one or more types of energy dissipation elements to an SMRF. The standard and hybrid energy dissipation systems are used with the reduced strength SMRF.

The next three systems are typical energy dissipation systems that have been successfully implemented in structures. The BRB frame (BRBF) system is created by adding buckling-restrained braces to the reduced strength SMRF. This type of system would be considered a dual system by ASCE 7-05. Another way to add energy dissipation is by adding viscous fluid dampers (VFD) or high-damping rubber dampers (HDRD). The primary difference between these systems is that an HDRD adds static stiffness to the structure while a VFD does not.

The final four configurations are referred to as hybrid systems because they combine rate-independent and rate-dependent energy dissipation devices. The hybrid passive control device (HPCD) consists of a rubber damper in series with a BRB. The damper has a lockout mechanism which allows it to transfer enough force to yield the BRB. Part of the locking mechanism is the initial gap prior to locking. This gap forces deformation to occur primarily in the damper prior to the steel brace engaging. It permits the behavior of the initial phase of the device with the rubber

damper providing energy dissipation at low displacements. Similar to the concept of the HPCD is the hybrid passive control device using a viscous fluid damper (HPCD-VFD). The only difference is that a standard viscous fluid damper is used. A similar locking mechanism with little initial stiffness is used to provide the gap.

The final two configurations are variations on the previously described hybrid systems. The hybrid frame (HYFR) configuration places an HDRD in parallel with a BRB. This is done by placing the BRB on one side of a chevron brace and the damper on the other side. Because the damper element and the yielding element are on opposite sides of the chevron brace, one will be in tension and the other in compression during seismic events. To maintain equivalent strength and stiffness of the frame in both directions in-plane, the HYFR devices must be used in two bays. In the second location, the damper element must be on the opposite side of the chevron brace from the first location. The same must be done with the BRB element. With this layout of the devices, the same stiffness and damping is provided in both directions of the frame. The two-phase behavior is provided by placing a lockout mechanism having essentially zero initial stiffness in series with the BRB. One benefit of this configuration is that the damper can continue to be effective when the BRB is yielding. Placing a BRB in parallel with a viscous fluid device creates the hybrid frame with a viscous damper (HYFR-VFD). The same lockout mechanism is used with the BRB from the HYFR system. A simplified diagram of the hybrid systems is shown in Figure 7-3. Note that for the HYFR and HYFR-VFD, denoted (c) and (d) in the figure, two bays are required for symmetry.

This collection of standard and hybrid energy dissipation systems allows for a comparison of the performance of typical passive seismic protection systems with the hybrid systems. Table 7-1 presents the abbreviations and a short description of each system used in this work. For the hybrid systems, a number will be added to the end of each abbreviation. This number refers to the size of the gap before the lockout mechanism engages. For this study two sizes, 0.5 in. and 1.0 in., were used. The reasons for selecting these two gaps are discussed in a later section. As an example of a model abbreviation, an HPCD with a 0.5 in. gap would be referred to as HPCD-050. The 1 in. gap version of the same device would be HPCD-100. The same pattern would apply to all the hybrid systems. The results also display the earthquake record for the analysis with NR and IV for Northridge and Imperial Valley, respectively. For example HPCD-050-NR is an HPCD model with a 0.5 in. gap subjected to the Northridge ground motion.

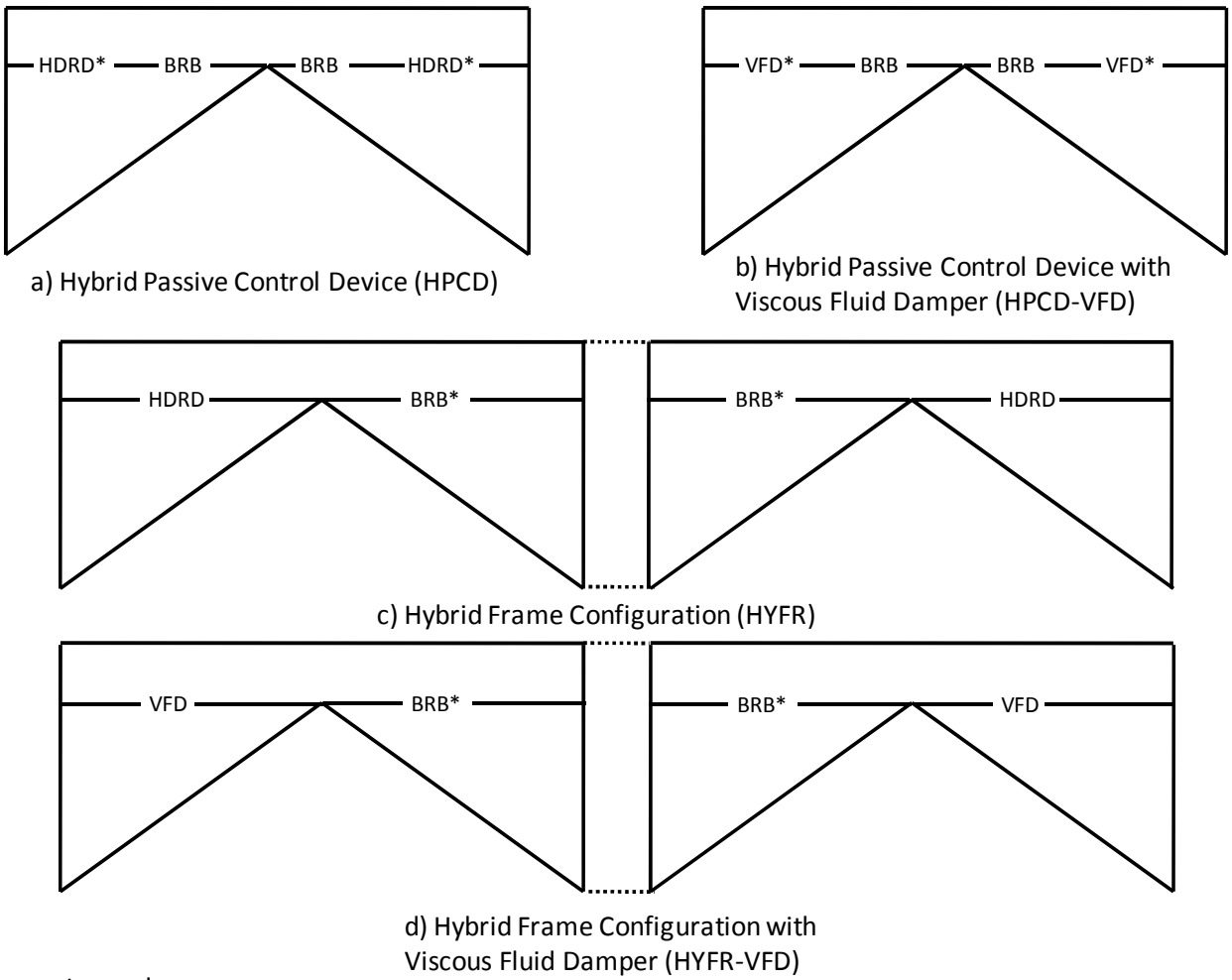

a) Hybrid Passive Control Device (HPCD)

b) Hybrid Passive Control Device with Viscous Fluid Damper (HPCD-VFD)

c) Hybrid Frame Configuration (HYFR)

d) Hybrid Frame Configuration with Viscous Fluid Damper (HYFR-VFD)

Legend:

HDRD – High Damping Rubber Damper VFD – Viscous Fluid Damper
BRB – Buckling Restrained Brace
Note – An "*" denotes the element with a locking mechanism.

Figure 7 - 3 Diagram of Hybrid Energy Dissipation Systems

Table 7 - 1 Seismic Resisting System Descriptions and Abbreviations

SMRF	Fully Code Compliant Special Steel Moment Resisting Frame (LA9 or CHA9)
BRBF	Reduced Strength SMRF with Buckling Restrained Braces
HDRD	Reduced Strength SMRF with High Damping Rubber Dampers
VFD	Reduced Strength SMRF with Viscous Fluid Damper
HPCD	Reduced Strength SMRF with Hybrid Passive Control Device
HYFR	Reduced Strength SMRF with Hybrid Frame Configuration
HPCD-VFD	Reduced Strength SMRF with Hybrid Passive Control Device Using a Viscous Fluid Damper
HYFR-VFD	Reduced Strength SMRF with Hybrid Frame Configuration Using a Viscous Fluid Damper

7.3.3. Modeling Energy Dissipation Elements

The energy dissipation elements were modeled using a combination of linear and nonlinear link elements in SAP2000. Figure 7-4 illustrates the types of springs used in the various configurations of hybrid damping systems. The abbreviation in parentheses represents the type of damper used. The HPCD is illustrated in Figure 7-4(a). The rubber damper is modeled using a multilinear elastic spring in parallel with a linear viscous damper. A multilinear elastic spring provides the capability to have several legs with different elastic stiffness. Figure 7-5 illustrates the force-deformation relationships for the various multilinear elastic spring elements. The multilinear spring in the HPCD is used to represent the initial stiffness of the rubber damper followed by an increased stiffness when the locking mechanism engages. The linear damper is used to represent the viscous damping. These two elements in parallel are then placed in series with a multilinear plastic spring which represents the BRB. The multilinear plastic spring allows for representation of yielding including strain hardening. This pattern of link elements is then mirrored on the opposite side of the chevron brace. Because the link elements only have stiffness in the axial direction, problems were encountered with links in series. This was overcome by providing bending stiffness with parallel frame elements. The frame elements had an axial release at one end so all the axial force was in the link elements,but are not shown in the figure for clarity.

The HYFR is shown as Figure 7-4(c). In this configuration, a rubber damper is placed in parallel with a BRB element. The two-phase behavior is achieved by placing a gap element in series with the BRB. This configuration allows the damper to continue dissipating energy when the BRB engages. It also removes the requirement of a lockout mechanism in the damper. The rubber damper is again represented by a multi-linear elastic link and linear damper. In this case, the second leg of the spring represents the hyperelastic nature of the rubber damper. The element used to model the gap is a multi-linear elastic element with nearly zero initial stiffness. An initial stiffness of 0.5 k/in. was used to represent friction in a slotted connection locking mechanism.

The two remaining models, Figures 7-4(b) and (d), are the HPCD and HYFR with a viscous damper replacing the rubber damper. For the HPCD with a viscous fluid damper (HPCD-VFD), the multilinear elastic spring with zero initial stiffness is used to lockout the damper. The damper is locked out at the specified displacement allowing the BRB to engage. The hybrid frame configuration with a viscous device (HYFR-VFD) is shown in Figure 7-4(d). In this case both

the multilinear spring and damper, representing the rubber damper, are replaced by the linear viscous damper. For both the rubber damper and the fluid damper, the damping constant is designed to provide the same first mode damping ratio as the HDRD.

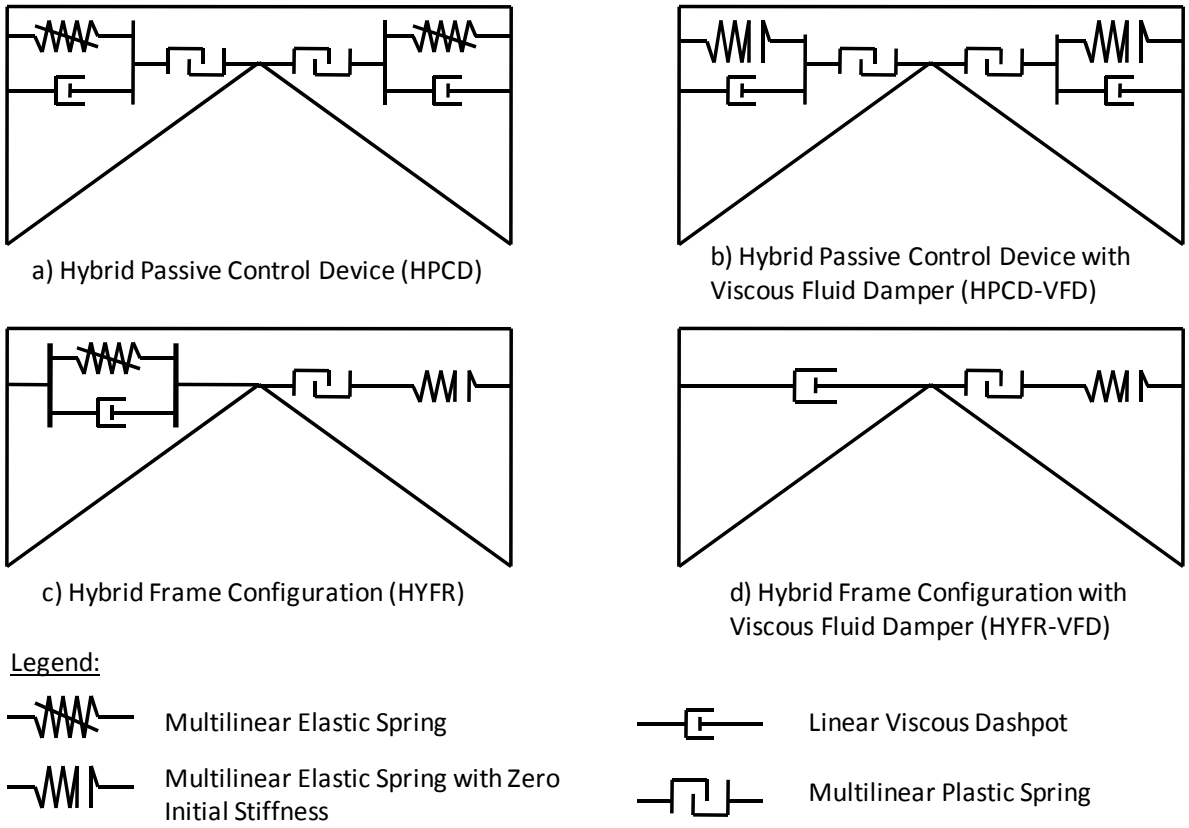

Figure 7 - 4 Modeling of Hybrid Energy Dissipation Configurations

In addition to the four cases shown in Figure 7-4, the same link elements were used to model the energy dissipation elements used in the BRBF, VFD and HDRD models. A BRB was modeled using the same multilinear plastic element modified for a longer core length. The longer yield length reduced the stiffness of the multilinear plastic spring. The frames with added viscous fluid or high-damping rubber dampers were modeled using the same individual or combinations of link elements. It is noted that the energy dissipation elements were connected at the beam-column joint. Figure 7-5 shows examples of the three multilinear elastic curves used in the SAP models.

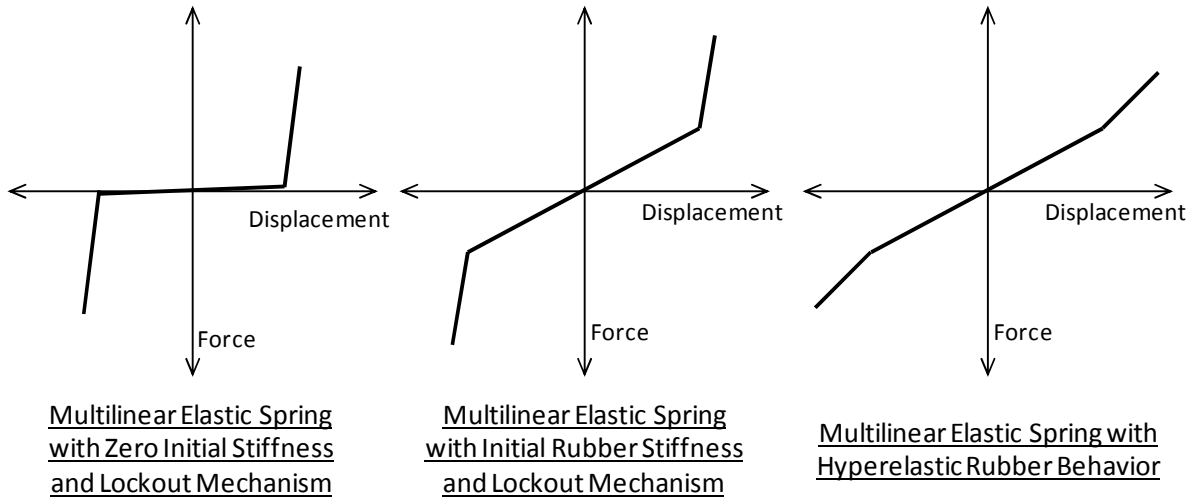

Figure 7 - 5 Diagram of Multilinear Elastic Elements Used in SAP2000

7.4. Structural Design

The 9-story special steel moment resisting frame (SMRF) models are based on the SAC Steel Project model buildings (FEMA 2000). The geometry, design loads and seismic weights were used directly from the SAC project report. The sizes of the members for the SAC Los Angeles 9-story structure were used as a starting point but were modified to meet the current provisions of ASCE 7-05 (ASCE 2006) and the AISC Seismic Provisions (AISC 2005). The Charleston, SC structure used the same geometry, design loads and seismic weight as the SAC structure but was designed for lateral loads based on local seismicity. The purpose of the Charleston structure is to investigate the performance of hybrid devices when the p-delta effects are greater due to a weaker and more flexible lateral system. Two steel moment frame structures were designed for each location. The first is code compliant for both strength and drift including p-delta. The loads used for strength requirements were developed using the Equivalent Lateral Force (ELF) method using the maximum period allowed by the code. The loads for calculating displacements were based on the analytical period provided by the analysis software unless it was also limited by the code. The second structure meets code specified strength criteria but not drift. Both structures were designed to meet strength requirements including p-delta. The purpose of the second model is to provide a structure where the effects of the added energy dissipation can be demonstrated. It is referred to in this work as the modified steel moment frame.

7.4.1. Seismic Hazard

The structures were designed as typical office buildings on Site Class D soil. The gravity load design for each structure is exactly the same. The only difference is the seismic hazard. The first location is Los Angeles, CA with a latitude and longitude of 34.05 and -118.25. The spectral acceleration values were taken from the USGS Java program, "Seismic Hazard Curves, Response Parameters and Design Parameters," which is available for free download.[2] The program reported the short and 1 s period accelerations for a site class B soil as 2.159 g and 0.723 g respectively. These values were modified for site class and multiplied by 0.667 to produce design spectral accelerations of 1.439 g for short period and 0.723 g for a 1 s period.

The second location, Charleston, SC, has a latitude and longitude of 32.79 and -79.94. The USGS program reported the short and 1 s spectral accelerations of 1.471 g and 0.361 g for site class B soil. The design spectral values for this location are 0.981 g and 0.404 g. The design response spectra from ASCE 7-05 are shown in Figure 7-6.

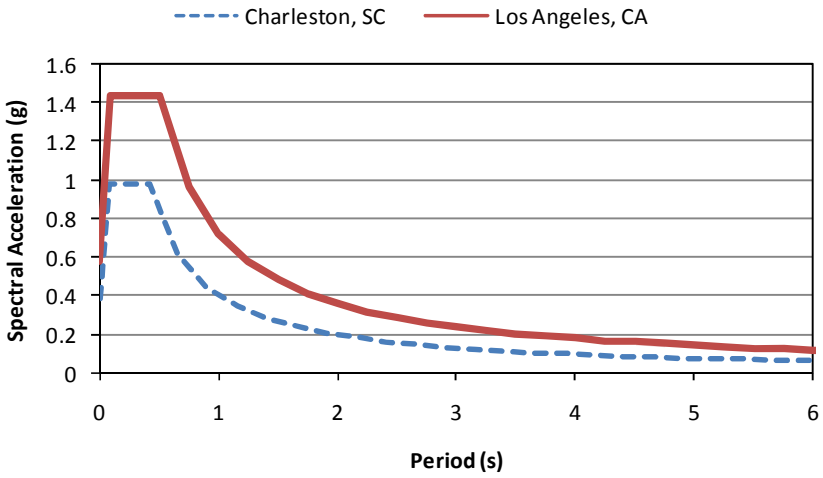

Figure 7 - 6 Design Response Spectrum for Los Angeles, CA and Charleston, SC

7.4.2. Los Angeles Structure

7.4.2.1. Structure Description and Design

Based on the design spectral acceleration values from the Los Angeles area for short and 1 second periods of 1.439 and 0.723 g respectively, the structure falls into ASCE 7-05 Seismic Design Category D. The approximate period, T_a, of the structure based on equation 12.8-7 of ASCE 7-05 gives 1.31 s which is significantly less than SAP 2000 which calculates a first mode

[2] http://earthquake.usgs.gov/research/hazmaps/design/

period of 2.48 s for the LA moment frame structure. The code provides an upper limit on the period by specifying a coefficient, C_u, multiplied by the approximate period, T_a . The upper limit period, C_uT_a, is 1.83 s. The response modification factor, R, was taken as 8 for a special steel moment resisting frame, which resulted in a seismic response coefficient, C_s, of 0.049. C_s was then used to determine the strength level earthquake forces using the ELF method. The total base shear is 980.2 k. These forces were used to design the structure for strength including p-delta using the SAP 2000 design module. The design for drift limits was done using loads generated without the C_uT_a cap. The full period of 2.48 s could not be used due to equation 12.8-6 in ASCE 7-05 which is required for structures with S_1 greater than 0.6 g. For the LA structure, the minimum allowed value for C_s is 0.045. This provided some reduction in forces but it was not significant. The base shear for drift checks is 896.7 k. The strength and drift level story forces are shown in Figure 7-7. The code compliant structure with the p-delta ghost column on the right is shown in Figure 7-8.

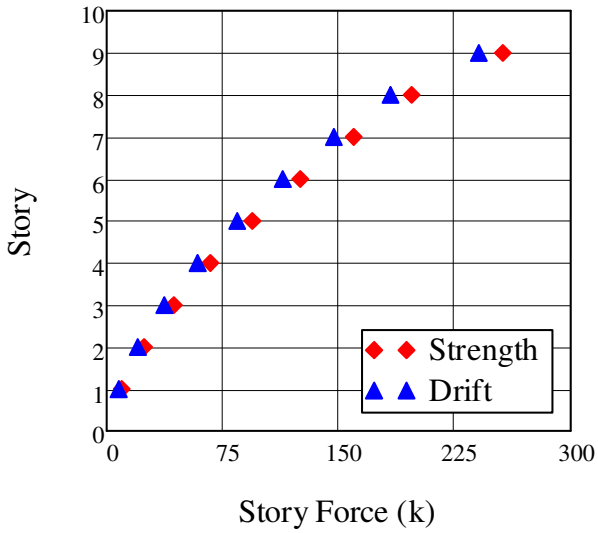

Figure 7 - 7 Story Forces for Los Angeles 9-Story Frame

The reduced strength steel moment frame structure including the location of energy dissipation devices is shown in Figure 7-9. This is the base LA frame to which the energy dissipation devices were added. This structure was generated by reducing the beam and column sizes by approximately 45% and 30%, respectively. The beam sizes were reduced more than the columns for two reasons. The first is that additional axial load is expected in the columns due to the forces in the energy dissipation devices. The secondary reason was to ensure that strong column-weak

beam was maintained. The structure still meets all strength requirements including p-delta requirements but exceeds drift limits. The typical drift ratios for the stories for the weakened structure range from 0.025 to 0.037.

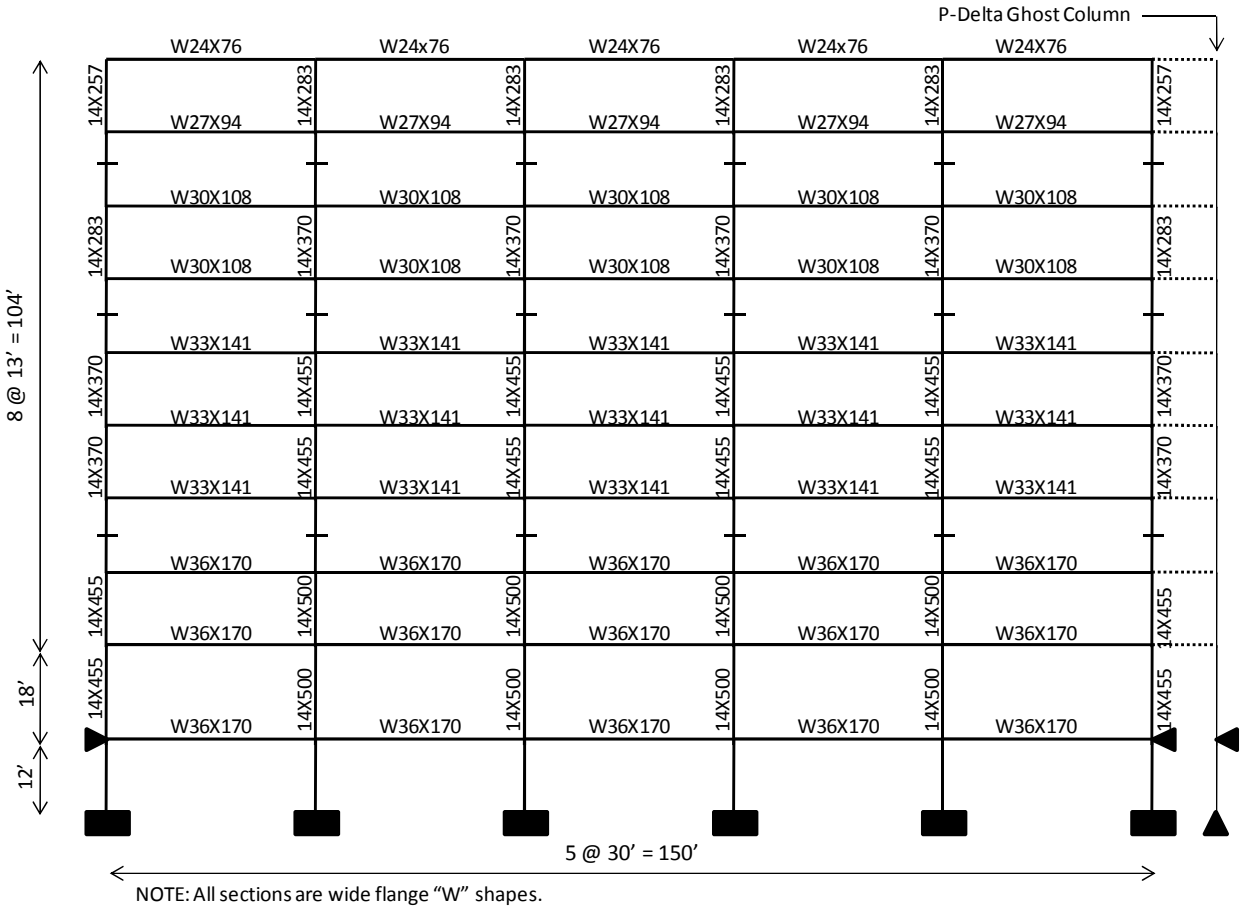

Figure 7 - 8 Los Angeles 9-Story Frame

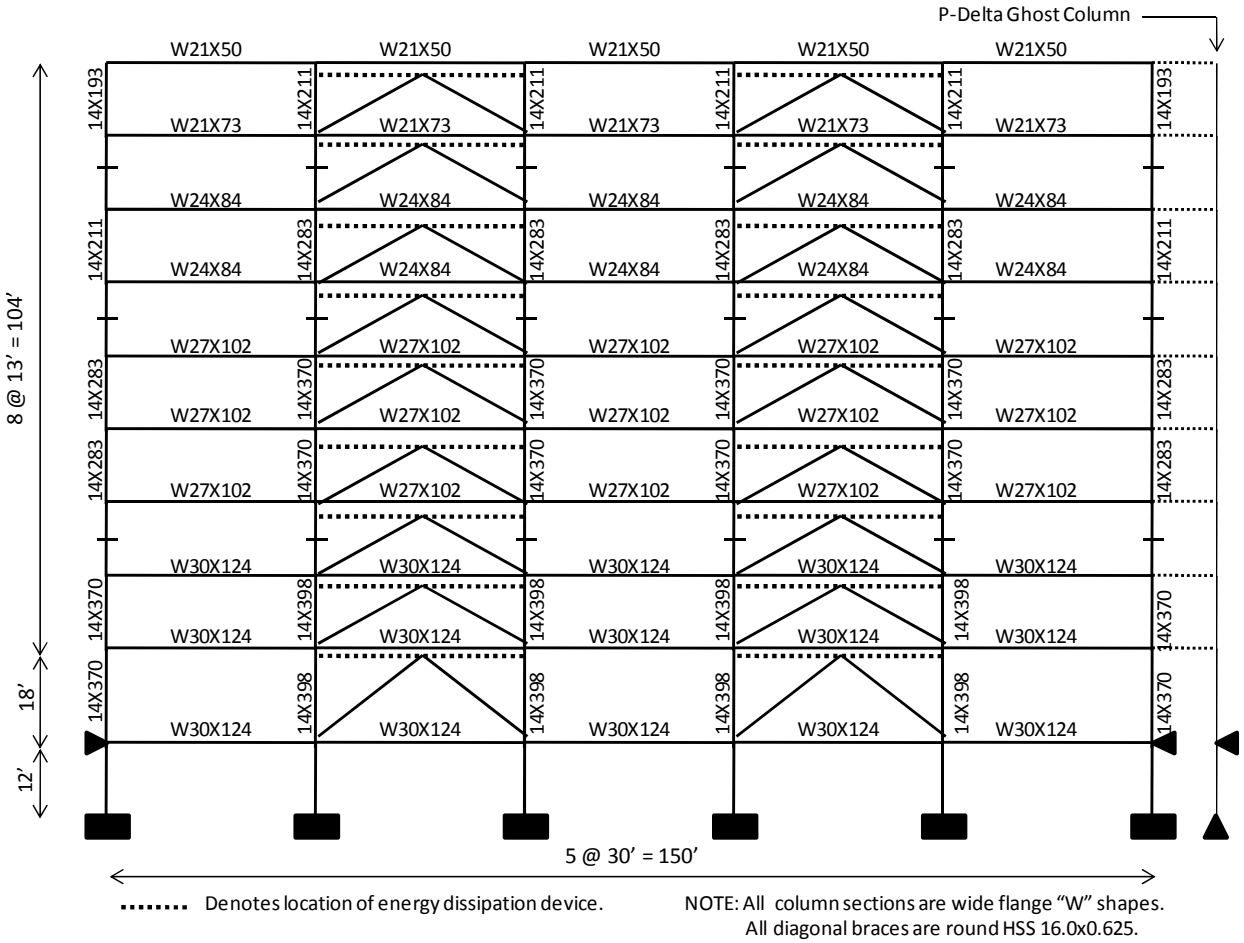

Figure 7 - 9 Reduced Strength Los Angeles 9-Story Frame

7.4.2.2. Scaled Earthquake Records

The next step in the process was the scaling of the earthquake acceleration records. This was done using the design spectrum shown in Figure 7- 6. At the code specified maximum period of 1.83 s, the design acceleration was determined to be 0.395 g. Although it is more common to scale at the actual structural period, the scaling at the code maximum period produced larger accelerations. The scale factor for each earthquake was calculated by determining a multiplier required to produce the design acceleration in a linear elastic structure with the same period. The scale factors for the Imperial Valley and Northridge earthquakes are 2.296 and 0.938 respectively. The scaled acceleration response spectrums for the two earthquakes are shown with the Los Angeles design spectrum in Figure 7-10. The graph shows the curves being coincident at a period of 1.83s and an acceleration of 0.395 g.

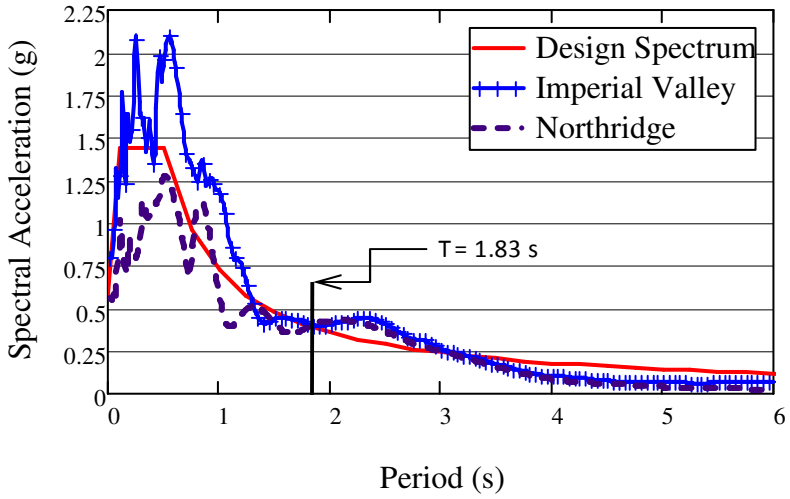

Figure 7 - 10 Acceleration Spectrum for Los Angeles 9-Story Structure

7.4.2.3. Seismic Resisting Systems

The sizing of the rubber and viscous devices was based on the goal of providing approximately 10% total damping, including inherent damping, in the first mode of the structure. Inherent damping was provided by specifying Rayleigh proportional damping of 2% in the first and fifth modes. The determination of required damper size was done using an iterative approach. A size was specified and then a linear free vibration analysis was done to determine the first-mode damping. This was done by applying a sinusoidal acceleration at the base of the structure at the first modal frequency for a few cycles and then letting the motion decay. The damping was calculated using the log decrement method. Two sizes of dampers were used over the height of the structure. One size was used on the first five stories, with a smaller size used for the top four stories. The same size rubber or viscous damper was used in all configurations. This means that for the HDRD and HPCD structures the same size rubber damper was used. It also applies to the viscous damper in the VD and HPCD-VFD. For the hybrid configurations, HYFR and HYFR-VFD, the size of the damper must be doubled since the damper was only on one side of the chevron brace. To maintain the same level of damping with half the number of damping devices, the elements had to be doubled in capacity. As an example, for the VFD structure, the required damping constant for the lower stories is 9 k-s/in. The same damper would be used in the HPCD-VFD structure. For the HYFR-VFD structure the damper would require a damping constant of 18 k-s/in. to maintain the same level of structural damping. The same doubling occurs for the

strength of the BRB elements. In the HYFR and HYFR-VFD structures, the BRB elements have twice the yield strength as for the BRBF, HPCD and HPCD-VFD structures.

Design of the BRB elements was done using the strength level ELF forces. The BRBs were designed to yield at the strength level forces. Like the damping devices, one size brace was used up to the fifth floor and a smaller size was used for the remaining stories. The BRB yield force is doubled in the hybrid configurations as with the dampers so the same yield force and energy dissipation is provided. Table 7-2 shows the sizes of the various elements along with some dynamic properties including the first-mode period and approximate damping ratio.

Table 7 - 2 Model Properties for Los Angeles 9-Story Structure

Seismic Resisting System	1st Mode Period (s)	1st Mode Damping Ratio (%)	Story 1 - 5			Story 6 - 9		
			Damper Size (in)	Damping Coefficient (k-s/in)	BRB Yield (k)	Damper Size (in)	Damping Coefficient (k-s/in)	BRB Yield (k)
SMRF (LA9)	2.48	2.0	N/A	N/A	N/A	N/A	N/A	N/A
BRBF	1.54	2.0	N/A	N/A	200	N/A	N/A	150
VFD	3.25	10.1	N/A	9	N/A	N/A	7	N/A
HDRD	2.15	9.6	15x54x0.75	22.9	N/A	15x42x0.75	17.8	N/A
HPCD	2.19	8.6	15x54x0.75	23.3	200	15x42x0.75	18.2	150
HYFR	2.16	9.2	15x108x0.75	46	400	15x84x0.75	35.8	300
HPCD-VFD	3.23	10.0	N/A	9	200	N/A	7	150
HYFR-VFD	3.24	10.1	N/A	18	400	N/A	14	300

It should be noted from the table that the same size damper is used in the HDRD, HPCD and HYFR models. What is different is the damping coefficient. This occurs because the coefficient, C, depends on the first natural frequency of the frame. This can be seen in Equation 6-2 for the damping constant where the frequency is in the denominator. The minor differences in the periods of the three systems cause similar differences to occur in the damping coefficients. It is also interesting to note that for roughly the same device damping coefficients, the HPCD experiences lower damping. This reduction in damper effectiveness occurs because the damper acts in series with a BRB. This configuration reduces the effectiveness of the device due to the deformation across the brace. The same reduction in effectiveness happens with the viscous devices, but it is not as apparent. The VFD is more flexible relative to the BRB, so the deformation across the BRB is not as significant.

The gap sizes for the hybrid configurations were selected based on the requirement to engage the braces prior to yielding of the moment frame. For a typical story, 0.5 in. of story displacement is

less than the drift which would cause yielding of a moment frame. An additional criterion was the maximum strain in the rubber. The rubber testing illustrated that the rubber had a higher loss factor at lower strains. With a rubber thickness of 0.75 in. for the LA structure and 1.0 in. for the Charleston structure, a maximum of 0.5 in. was a good size to keep the rubber strain within reasonable limits. The selection of 1.0 in. was to provide another gap size to investigate the effects on structural response. The same gap sizes are used in both structures.

7.4.3. Charleston Structure

7.4.3.1. Structure Description and Design

The design of the Charleston structure follows the same pattern as the LA structure. The difference is the severity of the seismic loads. The Charleston area was selected to remain in a significant seismic zone but reduce the strength of the structure under the same gravity loads. This provides an opportunity to see how these devices function in a case where the p-delta loads are more significant.

The design values for the short and 1 second period spectral accelerations are 0.981 g and 0.404 g respectively. Even though these values are significantly reduced from the LA structure, the structure is still classified as seismic design category D. The first mode period used to calculate design forces is again limited to 1.83 s, although the SAP model calculates a period of 3.38 s. The seismic response coefficient, C_s, using a response modification factor, R, equal to 8 is 0.028. Using this value, the strength level ELF forces generated a base shear of 547.5 kip. In this case, the reduction of story forces for drift calculations was more significant since equation 12.8-6 in ASCE 7-05 does not apply. The loads for displacement checks were generated using the minimum value for the response coefficient of 0.02. The analytically determined period of 3.38 s resulted in a response coefficient below the minimum required by ASCE 7-05. This resulted in a base shear for drift checks of 400.7 kip. The story forces along the height of the structure for strength and drift are shown in Figure 7-11.

The ELF forces were then used to design a fully code compliant structure for the Charleston seismic loads. This structure is shown in Figure 7-12. The full strength model was then reduced in stiffness by approximately 45% and 30% in the beams and columns, respectively, to produce a reduced strength structure. This structure still meets strength requirements including p-delta

effects but exceeds drift requirements. The reduced strength model showing the locations of added energy dissipation devices is shown in Figure 7-13.

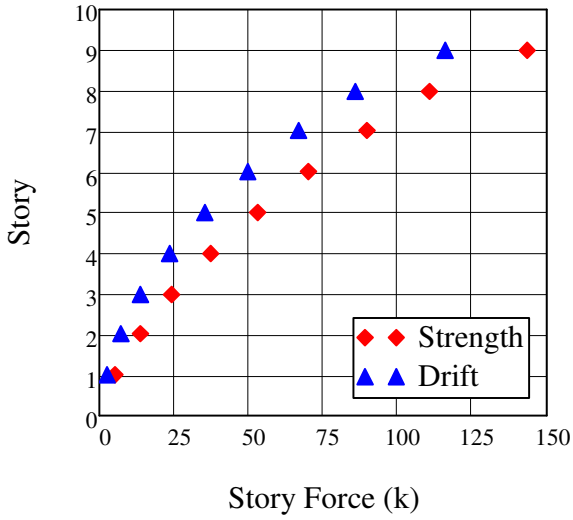

Figure 7 - 11 Story Forces for Charleston 9-Story Frame

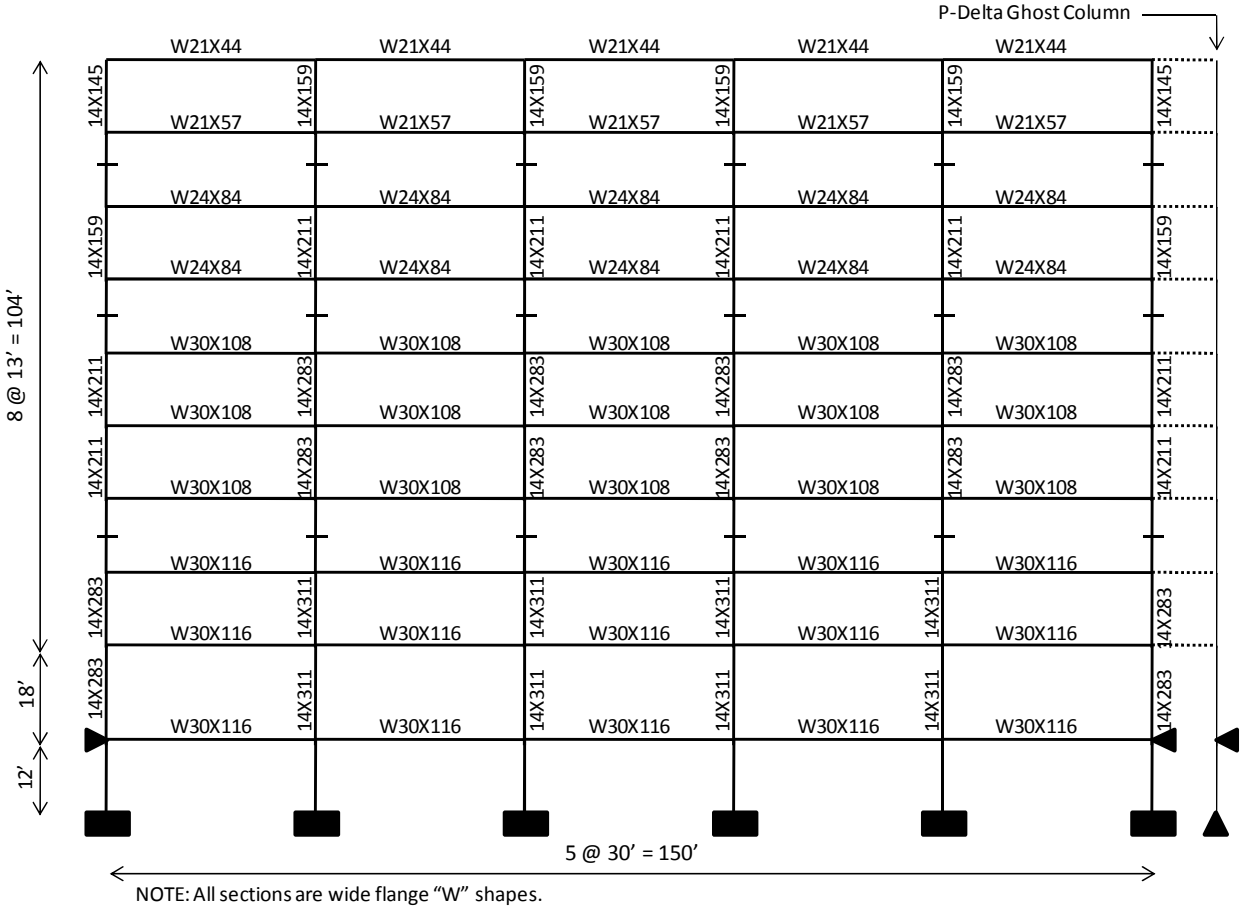

Figure 7 - 12 Charleston 9-Story Frame

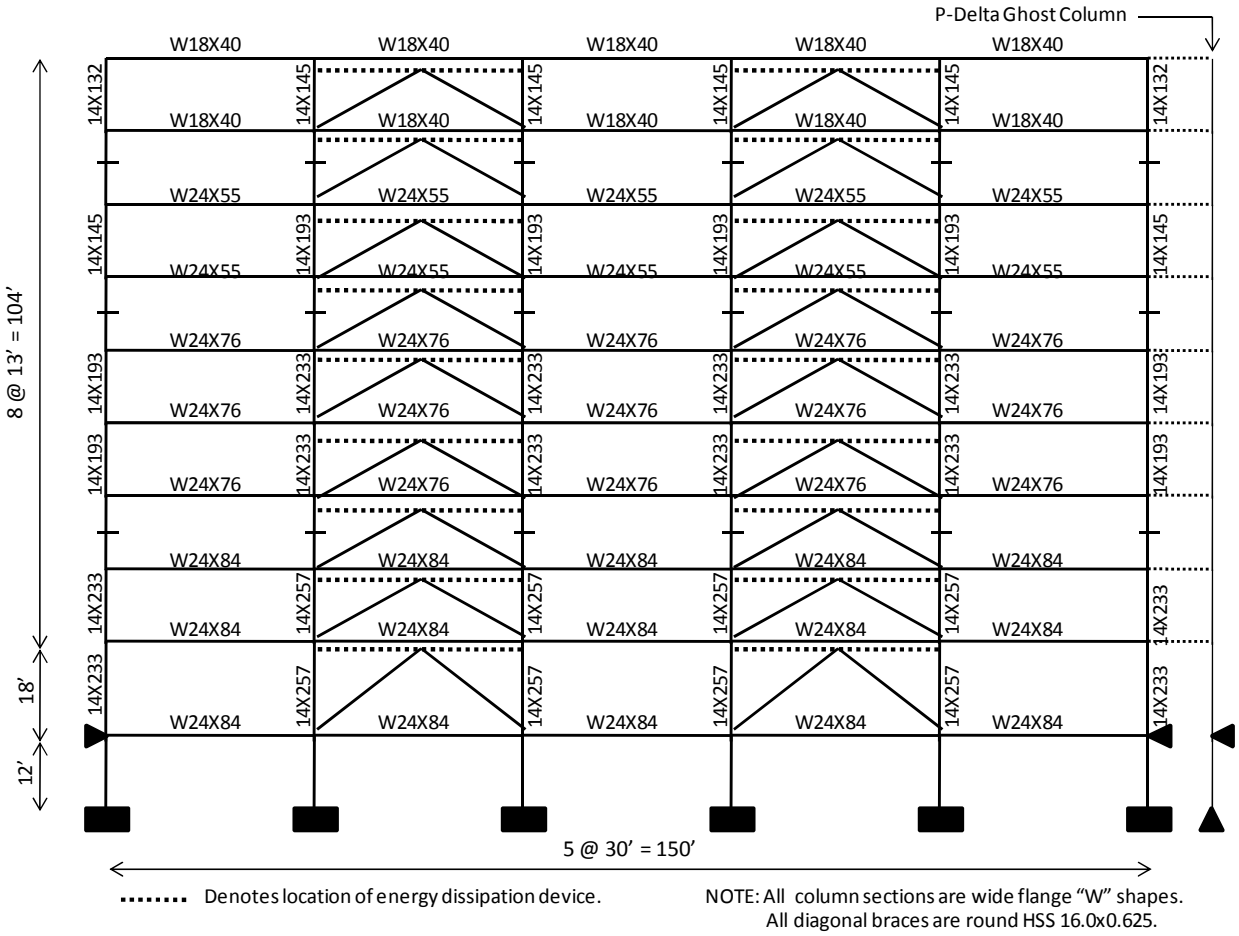

Figure 7 - 13 Reduced Strength Charleston 9-Story Frame

7.4.3.2. Scaled Earthquake Records

The same process for scaling the earthquake acceleration records was used for the Charleston structure. At the code limited maximum period of 1.83 s, the design acceleration was determined to be 0.220 g. The scale factor for each earthquake was calculated by determining the multiplier required to produce the design acceleration in a linear elastic structure having the same period. The scale factors for the Imperial Valley and Northridge earthquakes are 1.285 and 0.525 respectively. The scaled acceleration response spectrums for the two earthquakes are shown with the design spectrum in Figure 7-14. It can be seen in the graph that all three curves are coincident at a period of 1.83 s and an acceleration of 0.220 g.

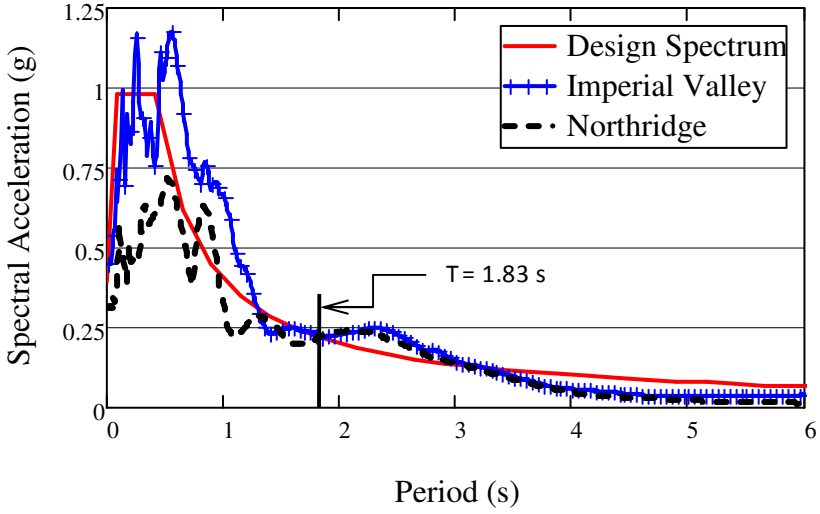

Figure 7 - 14 Acceleration Spectrum for Charleston 9-Story Structure

7.4.3.3. Seismic Resisting Systems

The same seismic resisting systems and design rules were used for the Charleston structure. The goal of 10% first-mode damping was used to size the viscous and rubber dampers. The BRBs were designed to yield at the ELF strength level forces. The summary of device sizes and model properties is shown in Table 7-3. The same observations about the damping coefficients for the LA structure apply to the Charleston model.

Table 7 - 3 Model Properties for Charleston 9-Story Structure

Seismic Resisting System	1st Mode Period (s)	1st Mode Damping Ratio (%)	Story 1 - 5			Story 6 - 9		
			Damper Size (in)	Damping Coefficient (k-s/in)	BRB Yield (k)	Damper Size (in)	Damping Coefficient (k-s/in)	BRB Yield (k)
SMRF (CHA9)	3.38	2.0	N/A	N/A	N/A	N/A	N/A	N/A
BRBF	1.92	2.0	N/A	N/A	100	N/A	N/A	75
VFD	4.41	10.1	N/A	6.5	N/A	N/A	5.2	N/A
HDRD	3.03	10.1	15x30x1.0	13.5	N/A	15x22x1.0	9.9	N/A
HPCD	3.1	9.5	15x30x1.0	13.8	100	15x22x1.0	10.1	75
HYFR	3.03	9.7	15x60x1.0	26.9	200	15x44x1.0	19.7	150
HPCD-VFD	4.33	9.8	N/A	6.5	100	N/A	5.2	75
HYFR-VFD	4.36	10.0	N/A	13	200	N/A	10.4	150

7.5. Analysis Results

The results of the analyses are shown in multiple types of graphs. One type of plot is the result of an IDA, which shows a maximum damage measure versus increasing levels of the design

earthquake. The three damage measures reported include maximum roof drift, maximum base shear and maximum total roof acceleration. In addition to roof quantities, plots are presented showing the maximum story drift and residual deformations for each story. This data is only presented for the DBE level. A response history of a quantity such as base shear or roof displacement shows the response as it changes with time. An SPO plot shows the nonlinear force versus displacement behavior of a structure. A multiplier on the ELF force distribution was used for these pushover analyses.

7.5.1. Los Angeles Structure

The LA structure provided some very interesting results. Figure 7-15 shows three IDA plots representing the response of the non-hybrid seismic resisting systems for both earthquakes. The LA9 structure represents the code compliant steel moment resisting frame (SMRF). The other abbreviations can be found in Table 7-1. At a scale factor of 1.2 of the IV record, the LA9 structure fails in the analysis due to extreme lateral drift, however there is a resurrection at the 1.4 and MCE levels. The LA9 structure which has no added energy dissipation is one of the worst performing structures for all the damage measures. The original plan was to use the LA9 as the baseline for comparison. The erratic performance of the LA9 makes the BRBF structure a better option. As BRB systems are seeing significant usage in new structures and the research arena, this provides a good baseline for the hybrid configurations. The symbols for the various resisting systems will remain constant in each plot for simplicity and ease in comparisons between the various figures.

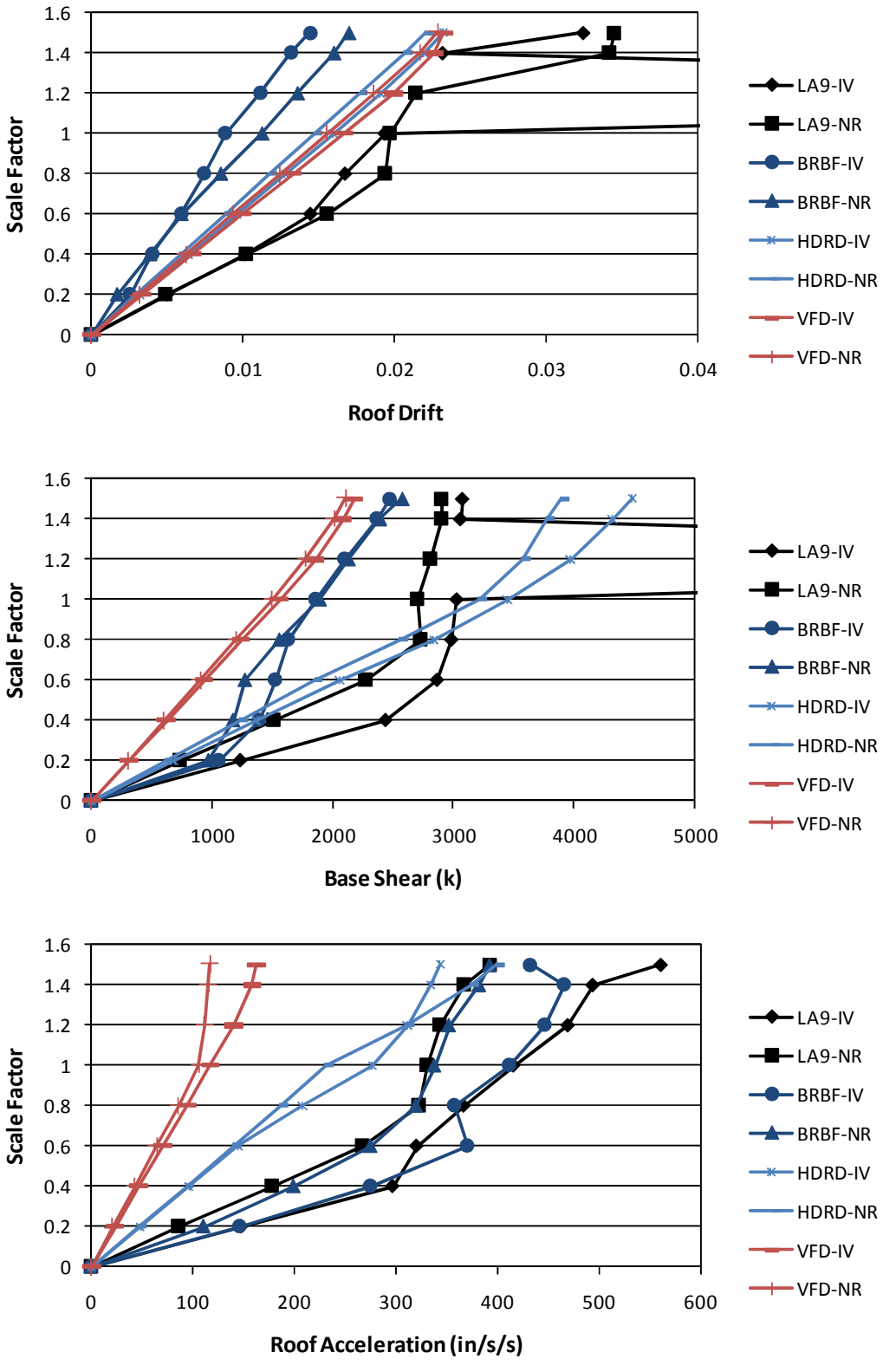

Figure 7 - 15 IDA Plots for Los Angeles Structure with Non-hybrid Systems

The results of the non-hybrid systems demonstrate that each of the systems has different strengths. The BRBF system provides the lowest roof drifts but falls in the middle of the pack for base shear. The weakness of the BRBF system is illustrated with the roof acceleration response. The increased stiffness results in higher accelerations. On the other hand, the viscous dampers provide the lowest base shears and accelerations but at the expense of higher deformations. One of the very interesting results is the HDRD which performs near the middle of the response quantities with the exception of the high scale factors for base shear and roof acceleration. The large base shear and roof acceleration become significant at the higher scale factors. This is attributed to the increasing stiffness and large elastic deformation capacity of the rubber. The LA9 structure performs poorly for all the damage measures and exceeds the standard drift limits for both earthquakes at the DBE level. ASCE 7-05 allows for an increase of 25% on drift limits when nonlinear response history analysis is used. This increase allows the LA9 structure to meet drift limitations for this case. All the other systems meet the standard drift requirements.

In addition to looking at the roof response, individual story drifts from the DBE level ground motion are shown in Figure 7-16. For these plots, a straight vertical line would represent a structure with equivalent story drifts at each level. The LA9 structure is the worst performer, with the BRB being the best. In addition to having lower magnitude drift ratios, the drifts are not as erratic as for the LA9 structure. The highest drift ratios typically occur near the bottom of the structure. The LA9 curve is typical of a structure experiencing significant yielding. In this case, several column hinges were formed, nearly creating a collapse mechanism.

Residual displacements for the non-hybrid frames are shown in Figure 7-17. This plot gives a numerical and visual representation of where the structure will be at the end of the earthquake. The LA9 structure is the worst case, with the remaining systems having relatively small residual drifts. Figure 7-18 shows the same plot without the LA9 results. We can see that the HDRD has the lowest residual drift problems while the BRB has the worst residual deformations. The likely explanation for the low residual deformations is a combination of two things. The first is the self-centering force the dampers provide. The second is that the elastic stiffness OF to the dampers takes load away from the steel frame, thereby reducing the deformations in the framing.

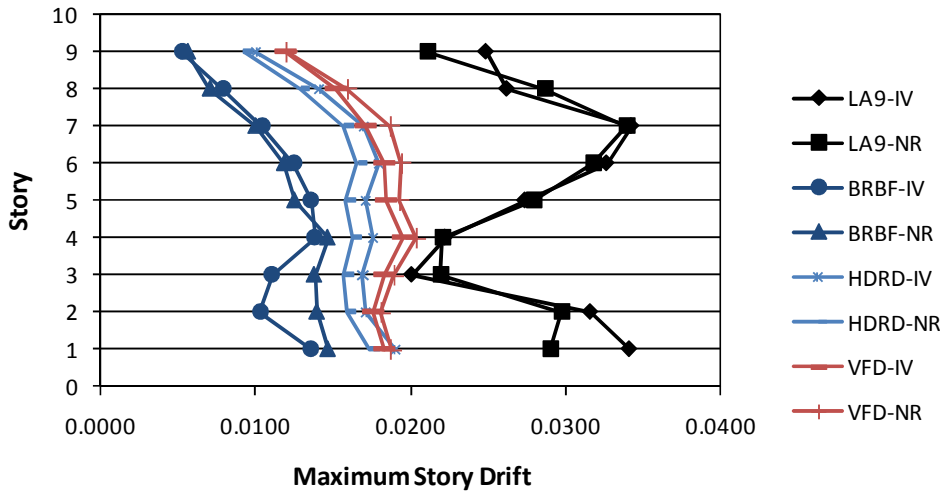

Figure 7 - 16 DBE Maximum Story Drifts with Non-hybrid Systems (LA)

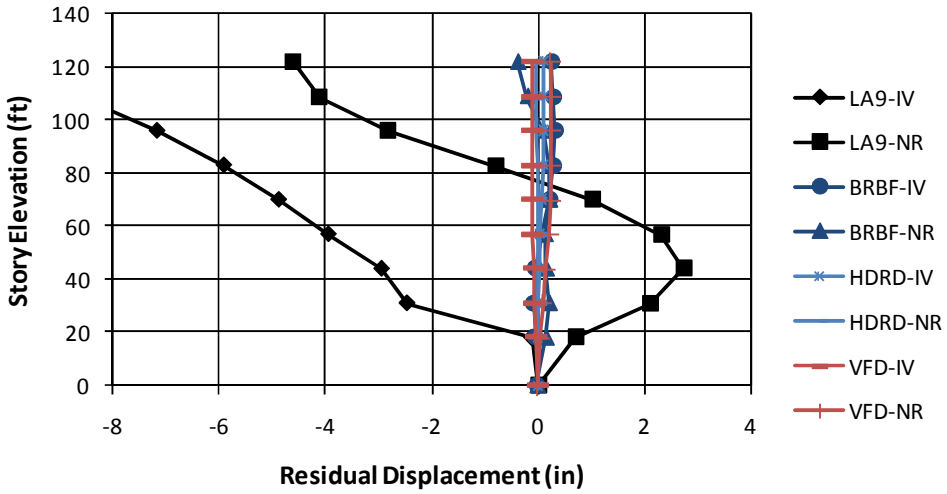

Figure 7 - 17 DBE Residual Displacements with Non-hybrid Systems (LA)

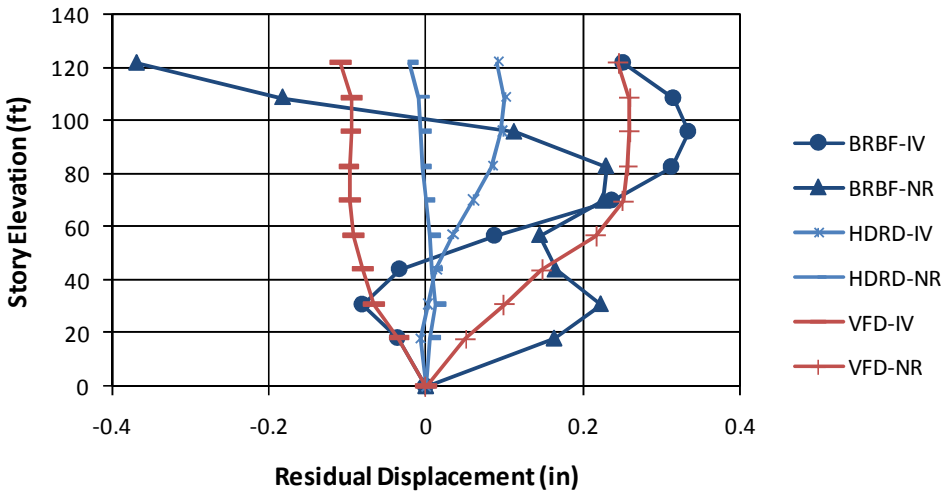

Figure 7 - 18 DBE Residual Displacements with Non-hybrid Systems (Excluding LA9)

Figure 7-19 shows the IDA results for the hybrid systems with an HDR device. The numbers at the end of the abbreviation represent the gap prior to engagement of the BRB element. Two sizes, 0.5 in. and 1.0 in., were analyzed for this study with 050 and 100 representing these gaps respectively. Although all the hybrid damping systems meet the code requirement of 0.02, the BRB system still performs better in reducing deformations. On the base shear plot, all of the devices are grouped together with the exception of the HYFR structures. These devices show the same tendency for high base shear and roof accelerations at large deformations as the plain HDRD system due to the properties of the rubber. The HPCD devices demonstrate their strength on the plot of roof accelerations. They reduce the acceleration below the BRBF and significantly below the hybrid frame devices, demonstrating that in some cases the stiffness associated with the BRBF can be detrimental. The hybrid frame configuration performs well on the acceleration plots until the stiffness of the rubber has the effect of continuously increasing base shears and accelerations. This problem does not occur with the HPCD devices because the rubber is locked out and the force is limited by the strength of the BRB.

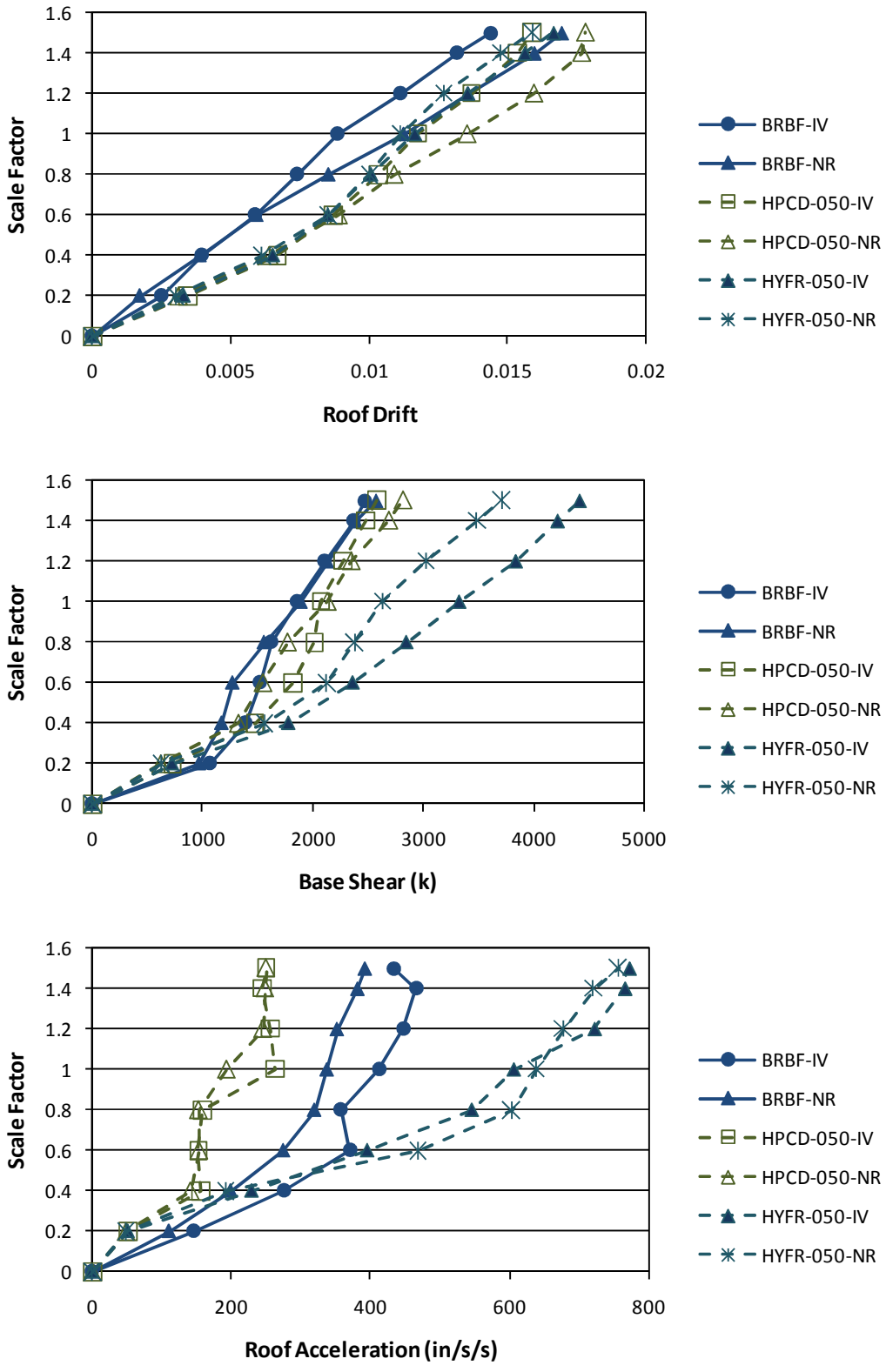

Figure 7 - 19 IDA Plots for Los Angeles Structure with Hybrid HDRD Systems

For the HPCDs, the higher base shear values in the upper scale factors can be explained by the relative stiffness of the structures when the damper is locked out. The yield force for the BRBs is held constant for all systems. The BRB frame assumes a core length of 12 ft based on the geometry of the frame. Due to the need for the HDRD in series with the BRB, the yield length of the steel core is assumed to be 7 ft. This creates a brace that is nearly twice as stiff. Higher stiffness translates to higher seismic forces and greater base shear. The HYFR structures have an equivalent brace to the BRBF structure but have the additional stiffness associated with the rubber dampers acting in parallel.

Figures 7-20 and 7-21 present the maximum story drifts and residual displacements for the hybrid systems with rubber dampers. The story drift plot shows a similar behavior for all the systems, with the BRB having the lowest ratios. The HYFR system is clearly superior at reducing residual drifts. This can be explained by the rubber dampers acting as a restoring force and having the capacity for large elastic deformation. This capacity of the rubber is limited in the HPCD because of the lockout mechanism.

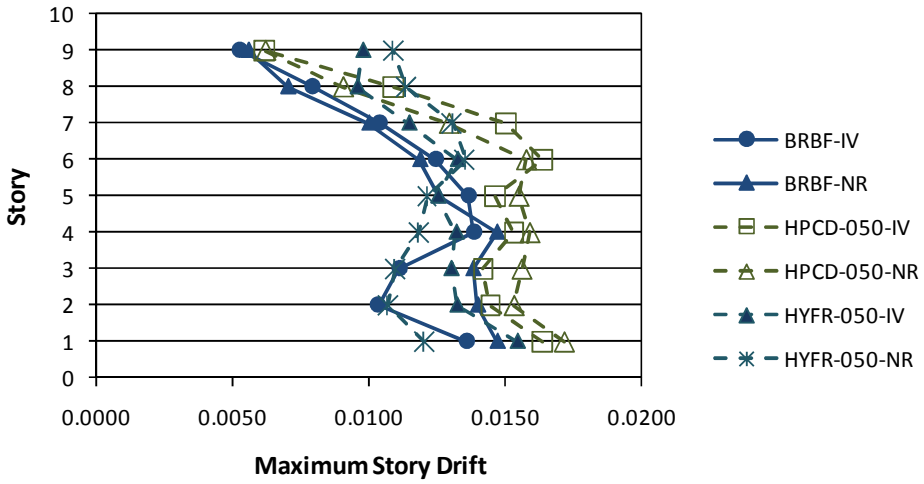

Figure 7 - 20 DBE Maximum Story Drifts with Hybrid HDRD Systems (LA)

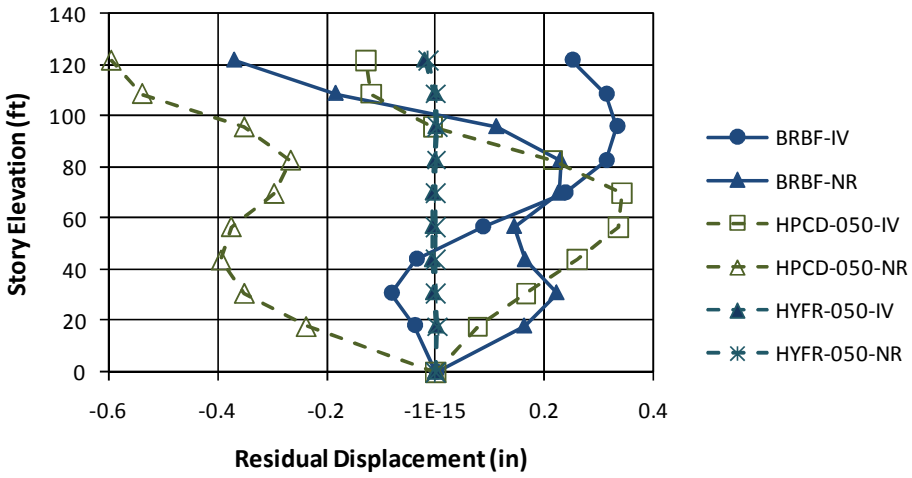

Figure 7 - 21 DBE Residual Displacements with Hybrid HDRD Systems (LA)

The increase in the maximum base shear in the hybrid systems is only element of the comparison. The increased shear in the HPCD-050 over the BRBF system at the DBE level for the Imperial Valley and Northridge ground motions are 11.5% and 20.6%, respectively. The benefit of the damping can be seen in Figure 7-22. The HPCD frame experiences higher shear early portion in the earthquake. During the latter part, the shear and number of cycles decrease.

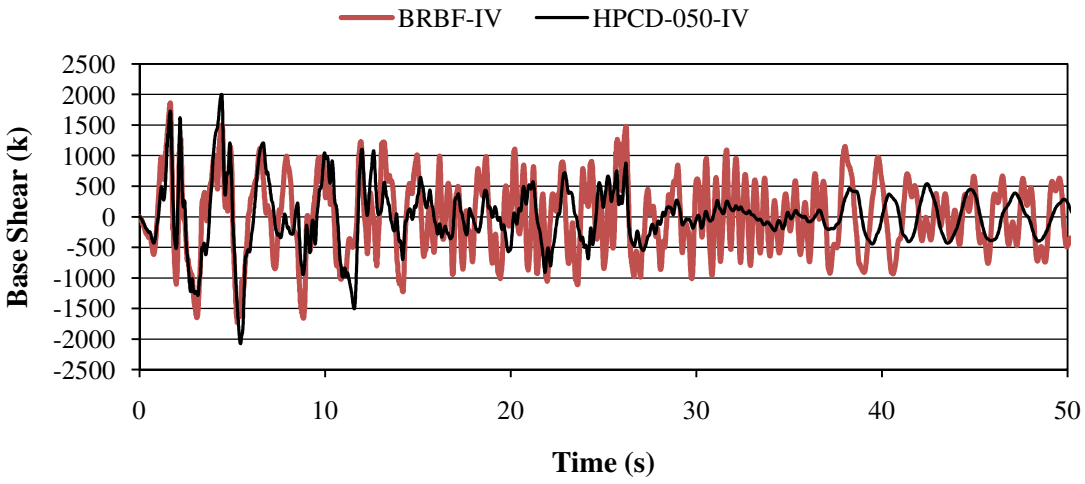

Figure 7 - 22 DBE Base Shear Response History - Imperial Valley Ground Motion (LA)

Figure 7-23 shows the results of a nonlinear static pushover analysis for several non-hybrid and hybrid systems. The LA9 structure has the typical linear elastic to yield trace. The curve shows a good amount of ductility, achieving a roof drift of nearly 4%. The BRBF has the highest initial

stiffness and two distinct yield points. The first is the braces, followed by the moment frame. The two HPCD traces are coincident until the HPCD-050 locks out and increases in stiffness. The transition in the HPCD-100 curve is not as apparent because the lockout occurs as the brace yields. Both hybrid curves have approximately the same yield for the moment frame. The larger post-yield stiffness of the HPCD frames due to the shorter yield length can be seen in the traces. This curve illustrates the reason for an increased base shear for the same BRB yield force.

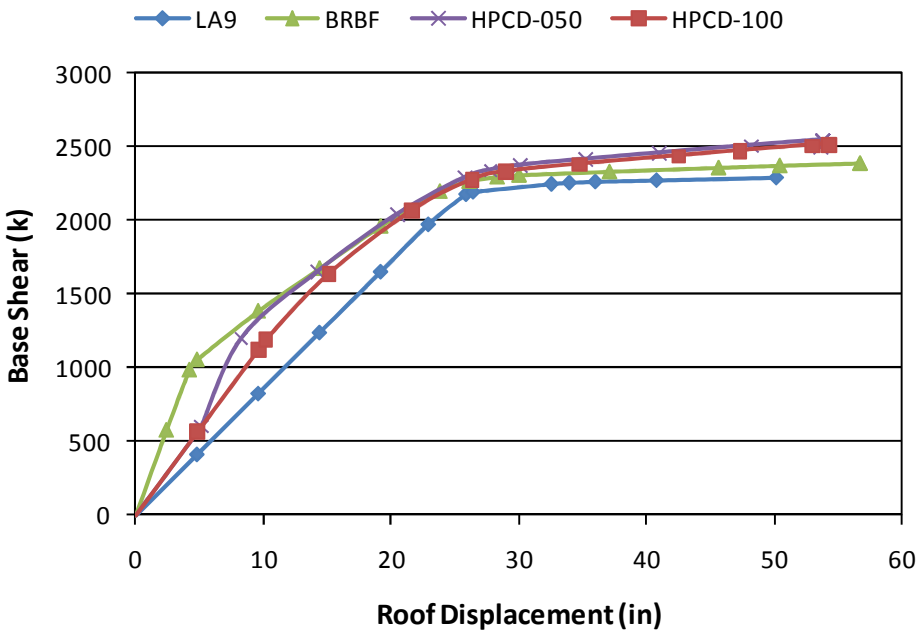

Figure 7 - 23 Nonlinear Static Pushover Plot for Los Angeles Structures

Figure 7-24 shows the SPO plots for the HYFR structures with the BRBF and LA9 structure. The increased strength of these structures is apparent. However, the additional strength comes at the expense of ductility. The HYFR frames reach the yield of the moment frame at a higher value but the frame does not have the long plastic plateau. The phased nature of the device shows the initially lower stiffness which is increased as the BRBs engage. The yield of the BRBs is apparent, but it is not as significant as for the HPCD elements because the additional stiffness of the rubber dampers is still present. Because these dampers remain elastic, they are able to take significant load away from the moment frame. When the frame does begin to yield, it quickly reaches the point where the structure becomes unstable. The plot does not show a descending branch, but the analysis could not progress as the frame developed a collapse mechanism.

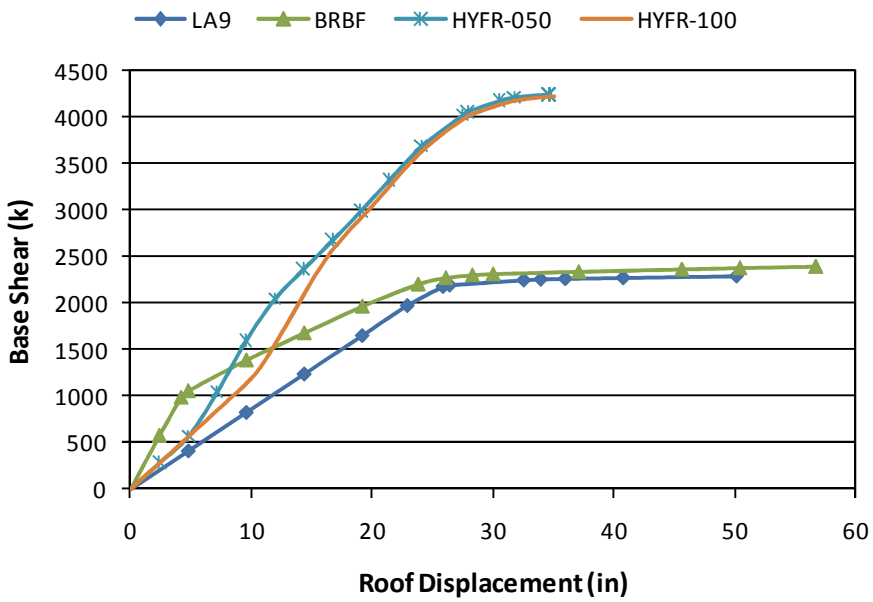

Figure 7 - 24 Nonlinear Static Pushover Plot for Los Angeles Structure

Another element that was explored was the effect of the gap on the structural response. The static analysis illustrates the phased stiffness. Figure 7-25 shows the IDA plots of the hybrid HDRD systems comparing a gap of 0.5 in. to 1.0 in. The results demonstrate that roof drift and base shear are affected by the change in gap. For the HPCD and HYFR, the smaller gap produces less drift. A smaller gap also results in less base shear and lower accelerations. The effect is more distinct for the higher scale factors.

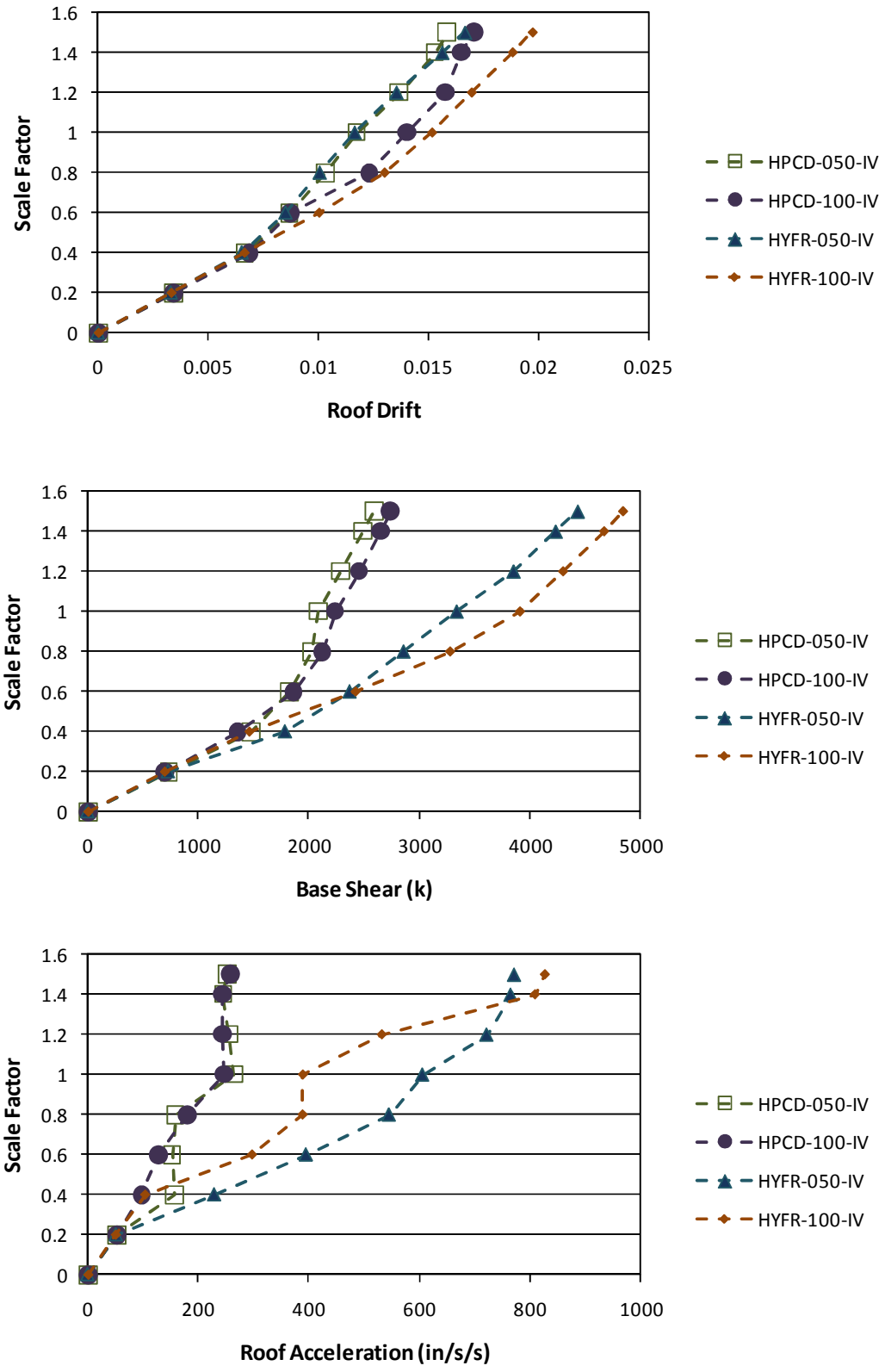

Figure 7 - 25 IDA Plots for Hybrid Systems with HDR Dampers Comparing Gaps (LA)

The minor difference in the base shear based on gap size is illustrated in Figures 7-26 and 7-27. The small differences in the base shear due to the larger gap do not have a significant effect on the overall behavior of the structure. The same trend applies for both the HPCD and HYFR, although the difference is larger for the HYFR configuration because of the added stiffness.

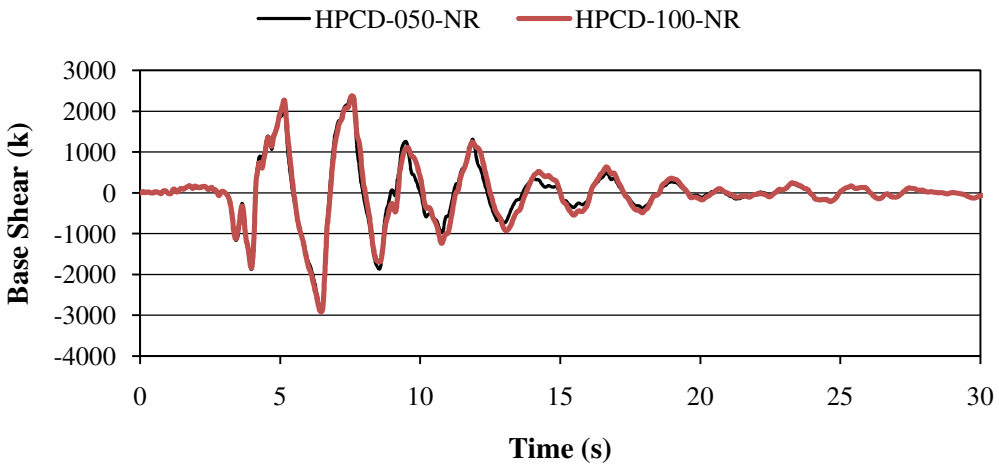

Figure 7 - 26 MCE Base Shear Response History - Northridge Ground Motion (LA)

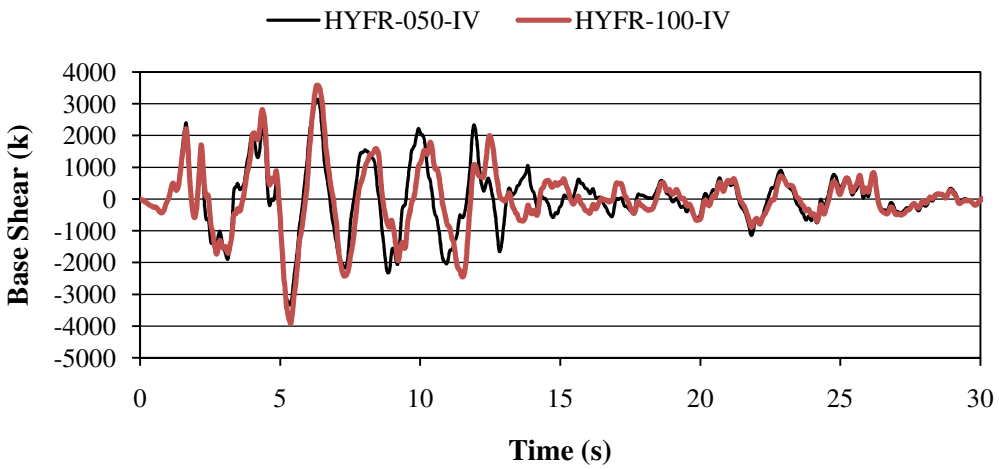

Figure 7 - 27 DBE Base Shear Response History – Imperial Valley Ground Motion (LA)

Figures 7-28 and 7-29 show the effect of the gap size on the maximum story drift and residual displacements. The story drift and residual displacement tend to increase with increasing gap. Having a larger gap puts more of the force into the moment frame for a longer period of time, resulting in larger story drifts and residual deformations in the moment frame. For the HPCD-100 the larger gap results in a significant increase in residual deformations. Small residuals are

again demonstrated by the HYFR system. This provides further proof that the increased base shear originates in the HDRD.

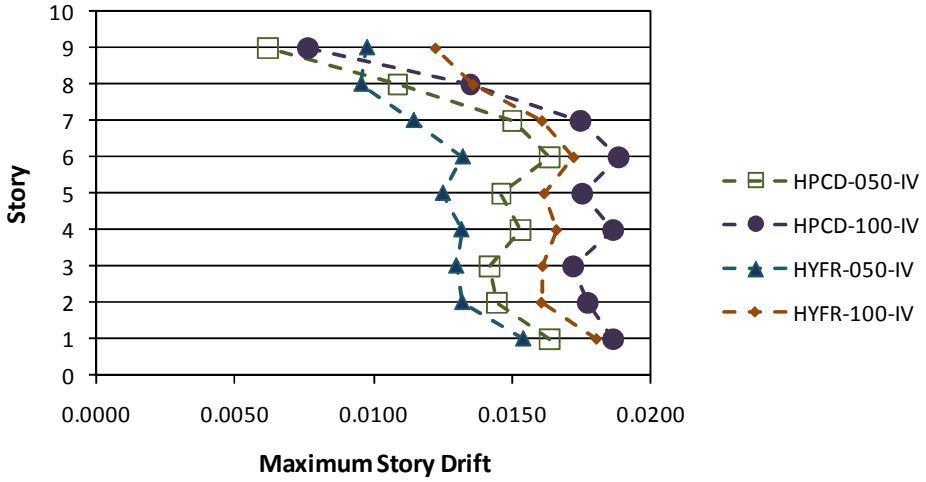

Figure 7 - 28 DBE Maximum Story Drifts - Comparing Gaps HDRD Hybrid Systems (LA)

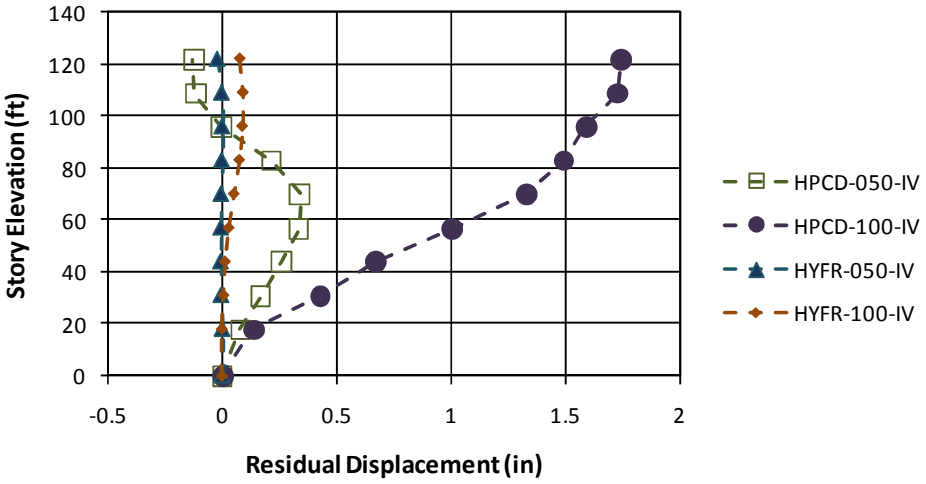

Figure 7 - 29 DBE Residual Displacements - Comparing Gaps in HDRD Hybrid Systems (LA)

Figure 7-30 presents a plot of the base shear response of two hybrid systems. The HYFR frame experiences a large increase in base shear early in the event when the lockout mechanism is engaged. The rubber damper and brace in parallel are stiffer and hence experience larger shear forces. The later part of the earthquake shows that prior to the lockout displacement, the two systems behave in a nearly identical fashion.

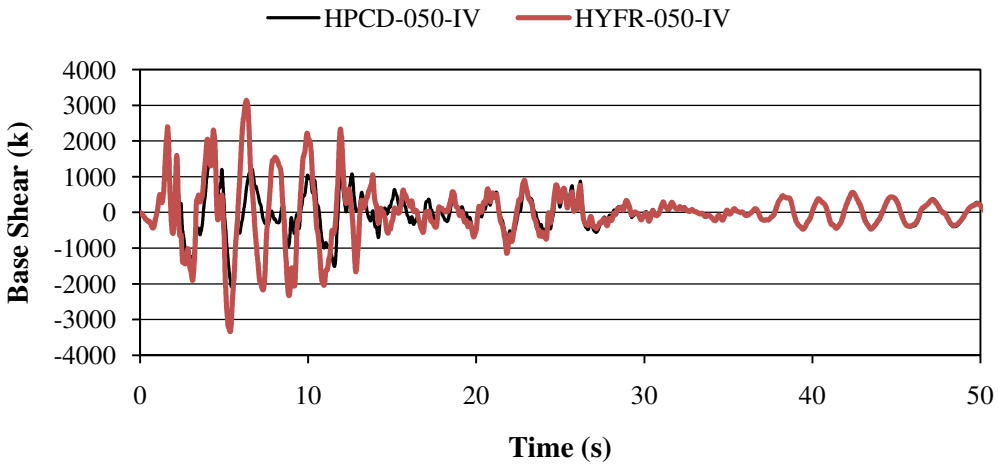

Figure 7 - 30 DBE Base Shear Response History - Northridge Ground Motion (LA)

Figure 7-31 presents the IDA results of the hybrid configurations with a viscous fluid damper. These configurations do not have the static stiffness of the rubber dampers, so the behavior can vary significantly. The BRBF is the best option when it comes to drift control. The BRBF is also the best option for base shear above a scale factor of 0.4. This is not intuitive considering the effectiveness of the VFD model for base shear and roof accelerations. The difference with the HPCD-VFD models is again the increased stiffness due to a shorter brace. The even larger base shear in the HYFR-VFD models is due to the forces in the dampers in parallel with the braces. When looking at the roof accelerations, it is difficult to find a clear advantage, as the traces are grouped closely together.

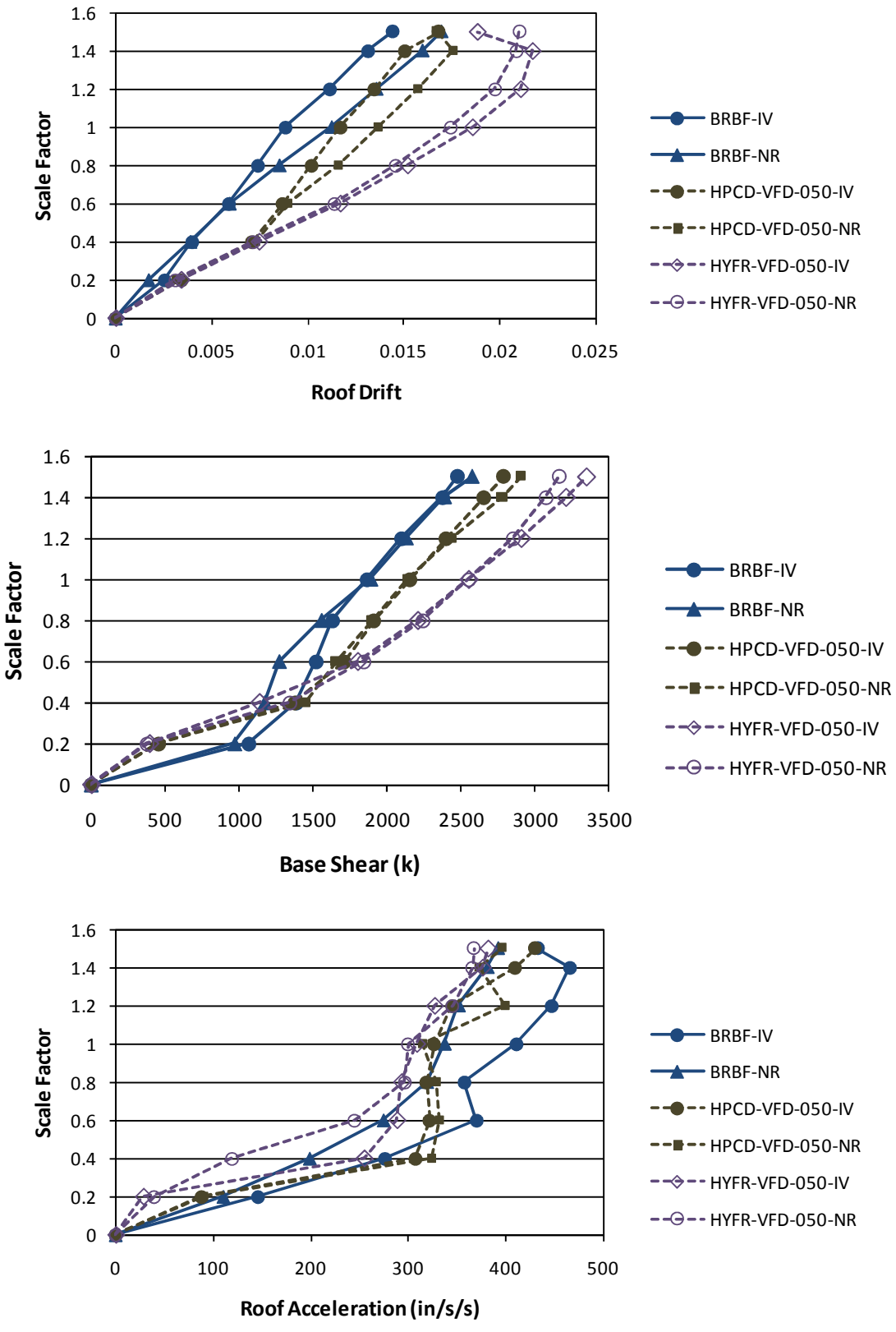

Figure 7 - 31 IDA Plots for Los Angeles Structure with Hybrid VFD Systems

Figures 7-32 shows base shear response histories of the BRBF and the HYFR-VFD. Similar comments about the difference in the responses have been made during past comparisons. The increased damping reduces the base shear excursions in the latter part of the event at the expense of a larger maximum base shear. The larger base shear for this plot comes from two sources. The first is the shorter, stiffer yielding brace element. The second is the damping force in parallel with the BRB, making the two forces additive. The longer period of the HYFR-VFD structure is apparent in the later cycles, illustrating the benefit of the reduced stiffness due to the initial gap.

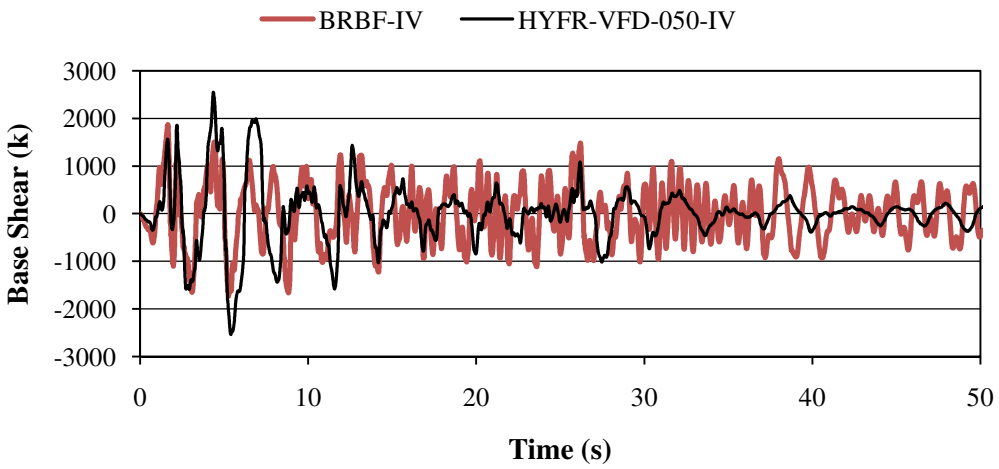

Figure 7 - 32 DBE Base Shear Response History - Imperial Valley Ground Motion (LA)

Figure 7-33 provides a comparison of the base shear response history for the two configurations of hybrid systems with viscous dampers. The larger base shear in the HYFR-VFD is generated by the viscous device in parallel with the BRB. The force in the damper in the HPCD-VFD is limited by the brace yield. When the brace is not engaged, the response is nearly identical.

Figure 7-34 displays the response history for an HPCD and an HPCD-VFD structure. Both traces are similar during the initial pulses of the ground motion. The difference between them is visible when the displacement is not enough to engage the braces in the second half of the event. In this range the difference in the periods of the structures is evident. The base shear for the HPCD is slightly higher, as the structure has greater stiffness and a shorter period.

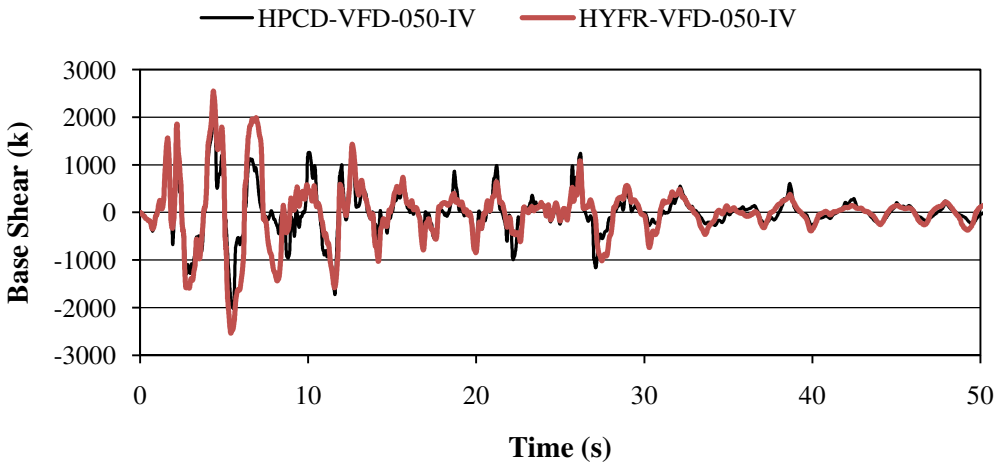

Figure 7 - 33 DBE Base Shear Response History - Imperial Valley Ground Motion (LA)

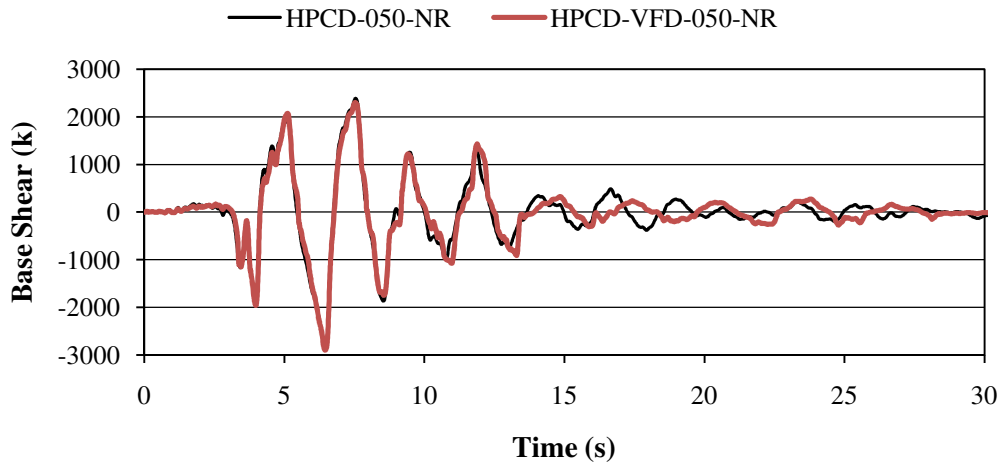

Figure 7 - 34 MCE Base Shear Response History - Northridge Ground Motion (LA)

Figures 7-35 and 7-36 provide the maximum drifts and residual displacements for the VFD hybrid systems. The BRBF is the better option for story drift, with the HPCD-VFD meeting the code drift limits. The HYFR-VFD does not meet standard drift requirements in the lower stories. This is the first case where a hybrid system has exceeded the standard drift limits. For the VFD hybrid systems, the HPCD-VFD system clearly does the best job of limiting residual deformations. The HYFR-VFD system results in significant residual drifts.

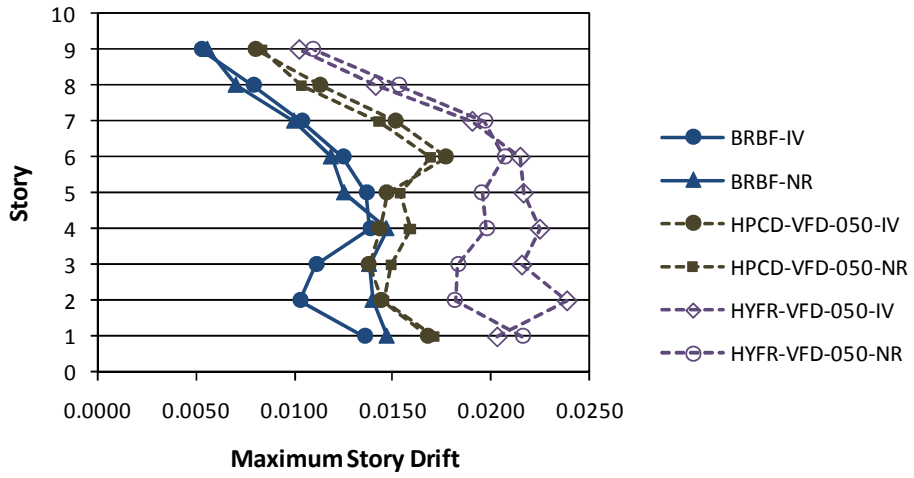

Figure 7 - 35 DBE Maximum Story Drifts with Hybrid VFD Systems (LA)

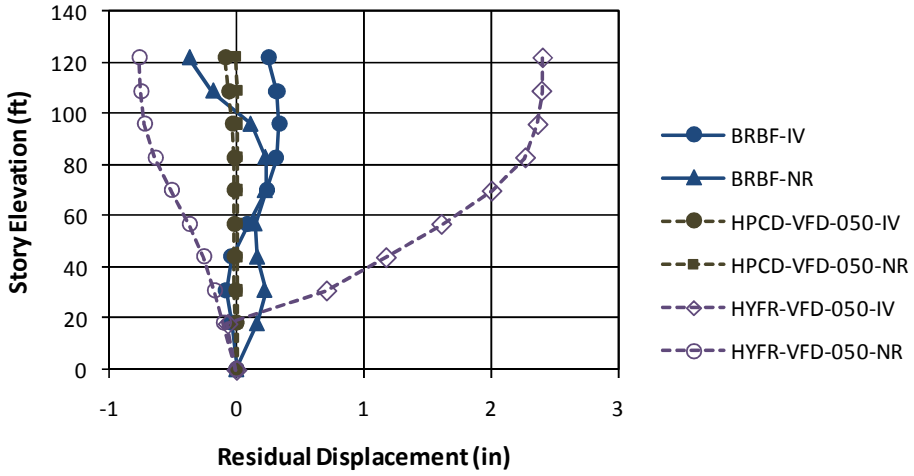

Figure 7 - 36 DBE Residual Displacements with Hybrid VFD Systems (LA)

Figure 7-37 provides IDA plots comparing gap size for VFD hybrid systems. The gap has minimal effect on the roof drift. For smaller scale factors, a larger gap results in reduced base shear. Around a scale factor of 0.6, the traces switch and a smaller gap produces smaller shears. The traces for both systems join at the MCE level. The acceleration plot shows that a larger gap produces lower accelerations in most cases. At some scale factors, the gap has little effect, while the difference is significant at other scale factors.

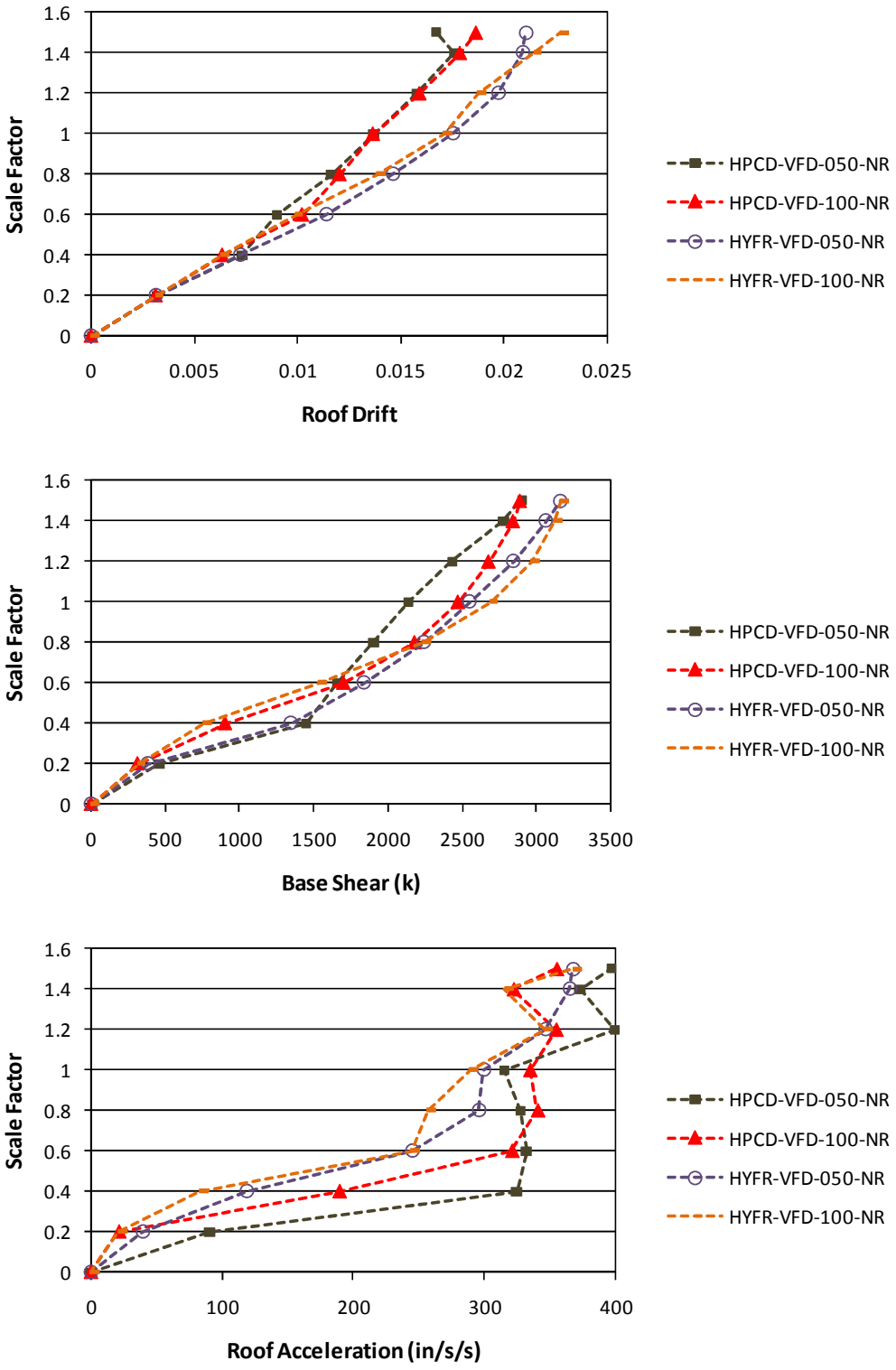

Figure 7 - 37 IDA Plots for Hybrid Systems with VFD Comparing Gaps (LA)

There is a difference in the base shear response history of hybrid systems with viscous dampers due to the gap. Figures 7-38 and 7-39 illustrate this for both the HPCD-VFD and HYFR-VFD.

Both plots show similar trends. During the initial strong pulse, the BRBs in both structures are engaged, so the base shear and period are similar. The second portion of the earthquake shows the 0.5 in. gap structure engaging the BRB with a shorter period and higher base shear. The 1.0 in gap structure is only engaging the viscous damper. The final stage is when both structures are in the gap phase. The traces are very similar in both magnitude and frequency. These stages are easier to see in the Northridge record which has a large initial pulse followed by what appears to be a nearly a free vibration response.

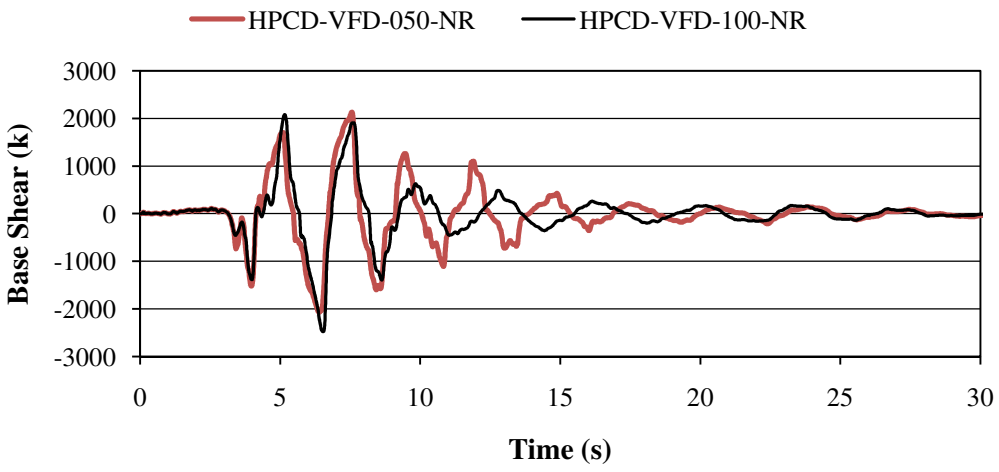

Figure 7 - 38 DBE Base Shear Response History - Northridge Ground Motion (LA)

Figures 7-40 and 7-41 show the effect that gap size has on the response of hybrid systems with viscous fluid dampers. The effect is not as clear as it was for the other hybrid devices. The bottom stories and top stories experience larger drifts with a larger gap. The 4th through 6th stories experience greater drift with a smaller gap. When it comes to residual deformations, the HPCD-VFD solution is superior to the HYFR-VFD. The HPCD-VFD-100 has significant residual deformations but only in the bottom two stories. For HYFR-VFD structures, less residual displacement occurs with a larger gap.

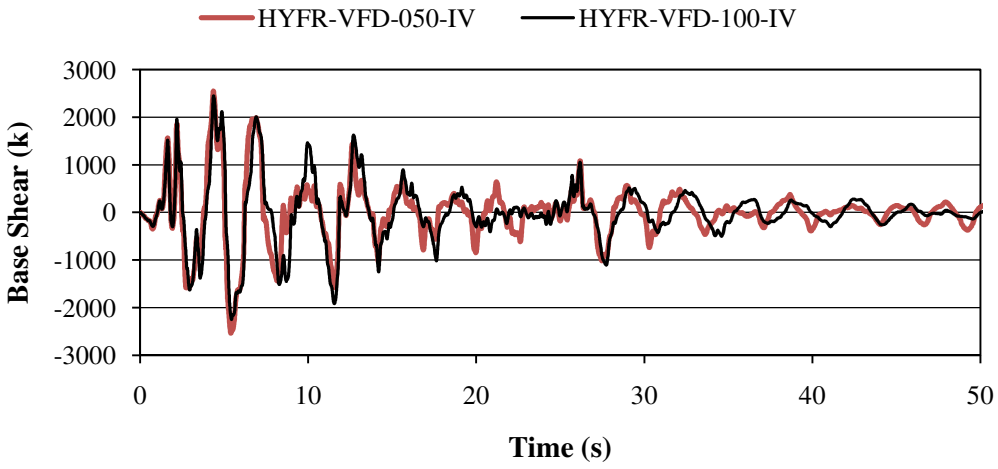

Figure 7 - 39 DBE Base Shear Response History - Imperial Valley Ground Motion (LA)

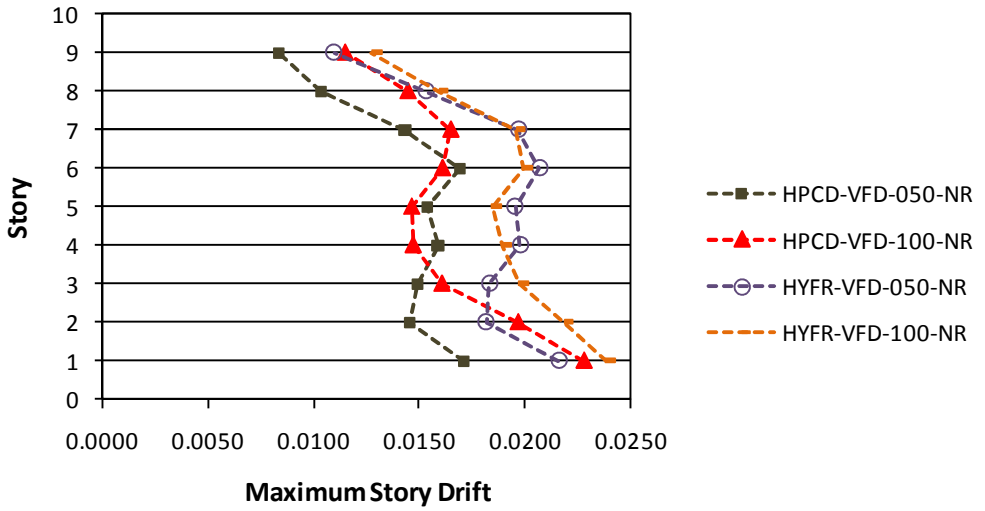

Figure 7 - 40 DBE Maximum Story Drift - Comparing Gaps in VFD Hybrid Systems (LA)

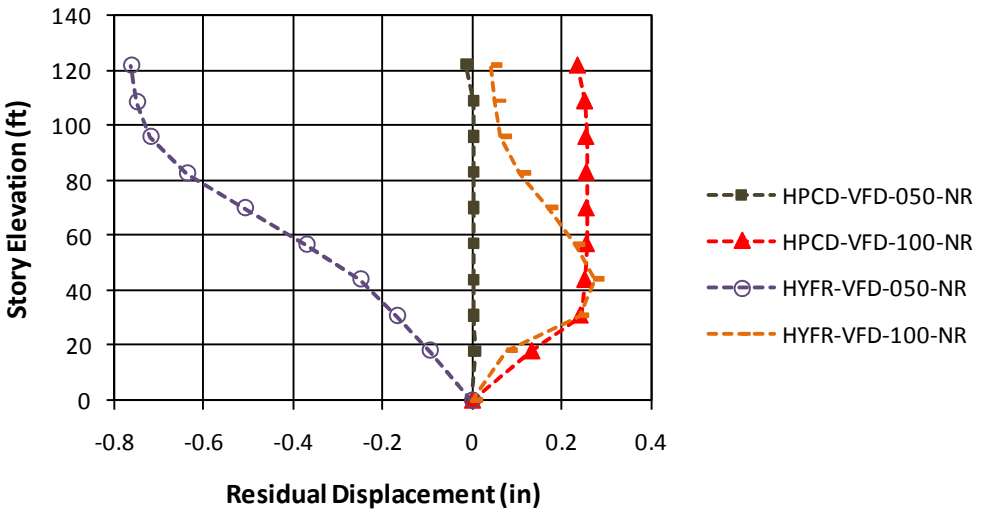

Figure 7 - 41 DBE Residual Displacement - Comparing Gaps in VFD Hybrid Systems (LA)

7.5.2. Charleston Structure

Figure 7-42 shows the IDA plots for the non-hybrid seismic resisting systems of the Charleston 9-story structures. The plain moment frame structure, CHA9, while still experiencing the greatest roof drift, remained essentially linear up to the DBE level. Only one plastic hinge formed at the DBE level in the NR earthquake. CHA9 actually outperformed or equaled the performance of the HDRD and BRB structures when considering base shear and roof acceleration. The BRBF structure performed well in drift reduction but was not the best. The BRBF system results are grouped with the other systems in base shear and are the worst case for roof accelerations. It was also the only system in this group to experience significant yielding. The HDRD and VFD frames remained essentially linear for all scale factors, which is evident in the plots. The HDRD performed well for roof accelerations but again displayed the large base shear values. For this structure, the VFD structure appears to be by far the best option. It performed arguably the best in roof drift and unquestionably for base shear and roof acceleration.

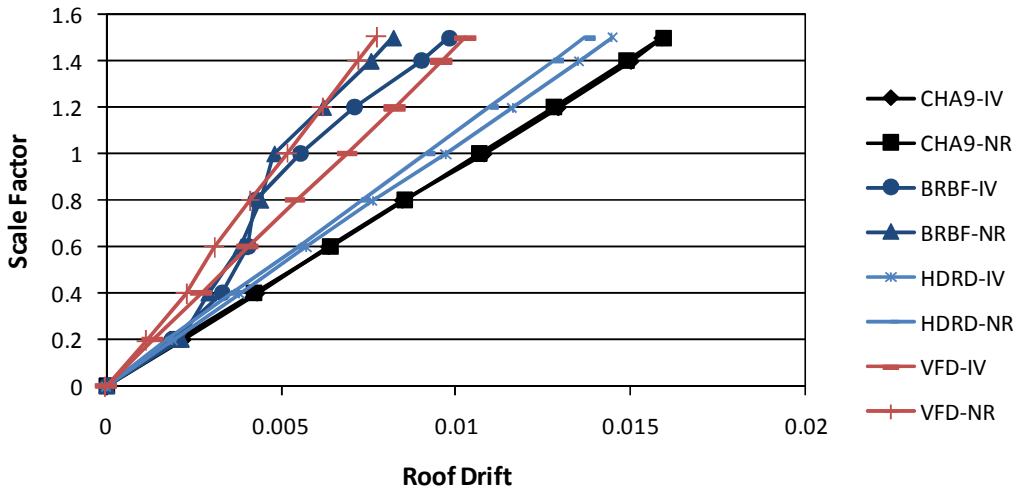

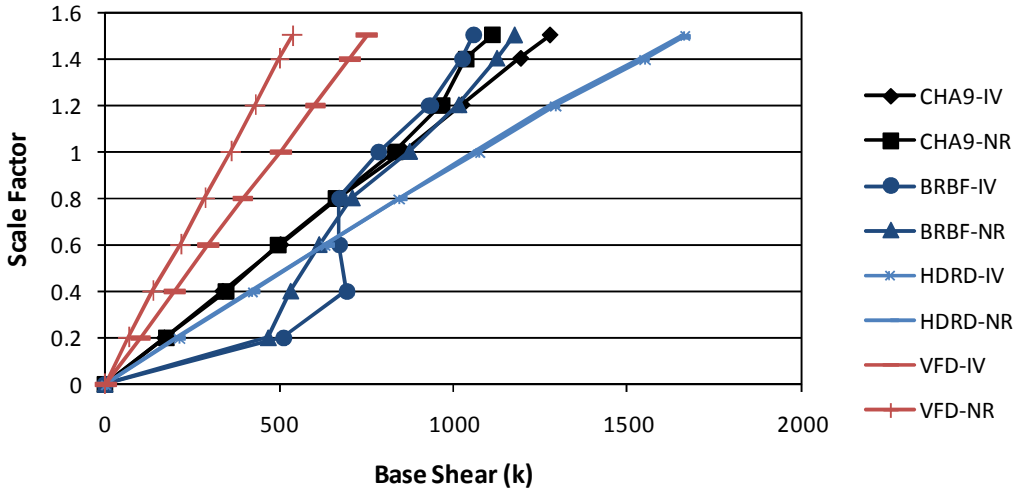

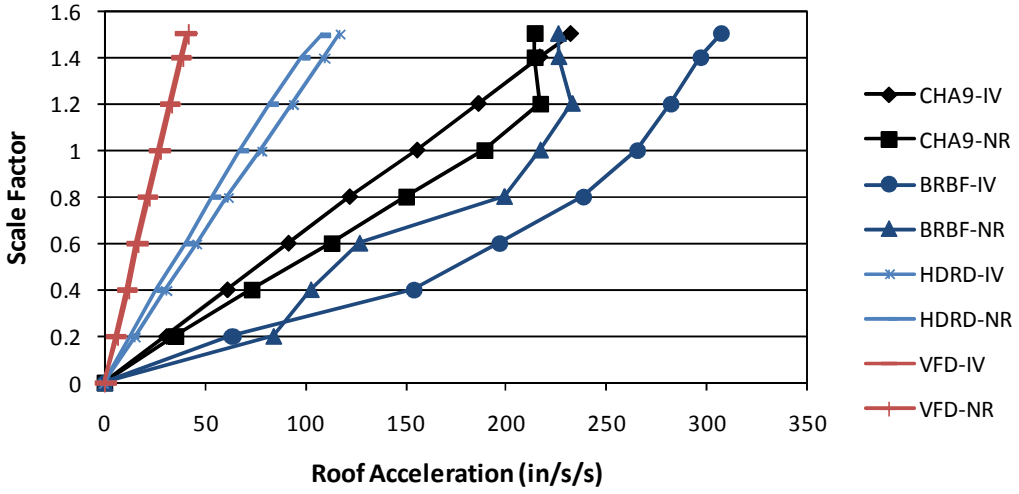

Figure 7 - 42 IDA Plots for Charleston Structure with Non-hybrid Systems

There are several differences between the behavior of the Charleston and LA structures. The Charleston moment frame performed very well from a damage perspective, but experienced large accelerations due to the frame remaining elastic. Both the frames were designed according to code, so the difference in the performance poses the question as to why. One reason for this may be the upper limit on the period prescribed by the code. The period calculated by the analysis program of 3.38 s is significantly larger than the 1.83 s used to calculate the ELF forces. Referring to Figure 7-13, the response to the scaled earthquakes for structures having a period of around 3.4 s is lower than at 1.83 s where the scale factor was calculated. More discussion of this difference in performance is presented in the discussion of results.

Figures 7-43 and 7-44 display the story drifts and residual displacements along the height of the building. The one thing of interest to note is that for the CHA9-NR record, the top two floors exceeded the story drift limits for the NR record. This was the location of the yielding at the DBE level. Because the only structure with any yielding is the BRBF, it is the only trace with any residual displacements. It is interesting to note that the shape of the BRBF curve for the two earthquakes is similar, although the Northridge record caused greater residual displacements.

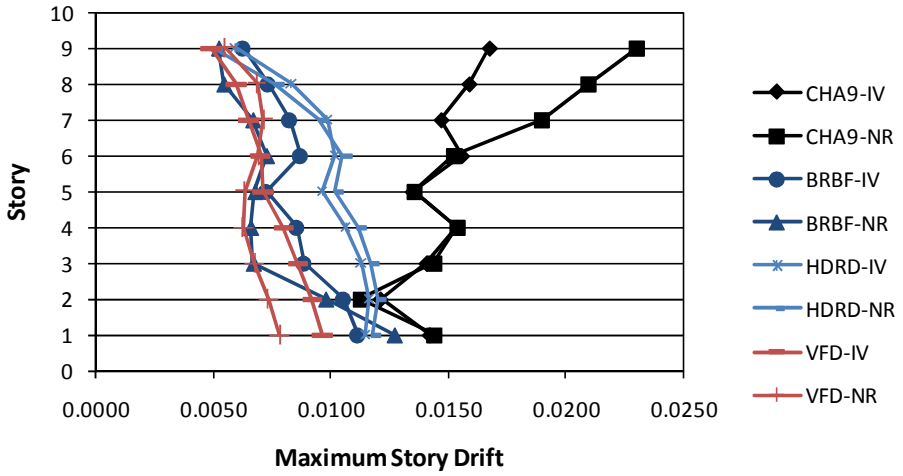

Figure 7 - 43 DBE Maximum Story Drifts for Non-hybrid Systems (CHA)

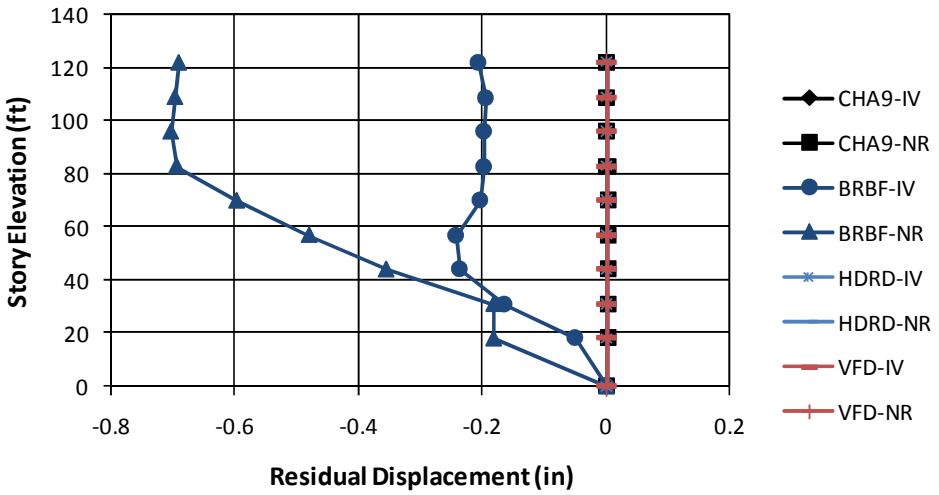

Figure 7 - 44 DBE Residual Displacements with Non-hybrid Systems (CHA)

The IDA results for the Hybrid HDRD systems are shown in Figure 7-45. For all these models at the DBE level, no hinges formed in the moment frames. The plots are not linear for base shear and roof drift because yielding occurred in the BRB elements. Similar trends to the LA structures are apparent in the plots. The BRBF provided the lowest roof drifts, with the hybrid systems experiencing slightly larger drifts. It should be noted that for all these systems the roof drifts are well below the code maximum. The base shear shows that the HPCD and BRBF systems provide similar levels of base shear, with the HYFR structure having the highest shears. For low levels of acceleration, the hybrid systems have a reduced base shear, highlighting the benefits of the damper. Another benefit of the rubber damper is apparent in the roof acceleration plots. At lower seismic levels, the HPCD and HYFR systems both experience lower roof accelerations. The HPCD continues to have the lowest accelerations by a significant margin up to the MCE level. The HYFR experiences the continued elastic stiffness of the rubber and BRB. Due to this additional stiffness, the HYFR experiences greater accelerations above a scale factor of 0.6.

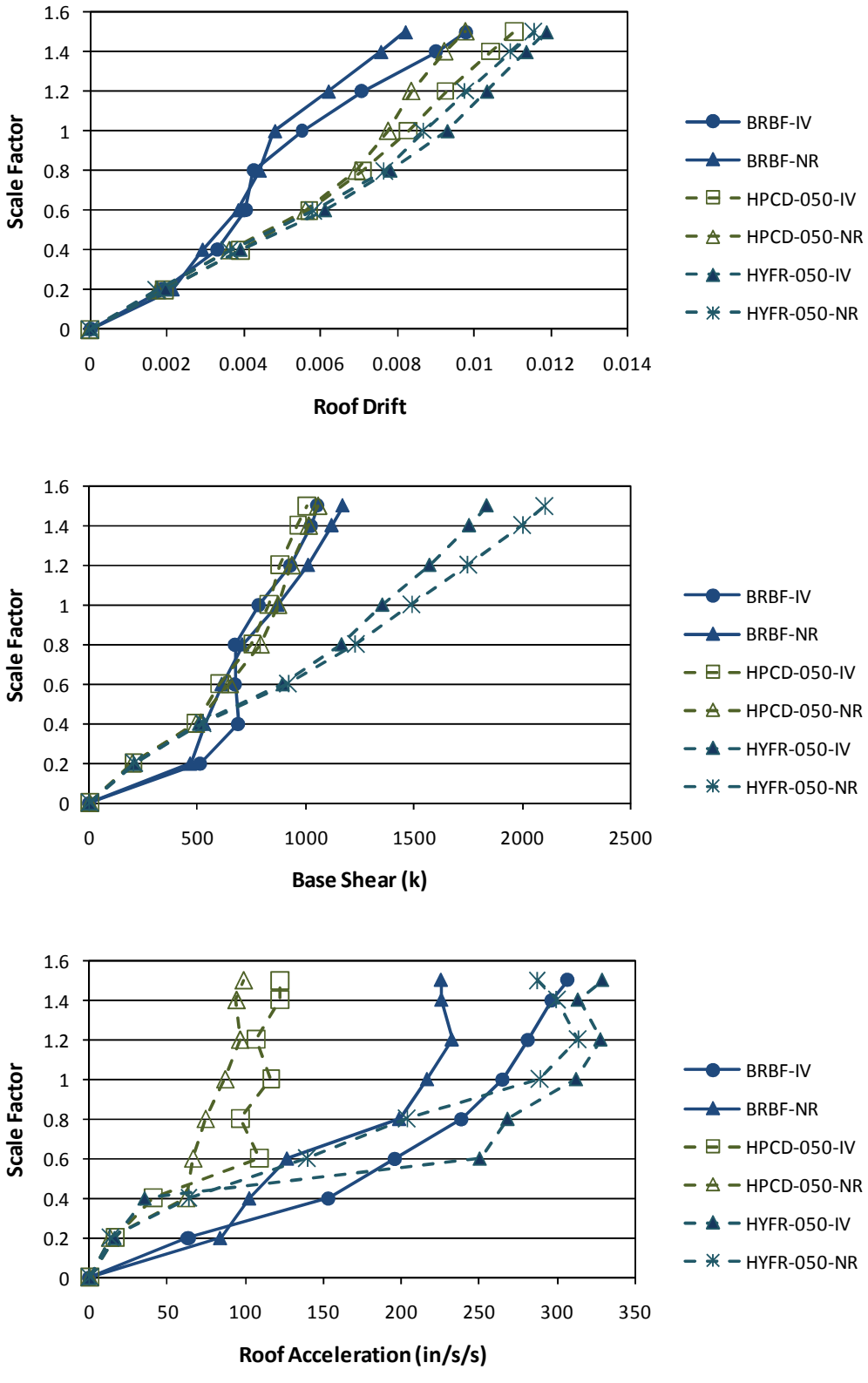

Figure 7 - 45 IDA Plots for Charleston Structure with HDRD Hybrid Systems

The DBE maximum story drifts and residual displacements are illustrated in Figures 7-46 and 7-47. The traces for story drift show similar levels and distribution of drift along the height of the structure. Some differences are apparent in the plot of residual displacements. Both BRBF responses show residual deformations. For the hybrid systems, the HPCD-050-NR experienced the most significant residual drift. The BRBF subjected to the Northridge ground motion experienced larger residuals than for the Imperial Valley. Both HYFR models experienced little or no residual deformations. This result is similar to the LA structure performance.

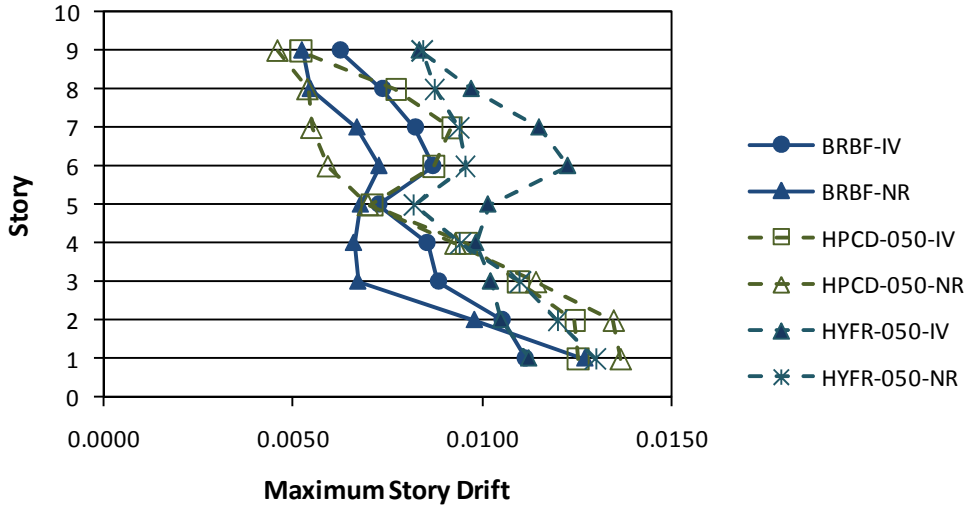

Figure 7 - 46 DBE Maximum Story Drifts with HDRD Hybrid Systems (CHA)

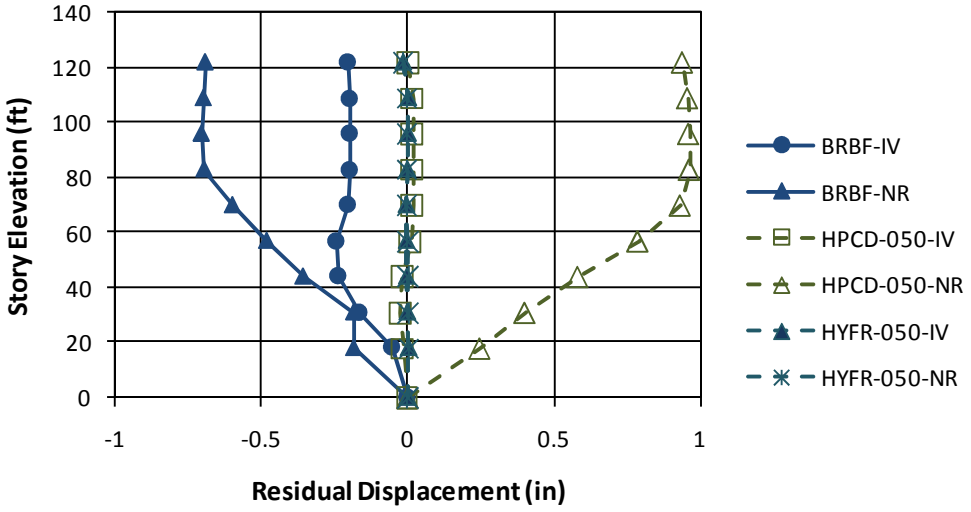

Figure 7 - 47 DBE Residual Displacements with HDRD Hybrid Systems (CHA)

Figure 7-48 shows the nonlinear static plot for the Charleston structure. The CHA9 structure shows a linear curve with yielding around 1300 k. This value explains why there was not yielding during the dynamic analysis, as the maximum base shear during the event was less than the strength at first yield. The ductility of the Charleston structures is not as good as LA. After first yield, column hinges formed earlier, causing instability at a drift of 2.5%. The BRBF shows a yielding of the BRB elements around 500 k. This is followed by the moment frame beginning to yield around 1200 k. The HPCD-050 and HPCD-100 are initially more flexible. The HPCD-50 reaches lockout and the stiffness increases until the BRB elements yield. The HPCD-100 does not have a defined lockout point, as it occurs when the damper has enough force to yield the brace. For the HYFR models, a similar phasing happens, but because the dampers are not locked out, they are able to take significant load. The added element increases the strength of the frame and the moment frames do not yield until nearly double the strength of the other models. This plot helps to illustrate the reason the HYFR dynamic models experience significantly higher base shears. Overall, this plot shows the phasing expected of the hybrid devices during the analysis.

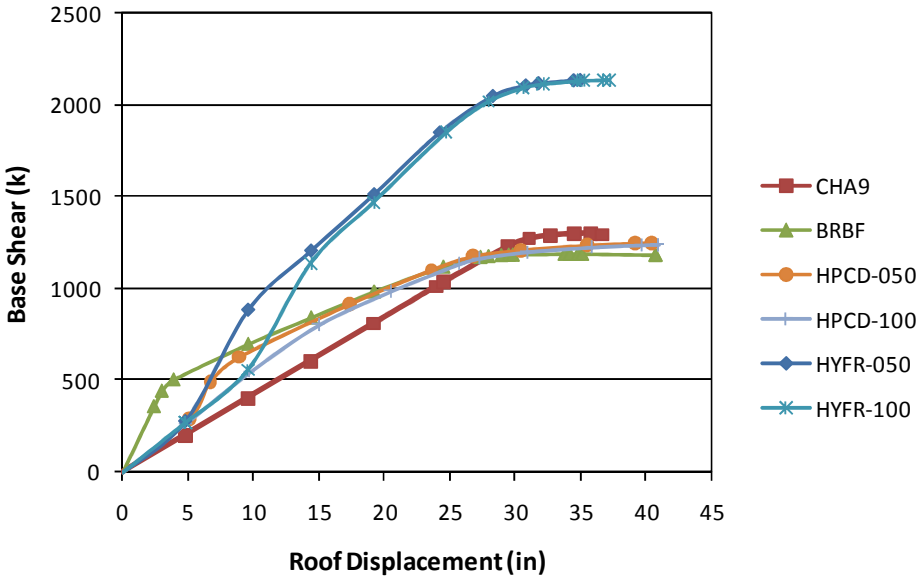

Figure 7 - 48 Static Pushover Plot for Charleston Structure

Figures 7-49 and 7-50 are plots of base shear response histories. These figures compare the HPCD frame to the CHA9 and the BRBF structures. The graphs help to illustrate the differences between a frame with and without added damping. The BRBF can be considered added damping but only at times where the structure is yielding. Both plots show that during the initial pulse of

the earthquake, the base shear in the HPCD is slightly higher. The benefit of the HPCD is that as the motion continues, the response is reduced in both magnitude and number of cycles. This is particularly apparent for the NR ground motion.

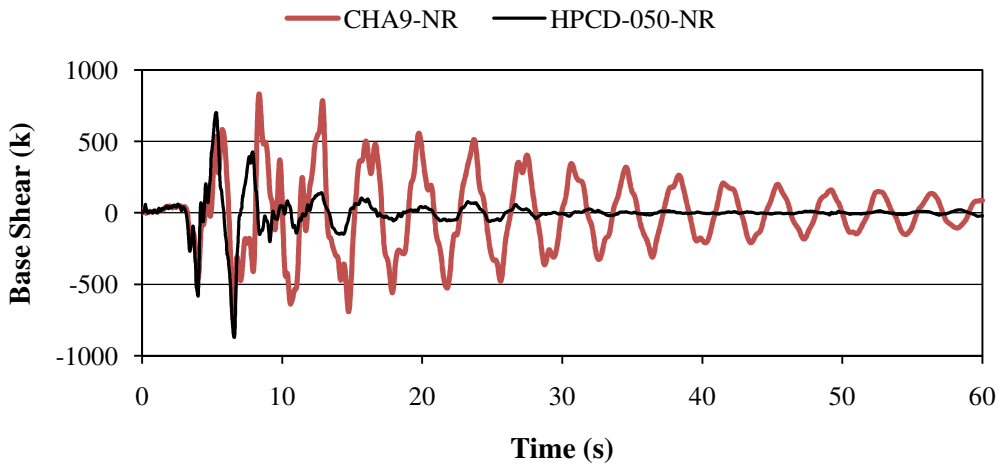

Figure 7 - 49 DBE Base Shear Response History - Northridge Ground Motion (CHA)

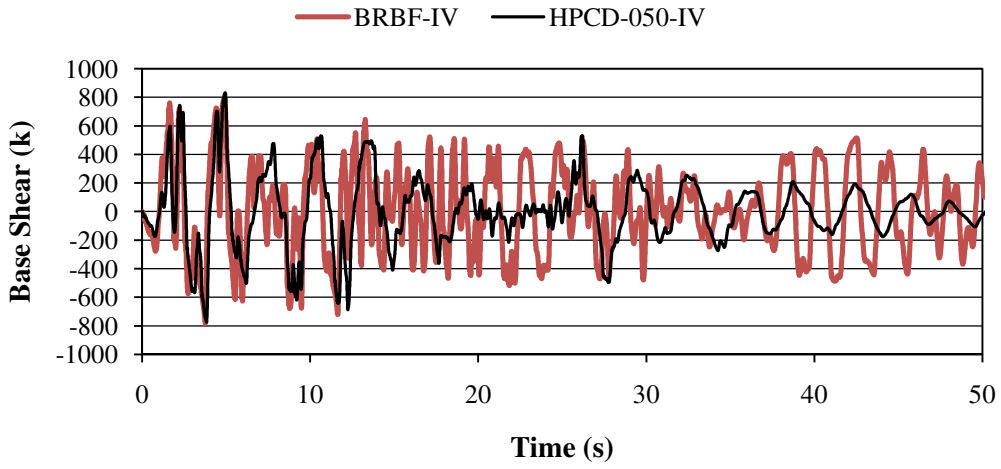

Figure 7 - 50 DBE Base Shear Response History - Imperial Valley Ground Motion (CHA)

Figure 7-51 shows a base shear response history that illustrates the difference between an HDRD system and the HPCD-050 system for the Imperial Valley DBE. It can be seen that the force in the damper in the HPCD is limited by the yield of the BRB element. The performance when the damper is not locked out is nearly identical.

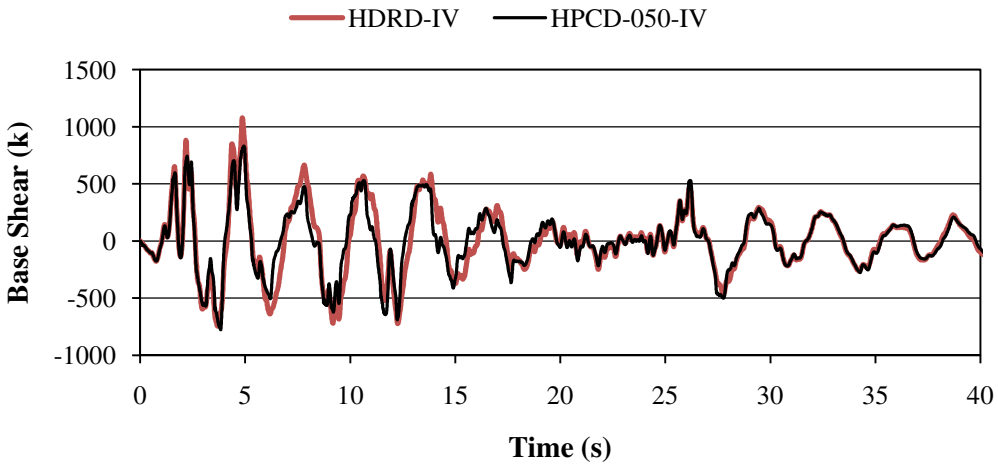

Figure 7 - 51 DBE Base Shear Response History – Imperial Valley Record (CHA)

Figure 7-52 illustrates the difference between the HPCD and HYFR systems. Because the rubber damper in the HYFR does not lockout, the system has a higher stiffness once the mechanism is engaged. This can be seen in both the magnitude of the base shear and the shortened period. Once the displacement is below the level of the lockout, the traces are nearly identical.

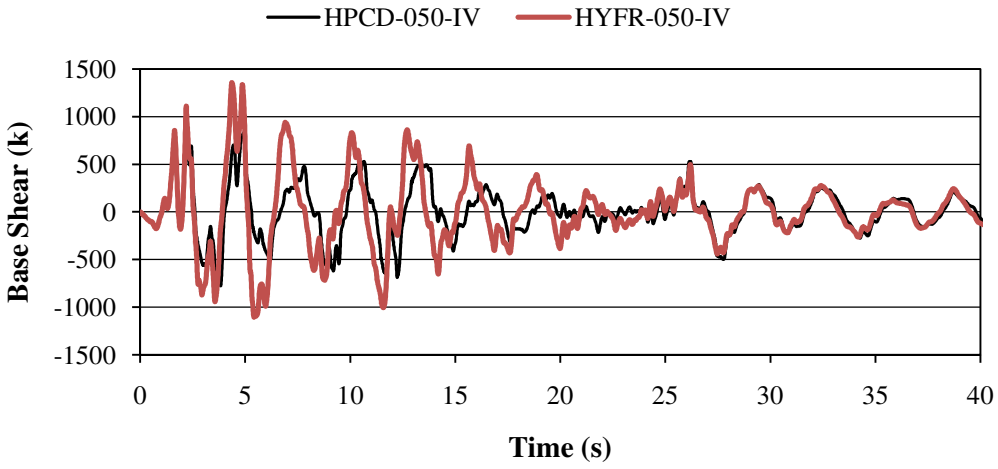

Figure 7 - 52 DBE Base Shear Response History – Imperial Valley Ground Motion (CHA)

Figure 7-53 presents the IDA results illustrating the effect of the gap for the hybrid systems with rubber dampers. Near linearity in response occurs for roof drift up to a scale factor of 0.6 and up to 0.4 for base shear. This highlights the benefit of the initial phase of the hybrid systems with reduced stiffness and higher damping. Once the two traces diverge, an increase in gap size leads to higher roof drifts and slightly lower base shears. The traces converge again and are essentially

equivalent above a scale factor of 1.2 for base shear. The roof acceleration plot illustrates the effect of the gap. At a scale factor of 0.2, the traces with a 0.5 in. gap diverge to the right, indicating the change in stiffness. This same event occurs for the 1 in. gap systems at a scale factor of 0.6. The curves follow a similar shaped path after that point. The HPCD traces are limited by the brace strength which causes them to be nearly vertical. The HYFR traces have the large elastic capacity of the rubber in parallel with the braces. This results in increasing accelerations until they level off above the DBE.

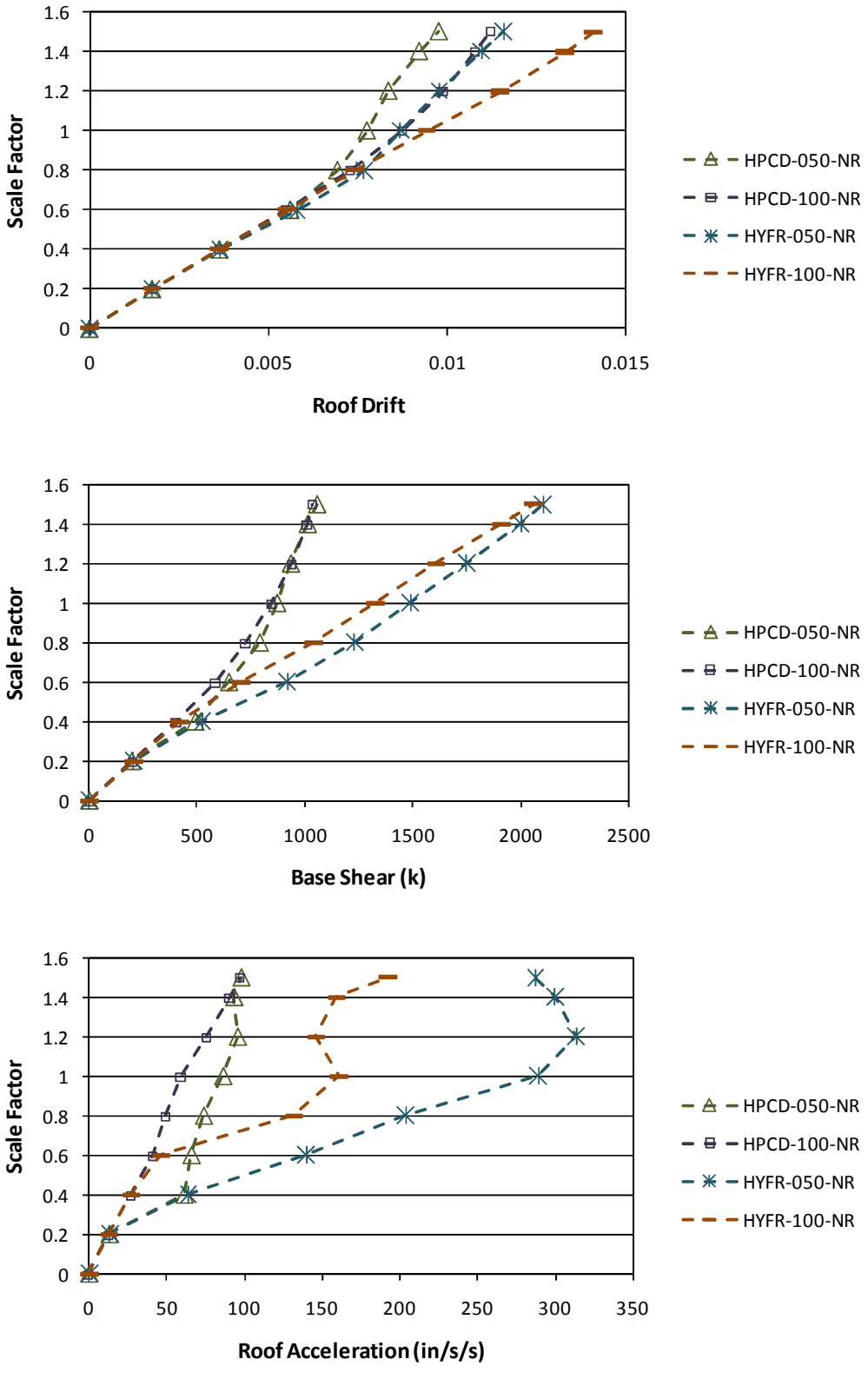

Figure 7 - 53 IDA Plots for Hybrid Systems with HDRD Comparing Gaps (CHA)

The effect of the gap size on story drift and residual displacements is shown in Figures 7-54 and 7-55. For the two different systems, the trends appear to be similar. The lower stories experience smaller drifts with the larger gap, while the trend is reversed for the upper stories. The crossover occurs around the 3rd or 4th floor. As far as residual displacements, the HYFR system performed extremely well. The HPCD experiences increased residual displacements with a larger gap.

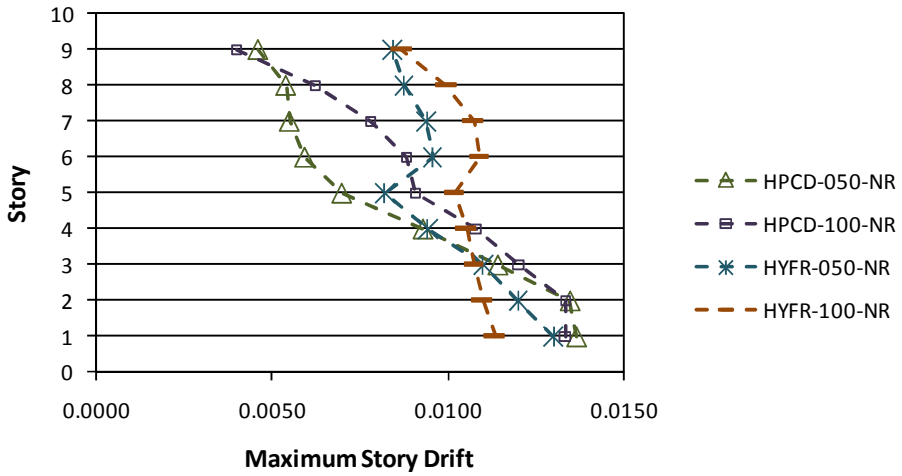

Figure 7 - 54 DBE Maximum Story Drifts - Comparing Gaps in HDRD Hybrid Systems (CHA)

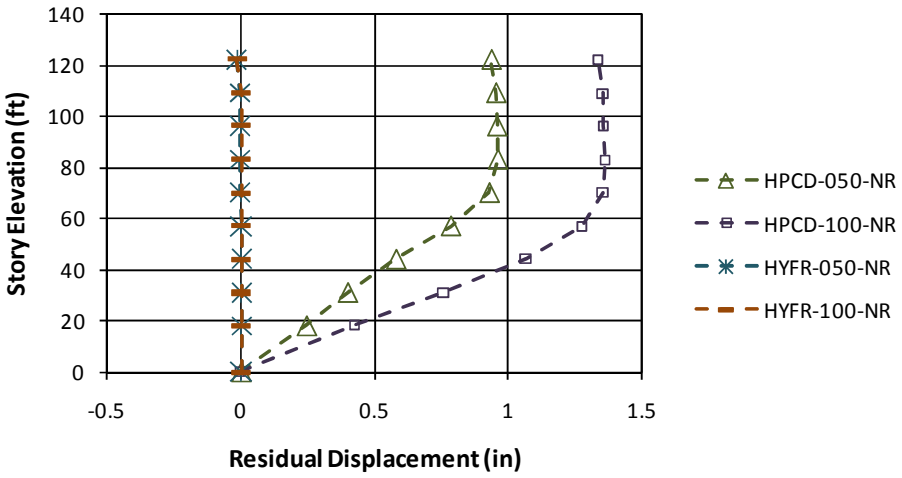

Figure 7 - 55 DBE Residual Displacements - Comparing Gaps in HDRD Hybrid Systems (CHA)

The base shear response history of the HYFR systems subjected to the DBE level Imperial Valley ground motion, shown in Figure 7-56, shows the variance between the systems. The

smaller gap locks out first, producing higher shears and shorter periods. Then the larger gap model experiences larger shears as the braces are engaged. Finally the two traces again match up as the displacements are reduced below the level of both gaps.

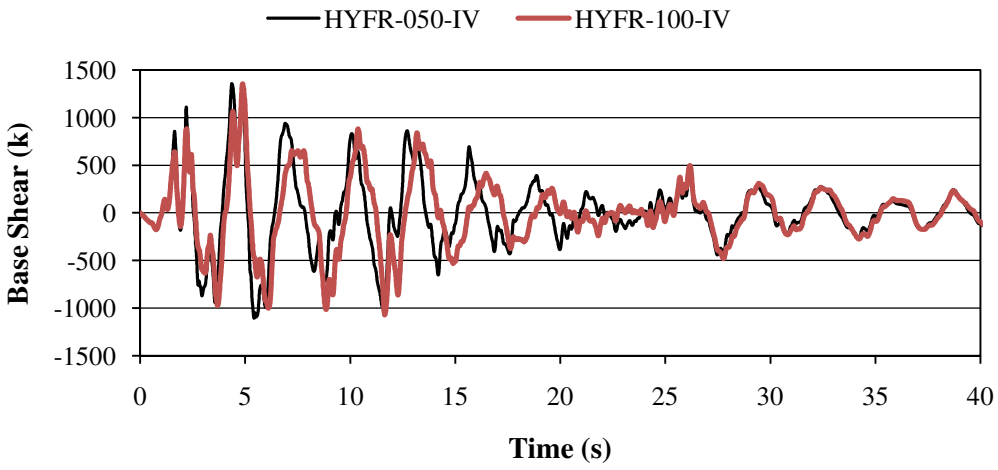

Figure 7 - 56 DBE Base Shear Response History – Imperial Valley Ground Motion (CHA)

The IDA plots for hybrid systems with viscous devices are presented in Figure 7-57. These plots show the benefits of providing damping at low levels. The hybrid configurations have lower drift values, with the crossover occurring between 0.4 and 0.6. The base shear plot illustrates the same trend, with the crossover occurring at 0.8. Above the crossover point, the base shear values for the hybrid systems are equivalent or slightly less than for the BRBF. The hybrid devices have a significantly decreased shear, with a minor difference in roof drift. This can be explained by the effect of damping and the nature of the viscous devices. The maximum damper force is out of phase with the base shear, so they do not occur simultaneously. For roof accelerations, the hybrid devices perform better with a single exception. The HPCD traces have slightly higher accelerations at a scale factor of 0.6. The hybrid curves turn from the initial slope at the same point with different slopes. The HYFR-VFD structures experience less acceleration, as the dampers are still effective while being locked out in the HPCD-VFD.

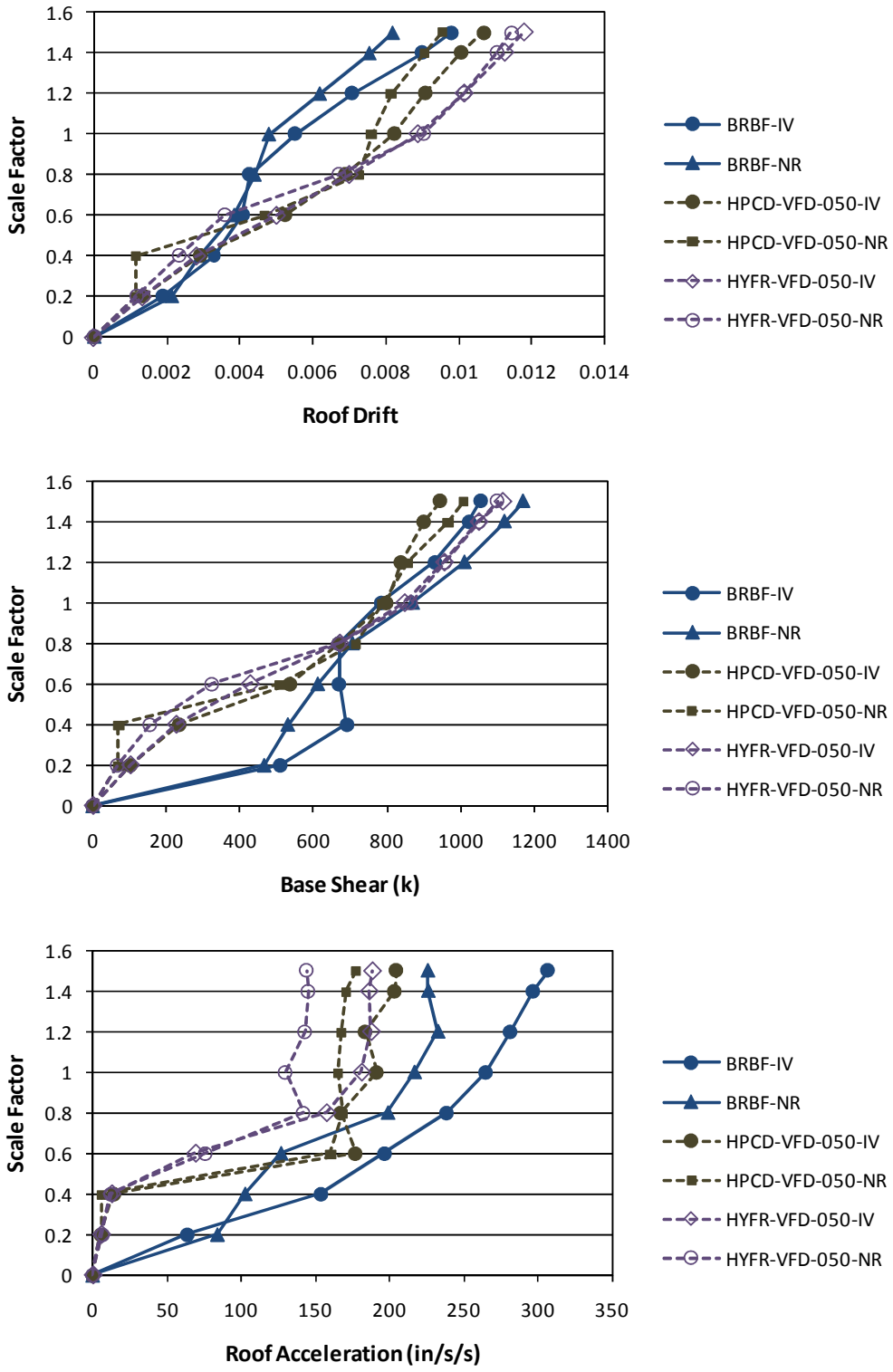

Figure 7 - 57 IDA Plots for Charleston Structure with VFD Hybrid Systems

Figures 7-58 and 7-59 are plots of the DBE level maximum story drifts and residual displacements of hybrid seismic systems with viscous fluid dampers. The hybrid systems

experience slightly higher story drifts, although they are still well below the code maximum. The BRBF experiences larger residual drifts than any of the hybrid systems. They do have in common the fact that the majority of the residual deformations are in the lower levels of the structure, which correlates with the higher drift ratios in the lower portion of the structure.

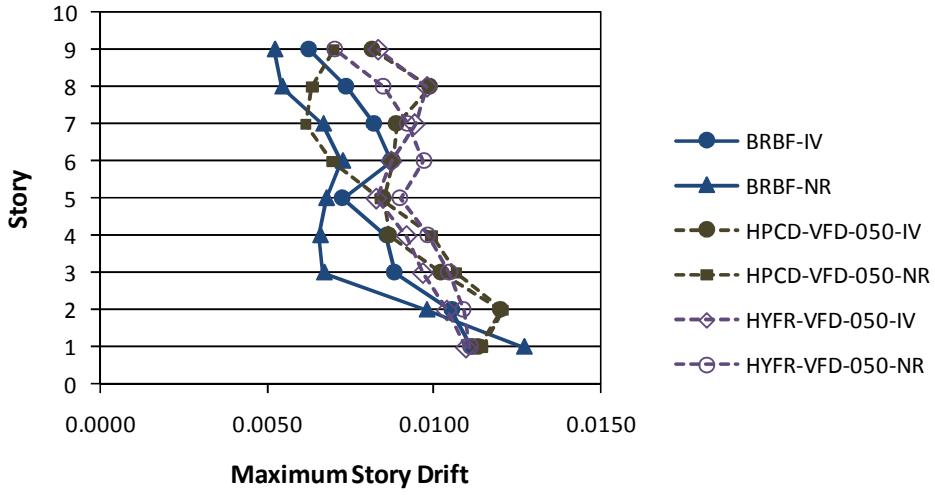

Figure 7 - 58 DBE Maximum Story Drifts with VFD Hybrid Systems (CHA)

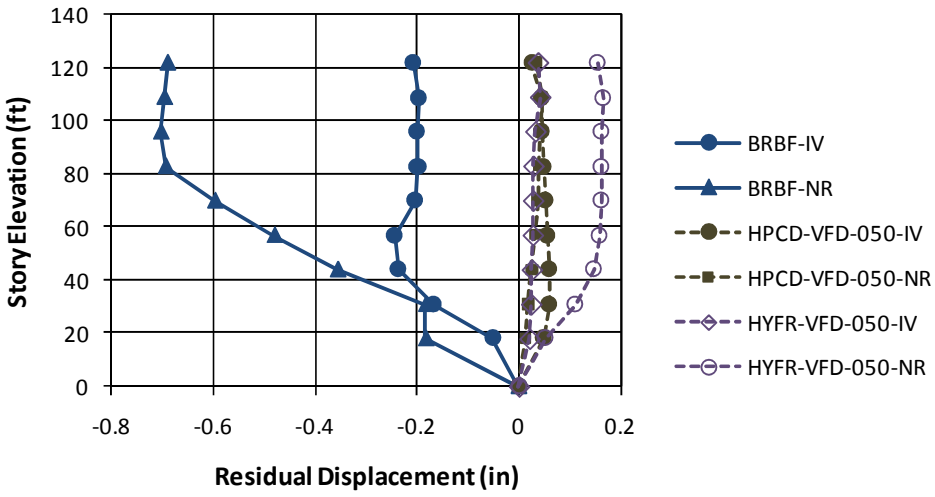

Figure 7 - 59 DBE Residual Displacements with VFD Hybrid Systems (CHA)

The difference between the HPCD-VFD and HYFR-VFD is less than for the hybrid systems with rubber dampers. Without the static stiffness to increase the base shear in the HYFR-VFD structure, the devices perform similarly. Figure 7-60 is a base shear response history plot showing an HPCD-VFD and HYFR-VFD structure. The traces are nearly identical for most of

the response. The only noticeable difference occurs between 15 and 35 seconds. The explanation of this difference is likely the fact that when the HPCD-VFD engages the BRB element, the viscous damper is locked out and not effective. This is not the case with the HYFR-VFD where the damper remains operational, as the lockout mechanism is attached to the BRB element.

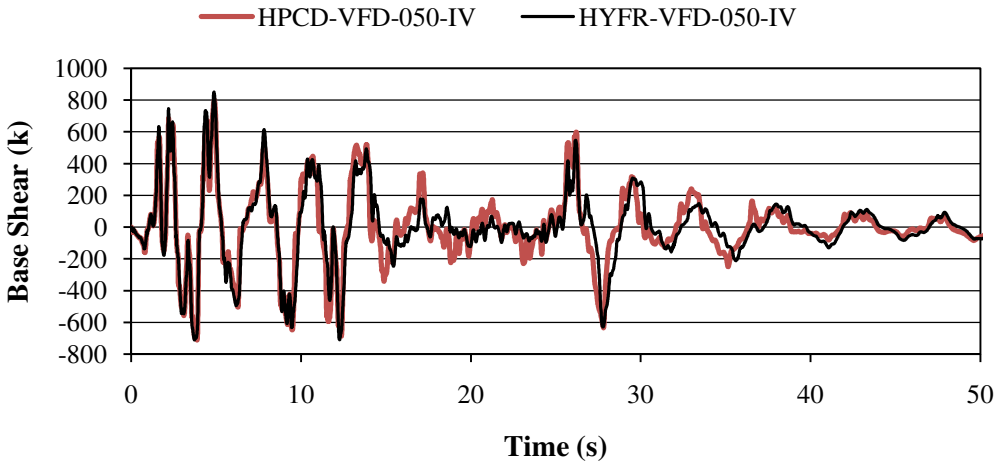

Figure 7 - 60 DBE Base Shear Response History – Imperial Valley Ground Motion (CHA)

The IDA results showing the effects of gap size for the hybrid systems with viscous devices are shown as Figure 7-61. The trend seen in the roof drift plot is that for a larger initial gap, a reduced roof drift occurs at and above a scale factor of 0.6. A similar trend occurs for base shear with the exception being the divergence occurring at 0.4. The gap is again visually apparent in the roof acceleration plot. The hybrid systems with the smaller gap diverge from the common path at a scale factor of 0.4 with different slopes. The larger gap models diverge with two different slopes at a scale factor of 0.8. Above the DBE, the larger gap traces cross the smaller gap curves, resulting in larger accelerations for a bigger gap.

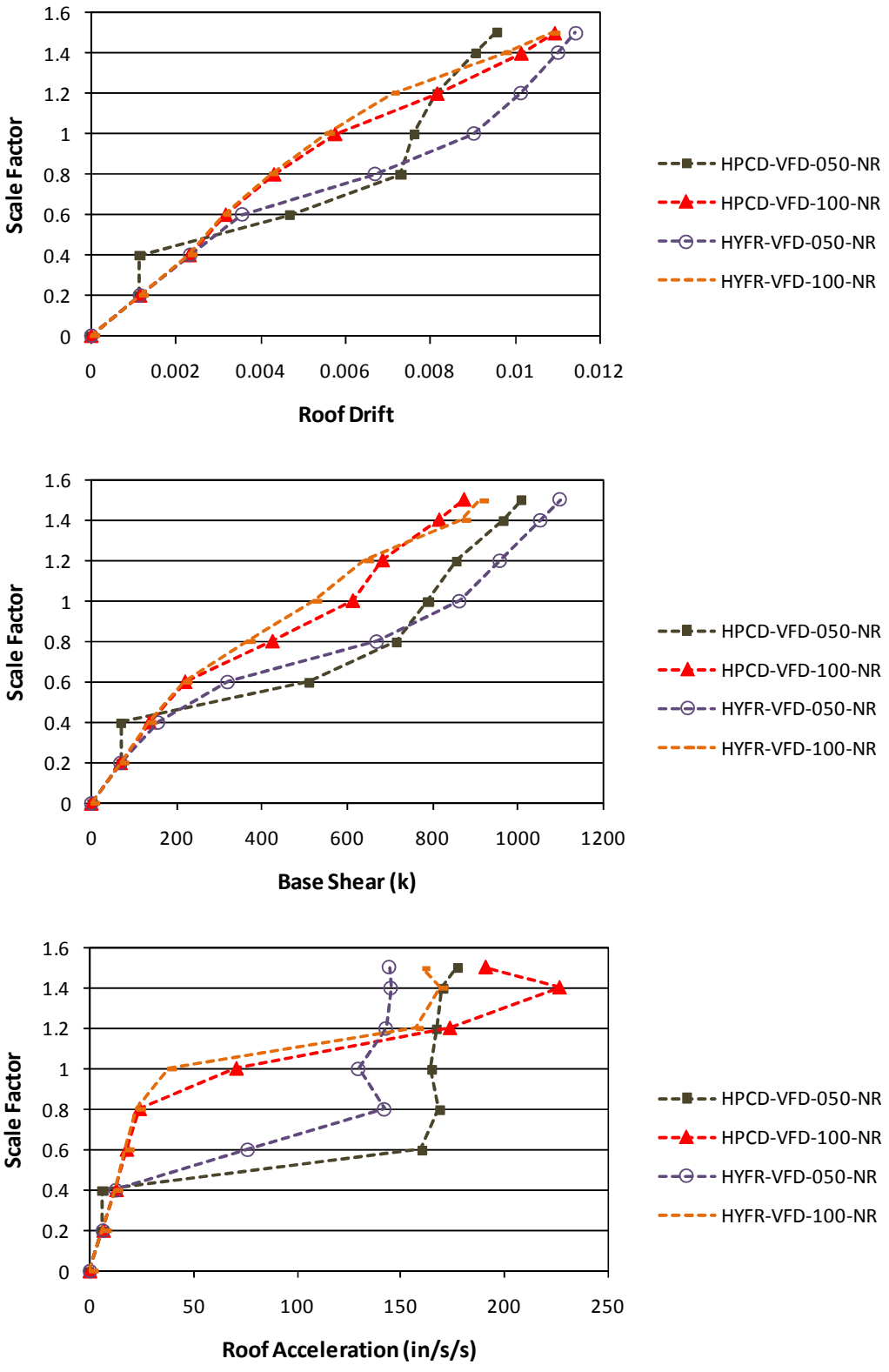

Figure 7 - 61 IDA Plots for Hybrid Systems with VFD Comparing Gaps (CHA)

Figures 7-62 and 7-63 show the comparison of the maximum story drift and residual displacements based on gap size. For the lower stories, a larger gap results in less drift. For the HPCD-VFD system the trend reverses at the 6th story with less drift for a smaller gap and then switches back again at the roof level. The HYFR-VFD system experiences reduced story drift over the height of the structure with a larger gap. The trend for residual deformations is the same for both systems. Both systems experience reduced residual deformations with a larger gap.

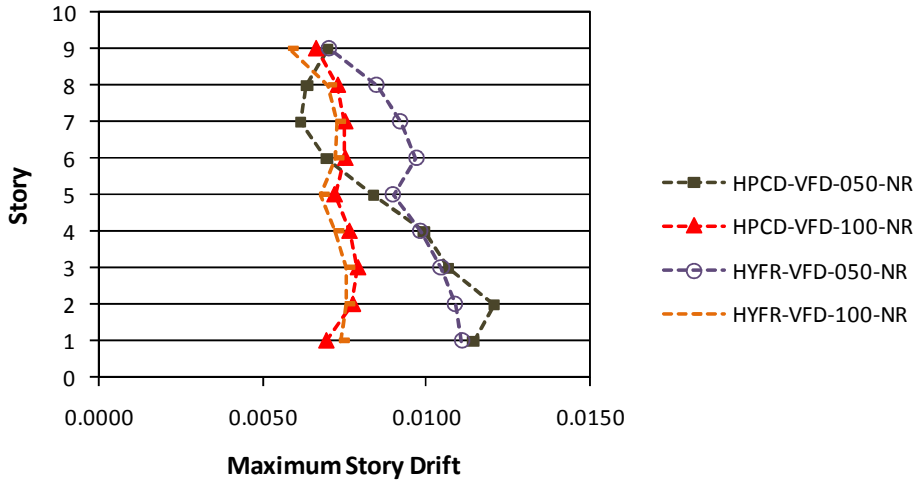

Figure 7 - 62 DBE Maximum Story Drifts – Comparing Gaps in VFD Hybrid Systems (CHA)

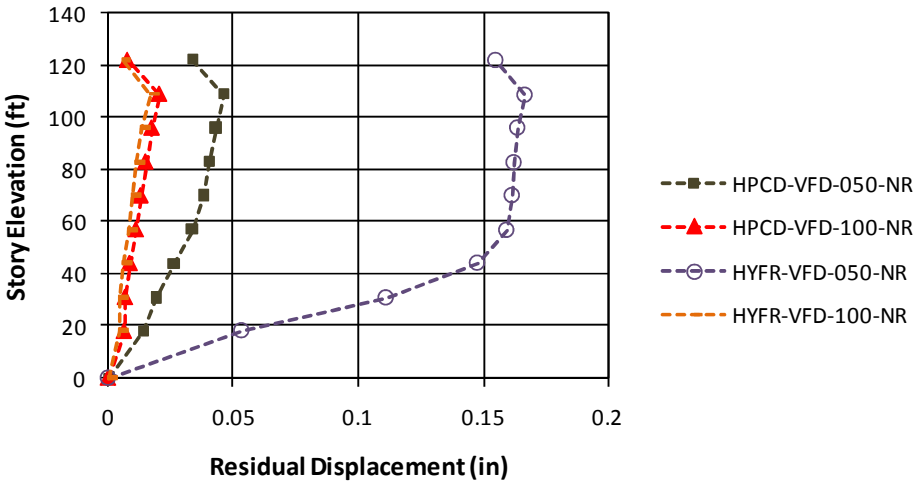

Figure 7 - 63 DBE Residual Displacements – Comparing Gaps in VFD Hybrid Systems (CHA)

The difference the gap makes on the VFD hybrid systems can be seen in the DBE base shear response history plots in Figures 7-64 and 7-65. The smaller gap results in larger base shear values and more excursions into the higher shears. This trend applies to both the HPCD-VFD and the HYFR-VFD.

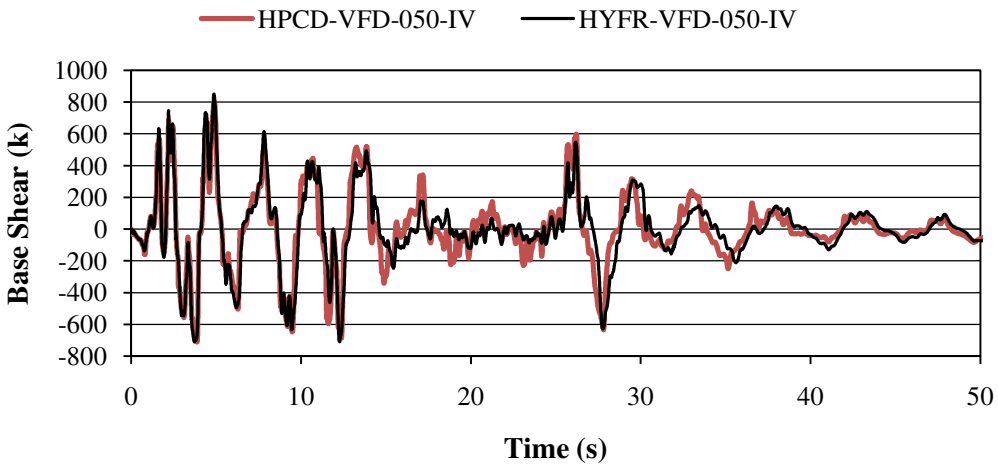

Figure 7 - 64 DBE Base Shear Response History – Imperial Valley Ground Motion (CHA)

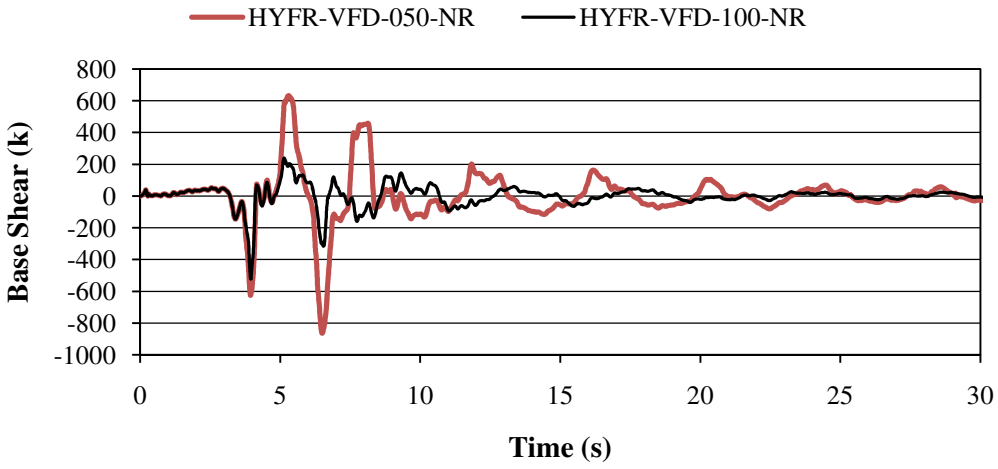

Figure 7 - 65 DBE Base Shear Response History – Northridge Ground Motion (CHA)

7.6. Discussion of Results

A significant amount of data has been presented in the previous sections of this chapter. The purpose of this section is to discuss the implications of what has been shown. The goal of this study was an initial investigation into the possibility of the hybrid passive control system for protection of structures from seismic events. The results have been presented in graphical form

and have shown some strengths and some weaknesses of the hybrid configurations analyzed. One weakness in the analysis is the limited number of earthquake records. Only two different ground motions were used. Even though the records represent two generally different types of ground shaking, a larger suite of motions should be used to indicate whether or not the type of earthquake can have an effect on the performance of the hybrid systems. Because of this limitation, the effect of the type of ground motion is not discussed.

Structural performance during earthquakes is rated based on the condition of the structure after the event. This can be investigated analytically by looking at the maximum story drifts, residual displacements and applied dynamic loads. An additional aspect is the total accelerations the structure experiences, as sensitive equipment and non-structural components can be affected by large accelerations. The best case scenario would be a reduction in all of the aforementioned quantities while maintaining economic feasibility. Unfortunately, that is typically not possible. For the sake of this study, the discussion focuses on determining if the results presented here justify further development, analysis and experimental testing of the hybrid concept.

The starting point is the plain steel moment frames. These frames have no added energy dissipation and hence perform poorly for most of the damage measures. Exceptionally poor performance occurred for the LA structure, with the structure essentially failing for some records. The Charleston SMRF structure performed well in the analysis, but the added damping devices provided an improved performance. The BRBF performed well in reducing deformations. Even with the increased stiffness, reduced base shears were reported compared to the SMRF structures. The weakness in the BRBF was that the accelerations were equivalent to or greater than the SMRF structures and residual deformations were significant for all the cases.

The VFD structures reduced deformations slightly compared to the undamped structures and experienced the lowest base shears and accelerations compared to all the analyzed systems. The reduction in displacement was not as significant as for the other added damping configurations. One point to highlight is that the improved performance occurred with only 10% critical damping in the first mode. Overall, the VFD structures provided good performance with the exception of residual drifts on the LA structure. The HDRD structures were effective at reducing drift and acceleration but caused large base shears due to the large elastic capacity of the rubber. The elastic re-centering force of the dampers did provide the benefit of reduced residual

deformations. Rubber or other viscoelastic dampers can provide improvements in seismic response, especially if modifications can be made to limit the base shear.

The HPCD configuration performed well compared to the other systems, especially in the lower scale factors. The reduction in drift was not as significant as for the BRBF but was still considerable. The base shear values were nearly equivalent to the BRBF but were lower at the smaller scale factors due to the added damping. The structure experienced fewer displacement cycles, especially in the later part of the earthquakes, due to the increased damping. The accelerations were significantly reduced compared to the BRBF and SMRF structures. The VFD structures had lower accelerations and base shears but had larger drifts. The HDRD structure had similar accelerations and larger base shears in the higher scale factors. The HPCD experienced significant residual deformations in some cases. The behavior of the HPCD shows that the yielding of the structure can be modified based on the gap. This feature demonstrates the possibility of performance-based design of structures with the option of modifying the ground acceleration level where the structure begins yielding the BRBs. The HPCD demonstrates potential for being an effective performance-based seismic protection strategy.

The HYFR configuration had similar levels of reduction to the HPCD for roof drift. In the lower scale factors it performed well in both base shear and roof acceleration reduction. The problem with the HYFR is the added elastic stiffness of the dampers. The increased stiffness caused large base shears and accelerations in the higher scale factors. One good characteristic of the HYFR is the near elimination of residual drifts. It is apparent in the results for both the LA and Charleston structures. This reduction is likely due to the re-centering force the damper provides the structure. The engagement of the BRB element is not as apparent in the IDA figures because the damper is still effective. The HYFR configuration shows promise for reducing response. It does require modifications to deal with the large elastic forces. An example could be to put a slotted bolted friction device in series with the HDR damper to limit force and provide energy dissipation for large-scale events.

The HPCD-VFD structure performed well in the lower scale factors. It follows the same initial paths as the VFD structures until the BRB engages. It provides the same possibility as the HPCD for performance-based design. In the larger scale factors the reduction in roof drift is not as significant as for the BRBF but the base shear values are similar. The HPCD-VFD reduced roof

accelerations better than the BRBF but the reduction was not as significant as it was for the HPCD. Residual deformations were similar to that of a BRBF. The HPCD-VFD demonstrates the ability to reduce seismic response and has the capacity to be a tool for performance based design.

The HYFR-VFD also performed well in the lower scale factors. It experienced slightly increased base shears over the HPCD-VFD due to the damper still being effective after the BRB engages. The benefit of the effective damper is reduced roof accelerations. It exhibits the capacity for use in performance-based framework with the engagement of the BRB being clear in the IDA plots. One drawback of the HYFR-VFD is the large residual deformations. The HYFR-VFD displays the ability to reduce the response of structures to seismic events. Further work is needed to develop solutions to reduce the large residual deformations.

7.7. Summary

The concept of the hybrid device has been analytically studied with several configurations applied to 9-story structures designed for conditions in Los Angeles, CA and Charleston, SC. The results of the study demonstrate the capabilities of hybrid devices to reduce seismic response. An additional benefit is the multi-phase nature of the device which can be applied to performance-based seismic design. All the hybrid configurations reduced some aspect of structural response. Some hybrid configurations had weaknesses that need to be investigated to provide better overall response. The effect of the gap was visible in the results and requires a more in-depth study.

This is a limited initial study that needs to be expanded in the future for a more detailed look at hybrid devices. A larger suite of earthquakes needs to be selected as well as adding additional levels of seismic hazard. The type of structures the devices are added to needs to be expanded as well. A single degree of freedom study could be used to look at some of the variables such as initial gap size, amount of added damping, and strength ratio of the BRB-to-SMRF. Various height structures should also be investigated to determine the size of structures these devices would benefit. The hybrid concept provides promise, but is still in its initial stages of development. Another aspect of future studies should include the economic feasibility of the device. It needs to be determined if the improved structural performance merits the additional cost of design and fabrication of hybrid devices.

Chapter 8. Summary and Conclusions

8.1. Summary

The goal of this research was to develop, analyze and experimentally test the concept of the hybrid passive control device. The first step in the process was to develop the configuration of the device. The decision was made to use a high-damping rubber device in combination with a metallic yield device. Multiple configurations were investigated with these options in mind. The desired characteristics of the device included a first-phase behavior with damping for any level of deformation. The second-phase behavior required an increase in stiffness and additional energy dissipation for significant seismic events. Considerations of cost and manufacturing were also considered in the selection process. The HPCD, which consists of an HDR damper with a lockout mechanism in series with a BRB, was selected as the most promising configuration meeting all requirements.

The next phase of the research was the development of an analytical device model. The first step in this process was to create a model of the high-damping rubber materials. Corry Rubber Corporation provided samples of six compounds of vulcanized rubber. The six compounds were characterized through static and cyclic testing. The testing measured the highly nonlinear static, dynamic and hysteretic properties of each compound. In the end, two compounds were selected as the best option for inclusion in the device. A high-damping natural rubber compound had the largest stiffness with a loss factor on the order of 0.16. The second compound was a highly-damped butyl rubber. The butyl rubber material had about half the stiffness of the natural rubber but had a loss factor on the order of 0.36. Corry Rubber recommended the butyl material, as it was specifically tailored for seismic applications.

The next step was creation of the material models including the stiffness and damping properties in the finite element program ABAQUS. Test data was used as an input for the Automatic Material Evaluation module in ABAQUS. The result of the material evaluation was the best fit hyperelastic function defining the elastic stiffness of the rubber compounds. Creation of the damping properties was done through the Hysteresis module of ABAQUS using the Bergstrom-Boyce model. The required coefficients were determined through a trial and error approach. In the end, the analytical model provided good correlation at a frequency of 1 Hz. The Mullins

effect was not accounted for in the model. The steady state behavior of the rubber was used in all the models.

Analytical models of the HPCD were created using both rubber compounds. The BRB core plate was modeled as a single plate with a reduced section for yielding. The steel material was modeled as a 36 ksi yield material with kinematic strain hardening. The buckling was restrained using edge boundary conditions configured in a way that would not restrain the Poisson effect. The lockout mechanism for the damper was modeled using nonlinear springs. The springs had no initial stiffness. Upon reaching the specified engagement of the mechanism, the springs had the stiffness of bolts in bending, simulating the lockout mechanism. The analytical performance of the HPCD for both rubber compounds verified the theorized behavior. Below the level of the lockout, the device performed as an HDR damper. Once the lockout was reached, an increase of stiffness resulted, followed by yielding of the BRB element.

Experimental testing of two prototype HPCDs was the next phase of the research. The first prototype was partially destroyed by a malfunctioning controller. It was subsequently used to test the reaction frame and fine tune the testing protocol. The tests run on HPCD #1 were qualitative but beneficial, as an error in the design was found and repaired prior to testing the second specimen.

HPCD prototype #2 was tested cyclically and statically to validate the concept of the hybrid device. The cyclic testing, although marred by partial bond failure of the damper, demonstrated the expected performance of the device. One drawback of the damper in series with the BRB is that the effectiveness of the damper is reduced for the same relative displacement due to deformation across the steel core. The static testing proved that the lockout mechanism in the damper worked well. The HPCD demonstrated the change in phase from damper to BRB without any problems. The BRB element did not complete the required displacement protocol. An unexpected local failure of the steel core terminated the testing. The device reached a ductility demand of 15.3 in compression before failure. The initiation of the failure was the result of an inadequate web thickness of the restraining member at a penetration. The flexibility of the web allowed the core to develop a buckling mechanism in the weak direction. The device demonstrated both the potential to be successful and the requirement for further development of the BRB restraining element.

The problem of bond failure between the rubber and steel in the damper was encountered during the HPCD #2 testing. Using surplus materials from the HPCD damper, smaller shear specimens were tested in an effort to determine why the bond failure was occurring. It was determined that the adhesive system used was appropriate for the application provided the steel surface is properly prepared. The reason for the bond failure of the rebuilt HPCD #2 was not discovered.

Using the material properties developed during testing, hybrid devices were analyzed and compared to typical passive control devices in a 9-story steel frame subjected to ground shaking. SAP 2000 by Computers and Structures, Inc. was used to analyze structures with two different seismic hazards. The first structure is based on designs for Los Angeles, CA. Charleston, SC was the second location used to determine seismic hazard. For each location, eight different lateral systems were analyzed and compared. The primary system was a special steel moment frame. The energy dissipation systems including the hybrid configurations were added to a reduced strength moment frame. The standard passive control systems included a BRB system, viscous fluid dampers and high damping rubber dampers. The hybrid configurations included various combinations of the three added damping systems. Table 8-1, originally presented as Figure 7-1, is shown here as a reminder of the abbreviations for the seismic resisting systems analyzed with the 9-story moment frame structure.

Table 8 - 1 Seismic Resisting System Descriptions and Abbreviations

SMRF	Fully Code Compliant Special Steel Moment Resisting Frame (LA9 or CHA9)
BRBF	Reduced Strength SMRF with Buckling Restrained Braces
HDRD	Reduced Strength SMRF with High Damping Rubber Dampers
VD	Reduced Strength SMRF with Viscous Fluid Damper
HPCD	Reduced Strength SMRF with Hybrid Passive Control Device
HYFR	Reduced Strength SMRF with Hybrid Frame Configuration
HPCD-VFD	Reduced Strength SMRF with Hybrid Passive Control Device Using a Viscous Fluid Damper
HYFR-VFD	Reduced Strength SMRF with Hybrid Frame Configuration Using a Viscous Fluid Damper

The previously described HPCD is one of the four hybrid systems analyzed. The HYFR system places an HDRD in parallel with a BRB. The phased behavior is provided by a slotted connection in series with the BRB. The slotted connection allows the first phase to engage the damper exclusively until the lockout displacement. The other two hybrid configurations are the HPCD-VFD and HYFR-VFD. These configurations are exactly like the HPCD and HYFR with the rubber damper being replaced by a viscous damper.

The analytical study was done in the form of an incremental dynamic analysis using two scaled earthquake records for each geographic location. The analysis included plastic hinges in the beams and interacting axial-flexural hinges in the columns. The BRBs, viscous dampers, rubber dampers and lockout mechanisms were modeled using linear and nonlinear link elements. P-delta effects were modeled using a ghost column with all the gravity loads from the leaner columns tributary to the modeled frame. In addition to the IDA, nonlinear static pushover analyses were run to investigate the phased behavior of the structure for the various configurations. The results of the study confirmed that the hybrid configurations have potential for reduction of seismic response. Each system demonstrated different strengths and weaknesses compared to the steel moment frame and other passive control systems.

The experimental and analytical work in the development of the HPCD and other hybrid configurations has demonstrated the potential of hybrid passive control. The ability to tailor a device to the structure and the seismic hazard provides an exceptional tool for performance-based seismic design. The only limitations that exist for applications of hybrid control are the imagination of the engineers who design them. This work has provided a kick start in the development, analysis and testing of hybrid prototypes. The future of seismic protection strategies should include this class of passive control.

8.2. Conclusions

The following section is a presentation of the conclusions generated throughout the body of this work. The first section talks about the testing, analysis and application of high damping rubber to reduce response of structures to dynamic loads. The second section discusses the performance and experimental testing of the HPCD. The last set of conclusions is based on the analytical study of steel moment frames with added hybrid and standard passive control systems.

8.2.1. High Damping Rubber

Filled vulcanized rubber is a unique and valuable engineering material. The highly nonlinear properties and high loss factor make it ideal for energy dissipation in structures. This is particularly true with the concept of a rubber damper as a structural brace. The HDRD model performed well in reduction of displacements and accelerations. An HDRD brace is able to dissipate energy at all levels of deformation while remaining elastic for large deformations. This

large deformation capacity creates a self-centering force to aid in the reduction of residual displacements.

The difficulty associated with rubber is the analytical modeling. Even in ABAQUS, limitations on the adequacy of the model were apparent. The Mullins effect could not be modeled at the same time as the hysteresis effect. The hysteresis properties could be correlated to the frequency dependence or the displacement dependence but not both. This creates problems for the implementation of rubber in engineering structures, as the typical designer does not have the tools readily available to analyze the material or structures using this material. Some relief is available due to the limited range of frequencies encountered in typical structures. The testing showed that the properties could be assumed to be relatively constant over this range without introducing significant error in the analysis.

The Mullins effect or stress softening of rubber is one area where neglecting the changing properties may have a significant effect. The virgin cycle for the material has a higher stiffness and a more robust hysteresis. In neglecting the higher initial stiffness, the analysis may underestimate the maximum base shear at the maximum device displacement. On the other hand, the actual displacement may be overestimated because of the higher loss factor associated with the first cycle. This is an area where more research is required. The stress-softening effect should be considered in applications of this material.

High-damping rubber is a unique and valuable material with properties specifically applicable to removing unwanted dynamic loads and deformations from structures. The analytical and experimental complexities of the material are the roadblocks to common usage.

8.2.2. Hybrid Passive Control Device

The HPCD concept provides a unique idea in passive control technology. The ability to tailor a device to desired structural performance is a powerful tool. The development of the HPCD was the result of examining multiple hybrid control options and finding the one that met the performance and economic criteria. Based on the experimental tests of the HPCD, the following conclusions can be drawn:

- The lockout mechanism in the damper performed well and created the desired phasing from the initial damper to the metallic yielding element.

- The reduction in the damper effectiveness due to deformation across the BRB element is in the range of 20% for the device tested. This reduced effectiveness must be considered when designing the device for an actual structure.
- The HDR damper experienced partial bond failure during cyclic testing. The root cause of the failure was not determined. The adhesive was shown to be appropriate for the application provided the steel and rubber surfaces are properly prepared. This issue must be studied in greater depth to ensure that a reliable bond can be developed.
- The loss factor for the damper alone is in the same range as the loss factor for the specimens tested during material characterization. A direct comparison is not possible in this situation due to the unknown loss of bond. The variability in the loss factor of the damper can also be attributed to the debonding.
- The performance of the device during cyclic testing over the range of frequencies and deformation levels applicable to typical structures was relatively constant. The loss factor and the dynamic stiffness of the device remained relatively unchanged throughout the tests. Considering the variable of the bond failure, this result is exceptional.
- The BRB device performed well up to the design displacement and achieved significant levels of ductility in both tension and compression. It did not reach the displacement demand required by the AISC Seismic Specification.
- The failure of the buckling restraining mechanism highlighted unforeseen behavioral characteristics in the prototype device. Future development of the device is required to eliminate undesirable failure modes.
- The overall behavior of the device during testing demonstrates multi-phased behavior with the capability for energy dissipation at all deformation levels and significant energy dissipation for significant seismic events.

8.2.3. Hybrid Damping Configurations in Steel Frame Structures

Using hybrid devices in steel moment frame structures to reduce seismic response was studied for two geographic areas, Los Angeles, CA and Charleston, SC. Both structures belong to seismic design category D according to ASCE 7-05, although the severity of the seismic loads was greater in Los Angeles. The BRBF structure was used as the baseline for comparisons, as the plain moment steel structure had the worst overall response and the hybrid devices must be an improvement over a successful energy dissipation system to have merit. Approximately 10%

total damping, including inherent damping, was provided by the viscous and rubber dampers. The results of this initial study are presented in the following conclusions:

- All the added passive control devices reduced seismic response in some manner over the plain steel moment frame structure.
- The HPCD structure performed well in the analyses. The BRBF had slightly better performance in reducing roof drift and base shear. The HPCD reduced accelerations significantly compared to the BRBF. The HPCD performed better in both base shear and roof acceleration at and below a ground motion scale factor of 0.4. The additional damping also reduced the number of large-displacement cycles the frame experienced. The HPCD exhibited good performance overall compared to the other systems.
- The HYFR structure displayed both strengths and weaknesses in its performance. The restoring force and large elastic capacity of the damper nearly eliminated residual deformations. The drawbacks of the large elastic capacity are the large shear forces and roof accelerations at higher scale factors. At small scale factors the acceleration and base shear performance was very good. The roof drift performance was very similar to that of the HPCD and the BRBF. The HYFR configuration shows promise but needs more work to eliminate the problems.
- The HPCD-VFD structure performed in a similar fashion to the BRBF for the three IDA damage measures. The added damping reduced the number of displacement and base shear cycles the structure experienced. It also reduced the severity of residual displacements over the BRBF. The HPCD-VFD as analyzed provides some benefits over the BRBF system. More study of this system to optimize the amount of damping could provide better performance.
- The HYFR-VFD was the only hybrid configuration to exceed the maximum drift requirements for the LA structure. In other damage measures, the HYFR-VFD structure experienced similar reductions to the HPCD-VFD. This system requires further study to investigate improved performance with larger dampers.
- The size of the gap before engagement of the BRB element had a variety of effects. For some damage measures, the gap reduced response. For other response quantities, the response increased. The effect of the gap was visible on many of the plots, as a larger gap allowed the structure to remain linear up to larger scale factors. The main effect of the

gap was to reduce forces and accelerations for small scale factors. More study on the effect of the gap on various damage measures is required.

8.3. Recommendations for Future Work

As with all research, success does not mean all the problems have been solved. Failure, although not an enjoyable experience, teaches many valuable lessons. This section focuses on recommendations for future research based on the successes, failures and findings of the current work. These are again broken down into high-damping rubber, the HPCD prototype and applying hybrid devices to steel frame structures.

8.3.1. High-Damping Rubber

The following list presents ideas for future work with high-damping rubber for seismic protection of structures. This is a multi-disciplinary type of research which should be completed with the cooperation of materials engineers, mathematicians, chemists or chemical engineers and rubber manufacturers.

- Development of models for high-damping rubber materials is an active research area. For these materials to move into mainstream usage, simplified models need to be developed. Although it may not be possible to include all the variables in a simplified model, some of the property variations could be excluded. Analytical studies which determine the sensitivity to the variations can be completed to determine which elements are not significant to the structural response.
- Many highly damped rubber materials are proprietary compounds. Because of this, published material properties are not available. It would be highly beneficial to experimentally compare the various high-damping rubber materials and generate standard properties for each different compound.
- Another analytical study could be completed using the material properties developed in the study listed previously. The purpose would be to determine how various combinations of stiffness and loss factor affect the performance of an HDR damper or a hybrid device with a rubber damper. This study could also be completed by choosing reasonable ranges of stiffness and loss factor and finding the combination with the best performance.

- The effect of aging on rubber needs to be studied to determine how the stiffness and hysteretic properties of the rubber change over time. This study also needs to include the condition and performance of the steel-rubber bond over time.
- A study of the type of structures for which an HDR damper is effective should be conducted. This should include multiple variables such as the number of stories, structural system, and type of dynamic loading. These results should be compared to other types of energy dissipation including viscous dampers, friction dampers and metallic yielding dampers.
- Because of the flexibility and high loss factor of these materials, HDR could be used to reduce small scale vibrations due to human activity, vehicles or machinery. The key is to find a location where the material can be placed to maximize deformations in the rubber without sacrificing the stiffness of the structure.

8.3.2. Hybrid Passive Control Device

The future development of the HPCD depends on the ability to refine the design of the prototype tested in this work. Additional ideas for development of this class of device are presented below.

- An experimental and analytical study should be carried out to further develop the HPCD to determine the appropriate ratio of core size to web thickness. The goal of this work would be to prevent localized failure of the core and the restraining web. The study should also include further refinement of the detailing of the buckling restraining mechanism.
- An experimental study needs to be done to develop a manufacturing process to achieve a reliable steel-rubber bond for the HDR damper. This study should focus on choosing the correct adhesive system for a hybrid device of typical size. A comparison of a post-cured and co-cured bond should be completed as part of the development. This study should include a feasibility study for manufacturing a damper with a lockout mechanism that could be co-cured during rubber compounding.
- Development, refinement and testing of other hybrid devices should be done. The concept of the hybrid device has boundless alternatives. The option of using a friction device in combination with a viscous or rubber damper has not been explored as part of

this work. This should also include development of the devices analyzed in the 9-story structures.

- One caveat of the BRB in the hybrid device is the shortened yield length. This tends to produce higher ductility demands at design displacements. This has generally been avoided with previous BRBs to avoid the strain hardening region of the steel stress-strain curve. One option would be to replace the low carbon steel with aluminum or stainless steel. Both these materials have significant ductility but do not experience the strain hardening at large inelastic strains.
- Development of a practical hybrid device which amplifies the strains across the rubber would be desirable. The previously discussed Visco-Plastic Device is one example of this idea. A large variety of configurations with this behavior could be developed, investigated and tested.

8.3.3. Hybrid Energy Dissipation in Steel Frame Structures

The future research under this heading will be to take the HPCD from element to system testing. It also includes further studies on the effects of the various parameters of the hybrid control system. The experimental projects in this section would be ideally suited for a National Science Foundation (NSF) Network for Earthquake Engineering Simulation (NEES) project, as large-scale testing would be required.

- A more detailed and rigorous analytical study of the effect of hybrid devices on structures subjected to earthquakes needs to be completed. One portion of this study should be a single degree of freedom system. At such a reduced level, it is easier to discern the effects of variables on performance. The variables needing research include gap size, amount of damping, type of damper and the ratio of BRB to moment frame stiffness or strength. The study also needs to be expanded to include buildings of various heights to determine the range of buildings for which hybrid devices are effective. The economic feasibility of the device must be investigated as well.
- Analytical studies with hybrid devices should be conducted to study the best distribution of hybrid devices through a structure. This should include vertical distribution and the number of devices producing the greatest effect.

- An analytical study should be completed to develop design guidelines and procedures for hybrid devices in a performance-based earthquake engineering environment. The capability to tailor damping, onset of BRB yield and ultimate strength creates an ideal opportunity for a performance-based approach.
- Prior to an HPCD being used in standard earthquake engineering, an analytical study needs to be completed to determine the appropriate response modification factor for this system. The study needs to explicitly model all the elements of the structural frame to determine probabilities of collapse and the amount of ductility the system can provide.
- Another type of hybrid frame could be developed and analyzed using only BRB elements. The BRB devices would be used with a lockout mechanism which would engage at a specified displacement. The BRBs could be engaged all at the same level or in various stages. This would help to reduce accelerations under low level earthquakes by having a longer period initially and put off yielding under small ground motions. The analytical study should include various sizes of structures and various distributions of BRBs along the height. It should also look at the effect of engaging BRBs in phases.
- Once the HPCD or another hybrid device has been refined and has performed successfully in an element test, a full or scaled structural frame with hybrid devices should be tested on a shaking table.

REFERENCES

ABAQUS. (2007). *Abaqus Analysis User's Manual*, Dassault Systems, United States of America.

Ahn, S.-K., Min, K.-W., Park, J.-H., Lee, S.-H., Lee, D.-G., Oh, J.-K., Kim, K.-S., and Lee, S.-K. (2008). "Practical Issues and Solutions on Installation of Viscoelastic Dampers in a 46-Story Reinforced Concrete Building Structure." *Structural Design of Tall and Special Buildings*, 17(1), 231-243.

Aiken, I. D., Kelly, J. M., and Pall, A. S. (1988). "Seismic Response of a Nine-Story Steel Frame with Friction-Damped Cross-Bracing." Earthquake Engineering Research Center, University of California, Berkeley, Berkeley, CA.

Aiken, I. D., Nims, D. K., Whiitaker, A. S., and Kelly, J. M. (1993). "Testing of Passive Energy Dissipation Systems." *Earthquake Spectra*, 9(3), 335-370.

AISC. (2005). *Seismic Provisions for Structural Steel Buildings*, American Institute of Steel Construction, Chicago, IL.

Amadio, C., Clemente, I., Macorini, L., and Fragiacomo, M. (2008). "Seismic Behaviour of Hybrid Systems Made of Pr Composite Frames Coupled with Dissipative Bracings." *Earthquake Engineering and Structural Dynamics*, 37(6), 861-879.

Amin, A. F. M. S., Alam, M. S., and Okui, Y. (2002). "An Improved Hyperelasticity Relation in Modeling Viscoelasticity Response of Natural and High Damping Rubbers in Compression: Experiments, Parameter Identification and Numerical Verification." *Mechanics of Materials*, 34(2), 75-95.

Amin, A. F. M. S., Lion, A., Sekita, S., and Okui, Y. (2006a). "Nonlinear Dependence of Viscosity in Modeling the Rate-Dependent Response of Natural and High Damping Rubbers in Compression and Shear: Experimental Identification and Numerical Verification." *International Journal of Plasticity*, 22(9), 1610-1657.

Amin, A. F. M. S., Wiraguna, S. I., Bhuiyan, A. R., and Okui, Y. (2006b). "Hyperelasticity Model for Finite Element Analysis of Natural and High Damping Rubbers in Compression and Shear." *Journal of Engineering Mechanics*, 132(1), 54-64.

Anderson, T. L. (1989). "Seismic Isolation for the Los Angeles County Fire Command and Control Facility." 1989 Structures Congress, ASCE, San Francisco, CA.

ASCE. (2006). *Minimum Design Loads for Buildings and Other Structures*, American Society of Civil Engineers, Reston, VA.

Asher, J. W., Young, R. P., and Ewing, R. D. (2001). "Seismic Isolation Design of the Arrowhead Regional Medical Center." *Structural Design of Tall Buildings*, 10(5), 321-334.

Auricchio, F., Fugazza, D., and DesRoches, R. (2006). "Earthquake Performance of Steel Frames with Nitinol Braces." *Journal of Earthquake Engineering*, 10(SPEC ISS 1), 45-66.

Bartera, F., Dezi, L., and Giacchetti, R. (2004). "Cyclic Behaviour of a Reinforced Concrete Braced Frame with High Damping Rubber Devices." Eighth International Conference on Structures Under Shock and Impact, SUSI VIII, WIT Press, Southampton, SO40 7AA, United Kingdom, Crete, Greece, 439-451.

Bartera, F., and Giacchetti, R. (2004). "Steel Dissipating Braces for Upgrading Existing Building Frames." *Journal of Constructional Steel Research*, 60(3-5), 751-769.

Bergman, D. M., and Goel, S. C. (1987). "Evaluation of Cyclic Testing of Steel-Plate Device for Added Damping and Stiffness." University of Michigan, Ann Arbor, Michigan.

Bergstrom, J. S., and Boyce, M. C. (1998). "Constitutive Modeling of the Large Strain Time-Dependent Behavior of Elastomers." *Journal of the Mechanics and Physics of Solids*, 46(5), 931-954.

Bergstrom, J. S., and Boyce, M. C. (2000). "Large Strain Time-Dependent Behavior of Filled Elastomers." *Mechanics of Materials*, 32(11), 627-644.

Bergstrom, J. S., and Boyce, M. C. (2001). "Constitutive Modeling of the Time-Dependent and Cyclic Loading of Elastomers and Application to Soft Biological Tissues." *Mechanics of Materials*, 33(9), 523-30.

Black, C. J., Makris, N., and Aiken, I. D. (2004). "Component Testing, Seismic Evaluation and Characterization of Buckling-Restrained Braces." *Journal of Structural Engineering*, 130(6), 880-894.

Brown, R. (1996). *Physical Testing of Rubber*, Chapman & Hall, London, UK.

Buckle, I. G., and Mayes, R. L. (1990). "Seismic Isolation: History, Application, and Performance - a World View." *Earthquake Spectra*, 6(2), 161-202.

Cardone, D., Dolce, M., and Ponzo, F. C. (2004). "Experimental Behaviour of R/C Frames Retrofitted with Dissipating and Re-Centring Braces." *Journal of Earthquake Engineering*, 8(3), 361-396.

Chang, K.-C., and Lin, Y.-Y. (2004). "Seismic Response of Full-Scale Structure with Added Viscoelastic Dampers." *Journal of Structural Engineering*, 130(4), 600-608.

Chang, K. C., Chen, S. J., and Lai, M. L. (1996). "Inelastic Behavior of Steel Frames with Added Viscoelastic Dampers." *Journal of Structural Engineering*, 122(10), 1178-1185.

Chang, K. C., and El-natur, H. A. (1993). "Parametric Study of Structures with Added Viscoelastic Dampers." Symposium on Structural Engineering in Natural Hazards Mitigation, ASCE, Irvine, CA, USA, 724-729.

Chang, K. C., Soong, T. T., Oh, S. T., and Lai, M. L. (1995). "Seismic Behavior of Steel Frame with Added Viscoelastic Dampers." *Journal of Structural Engineering*, 121(10), 1418-1426.

Charney, F. A., and Marshall, J. D. (2006). "A Comparison of the Krawinkler and Scissors Model for Including Beam-Column Joint Deformations in the Analysis of Steel Moment-Resisting Frames." *Engineering Journal*, 63(11), 1515-1528.

Charney, F. A., and McNamara, R. J. (2008). "Comparison of Methods for Computing Equivalent Viscous Damping Ratios of Structures with Added Viscous Damping." *Journal of Structural Engineering*, 134(1), 32-44.

Chen, C.-S., Chen, K.-C., Pong, W. S., and Tsai, C. S. (2002). "Parametric Study for Buildings with Combined Displacement-Dependent and Velocity-Dependent Energy Dissipation Devices." *Structural Engineering and Mechanics*, 14(1), 85-98.

Christopoulos, C., Tremblay, R., Kim, H.-J., and Lacerte, M. (2008). "Self-Centering Energy Dissipative Bracing System for the Seismic Resistance of Structures: Development and Validation." *Journal of Structural Engineering*, 134(1), 96-107.

Ciampi, V. (1995). "Research and Development of Passive Energy Dissipation Techniques for Civil Buildings in Italy." International Post-SMiRT Conference Seminar on Seismic Isolation, Energy Dissipation and Control of Vibrations of Structures, 1-15.

Ciampi, V., Arcangeli, M., and Perno, S. (1993a). "Characterisation of the Low-Cycle Fatigue Life of a Class of Energy Dissipating Devices." Structural Dynamics - Eurodyn '93, Trondheim, Norway, 137-144.

Ciampi, V., De Angelis, M., and Paolacci, F. (1993b). "On the Seismic Design of Dissipative Bracings for Seismic Protection of Structures." Structural Dynamics - Eurodyn '93, Trondheim, Norway, 153-160.

Ciampi, V., and Samuelli-Ferretti, A. (1990). "Energy Dissipation in Buildings Using Special Bracing Systems." 9th European Conference on Earthquake Engineering, Moscow, 9-18.

Clark, P. W., and Kelly, J. M. (1996). "Energy-Based Modeling of High Damping Rubber Seismic Isolators for Dynamic Analysis." Conference on Analysis and Computation, ASCE, New York, NY, USA, Chicago, IL, USA, 200-211.

Constantinou, M. C., Soong, T. T., and Dargush, G. F. (1998). *Passive Energy Dissipation Systems for Structural Design and Retrofit*, Multidisciplinary Center for Earthquake Engineering Research Center, Buffalo, NY.

Constantinou, M. C., and Symans, M. D. (1993). "Experimental Study of Seismic Response of Buildings with Supplemental Fluid Dampers." *Structural Design of Tall Buildings*, 2(2), 93.

Constantinou, M. C., Tsopelas, P., Hammel, W., and Sigaher, A. N. (2001). "Toggle-Brace-Damper Seismic Energy Dissipation Systems." *Journal of Structural Engineering*, 127(2), 105-112.

CSI. (2007). *Csi Analysis Reference Manual*, Computers and Structures, Inc., Berkeley, CA.

Dall'Asta, A., and Ragni, L. (2006). "Experimental Tests and Analytical Model of High Damping Rubber Dissipating Devices." *Engineering Structures*, 28(13), 1874-1884.

Dall'Asta, A., and Ragni, L. (2008). "Dynamic Systems with High Damping Rubber: Nonlinear Behavior and Linear Approximation." *Earthquake Engineering and Structural Dynamics*, 37(13), 1511 - 1526.

De Luca, A., Mele, E., Molina, J., Verzeletti, G., and Pinto, A. V. (2001). "Base Isolation for Retrofitting Historic Buildings: Evaluation of Seismic Performance through Experimental Investigation." *Earthquake Engineering and Structural Dynamics*, 30(8), 1125-1145.

De Matteis, G., Mazzolani, F. M., and Panico, S. (2007). "Pure Aluminium Shear Panels as Dissipative Devices in Moment-Resisting Steel Frames." *Earthquake Engineering and Structural Dynamics*, 36(7), 841-859.

Derham, C. J., Kelly, J. M., and Thomas, A. G. (1985). "Nonlinear Natural Rubber Bearings for Seismic Isolation." *Nuclear Engineering and Design*, 84(3), 417-428.

DesRoches, R., and Smith, B. (2004). "Shape Memory Alloys in Seismic Resistant Design and Retrofit: A Critical Review of Their Potential and Limitations." *Journal of Earthquake Engineering*, 8(3), 415-429.

Di Sarno, L., and Elnashai, A. S. (2003). "Special Metals for Seismic Retrofitting of Steel Buildings." *Progress in Structural Engineering and Materials*, 5(2), 60-76.

Dicleli, M., and Mehta, A. (2007a). "Efficient Energy Dissipating Steel-Braced Frame to Resist Seismic Loads." *Journal of Structural Engineering*, 133(7), 969-981.

Dicleli, M., and Mehta, A. (2007b). "Seismic Performance of Chevron Braced Steel Frames with and without Viscous Fluid Dampers as a Function of Ground Gotion and Damper Characteristics." *Journal of Constructional Steel Research*, 63(8), 1102-1115.

Dinehart, D. W., Shenton, H. W., and Elliott, T. E. (1999). "The Dynamic Response of Wood-Frame Shear Walls with Viscoelastic Dampers." *Earthquake Spectra*, 15(1), 67 - 86.

Dolce, M., and Cardone, D. (2006). "Theoretical and Experimental Studies for the Application of Shape Memory Alloys in Civil Engineering." *Journal of Engineering Materials and Technology*, 128(3), 302-311.

Dolce, M., Cardone, D., and Marnetto, R. (2001). "Sma Re-Centering Devices for Seismic Isolation of Civil Structures." Smart Systems for Bridges, Structures, and Highways-Smart Structures and Materials 2001, Society of Photo-Optical Instrumentation Engineers, Newport Beach, CA, 238-249.

Dolce, M., Cardone, D., Ponzo, F. C., and Valente, C. (2005). "Shaking Table Tests on Reinforced Concrete Frames without and with Passive Control Systems." *Earthquake Engineering and Structural Dynamics*, 34(14), 1687-1717.

El-Attar, A. G., Saleh, A. M., and Zaghw, A. H. (2005). "Conservation of a Slender Historical Mamluk-Style Minaret by Passive Control Techniques." *Structural Control and Health Monitoring*, 12(2), 157-177.

Fahnestock, L. A., Ricles, J., and Sause, R. (2007a). "Experimental Evaluation of a Large-Scale Buckling-Restrained Braced Frame." *Journal of Structural Engineering*, 133(9), 1205-1214.

Fahnestock, L. A., Ricles, J. M., and Sause, R. (2006). "Experimental Study of a Large-Scale Buckling Restrained Braced Frame Using the Pseudo-Dynamic Testing Method." 8th US National Conference on Earthquake Engineering, Earthquake Engineering Research Institute, San Francisco, CA.

Fahnestock, L. A., Sause, R., and Ricles, J. (2007b). "Seismic Response and Performance of Buckling-Restrained Braced Frames." *Journal of Structural Engineering*, 133(9), 1195-1204.

FEMA. (2000). "State of the Art Report on Systems Performance of Steel Moment Frames Subject to Earthquake Ground Shaking (Fema 355c)." Federal Emergency Management Agency, Washington, D.C.

FEMA. (2003). *Nehrp Recommended Provisions for Seismic Regulations for New Buildings and Other Structures (Fema 450)*, Federal Emergency Management Agency, Washington, D.C.

Filiatrault, A., Tremblay, R., and Kar, R. (2000). "Performance Evaluation of Friction Spring Seismic Damper." *Journal of Structural Engineering*, 126(4), 491-499.

Freakley, P. K., and Payne, A. R. (1978). *Theory and Practice of Engineering with Rubber*, Applied Science Publishers LTD, London.

Fu, Y., and Kasai, K. (1998). "Comparative Study of Frames Using Viscoelastic and Viscous Dampers." *Journal of Structural Engineering*, 124(5), 513-522.

Fujita, S., Fujita, T., Furuya, O., Morikawa, S., Suizu, Y., Teramoto, T., and Kitamura, H. (1992). "Development of High Damping Rubber Damper for Vibration Attenuation of High-Rise Buildings." 10th World Conference on Earthquake Engineering, A.A. Balkema, Madrid, Spain, 2097.

Fujita, S., Furuya, O., Fujita, T., Kasahara, Y., Suizu, Y., Morikawa, S., Teramoto, T., and Kitamura, H. (1995). "Research and Development of High-Damping Rubber Damper for Vibration Control of Tall Buildings." 1995 Joint ASME/JSME Pressure Vessels and Piping Conference, ASME, New York, NY, USA, Honolulu, HI, USA, 265-272.

Fukukita, A., Saito, T., and Shiba, K. (2002). "Seismic Control Effect for Nonlinear Benchmark Building Using Passive or Semi-Active Damper." 2002 ASME Pressure Vessels and Piping Conference, American Society of Mechanical Engineers, Vancouver, BC, Canada, 197-204.

Fuller, K. N., Ahmadi, H. R., and Pond, T. J. (1996a). "High Damping Natural Rubber Seismic Bearings: Longevity and Modelling." 1996 ASME Pressure Vessels and Piping Conference, ASME, Montreal, Canada, 71-79.

Fuller, K. N. G., Gough, J., and Pond, T. J. (1996b). "High Damping Natural Rubber Compounds for Seismic Isolators: Properties and Specifications." 1st European Conference on Structural Control, Barcelona, Spain, 288.

Furuya, O., Fujita, S., Fujita, T., Masaki, N., Kitamura, H., and Ozaki, H. (1999). "Vibration Control Performance of High-Damping Rubber Damper Evaluating from Seismic Observation in Actual Building." 1999 ASME Pressure Vessels and Piping Conference, American Society of Mechanical Engineers, Fairfield, NJ, USA, Boston, MA, USA, 305-310.

Gent, A. N. (2001). "Engineering with Rubber." Hanser Publishers, Munich.

Ghaemi, H., Behdinan, K., and Spence, A. (2006a). "On the Development of Compressible Pseudo-Strain Energy Density for Elastomers: Part 2: Application to Finite Element." *Journal of Materials Processing Technology*, 178(1-3), 317-327.

Ghaemi, H., Behdinan, K., and Spence, A. (2006b). "On the Development of Compressible Pseudo-Strain Energy Density Function for Elastomers. Part 1: Theory and Experiment." *Journal of Materials Processing Technology*, 178(1-3), 307-316.

Grant, D. N., Fenves, G. L., and Whittaker, A. S. (2004). "Bidirectional Modelling of High-Damping Rubber Bearings." *Journal of Earthquake Engineering*, 8(Special Issue 1), 161-185.

Grigorian, C. E., Yang, T. S., and Popov, E. P. (1993). "Slotted Bolted Connection Energy Dissipators." *Earthquake Spectra*, 9(3), 491-504.

Guerreiro, L., Craveiro, A., and Branco, M. (2006). "The Use of Passive Seismic Protection in Structural Rehabilitation." *Progress in Structural Engineering and Materials*, 8(4), 121-132.

Hanson, R. D., and Soong, T. T. (2001). *Seismic Design with Supplemental Energy Dissipation Devices*, Earthquake Engineering Research Institute, Oakland, CA.

Higgins, C. (2001). "Hysteretic Dampers for Wood Frame Shear Walls." 2001 Structures Congress and Exposition, P. C. Chang, ed., ASCE, Washington DC.

Higgins, C., and Kasai, K. (1998). "Experimental and Analytical Simulation of Wind Response for a Full-Scale Ve-Damped Steel Frame." *Journal of Wind Engineering and Industrial Aerodynamics*, 77-78, 297-313.

Higgins, C. C., and Newell, J. D. (2004). "Confined Steel Brace for Earthquake Resistant Design." *Engineering Journal*, 41(4), 187-202.

Housner, G. W., Bergman, L. A., Caughey, T. K., Chassiakos, A. G., Claus, R. O., Masri, S. F., Skelton, R. E., Soong, T. T., Spencer, B. F., and Yao, J. T. P. (1997). "Structural Control: Past, Present, and Future." *Journal of Engineering Mechanics*, 123(9), 897-971.

Hwang, J.-S., Huang, Y.-N., and Hung, Y.-H. (2005). "Analytical and Experimental Study of Toggle-Brace-Damper Systems." *Journal of Structural Engineering*, 131(7), 1035-1043.

Hwang, J.-S., Tsai, C.-H., Wang, S.-J., and Huang, Y.-N. (2006). "Experimental Study of Rc Building Structures with Supplemental Viscous Dampers and Lightly Reinforced Walls." *Engineering Structures*, 28(13), 1816-1824.

Hwang, J. S., and Ku, S. W. (1997). "Analytical Modeling of High Damping Rubber Bearings." *Journal of Structural Engineering*, 123(8), 1029-1036.

Ibrahim, Y. E. (2005). "A New Visco-Plastic Device for Seismic Protection of Structures," Ph.D. Dissertation, Virginia Polytechnic Institute and State University, Blacksburg, VA.

Ibrahim, Y. E., Marshall, J. D., and Charney, F. A. (2007). "A Visco-Plastic Device for Seismic Protection of Structures." *Journal of Constructional Steel Research*, 63(11), 1515-1528.

Inoue, K., Suita, K., Takeuchi, I., Chusilp, P., Nakashima, M., and Zhou, F. (2006). "Seismic-Resistant Weld-Free Steel Frame Buildings with Mechanical Joints and Hysteretic Dampers." *Journal of Structural Engineering*, 132(6), 864-872.

Iwata, M., and Murai, M. (2006). "Buckling-Restrained Brace Using Steel Mortar Planks; Performance Evaluation as a Hysteretic Damper." *Earthquake Engineering and Structural Dynamics*, 35(14), 1807-1826.

Jankowski, R. (2003). "Nonlinear Rate Dependent Model of High Damping Rubber Bearing." *Bulletin of Earthquake Engineering*, 1(3), 397-403.

Joye, D. D., and Dinehart, D. W. (2007). "Improved Viscoelastic Damping for Earthquake-Resistant Wood Structures." *International Journal of Polymeric Materials*, 56(1), 55-64.

Kani, N., Takayama, M., and Wada, A. (2006). "Performance of Seismically Isolated Buildings in Japan." 8th US National Conference on Earthquake Engineering, Earthquake Engineering Research Institute, San Francisco, CA.

Kareem, A., Kijewski, T., and Tamura, Y. (1999). "Mitigation of Motions of Tall Buildings with Specific Examples of Recent Applications." *Wind & Structures: An International Journal*, 2(3), 201-251.

Kasai, K., and Ooki, Y. (2006). "Current Status of Japanese Passive Control Technology Using Various Damping Materials." *Key Engineering Materials*, 319, 197-208.

Kato, S., Kim, Y.-B., Nakazawa, S., and Ohya, T. (2005). "Simulation of the Cyclic Behavior of J-Shaped Steel Hysteresis Devices and Study on the Efficiency for Reducing Earthquake Responses of Space Structures." *Journal of Constructional Steel Research*, 61(10), 1457-1473.

Kelly, J. M., Skinner, R. I., and Heine, A. J. (1972). "Mechanisms of Energy Absorption in Special Devices for Use in Earthquake Resistant Structures." *Bulletin of the New Zealand Society for Earthquake Engineering*, 5(3), 63-88.

Kiggins, S., and Uang, C.-M. (2006). "Reducing Residual Drift of Buckling-Restrained Braced Frames as a Dual System." *Engineering Structures*, 28(11), 1525-1532.

Kim, H.-J., and Christopoulos, C. (2008). "Friction Damped Posttensioned Self-Centering Steel Moment-Resisting Frames." *Journal of Structural Engineering*, 134(11), 1768-1779.

Kim, J., Ryu, J., and Chung, L. (2006). "Seismic Performance of Structures Connected by Viscoelastic Dampers." *Engineering Structures*, 28(2), 183-195.

Koetaka, Y., Chusilp, P., Zhang, Z., Ando, M., Suita, K., Inoue, K., and Uno, N. (2005). "Mechanical Property of Beam-to-Column Moment Connection with Hysteretic Dampers for Column Weak Axis." *Engineering Structures*, 27(1), 109-117.

Lai, M. L., Chang, K. C., Soong, T. T., Hao, D. S., and Yeh, Y. C. (1995). "Full-Scale Viscoelastically Damped Steel Frame." *Journal of Structural Engineering*, 121(10), 1443-1447.

Law, S. S., Wu, Z. M., and Chan, S. L. (2006). "Analytical Model of a Slotted Bolted Connection Element and Its Behaviour under Dynamic Load." *Journal of Sound and Vibration*, 292(3-5), 777-787.

Lee, D., and Taylor, D. P. (2001). "Viscous Damper Development and Future Trends." *Structural Design of Tall Buildings*, 10(5), 311-320.

Lee, K. S., Sause, R., Ricles, J., Ab-Malek, K., and Lu, L. W. (2004). "Non-Linear Rate-Dependent Hysteresis Model for Structural Dampers Made from Ultra-High Damping Natural Rubber." *Journal of Rubber Research*, 7(2), 79-103.

Lee, K. S., Sause, R., Ricles, J. M., and Lu, L. W. (2003). "Seismic Behavior of Steel Mrfs with Uhdnr Structural Dampers." Stessa 2003, Behavior of Steel Structures in Seismic Areas, F. M. Mazzolani, ed., Swets & Zeitlinger, Naples, Italy, 615-620.

Leon, R. T., DesRoches, R., Ocel, J., and Hess, G. (2001). "Innovative Beam Column Connections Using Shape Memory Alloys." Smart Systems for Bridges, Structures, and Highways-Smart Structures and Materials 2001, Society of Photo-Optical Instrumentation Engineers, Newport Beach, CA, 227-237.

Li, H.-N., and Li, G. (2006). "Seismic Analysis and Design of Rc Frame with New Metallic Dampers." 2006 ASME Pressure Vessels and Piping Conference, American Society of Mechanical Engineers, Vancouver, BC, Canada.

Liao, W.-I., Mualla, I., and Loh, C.-H. (2004). "Shaking-Table Test of a Friction-Damped Frame Structure." *Structural Design of Tall and Special Buildings*, 13(1), 45-54.

Lin, T. K., Chang, K. C., Chang, C. Y., and Chen, C. H. (2006). "Application of Viscoelastic Dampers in a Multi-Purpose Vibration Prevention System." 8th US National Conference on Earthquake Engineering, Earthquake Engineering Research Institute, San Francisco, CA.

Lu, X., and Zhao, B. (2004). "Recent Advances of Passive Structural Control and Its Applications in Mainland China." 13th World Conference on Earthquake Engineering, Vancouver, British Columbia, Canada.

Malek, K. A., and Basir, K. B. (2001). "Design and Characteristics of High Damping Natural Rubber Bearings for Base Isolation." Earthquake Resistant Engineering Structures III, Computational Mechanics Publications, Ashurst, United Kingdom, Malaga, Spain, 155-163.

Marckmann, G., and Verron, E. (2006). "Comparison of Hyperelastic Models for Rubber-Like Materials." *Rubber Chemistry and Technology*, 79(5), 835-58.

Martelli, A. (2006). "Modern Seismic Protection Systems for Civil and Industrial Structures." SAMCO.

Martinez-Romero, E. (1993). "Experiences on the Use of Supplementary Energy Dissipators on Building Structures." *Earthquake Spectra*, 9(3), 581-625.

Martinez-Rueda, J. E. (2002). "On the Evolution of Energy Dissipation Devices for Seismic Design." *Earthquake Spectra*, 18(2), 309-346.

Mazzolani, F. M. (2001). "Passive Control Technologies for Seismic-Resistant Buildings in Europe." *Progress in Structural Engineering and Materials*, 3(3), 277-287.

McCormick, J., DesRoches, R., Fugazza, D., and Auricchio, F. (2006). "Seismic Vibration Control Using Superelastic Shape Memory Alloys." *Journal of Engineering Materials and Technology*, 128(3), 294-301.

Min, K.-W., Kim, J., and Lee, S.-H. (2004). "Vibration Tests of 5-Storey Steel Frame with Viscoelastic Dampers." *Engineering Structures*, 26(6), 831-839.

Molina, F. J., Sorace, S., Terenzi, G., Magonette, G., and Viaccoz, B. (2004). "Seismic Tests on Reinforced Concrete and Steel Frames Retrofitted with Dissipative Braces." *Earthquake Engineering and Structural Dynamics*, 33(15), 1373-1394.

Monir, H. S. (2004). "The Enhancement of Earthquake Resistance of a Mrf by Using Tube Inversion Devices." Eighth International Conference on Structures Under Shock and Impact, SUSI VIII, WIT Press, Southampton, United Kingdom, Crete, Greece, 365-374.

Motamedi, M., and Nateghi-A., F. (2006). "Study of Seismic Energy Dissipation in Accordion Metallic Dampers." 8th US National Conference on Earthquake Engineering, Earthquake Engineering Research Institute, San Francisco, CA.

Mualla, I. H., and Belev, B. (2002). "Performance of Steel Frames with a New Friction Damper Device under Earthquake Excitation." *Engineering Structures*, 24(3), 365-371.

Muhr, A. H. (2005). "Modeling the Stress-Strain Behavior of Rubber." *Rubber Chemistry and Technology*, 78(3), 391-425.

Mullins, L. (1969). "Softening of Rubber by Deformation." *Rubber Chemistry and Technology*, 42, 339-362.

Munshi, J. A. (1997). "Effect of Viscoelastic Dampers on Hysteretic Response of Reinforced Concrete Elements." *Engineering Structures*, 19(11), 921-935.

Murthy, K. (2005). "Application of Visco-Hyperelastic Devices in Structural Response Control," M.S. Thesis, Virginia Polytechnic Institute and State University, Blacksburg, VA.

Naeim, F., and Kelly, J. (1999). *Design of Seismic Isolated Structures: From Theory to Practice*, John Wiley and Sons, Inc, New York, NY.

Nashif, A. D., Jones, D. G., and Henderson, J. P. (1985). *Vibration Damping*, John Wiley & Sons, Inc., New York, NY.

Ng, C.-L., and Xu, Y.-L. (2006). "Seismic Response Control of a Building Complex Utilizing Passive Friction Damper: Experimental Investigation." *Earthquake Engineering and Structural Dynamics*, 35(6), 657-677.

Nielsen, L. O., Mualla, I. H., and Iwai, Y. (2004). "Seismic Isolation with a New Friction-Viscoelastic Damping System." 13th World Conference on Earthquake Engineering, Vancouver, British Columbia, Canada.

Oliveto, G., Calio, I., and Marletta, M. (2004). "Retrofitting of Reinforced Concrete Buildings Not Designed to Withstand Seismic Action: A Case Study Using Base Isolation." 13th World Conference on Earthquake Engineering, Vancouver, Canada.

Pall, A. S., and Marsh, C. (1982). "Response of Friction Damped Braced Frames." *Journal of the Structural Division, ASCE*, 108(ST6), 1313-1323.

Patel, H. (2005). "Use of Permanent Magnets to Improve the Seismic Behavior of Light-Framed Structures," M.S. Thesis, Virginia Polytechnic Institute and State University, Blacksburg, VA.

Patten, W. N., Sun, J., Li, G., Kuehn, J., and Song, G. (1999). "Field Test of an Intelligent Stiffener for Bridges at the I-35 Walnut Creek Bridge." *Earthquake Engineering and Structural Dynamics*, 28(2), 109-126.

Pavlou, E., and Constantinou, M. C. (2006). "Response of Nonstructural Components in Structures with Damping Systems." *Journal of Structural Engineering*, 132(7), 1108-1117.

Perry, C. L., Fierro, E. A., Sedarat, H., and Scholl, R. E. (1993). "Seismic Upgrade in San Francisco Using Energy Dissipation Devices." *Earthquake Spectra*, 9(3), 559-579.

Phocas, M. C., and Pocanschi, A. (2003). "Steel Frames with Bracing Mechanism and Hysteretic Dampers." *Earthquake Engineering and Structural Dynamics*, 32(5), 811-825.

Pu, J.-P., Tsai, C. S., Huang, J.-F., Chen, B.-J., and Fang, Y.-M. (2004). "Analysis and Experiment on the Effect of Seismic Protection of Buildings by High Damping Rubber Bearings." 2004 ASME Pressure Vessels and Piping Conference, American Society of Mechanical Engineers, New York, NY San Diego, CA, 237-244.

Ribakov, Y., and Dancyoier, A. N. (2006). "High-Efficiency Amplifiers for Viscous Damped Structures Subjected to Strong Earthquakes." *Structural Design of Tall and Special Buildings*, 15(2), 221-232.

Roeder, C. W., Lehman, D. E., and Christopulos, A. (2006). "Seismic Performance of Special Concentrically Braced Frames with Buckling Restrained Braces." 8th US National Conference on Earthquake Engineering, Earthquake Engineering Research Institute, San Francisco, CA.

Rojas, P., Ricles, J. M., and Sause, R. (2005). "Seismic Performance of Post-Tensioned Steel Moment Resisting Frames with Friction Devices." *Journal of Structural Engineering*, 131(4), 529-540.

Rubber Engineering. (2000). McGraw-Hill, New York, NY.

Sabouri-Ghomi, S., and Roufegarinejad, A. (2005). "Non-Linear Behavior of Yielding Damped Braced Frames." *Structural Design of Tall and Special Buildings*, 14(1), 37-45.

Sakamoto, I., Ohashi, Y., and Fujii, Y. (1990). "Seismic Behavior of Base Isolated Two-Storied Wooden Building." 1990 International Timber Engineering Conference, Tokyo, Japan, 938-945.

Saunders, R. A. (2004). "Nonlinear Dynamic Analysis of Structures with Hyperelastic Devices," M.S. Thesis, Virginia Polytechnic Institute and State University, Blacksburg, VA.

Sause, R., Lee, K. S., Ricles, J., Ab-Malek, K., and Lu, L. W. (2001). "Non-Linear Hysteresis Models for Ultra-High Damping Nr Structural Dampers." *Journal of Rubber Research*, 4(4), 222-244.

Shen, K. L., Soong, T. T., Chang, K. C., and Lai, M. L. (1995). "Seismic Behaviour of Reinforced Concrete Frame with Added Viscoelastic Dampers." *Engineering Structures*, 17(5), 372-380.

Shih, M.-H., Sung, W.-P., and Go, C.-G. (2004). "Investigation of Newly Developed Added Damping and Stiffness Device with Low Yield Strength Steel." *Journal of Zhejiang University: Science*, 5(3), 326-334.

Sigaher, A. N., and Constantinou, M. C. (2003). "Scissor-Jack-Damper Energy Dissipation System." *Earthquake Spectra*, 19(1), 133-158.

Sinha, S. (2004). "Seismic Applications of Energy Dampers." *Defence Science Journal*, 54(1), 73-83.

Skinner, R. I., Kelly, J. M., and Heine, A. J. (1975). "Hysteretic Dampers for Earthquake Resistant Structures." *Earthquake Engineering and Structural Dynamics*, 3, 287-296.

Sorace, S., and Terenzi, G. (2008). "Seismic Protection of Frame Structures by Fluid Viscous Damped Braces." *Journal of Structural Engineering*, 134(1), 45-55.

Spencer, B. F., and Soong, T. T. (2002). "Supplemental Energy Dissipation: State-of-the-Art and State-of-the-Practice." *Engineering Structures*, 24(3), 243-259.

Spencer Jr., B. F., and Nagarajaiah, S. (2003). "State of the Art of Structural Control." *Journal of Structural Engineering*, 129(7), 845-856.

Suita, K., Inoue, K., Takeuchi, I., and Uno, N. (2004). "Mechanical Joint with Hysteretic Dampers as Bolted Beam-to-Column Moment Connection." 13th World Conference on Earthquake Engineering, Vancouver, B.C., Canada.

Symans, M. D., Charney, F. A., Whittaker, A. S., Constantinou, M. C., Kircher, C. A., Johnson, M. W., and McNamara, R. J. (2008). "Energy Dissipation Systems for Seismic Applications: Current Practice and Recent Developments." *Journal of Structural Engineering*, 134(1), 3-21.

Symans, M. D., Cofer, W. F., Du, Y., and Fridley, K. J. (2004). "Seismic Behavior of Wood-Framed Structures with Viscous Fluid Dampers." *Earthquake Spectra*, 20(2), 451-482.

Symans, M. D., Cofer, W. F., and Fridley, K. J. (2002). "Base Isolation and Supplemental Damping Systems for Seismic Protection of Wood Structures: Literature Review." *Earthquake Spectra*, 18(3), 549-572.

Symans, M. D., and Constantinou, M. C. (1999). "Semi-Active Control Systems for Seismic Protection of Structures: A State-of-the-Art Review." *Engineering Structures*, 21(6), 469-487.

Tan, X. M., Ko, J. M., Fang, E. H., and Qian, J. R. (1997). "Vibration Control with Viscoelastic Dampers in a High-Rise Building." International Modal Analysis Conference, SEM, Bethel, CT, Orlando, FL, 935-941.

Tarics, A. G., Way, D., and Kelly, J. M. (1984). "The Implementation of Base Isolation for the Foothill Communities Law and Justice Center." San Francisco, CA.

Tehranizadeh, M. (2001). "Passive Energy Dissipation Device for Typical Steel Frame Building in Iran." *Engineering Structures*, 23(6), 643-655.

Tena-Colunga, A., and Vergara, A. (1997). "Comparative Study on the Seismic Retrofit of a Mid-Rise Steel Building: Steel Bracing Vs Energy Dissipation." *Earthquake Engineering and Structural Dynamics*, 26(6), 637-655.

Tezcan, S. S., and Uluca, O. (2003). "Reduction of Earthquake Response of Plane Frame Buildings by Viscoelastic Dampers." *Engineering Structures*, 25(14), 1755-1761.

Towashiraporn, P., Park, J., Goodno, B. J., and Craig, J. I. (2002). "Passive Control Methods for Seismic Response Modification." *Progress in Structural Engineering and Materials*, 4(1), 74-86.

Treloar, L. R. G. (2005). *The Physics of Rubber Elasticity*, Oxford University Press, New York, NY.

Tremblay, R., Bolduc, P., Neville, R., and DeVall, R. (2006). "Seismic Testing and Performance of Buckling-Restrained Bracing Systems." *Canadian Journal of Civil Engineering*, 33(2), 183-198.

Tremblay, R., Lacerte, M., and Christopoulos, C. (2008). "Seismic Response of Multistory Buildings with Self-Centering Energy Dissipative Steel Braces." *Journal of Structural Engineering*, 134(1), 108-120.

Tsai, C. S., Chen, B.-J., Chiang, T.-C., Chen, W.-S., and Shih, H. (2004). "Component Test and Mathematical Modeling of Advanced Unbounded Brace." 2004 ASME Pressure Vessels and Piping Conference, American Society of Mechanical Engineers, New York, San Diego, CA, 231-234.

Tsai, C. S., Chen, K.-C., and Chen, C.-S. (1998). "Seismic Resistibility of High-Rise Buildings with Combined Velocity-Dependent and Velocity-Independent Devices." 1998 ASME Pressure Vessels and Piping Conference, ASME, Fairfield, NJ, San Diego, CA, 103-110.

Tsai, C. S., Chen, K.-C., and Chen, W.-S. (2005a). "Shaking Table Test of Structure with Reinforced Buckling Restrained Braces." 2005 ASME Pressure Vessels and Piping Conference, American Society of Mechanical Engineers, New York, NY Denver, CO, 307-312.

Tsai, C. S., Chen, W.-S., and Chen, B.-J. (2006). "Component Tests and Simulation of Advanced Buckling Restrained Braces." 2006 ASME Pressure Vessels and Piping Conference, American Society of Mechanical Engineers, New York, NY Vancouver, BC, Canada, 8.

Tsai, C. S., Chen, W.-S., Lee, G.-H., and Hsu, L.-T. (2005b). "Experimental Tests of Longitudinal Added Damping and Stiffness Device." 2005 ASME Pressure Vessels and Piping Conference, American Society of Mechanical Engineers, New York, NY Denver, CO, 101-107.

Tsai, C. S., Chiang, T.-C., Chen, B.-J., and Lin, S.-B. (2003a). "An Advanced Analytical Model for High Damping Rubber Bearings." *Earthquake Engineering and Structural Dynamics*, 32(9), 1373-1387.

Tsai, C. S., Chung, L. L., Chiang, T. C., Chen, B. J., and Chen, W. S. (2002). "Experimental Study for a New Energy Dissipation Device - Multiple-Direction Damper." 2003 ASME Pressure Vessels and Piping Conference, American Society of Mechanical Engineers, Vancouver, BC, Canada, 193-199.

Tsai, C. S., and Lee, H. H. (1993). "Applications of Viscoelastic Dampers to High-Rise Buildings." *Journal of Structural Engineering*, 119(4), 1222-1233.

Tsai, C. S., and Tsai, K. C. (1995). "Tpea Device as Seismic Damper for High-Rise Buildings." *Journal of Engineering Mechanics*, 121(10), 1075-1081.

Tsai, C. S., Wei, T. T., and Chen, W. S. (2003b). "Experimental Study for Highly Plastic Material Damper." 2003 ASME Pressure Vessels and Piping Conference, American Society of Mechanical Engineers, New York, NY Cleveland, OH, 97-102.

Tsai, K. C., Chen, H. W., Hong, C. P., and Su, Y. F. (1993). "Design of Steel Triangular Plate Energy Absorbers for Seismic-Resistant Construction." *Earthquake Spectra*, 9(3), 505-528.

Tsai, K. C., Chou, C. C., Lin, C. L., Chen, P. C., and Jhang, S. J. (2008). "Seismic Self-Centering Steel Beam-to-Column Moment Connections Using Bolted Friction Devices." *Earthquake Engineering and Structural Dynamics*, 37, 627-645.

Tyler, R. G. (1985). "Further Notes on a Steel Energy-Absorbing Element for Braced Networks." *Bulletin of the New Zealand Society for Earthquake Engineering*, 18(3), 270-279.

Uang, C.-M., and Bertero, V. V. (1990). "Evaluation of Seismic Energy in Structures." *Earthquake Engineering and Structural Dynamics*, 19(1), 77-90.

Vamvatsikos, D., and Cornell, C. A. (2002). "Incremental Dynamic Analysis." *Earthquake Engineering and Structural Dynamics*, 31(3), 491-514.

Vargas, R., and Bruneau, M. (2007). "Effect of Supplemental Viscous Damping on the Seismic Response of Structural Systems with Metallic Damping." *Journal of Structural Engineering*, 133(10), 1434-1444.

Vilcheck, M. G., and Pong, W. (2001). "Viscous and Metallic Dampers in a Building Structure Subjected to Varying Levels of Ground Motion." Smart Structures and Materials 2001-Damping and Isolation, Society of Photo-Optical Instrumentation Engineers, Newport Beach, CA, 175-185.

Walters, M. T., Honeck, B., and Elsesser, E. (1995). "Use of Seismic Isolation in New and Retrofit Construction." 1995 Joint ASME/JSME Pressure Vessels and Piping Conference, Seismic, Shock, and Vibration Isolation, Honolulu, HI.

Wang, W., and Chen, G. (2006). "Dynamic Behavior of a Damping-Enhanced Strengthening System for Seismic Retrofit of Rc Columns." 2006 Structures Congress and Exposition, American Society of Civil Engineers, Reston, VA St. Louis, MO, 84.

Whittaker, A. S., and Aiken, I. D. (1993). "Passive Energy Dissipation Systems for Earthquake-Resistant Design." Structural Engineering in Natural Hazards Mitigation, ASCE, New York, NY, Irvine, CA, 712-717.

Whittaker, A. S., Bertero, V. V., Thompson, C. L., and Alonso, L. J. (1991). "Seismic Testing of Steel Plate Energy Dissipation Devices." *Earthquake Spectra*, 7(4), 563-604.

Wilson, J. C., and Wesolowsky, M. J. (2005). "Shape Memory Alloys for Seismic Response Modification: A State-of-the-Art Review." *Earthquake Spectra*, 21(2), 569-601.

Wu, B., and Ou, J. (2003). "The Pseudo-Viscous Frictional Energy Dissipator: A New Device for Mitigating Seismic Effects." *Earthquake Engineering and Structural Dynamics*, 32(1), 31-48.

Xie, Q. (2005). "State of the Art of Buckling-Restrained Braces in Asia." *Journal of Constructional Steel Research*, 61(6), 727-748.

Xu, Y. L., and Zhang, W. S. (2001). "Modal Analysis and Seismic Response of Steel Frames with Connection Dampers." *Engineering Structures*, 23(4), 385-396.

Yang, L. M., Shim, V. P. W., and Lim, C. T. (2000). "Visco-Hyperelastic Approach to Modelling the Constitutive Behaviour of Rubber." *International Journal of Impact Engineering*, 24(6), 545-560.

Yeung, N., and Pan, A. D. E. (1998). "Effectiveness of Viscous-Damping Walls for Controlling Wind Vibrations in Multi-Story Buildings." *Journal of Wind Engineering and Industrial Aerodynamics*, 77-78, 337-348.

Yoshida, J., Abe, M., and Fujino, Y. (2004a). "Constitutive Model of High-Damping Rubber Materials." *Journal of Engineering Mechanics*, 130(2), 129-141.

Yoshida, J., Abe, M., Fujino, Y., and Watanabe, H. (2004b). "Three-Dimensional Finite-Element Analysis of High Damping Rubber Bearings." *Journal of Engineering Mechanics*, 130(5), 607-620.

Youssef, N., and Hata, O. (2005). "Seismic Retrofit and Instrumentation of Los Angeles City Hall." SMIP05 Seminar on Utilization of Strong-Motion Data, Los Angeles, CA, 115 - 130.

Zhang, X., and Erdman, A. G. (2001). "Dynamic Responses of Flexible Linkage Mechanisms with Viscoelastic Constrained Layer Damping Treatment." *Computers and Structures*, 79(13), 1265-1274.

Zhang, X. Z., Cheng, F. Y., and Jiang, H. P. (2006). "Hybrid Actuator-Damper-Bracing Control (Hdabc) System with Intelligent Strategy and Soil-Structure Interaction." *Engineering Structures*, 28(14), 2010-2022.

Zhu, S., and Zhang, Y. (2008). "Seismic Analysis of Concentrically Braced Frame Systems with Self-Centering Friction Damping Braces." *Journal of Structural Engineering*, 134(1), 121-131.

APPPENDIX A

Appendix A presents the test results for the static tests on the six rubber compounds. The first three plots for each compound represent the average of the traces used to determine the nonlinear stress-strain curve. The fourth plot shows the plot of all three stress-strain curves.

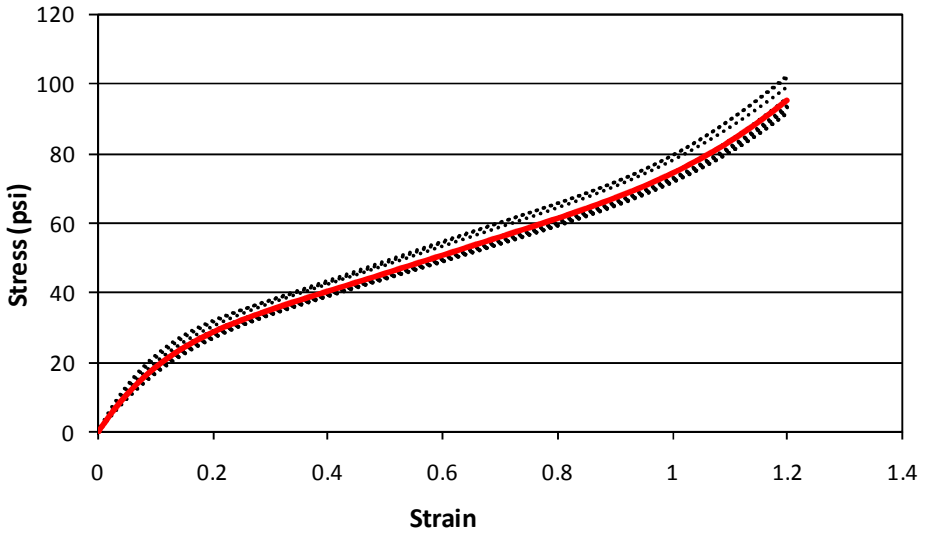

Figure A - 1 Uniaxial Tension - BR40H

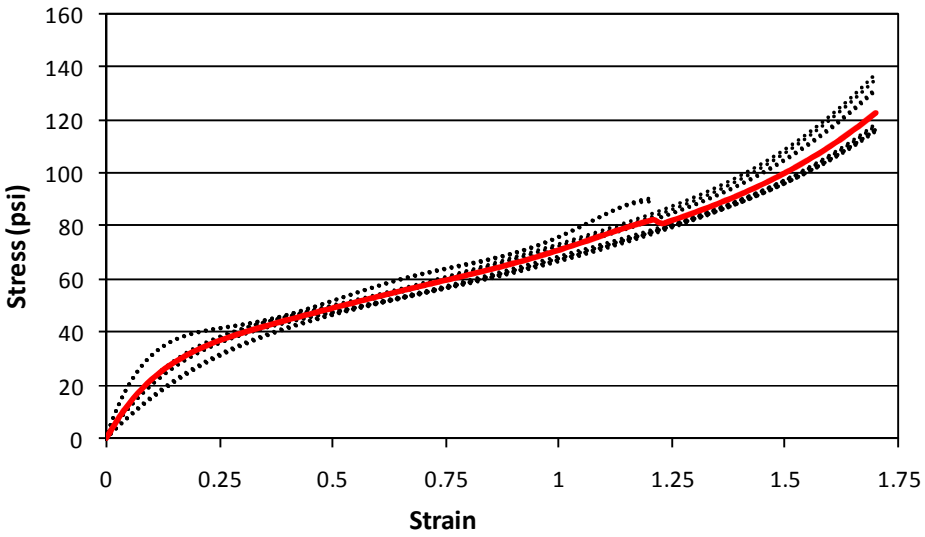

Figure A - 2 Planar Tension - BR40H

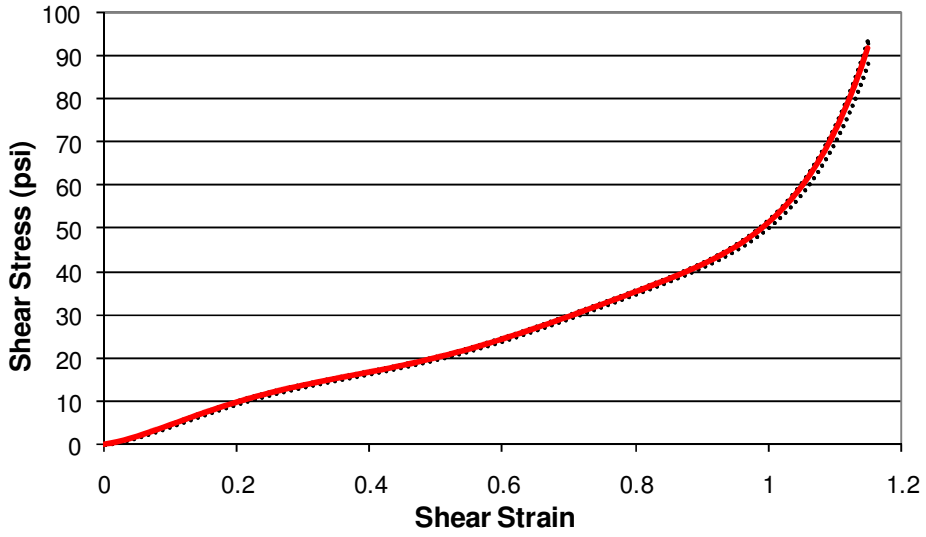

Figure A - 3 Simple Shear - BR40H

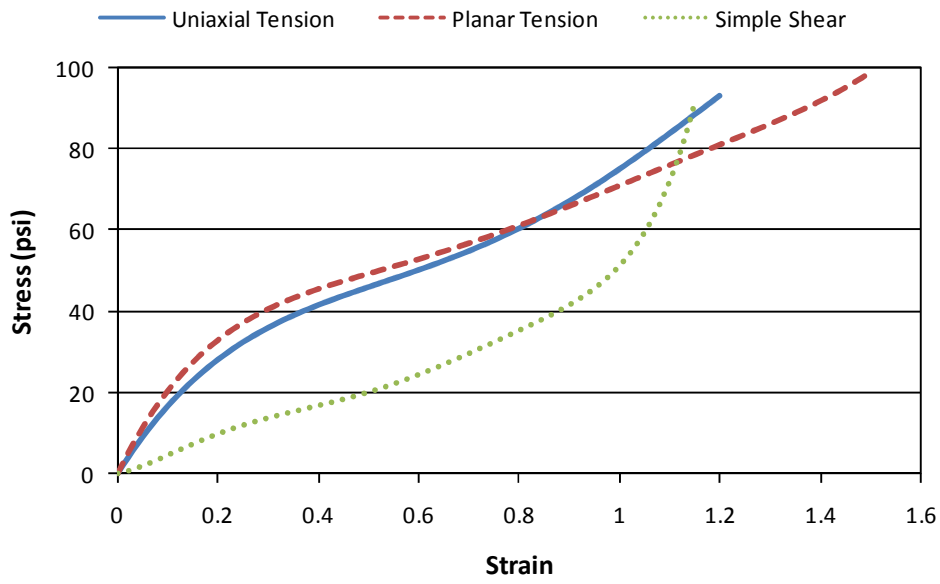

Figure A - 4 Stress-Strain Curves - BR40H

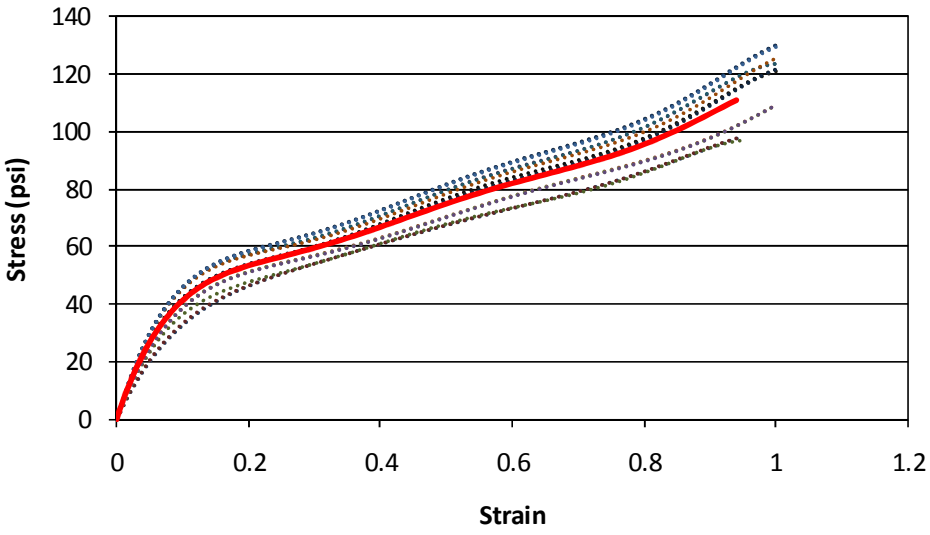

Figure A - 5 Uniaxial Tension - BR60H

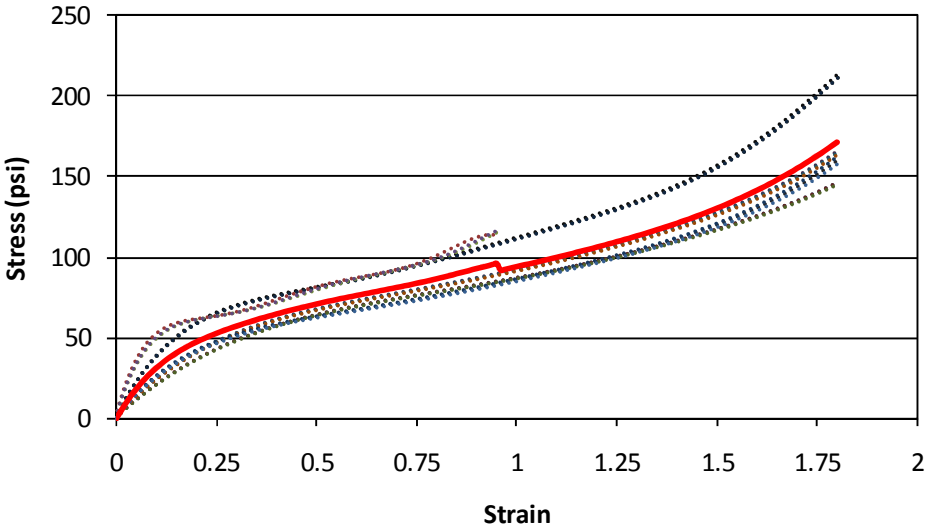

Figure A - 6 Planar Tension - BR60H

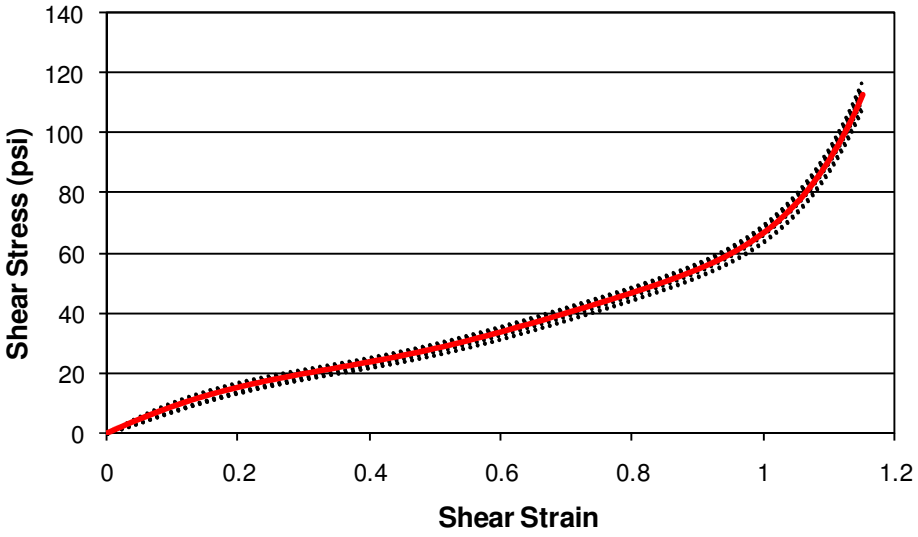

Figure A - 7 Simple Shear - BR60H

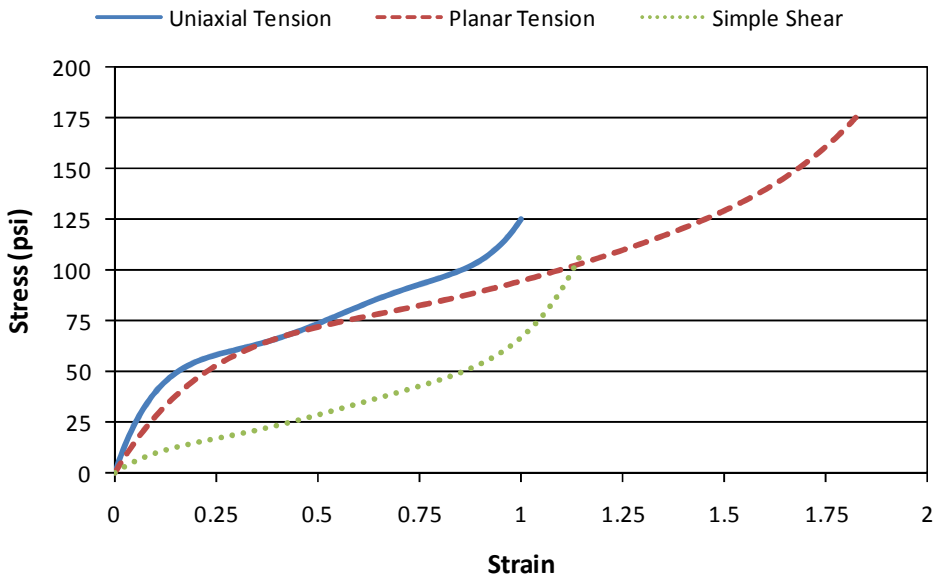

Figure A - 8 Stress-Strain Curves - BR60H

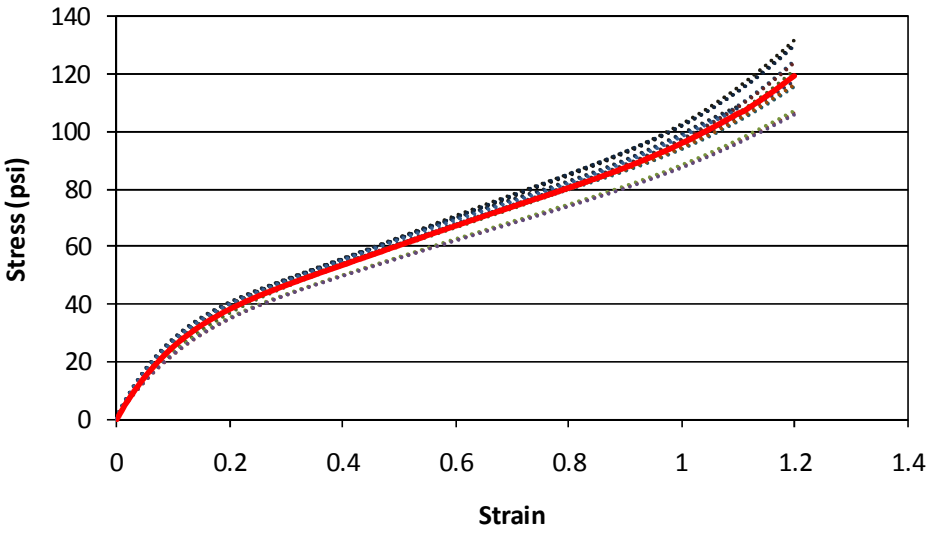

Figure A - 9 Uniaxial Tension - NR40H

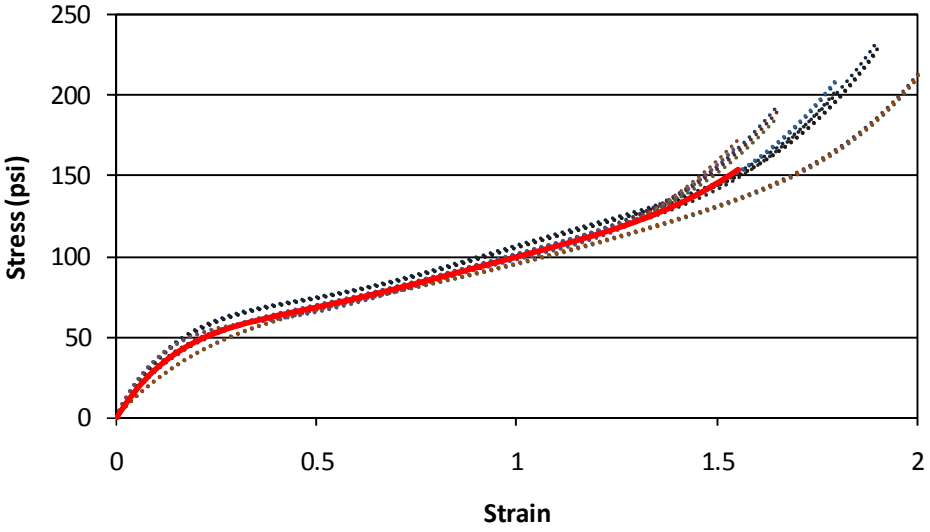

Figure A - 10 Planar Tension - NR40H

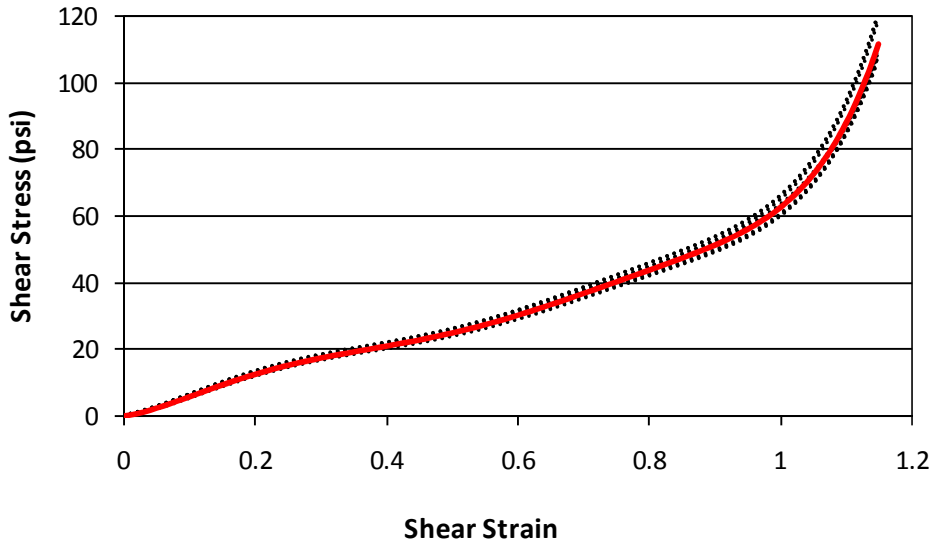

Figure A - 11 Simple Shear - NR40H

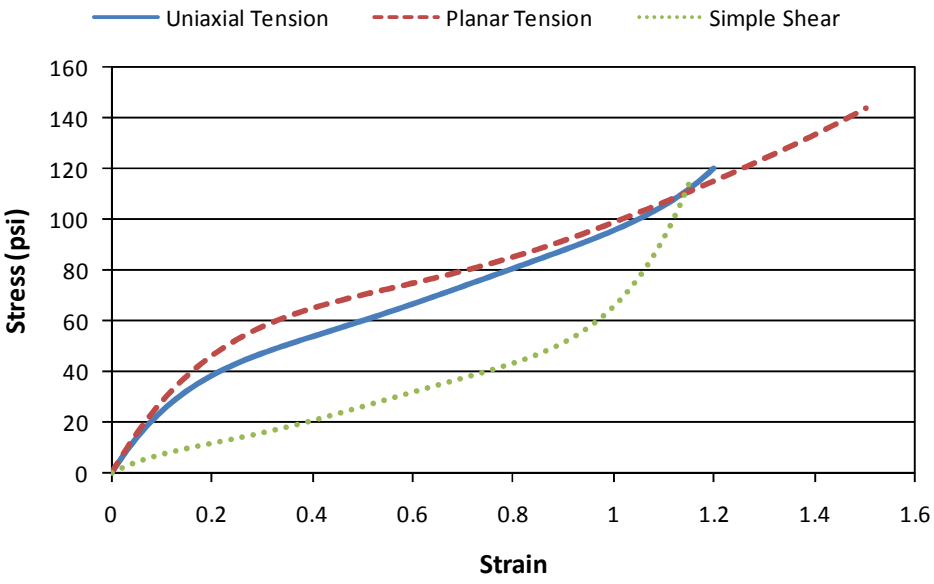

Figure A - 12 Stress-Strain Curves - NR40H

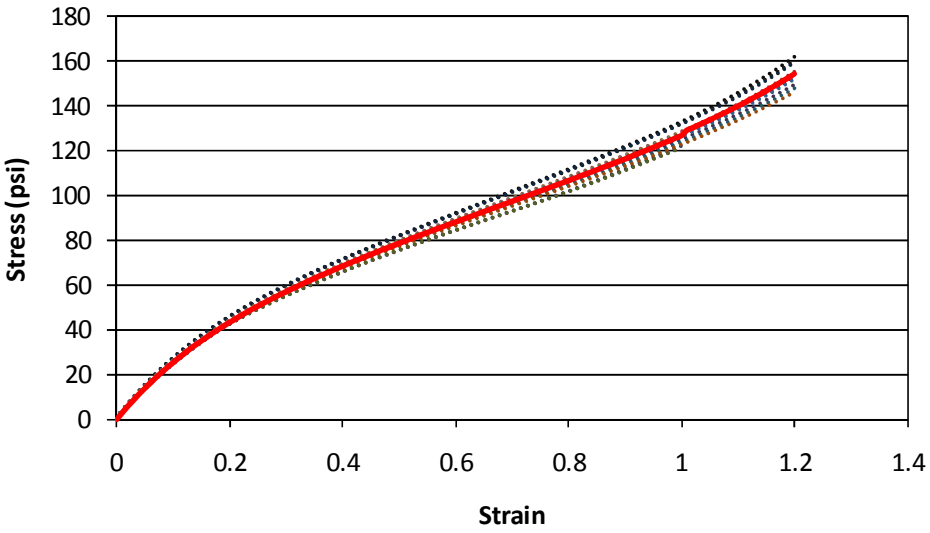

Figure A - 13 Uniaxial Tension - NR40L

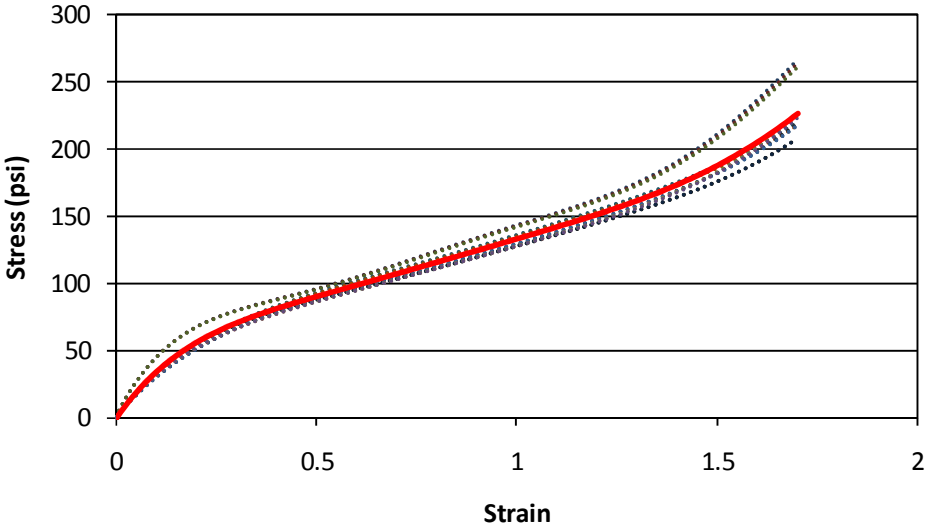

Figure A - 14 Planar Tension - NR40L

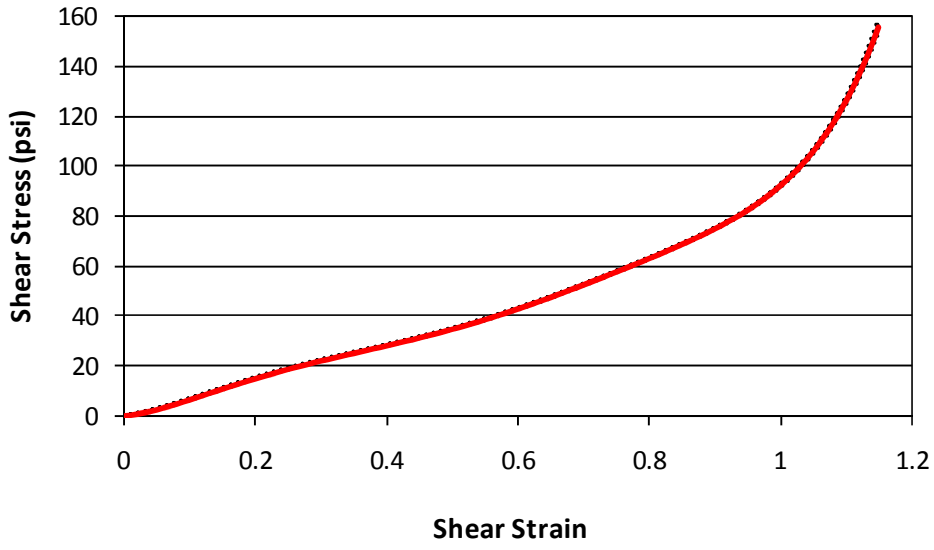

Figure A - 15 Simple Shear - NR40L

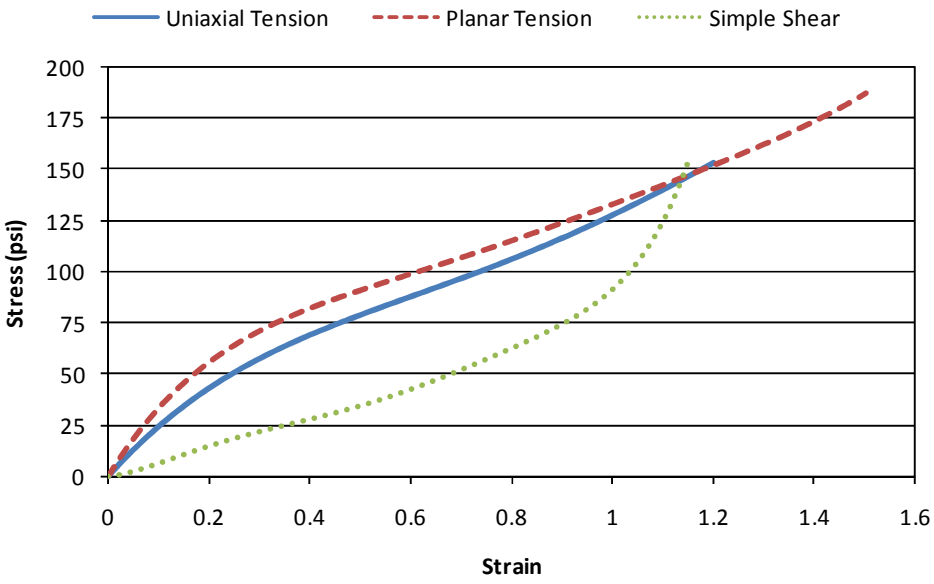

Figure A - 16 Stress-Strain Curves - NR40L

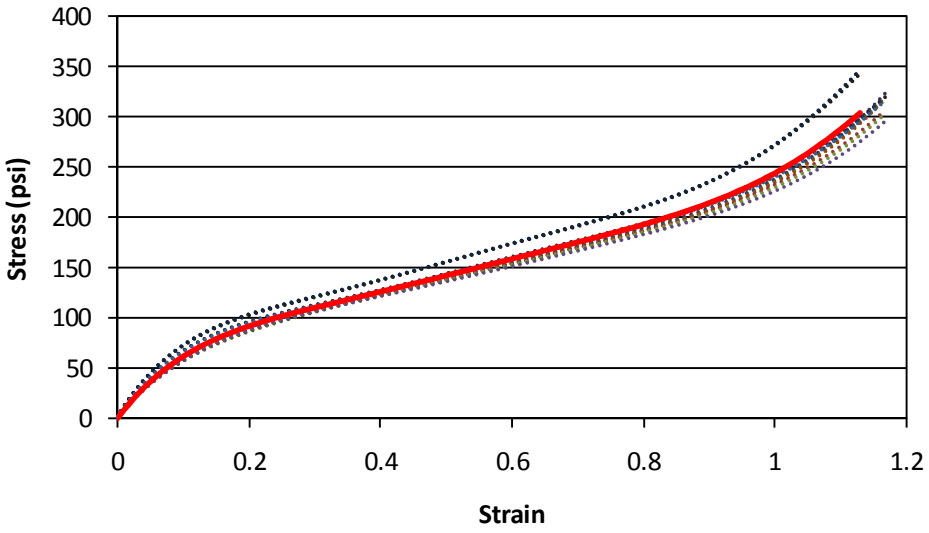

Figure A - 17 Uniaxial Tension - NR60H

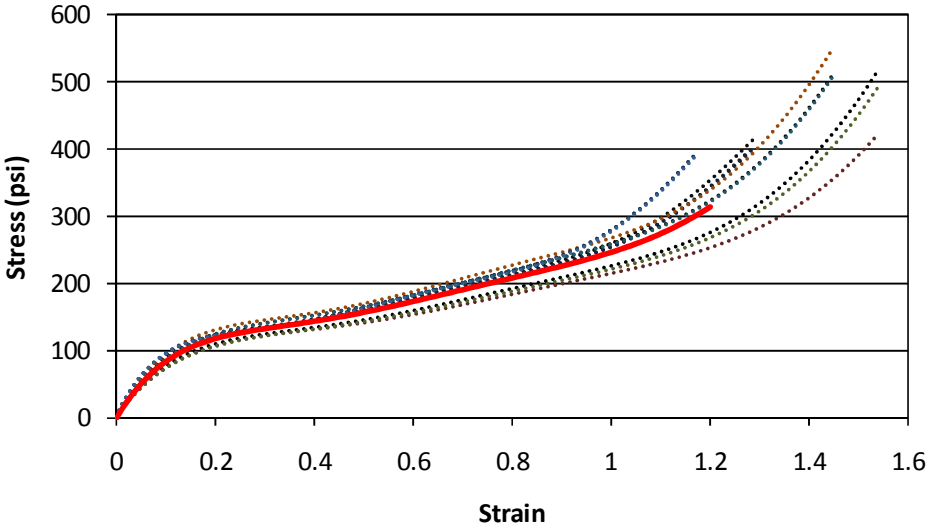

Figure A - 18 Planar Tension - NR60H

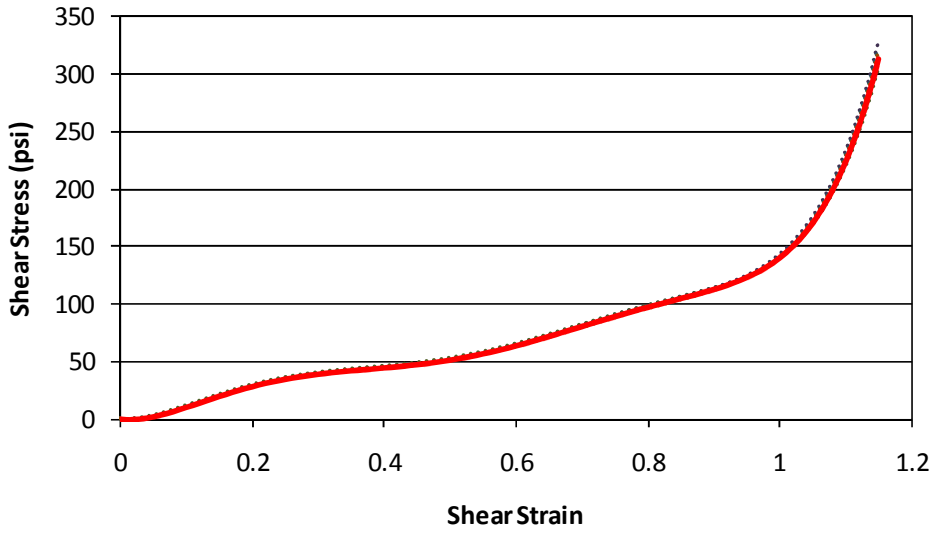

Figure A - 19 Simple Shear - NR60H

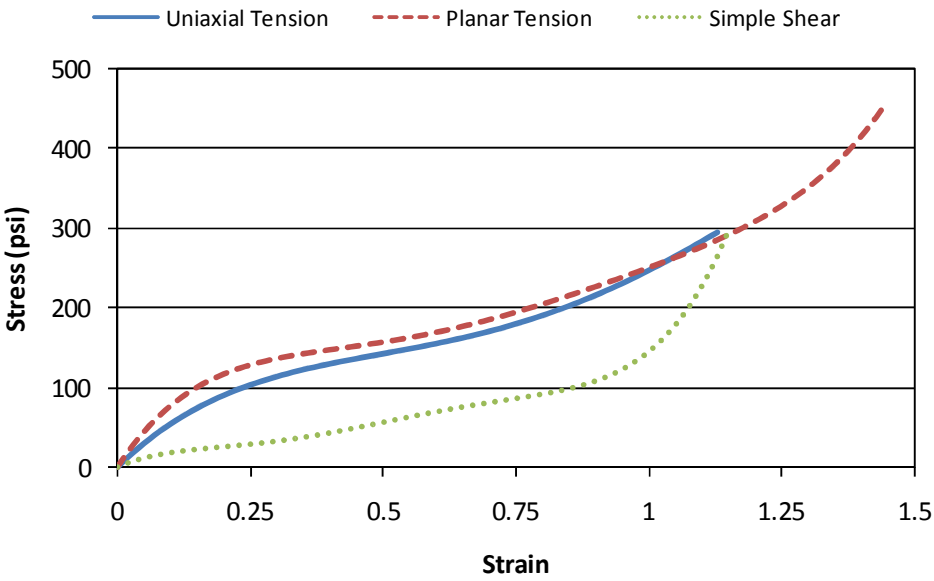

Figure A - 20 Stress-Strain Curves - NR60H

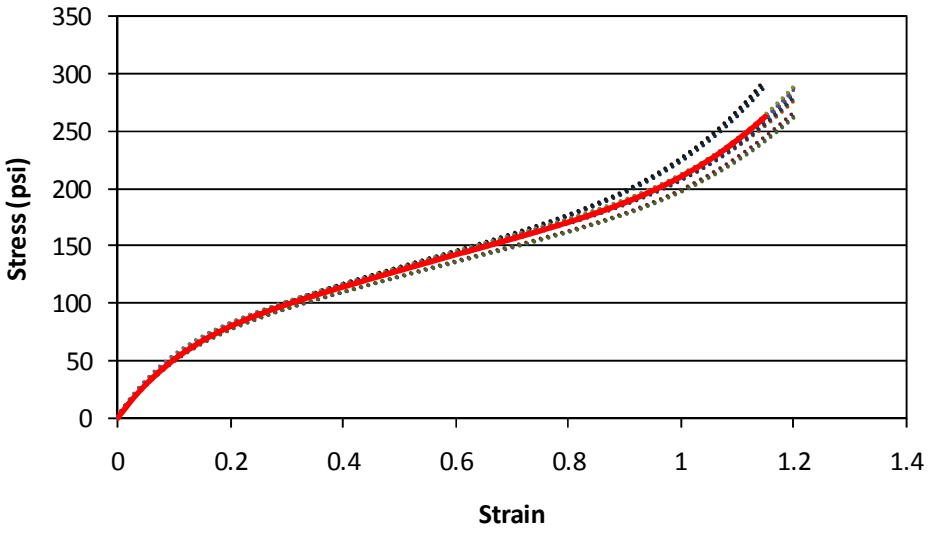

Figure A - 21 Uniaxial Tension - NR60L

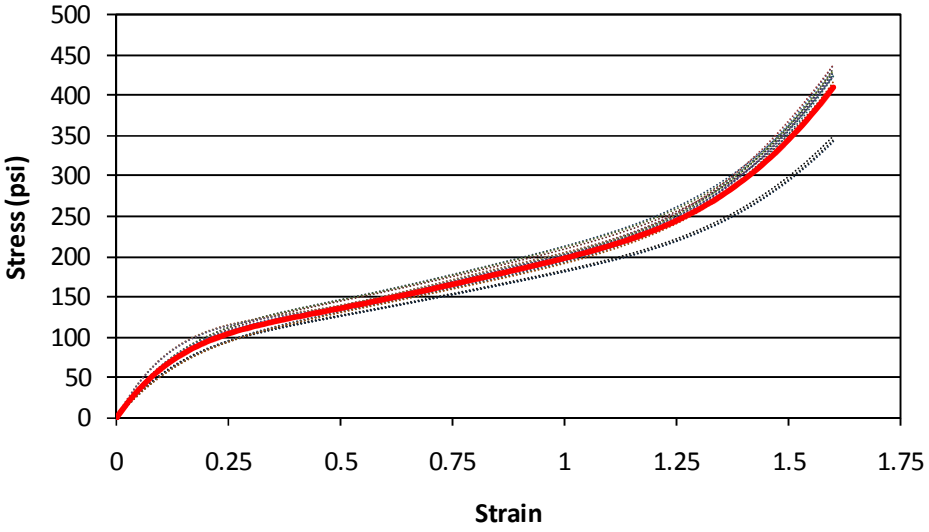

Figure A - 22 Planar Tension - NR60L

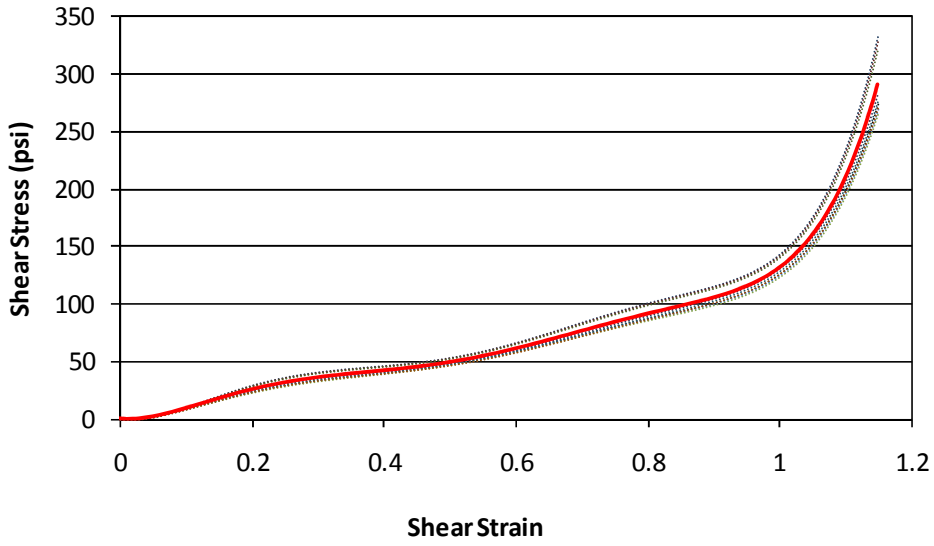

Figure A - 23 Simple Shear - NR60L

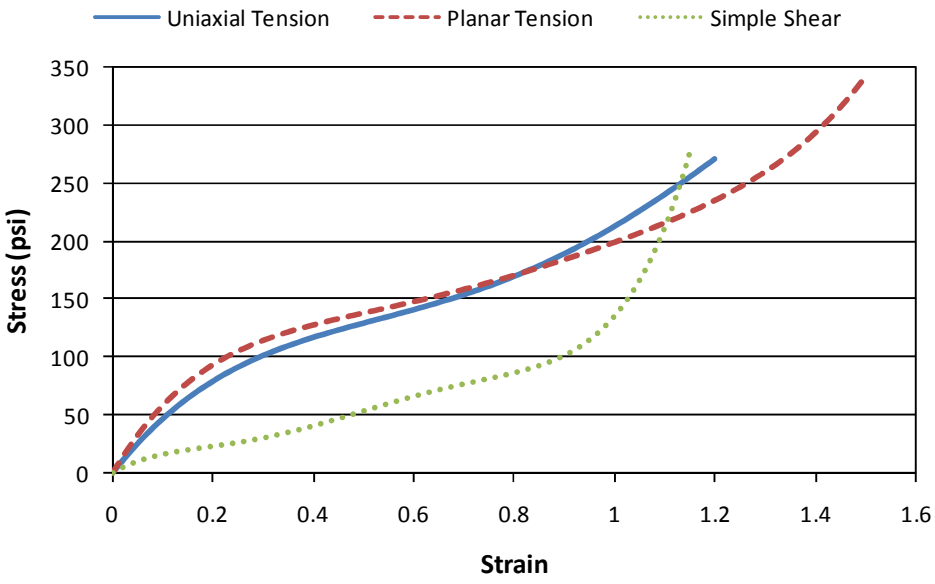

Figure A - 24 Stress-Strain Curves - NR60L

APPPENDIX B

Appendix B presents the design computations for the 1/2 scale prototype of the hybrid passive control device.

ORIGIN := 1

kip := 1000lbf

Initial Geometry and Material constants for HPCD Device:

$E := 29000 \frac{kip}{in^2}$

K := 1.0 L := 15ft (Overall Length including BRB and Sandwich Damper)

$F_y := 36 \frac{kip}{in^2}$ $F_u := 58 \frac{kip}{in^2}$ $F_{umax} := 80 \frac{kip}{in^2}$

BRB (Full Scale):

$t_{yc} := 1.5in$ $w_{yc} := 3.70in$ $A_{yc} := t_{yc} \cdot w_{yc}$ $A_{yc} = 5.55 \cdot in^2$

$P_y := F_y \cdot A_{yc}$ $P_y = 199.8 \cdot kip$ gap := 1.0in $\Delta := 3in$

$L_y := 8 \cdot 12in$ $K_B := \frac{A_{yc} \cdot E}{L_y} = 1.677 \times 10^3 \cdot \frac{kip}{in}$

$\varepsilon_y := \frac{F_y}{E} = 1.241 \times 10^{-3}$ $\delta_y := \varepsilon_y \cdot L_y = 0.119 \cdot in$ $\mu := \frac{\Delta - gap}{\delta_y} = 16.782$

HDRD (Full Scale):

T := 2.5s $\omega := \frac{2 \cdot \pi}{T} = 2.513 \cdot \frac{1}{s}$ $G_{dp} := 31 \frac{lbf}{in^2}$ $G_p := 87 \frac{lbf}{in^2}$

$t_r := 0.75in$ $l_r := 48in$ $w_r := 15in$

$A_r := 2 \cdot l_r \cdot w_r$

$C := \frac{G_{dp} \cdot A_r}{t_r \cdot \omega} = 23.682 \cdot \frac{kip \cdot s}{in}$ $K_D := \frac{G_p \cdot A_r}{t_r} = 167.04 \cdot \frac{kip}{in}$

$F_G := K_D \cdot gap = 167.04 \cdot kip$

BRB (Scaled):

$SF := 2$

$t_{ycs} := \frac{t_{yc}}{SF} = 0.75 \cdot in$ $w_{ycs} := \frac{w_{yc}}{SF} = 1.85 \cdot in$ $A_{ycs} := t_{ycs} \cdot w_{ycs}$ $A_{ycs} = 1.387 \cdot in^2$

$P_{ys} := F_y \cdot A_{ycs}$ $P_{ys} = 49.95 \cdot kip$ $gap_s := \frac{gap}{SF} = 0.5 \cdot in$ $\Delta_s := \frac{\Delta}{SF}$

$L_{ys} := \frac{L_y}{SF} = 48 \cdot in$ $K_{Bs} := \frac{A_{ycs} \cdot E}{L_{ys}} = 838.281 \cdot \frac{kip}{in}$

$\varepsilon_y := \frac{F_y}{E} = 1.241 \times 10^{-3}$ $\delta_{ys} := \varepsilon_y \cdot L_{ys} = 0.06 \cdot in$ $\mu_s := \frac{\Delta_s - gap_s}{\delta_{ys}} = 16.782$

HDRD (Scaled): $SF = 2$

$t_{rs} := \frac{t_r}{SF} = 0.375 \cdot in$ $l_{rs} := \frac{l_r}{SF} = 24 \cdot in$ $w_{rs} := \frac{w_r}{SF} = 7.5 \cdot in$

$A_{rs} := 2 \cdot l_{rs} \cdot w_{rs}$

$C_s := \frac{G_{dp} \cdot A_{rs}}{t_{rs} \cdot \omega} = 11.841 \cdot \frac{kip \cdot s}{in}$ $K_D := \frac{G_p \cdot A_{rs}}{t_{rs}} = 83.52 \cdot \frac{kip}{in}$

$F_G := K_D \cdot gap_s = 41.76 \cdot kip$

Design Calculations for Hybrid Passive Control Device (1/2 Scale)

References:

AISC Steel Construction Manual (13th Ed.) - AISCM
AISC Seismic Design Manual (2nd Printing - AISCSDM
AISC Specification for Structural Steel Buildings (2005) - AISCS

Initial Geometry and Material constants for HPCD Device:

$K := 1.0$ $L := 9.0ft$ (Overall Length including BRB and Sandwich Damper)

$F_y := 36\frac{kip}{in^2}$ $F_u := 58\frac{kip}{in^2}$ $F_{umax} := 75\frac{kip}{in^2}$

Design Values for Yielding Steel Core:

$t_{yc} := 0.75in$ $w_{yc} := 1.875in$ $A_{yc} := t_{yc} \cdot w_{yc}$ $A_{yc} = 1.406 \cdot in^2$

$P_n := F_y \cdot A_{yc}$ $P_n = 50.625 \cdot kip$ $P_{nmax} := F_{umax} \cdot A_{yc}$ $P_{nmax} = 105.469 \cdot kip$

$P_u := 1.25 \cdot P_{nmax}$ $P_u = 131.836 \cdot kip$

The design load is calculated based on the ultimate strength of the yielding core section multiplied by a load factor to have additional capacity in the other elements. This value also corresponds to the maximum load the hydraulic actuator can generate in tension. This value will be used to calculate the capacity of all the other elements. It should be also noted that the yielding will likely not reach the full strain hardened capacity so the amount of safety provided by the load factor 1.25 will be greater.

Design Buckling Restraining Member: (AISCS Section E6)
(Design the built-up section so it will not buckle for the design load of the yielding steel core.)

Try (2)-C8 x 13.7 with (2) - 2.5" x 0.75" steel blocks bolted at 6" o.c.

C8 x 13.7: $A_{gc} := 4.04in^2$ $I_{yyc} := 1.52in^4$ $x_{bar} := 0.554in$ $t_{wc} := 0.303$

$d_c := 8$ $I_{xxc} := 36.1in^4$ $b_{fc} := 2.34$ $t_{fc} := 0.39$

Check Seismic Local Buckling of Channel Section:

$0.30 \cdot \sqrt{\frac{E}{F_y}} = 8.515$ $\frac{b_{fc}}{t_{fc}} = 6$

$1.49 \sqrt{\frac{E}{F_y}} = 42.29$ $\frac{d_c}{t_{wc}} = 26.403$ (Seismically Compact Section)

Steel Block: $t_b := 0.75in$ $h_b := 2.5in$ $A_{gb} := t_b \cdot h_b = 1.875 \cdot in^2$

$$I_{xxb} := \frac{t_b \cdot h_b^3}{12} = 0.977 \cdot in^4 \qquad I_{yyb} := \frac{t_b^3 \cdot h_b}{12} = 0.088 \cdot in^4$$

$$\frac{h_b}{t_b} = 3.333$$ (Compact by inspection)

Overall Properties:

$$A_{gr} := 2 \cdot \left(A_{gc} + A_{gb}\right) = 11.83 \cdot in^2$$

$$I_{yyr} := 2 \cdot \left[I_{yyb} + I_{yyc} + A_{gc} \cdot \left(\frac{t_b}{2} + x_{bar}\right)^2\right] = 10.189 \cdot in^4 \qquad r_{yr} := \sqrt{\frac{I_{yyr}}{A_{gr}}} = 0.928 \cdot in$$

$$I_{xxr} := 2 \cdot \left[I_{xxb} + I_{xxc} + A_{gb} \cdot \left(\frac{w_{yc}}{2} + \frac{h_b}{2}\right)^2\right] = 92.097 \cdot in^4 \qquad r_{xr} := \sqrt{\frac{I_{xxr}}{A_{gr}}} = 2.79 \cdot in$$

Y axis is critical for buckling design.

Calculate Overall Slenderness for Restraining Member: (AISCS E6)

$$\frac{K \cdot L}{r_{yr}} = 116.372$$

$a := 6in$ $r_c := \sqrt{\frac{I_{yyc}}{A_{gc}}} = 0.613 \cdot in$ (Channel)

$$\frac{K \cdot a}{r_b} = 27.713$$

$r_b := \sqrt{\frac{I_{yyb}}{A_{gb}}} = 0.217 \cdot in$ (Stl Block)

Individual KL/r is less than 75% of overall KL/r therefore spacing of bolts is OK. Note spacing is controlled by the maximum spacing requirement of 24*twc in AISCS J3.5)

$$\sqrt{\left(\frac{K \cdot L}{r_{yr}}\right)^2 + \left(\frac{a}{r_b}\right)^2} = 119.626$$

$\phi F_{cr} := 15.2 \frac{kip}{in^2}$ (Table 4-22 AISCM)

$\phi P_{nr} := A_{gr} \cdot \phi F_{cr} = 179.816 \cdot kip$ (> Pu)

Connection Design at End of Brace:

$t_p := 0.625in$ $w_p := 6.0in$ $d_h := \left(0.75 + \frac{1}{8}\right)in$

$t_s := 0.5in$ $w_s := 1.5in$

(Assume A325N 3/4 in bolts)

Plate Yield and Rupture:

$A_{gp} := 2 \cdot t_s \cdot w_s + t_p \cdot w_p = 5.25 \cdot in^2$

$\phi R_{n_1} := 0.9 \cdot F_y \cdot A_{gp} = 170.1 \cdot kip$

$A_n := A_{gp} - 2 \cdot d_h \cdot t_p = 4.156 \cdot in^2$

$\phi R_{n_2} := 0.75 \cdot F_u \cdot A_n \cdot U = 154.159 \cdot kip$

Assume L3x3 Angle for connection:

$l := 6in$

$x_{bar} := 0.884in$

$U := 1 - \frac{x_{bar}}{l} = 0.853$

Connection Member: (Assume (4)-L3x3x3/8)

Block shear will not be a limit state due to the stiffeners.

$A_{ga} := 2.11in^2$ $t_a := 0.375in$

Member Yield and Rupture: (AISCS J4.1)

$\phi R_{n_3} := 0.9 \cdot F_y \cdot 4A_{ga} = 273.456 \cdot kip$

$A_{na} := A_{ga} - t_a \cdot d_h = 1.782 \cdot in^2$

$U = 0.853$

$\phi R_{n_4} := 0.75 \cdot F_u \cdot 4 \cdot A_{na} \cdot U = 264.366 \cdot kip$

Member Block Shear: (AISCS J4.3)

$ed_1 := 1.25in$ $ed_2 := 1.0in$ $s := 3in$

$A_{nv} := t_a \cdot \left(ed_1 + 2 \cdot s - 2.5 \cdot d_h\right) = 1.898 \cdot in^2$

$A_{gv} := t_a \cdot \left(ed_1 + 2 \cdot s\right) = 2.719 \cdot in^2$

$A_{nt} := t_a \cdot \left(ed_2 - 0.5d_h\right) = 0.211 \cdot in^2$

$\phi R_{n1} := 4 \times 0.75 \cdot \left(0.6 \cdot F_u \cdot A_{nv} + F_u \cdot A_{nt}\right) = 234.9 \cdot kip$

$\phi R_{n2} := 4 \times 0.75 \cdot \left(0.6 \cdot F_y \cdot A_{gv} + F_u \cdot A_{nt}\right) = 212.878 \cdot kip$

$\phi R_{n_5} := \min\left(\phi R_{n1}, \phi R_{n2}\right) = 212.878 \cdot kip$

Bolt Design:

Bolt shear (double shear): (AISCM Table 7-1)

$n_b := 6$

$\phi r_n := 31.8\text{kip}$ $\phi R_{n_6} := \phi r_n \cdot n_b = 190.8 \cdot \text{kip}$

Bolt bearing (bolt spacing): (AISCM Table 7-5) $s = 3 \cdot \text{in}$

$\phi r_n := 78.3 \frac{\text{kip}}{\text{in}}$ $\phi R_{n_7} := \phi r_n \cdot t_p \cdot n_b = 293.625 \cdot \text{kip}$

Bolt bearing (edge distance): (AISCM Table 7-6) $ed_1 = 1.25 \cdot \text{in}$

$\phi r_n := 49.4 \frac{\text{kip}}{\text{in}}$ $\phi R_{n_8} := \phi r_n \cdot t_p \cdot n_b = 185.25 \cdot \text{kip}$

Bolt Slip: (Slip as a Serviceability Limit State) (AISCM Table 7-3)

$\phi r_n := 22.1\text{kip}$ $\phi R_{n_9} := \phi r_n \cdot n_b = 132.6 \cdot \text{kip}$

Assume Class A Surface

Connection Capacity: (Controlled by bolt slip)

$\phi R_n := \min\left(\phi R_n\right) = 132.6 \cdot \text{kip}$

Design of HDR Damper:

Outer members: C8x13.7, Center Plate: 5/8" plate, Rubber: 0.375" thick rubber pads

C8 x 13.7: $A_{gc} := 4.04in^2$ $I_{yyc} := 1.52in^4$ $x_{bar} := 0.554in$ $t_{wc} := 0.303in$

$d_c := 8in$ $I_{xxc} := 36.1in^4$ $b_{fc} := 2.89in$ $t_{fc} := 0.390in$

Check Seismic Local Buckling of Channel Section:

$0.30 \cdot \sqrt{\frac{E}{F_y}} = 8.515$ $\frac{b_{fc}}{t_{fc}} = 7.41$

$1.49 \sqrt{\frac{E}{F_y}} = 42.29$ $\frac{d_c}{t_{wc}} = 26.403$ (Seismically Compact Section)

Try (4) - 1.25" diameter A325N bolts for locking mechanism of sandwich damper:

Bolt shear: (Double Shear) (AISCM Table 7-1) $n_b := 4$

$\phi r_n := 88.4kip$ $\phi R_{n_1} := n_b \cdot \phi r_n = 353.6 \cdot kip$

Bolt Bearing: (Edge Distance = 1.25" at edge of slotted hole) (AISCS J3.10)

$L_{c1} := (1.5 - 0.125)in$ $t_p = 0.625 \cdot in$ $t_{wc} = 0.303 \cdot in$ $d_b := 1.25in$

$\phi R_{n_2} := 1.2 \cdot L_{c1} \cdot t_p \cdot F_u \cdot n_b = 239.25 \cdot kip$ (Center Plate)

$\phi R_{n_3} := 2.4 \cdot d_b \cdot t_p \cdot F_u \cdot n_b = 435 \cdot kip$

$\phi R_{n_4} := 1.2 \cdot L_{c1} \cdot t_{wc} \cdot F_u \cdot 2 \cdot n_b = 231.977 \cdot kip$ (Outer Channel)

$\phi R_{n_5} := 2.4 \cdot d_b \cdot t_{wc} \cdot F_u \cdot 2 \cdot n_b = 421.776 \cdot kip$

Edge Distance = 1.25" so the spacing controls.

$\phi R_n := \min(\phi R_n) = 231.977 \cdot kip$ Capacity > Demand, therefore OK

Due to the size of the channel and the central plate, the bolts will be the critical link in the damper lock out mechanism. However the bolt must also be designed for the moment due to the spacing between the outer channel and the central plate.

$F_{yb} := 120 \frac{kip}{in^2}$ $d_{br} := 1.10in$ $A_{br} := \frac{\pi \cdot d_{br}^2}{4} = 0.95 \cdot in^2$ $t_r := 0.375in$

$I_{br} := \frac{\pi \cdot d_{br}^4}{64} = 0.072 \cdot in^4$ $S_{br} := \frac{I_{br}}{\frac{d_{br}}{2}} = 0.131 \cdot in^3$ $n_b = 4$

$\phi M_{nb} := 0.9 \cdot F_{yb} \cdot S_{br} \cdot n_b = 56.45 \cdot kip \cdot in$ $L_d := t_p + 2t_r + t_{wc} = 1.678 \cdot in$

$M_u := \frac{P_u \cdot L_d}{6} = 36.87 \cdot kip \cdot in$ (Assumes some fixity at outer channels)

Capacity > Demand, therefore 1.25" diameter bolts will work for lockout of damper.

Connection of C8x13.7: (Use 3/4" diameter A325N bolts)

$A_{gc} = 4.04 \cdot in^2$ $t_{wc} = 0.303 \cdot in$ $d_h = 0.875 \cdot in$ $x_{bar} = 0.554 \cdot in$ $l_c := 3in$

Member Yield and Rupture:

$\phi R_{n_1} := 0.9 \cdot 2A_{gc} \cdot F_y = 261.792 \cdot kip$

$A_{nc} := A_{gc} - 2 \cdot d_h \cdot t_{wc} = 3.51 \cdot in^2$ $U := 1 - \frac{x_{bar}}{l_c} = 0.815$

$\phi R_{n_2} := 0.75 \cdot 2A_{nc} \cdot U \cdot F_u = 248.961 \cdot kip$

Member Block Shear: (AISCS J4.3)

$ed_1 := 1.5in$ $g := 3.0in$ $s := 3in$

$A_{nv} := 2t_{wc} \cdot \left(ed_1 + 2s - 2.5 \cdot d_h\right) = 3.219 \cdot in^2$ $A_{gv} := 2t_{wc} \cdot \left(ed_1 + 2s\right) = 4.545 \cdot in^2$

$A_{nt} := t_{wc} \cdot \left(g - d_h\right) = 0.644 \cdot in^2$

$\phi R_{n1} := 2 \times 0.75 \cdot \left(0.6 \cdot F_u \cdot A_{nv} + F_u \cdot A_{nt}\right) = 224.068 \cdot kip$

$\phi R_{n2} := 2 \times 0.75 \cdot \left(0.6 \cdot F_y \cdot A_{gv} + F_u \cdot A_{nt}\right) = 203.275 \cdot kip$

$\phi R_{n_3} := \min\left(\phi R_{n1}, \phi R_{n2}\right) = 203.275 \cdot kip$

Bolt shear (single shear): (AISCM Table 7-1) $n_b := 12$

$\phi r_n := 15.9kip$ $\phi R_{n_4} := \phi r_n \cdot n_b = 190.8 \cdot kip$

Bolt bearing (bolt spacing): (AISCM Table 7-5) $s = 3 \cdot in$

$\phi r_n := 78.3 \frac{kip}{in}$ $\phi R_{n_5} := \phi r_n \cdot t_{wc} \cdot n_b = 284.699 \cdot kip$

Bolt bearing (edge distance): (AISCM Table 7-6) $ed_1 = 1.5 \cdot in$

$\phi r_n := 49.4 \frac{kip}{in}$ $\phi R_{n_6} := \phi r_n \cdot t_{wc} \cdot n_b = 179.618 \cdot kip$

Connection Capacity: (Controlled by edge distance)

$\phi R_n := \min\left(\phi R_n\right) = 179.618 \cdot kip$ Capacity > Demand, OK

Check compressive capacity of connection between BRB and HDR damper:

6" wide x 5/8" plate with (2)-1/2" x 1.5" stiffeners with (4)-L3x3x3/8

$w_p := 6in \quad t_p = 0.625 \cdot in \quad w_s := 0.5in \quad h_s := 1.5in \quad A_{gp} := w_p \cdot t_p + 2 \cdot w_s \cdot h_s = 5.25 \cdot in^2$

$$I_{gp} := \frac{(w_p - w_s) \cdot t_p^3}{12} + \frac{w_s \cdot (2 \cdot h_s + t_p)^3}{12} = 2.097 \cdot in^4 \qquad r_p := \sqrt{\frac{I_{gp}}{A_{gp}}} = 0.632 \cdot in$$

L3x3x3/8:

$A_{gl} := 2.11in^2 \quad I_{gl} := 1.75in^4 \quad x_{barl} := 0.884in \quad r_l := 0.910in$

$A_{gc} := 4A_{gl} + A_{gp} = 13.69 \cdot in^2 \quad a := 6in$

$$I_{gc} := 4I_{gl} + I_{gp} + 4 \cdot A_{gl} \cdot \left(x_{barl} + \frac{t_p}{2} \right)^2 = 21.179 \cdot in^4 \qquad r_g := \sqrt{\frac{I_{gc}}{A_{gc}}} = 1.244 \cdot in$$

$$\frac{L}{r_g} = 86.83 \qquad \sqrt{\left(\frac{L}{r_g}\right)^2 + \left(\frac{a}{r_p}\right)^2} = 87.347 \qquad \text{(AISCS E6.1)}$$

$\phi F_{cr} := 21.6 \frac{kip}{in^2}$ (AISCM Table 4-22)

$\phi P_n := \phi F_{cr} \cdot A_{gc} = 295.704 \cdot kip$ Capacity > Demand, OK

Check capacity of center plate for buckling:

$t_p = 0.625 \cdot in \quad w_{so} := 0.25in \quad h_{so} := 2.625in$

$w_p := 8.5in$

$A_{gp} := w_p \cdot t_p + 2(w_{so} \cdot h_{so}) = 6.625 \cdot in^2$

$$I_{gp} := \frac{(w_p) \cdot t_p^3}{12} + 2 \cdot \frac{w_{so} \cdot h_{so}^3}{12} + \frac{w_{so} \cdot (t_p)^3}{12} = 0.932 \cdot in^4$$

$$r_p := \sqrt{\frac{I_{gp}}{A_{gp}}} = 0.375 \cdot in$$

L3x3x3/8:

$A_{gl} := 2.11in^2$ $I_{gl} := 1.75in^4$ $x_{barl} := 0.884in$ $r_l := 0.910in$

$A_{gc} := 4A_{gl} + A_{gp} = 15.065 \cdot in^2$

$I_{gc} := 4I_{gl} + I_{gp} + 4 \cdot A_{gl} \cdot \left(x_{barl} + \frac{t_p}{2} \right)^2 = 20.014 \cdot in^4$ $r_g := \sqrt{\frac{I_{gc}}{A_{gc}}} = 1.153 \cdot in$

$\frac{L}{r_g} = 93.699$ $\sqrt{\left(\frac{L}{r_g}\right)^2 + \left(\frac{a}{r_p}\right)^2} = 95.055$ (AISCS E6.1)

$\phi F_{cr} := 20.1 \frac{kip}{in^2}$ (AISCM Table 4-22)

$\phi P_n := \phi F_{cr} \cdot A_{gc} = 302.807 \cdot kip$

Check buckling of core plate with stiffeners:

$w_p := 6in$ $t_p := 0.75in$ $w_s := 0.5in$ $h_s := 1.5in$ $A_{gp} := w_p \cdot t_p + 2 \cdot w_s \cdot h_s = 6 \cdot in^2$

$I_{gp} := \frac{(w_p - w_s) \cdot t_p^3}{12} + \frac{w_s \cdot (2 \cdot h_s + t_p)^3}{12} = 2.391 \cdot in^4$ $r_p := \sqrt{\frac{I_{gp}}{A_{gp}}} = 0.631 \cdot in$

$\frac{K \cdot L}{r_p} = 171.097$

$\phi F_{cr} := 7.73 \frac{kip}{in^2}$ (AISCM Table 4-22)

$\phi P_n := \phi F_{cr} \cdot A_{gp} = 46.38 \cdot kip$

Check buckling of core plate with stiffeners: (Modified)

$w_p := 6in \qquad t_p := 0.75in \qquad w_s := 0.5in \qquad h_s := 2.0in \qquad A_{gp} := w_p \cdot t_p + 2 \cdot w_s \cdot h_s = 6.5 \cdot in^2$

$$I_{gp} := \frac{(w_p - w_s) \cdot t_p^{\,3}}{12} + \frac{w_s \cdot (2 \cdot h_s + t_p)^3}{12} = 4.659 \cdot in^4$$

$$r_p := \sqrt{\frac{I_{gp}}{A_{gp}}} = 0.847 \cdot in$$

$$\frac{K \cdot L}{r_p} = 127.568$$

$$\phi F_{cr} := 13.7 \frac{kip}{in^2} \qquad \text{(AISCM Table 4-22)}$$

$$\phi P_n := \phi F_{cr} \cdot A_{gp} = 89.05 \cdot kip$$